UNIVERSITY OF SOUTHAMPTON

FACULTY OF ENVIRONMENTAL AND LIFE SCIENCES

School of Ocean and Earth Science

# Megabenthic ecology of the Angolan continental slope

by

**Simone Pfeifer**

Thesis for the degree of Doctor of Philosophy

November 2021

ORCID ID: 0000-0001-6725-613X

*Für meine Eltern*

UNIVERSITY OF SOUTHAMPTON

SCHOOL OF OCEAN AND EARTH SCIENCE

FACULTY OF ENVIRONMENTAL AND LIFE SCIENCES

Thesis for the degree of Doctor of Philosophy

**Megabenthic ecology of the Angolan continental slope**

Simone Pfeifer

# Abstract

The structure of deep-water benthic systems off Angola is poorly known. This thesis presents new information on the present-day spatial structure of epifaunal megabenthic communities from the Angolan continental slope using seabed imagery and environmental data obtained across a range of depths extending from 300 to 2500 m. At broader spatial scale, communities associated with soft sedimentary habitats on the upper to lower slope showed strong depth-related structuring. Evolutionary influences and ecological controls, such as food availability, hydrodynamic conditions, and dissolved oxygen concentrations were proposed to influence these patterns at different spatial and temporal extents. The study of the ecological and morphological characteristics of cold-water coral mounds along the upper continental slope highlighted the importance of habitat-forming scleractinian species in providing habitat heterogeneity and increasing regional diversity. The preliminary analysis of acoustic and photographic data collected on the lower slope revealed a variety of geomorphological and geochemical features on a wide range of scales that increased habitat heterogeneity. The regional-scale review of Angolan deep-water systems showed major gaps in our understanding of Angolan deep-water ecology. The data presented in this study contribute to filling some of those gaps, while simultaneously providing quantitative data for environmental managers and conservationists.

# Contents

# List of Figures

# Supporting Information

# List of Tables



# Supporting Information

# Abbreviations

| | |
|---|---|
| AABW | Antarctic Bottom Water |
| ABFZ | Angola-Benguela Frontal Zone |
| AC | Angola Current |
| AD | Angola Dome |
| AEB | Atlantic Equatorial Belt |
| AIW | Antarctic Intermediate Water |
| AUV | Autonomous underwater vehicle |
| BCC | Benguela Current Convention |
| BCLME | Benguela Current Large Marine Ecosystem |
| BP | British Petroleum plc |
| CBD | Convention on Biological Diversity |
| CCD | Carbon compensation depth |
| $C_{org}$ | Organic carbon |
| CTD | Conductivity, Temperature and Depth |
| CWCR | Cold-water coral reef |
| DELOS | Deep-ocean Environmental Long-term Observatory System |
| EBM | Ecosystem-based management |
| EBSA | Ecologically or Biologically Significant Area |
| EEZ | Exclusive Economic Zone |
| EIA | Environmental Impact Assessment |
| EIS | Environmental Impact Study |
| Exp *H'* | Exponential from of Shannon diversity index |
| EUC | Equatorial Undercurrent |
| g fwwt | Grams of fresh wet weight |
| ind | Individuals |
| LCB | Lower Congo Basin |
| Ma | Million years |
| mg | milligram |
| MPA | Marine Protected Area |
| msp | Morphospecies |
| MSP | Marine Spatial Planning |
| NADW | North Atlantic Deep Water |
| nMDS | non-metric Multi-dimensional scaling |
| NOC | National Oceanography Centre |
| NPP | Net primary productivity |
| OMZ | Oxygen minimum zone |
| PCA | Principle Component Analysis |
| POC | Particulate organic carbon |
| $r_s$ | Spearman's rank correlation coefficient |
| ROV | Remotely Operated Vehicle |
| SECC | South Equatorial Countercurrent |
| SEUC | South Equatorial Undercurrent |

| | |
|---|---|
| SST | Sea surface temperature |
| SVI | Season Variation Index |
| TN | Total nitrogen |
| TOC | Total organic carbon |
| TSW | Tropical Surface Water |
| VGPM | Vertically Generalized Production Model |
| WASP | Wide-Angle Seabed Photography |
| 1/D | Inverse of Simpson concentration index |

# Declaration of Authorship

I, Simone Pfeifer

declare that this thesis entitled “Megabenthic ecology of the Angolan continental slope” and the work presented in it is my own and has been generated by me as the result of my own original research.

I confirm that:

1. This work was done wholly or mainly while in candidature for a research degree at this University;
2. Where any part of this thesis has previously been submitted for a degree or any other qualification at this University or any other institution, this has been clearly stated;
3. Where I have consulted the published work of others, this is always clearly attributed;
4. Where I have quoted from the work of others, the source is always given. With the exception of such quotations, this thesis is entirely my own work;
5. I have acknowledged all main sources of help;
6. Where the thesis is based on work done by myself jointly with others, I have made clear exactly what was done by others and what I have contributed myself;
7. None of this work has been published before submission.

Signature: .....

Date: .....

# Acknowledgements

My first thanks go to my supervisors Dr. Daniel Jones and Dr. Brian Bett for their guidance, support, and inspiration throughout my PhD. I would particularly like to thank Dan for his advice and patience whenever I needed it. I am also grateful to Dr. Tammy Horton for her help and advice as my panel chair, and to Prof. Lawrence Hawkins and Dr. Phillip Fenberg for their valuable inputs to my project plan. I also thank all my fellow members of the DEEPSEAS group for answering questions, their support, and the many stimulating discussions about deep-sea science, which made NOC a pleasant and encouraging place to work. I also thank them for providing experiences outside of my PhD work, particularly the opportunities to go to sea and to participate in outreach activities. A special thanks goes to BP for providing access to their deep-water data, without which none of this work would have been possible. I particularly thank Philippe de Susanne, Alph Motsamai, and Robert O'Brien for help with data queries. I am also grateful to everyone who helped with the identification of species, including E. Anderson, N. Benoist, B. Bett, D. Billett, J. Durden, A. Gates, A. Goineau, A. Gooday, S. De Grave, T. Horton, A. Jamieson, D. Jones, E. Simon-Lledó, K. Sulak, and M. Thurston. I would also like to thank the team of GSNOCS for their support at challenging times. I gratefully acknowledge the funding provided by the UK Natural Environmental Research Council (grant number NE/L002531/1), and by BP under the CASE studentship 'Collaborative Awards in Science and Engineering' scheme. A very special thanks to my family and friends for their unconditional support.

Finally, I deeply thank my parents for raising my interest in science, and for their love and support throughout my life. I am deeply grateful to my mum! Without her love and support I could not have completed this project.

# Chapter 1

# Introduction

The deep sea is the largest ecosystem on Earth, and contrary to initial hypotheses it is a highly heterogeneous and dynamic environment (Danovaro et al., 2014; Ramirez-Llodra et al., 2010; Tyler, 1988). Research into deep-water systems has risen over the last decades as sampling and mapping techniques have improved (Ramirez-Llodra et al., 2010), and questions on how these systems may change in response to climate change and increasing human exploitation have become more prominent (Levin and Sibuet, 2012; Ramirez-Llodra et al., 2011). Nevertheless, only a small fraction of the deep water environment has been studied to date, with an estimated 95% of the deep sea and more than 99% of its seafloor still to be explored (Ramirez-Llodra et al., 2010). In addition, sampling effort across the deep sea remains geographically biased with the majority of historic research carried out in the North Atlantic and Pacific Oceans (Levin and Gooday, 2003; Smith and Demopoulos, 2003). Therefore, there is a strong need for continued sampling of the deep ocean to provide the data needed to ensure its effective environmental management (Glover et al., 2018; Howell et al., 2020; Levin et al., 2019), and to address fundamental questions of biodiversity and connectivity (McClain and Schlacher, 2015).

The research presented in this thesis aims to improve understanding of deep-water benthic ecology along the deep continental margin off Angola in the eastern tropical South Atlantic, which is one of the lesser studied region of the world's deep ocean. Specifically, the thesis examines the present-day spatial patterns of megabenthic assemblages on the Angolan continental slope in water depths between about 300 and 2500 m. Before outlining the objectives of the research, current knowledge relating to the study of megabenthic ecology on deep continental margins is introduced.

## 1.1 Deep continental margins

The deep continental margins include the continental slopes and rises, which comprise the portion of the seafloor between the shallow continental shelves and the deep abyssal plains. The upper boundary of deep margins is marked by the shelf break, whose depth varies geographically, ranging from about 100 m at lower altitudes down to about 600 m in polar areas (Heezen, 1974). Applying an average depth range of 140 to 3500 m, deep margins are estimated to cover an area of 40 million $km^2$, which represents approximately 11% of the ocean's surface (Menot et al., 2010). Geologically, two main types of continental margins are distinguished, based on their mode of development: (1) passive or "Atlantic" type margins, and (2) active or "Pacific" type margins (Wright and Rothery, 2007). Passive margins occur at the boundaries of ocean basins that were formed following rifting and subsequent break-up of continents. They are characterised by relatively low seismic activity and the occurrence of a gently sloping, often extensive continental rise at the foot of the continental slope. On the contrary, active margins develop at convergent plate boundaries where oceanic crust is subducted beneath continental or oceanic crust. They exhibit high seismic activity, and their slopes are often steeper than those on passive margins. Ocean trenches at the foot of the continental slope are a common feature of active margins, while the continental rise is less developed or absent (Harris et al., 2014; Wright and Rothery, 2007). The Angolan continental slope, which is the focus of this study, is part of the West African passive margin, which evolved following the breakup of the Gondwana supercontinent and the subsequent separation of the South American and African plates (Sabato Ceraldi et al., 2017).

Deep continental margins host a diverse set of habitats, reflecting the large environmental heterogeneity driven by often complex geological and topographical settings, and strong bathymetric gradients in hydrographic and physico-chemical conditions (reviewed in Levin and Sibuet, 2012; Menot et al., 2010). At broader scales, for instance, submarine canyon systems dissect continental margins, providing conduits for turbidite sediments and associated organic matter transport into the deep ocean (e.g. Khripounoff et al., 2003). At finer scales, hydrocarbon seepage and associated seabed features, such as pockmarks, cold seeps, and concretions of authigenic carbonates are common on margins affected by salt diaparism, such as the Gulf of Mexico (Sahling et al., 2016) and the Angolan Margin

(Gay et al., 2006; Sibuet and Vangriesheim, 2009), supporting a highly specialised chemosynthetic fauna (e.g. Cordes et al., 2007; 2010; Levin et al., 2016; Olu-Le Roy, 2007; Sibuet and Olu, 1998). Oxygen minimum zones impinging on the seabed at mid-water depths are prominent at several margins (Levin and Sibuet, 2012), like on the Indian (Hunter et al., 2011), Pakistan (Murty et al., 2009), and Peruvian (Mosch et al., 2012) margin.

## 1.2 Megabenthos

### 1.2.1 Fauna

The megabenthos comprises the largest organisms that live in, on, or near the seabed (Bett, 2019). It is a major component of the deep-sea benthos, represented by a large variety of taxonomic groups with varying morphologies, behaviours, and feeding modes (Gage and Taylor, 2010). This includes sessile suspension feeding sponges, cnidarian, and ascidians, mobile deposit-feeding echinoderms, predators, scavengers, and trophic generalists that can switch their feeding style with changing trophic conditions (e.g. Meyer et al., 2016). Deep-water benthic megafauna contributes substantially to benthic biomass (e.g. Haedrich and Rowe, 1977; Lampitt et al., 1986; Smith and Hamilton, 1983) and community respiration (Smith, 1983). Several taxa, such as sponges, corals, and xenophyophores, can enhance environmental heterogeneity (Buhl-Mortensen et al., 2010), for example by offering surfaces for attachment (e.g. Beaulieu, 2001), or by providing favourable microhabitats for shelter (e.g. Baillon et al., 2014; Gates et al., 2017; Moore and Auster, 2009), and spawning (e.g. Levin and Rouse, 2020). Mobile epibenthic megafauna can alter the structure of sediments in a variety of ways, for instance, through the production of moving traces, mucus, and fecal material and when foraging on infaunal organisms (Gage and Tyler, 2010; Smith et al., 1993). Moreover, deposit-feeding megafauna, in particular holothurians, are important consumers of detrital material and contributors in the recycling of nutrients (Miller et al., 2000).

### 1.2.2 Sampling

Common sampling devices in use for studying deep-sea benthic and benthopelagic megafauna are towed bottom samplers and imaging systems (Gage and Tyler, 2010). The former include deep-water trawls and epibenthic sledges, and can cover relatively large

areas of seabed, which makes them particularly useful in sampling sparsely distributed species, as found in many deep-water settings (Clark et al., 2016). The physical samples obtained with trawls and sledges have been pivotal to our current understanding of deep-water taxonomy, biogeography and population genetics, and continue to provide an important source of material for a range of biological studies such as analysis of diet, life history, histology, and body size. Widely recognised disadvantages of using trawls and sledges are the destructive nature of sampling, and the need for predominantly soft-bottom environments with relative flat relief to ensure effective gear deployment (Clark et al., 2016). Moreover, population densities and biomass tend to be underestimated when using these devices owing to the low catchability of several species and the unreliable estimation of the area sampled (Clark et al., 2016; Kaiser and Brenke, 2016).

Seabed photography, in the form of video and still images, have proven to provide more accurate estimates of megafaunal assemblage composition and standing stocks (Durden et al., 2016). Its application in deep-water research has expanded rapidly over the last decades, largely as a result of major advances in underwater imaging technology, and reduced development and deployment costs (Durden et al., 2016). Overviews of the different types of deep-sea imaging platforms currently available with examples of their use are given by Bowden and Jones (2016), Durden et al. (2016), and Kelley et al. (2016). In principle, two classes of camera platforms can be distinguished: mobile devices, which can be towed, tethered or free-moving, and stationary devices, which include moored instruments and autonomous free falling landers. Mobile imaging platforms can be employed along transects to provide quantitative data for spatial studies (e.g. Benoist et al., 2019; Hecker, 1990; Howell et al., 2010), or they may be used to conduct detailed observations (e.g. Gates et al., 2017), and to facilitate sampling and in-situ experimentation (e.g. McClain et al., 2016). Many advanced mobile systems, such as remotely operated vehicles (ROVs) and autonomous underwater vehicles (AUV), carry a suite of scientific sensors (e.g. echosounder, CTD) in addition to imaging equipment to simultaneously provide data on fauna and habitat characteristics. Stationary imaging systems on the other hand are employed to record time-lapse photography for analysis of ecological and environmental processes. Examples of time-lapse image studies conducted in deep waters include observations of feeding behaviour and animal growth, and long-term studies of seasonal variation in phytodetrital deposition (Bett, 2003). In addition,

time-lapse observations from baited landers are routinely used to investigate the distribution and foraging of bait-attending benthopelagic species (Bailey et al., 2007; Jamieson, 2016). Finally, imaging instruments are a key component of long-term deep-water observatories (e.g. Lampitt et al., 2010; Pfannkuche and Linke, 2003; Purser et al., 2013; Vardaro et al., 2013).

Unlike trawls and sledges, imaging devices can be deployed across a variety of bottom topographies, ranging from relative uniform soft sediments (e.g. slope sediments, abyssal plains) to areas with complex terrain (e.g. seamounts, submarine canyons). Moreover, photographic data retain information about the spatial structure of seabed features across the area sampled (Jones, 2009), allowing both transect-level community distributions and fine-scale patterns in species and habitat heterogeneity to be analysed (e.g. Grassle et al., 1975; Jones et al., 2007). The non-intrusive nature of underwater photography makes it the method of choice when studying sensitive habitats, such as cold-water coral reefs and sponge grounds, and also provides a best practise method in scientific and industrial studies to minimise disturbance and damage to the seabed. The major disadvantage of deep-water imaging studies is their lower taxonomic resolution compared to studies that yield physical specimens, and as a result they tend to underestimate taxonomic diversity (Durden et al., 2016).

Generally, the deep-sea benthos remains poorly described for lack of sampling as well as limited taxonomic capability (Gage, 2003; Ramirez-Llodra et al., 2010). For instance, in a study of the macrobenthos on the continental slope off New Jersey and Delaware, Grassle and Maciolek (1992) estimated that 58% of the species recorded were new to science, while more recent sequencing of environmental DNA samples from bathyal and abyssal surface sediments showed a large proportion of unknown genetic diversity of meio- and macrofaunal taxa (Sinniger et al., 2016). New species of deep-sea megabenthos are regularly reported for many taxonomic groups, including sponges (e.g. Cristobo et al., 2005; Lopes and Hajdu, 2014), corals (e.g. Cordeiro et al., 2005; Daly, 2006), arthropods (e.g. Arango, 2009; De Matos-Pita and Ramil, 2014), echinoderms (e.g. Martinez et al., 2019; Pawson et al., 2004), and fish (e.g. Linley et al., 2016). The use of image data poses an additional challenge for identification because characteristic morphological features are often not visible or obscured from view. For example, species-level identification of holothurians is typically based on the shape and size of body wall ossicles, which requires

microscopic examination of tissue samples, while fish species may be distinguished by their number and position of fins, which are difficult to discern from still images, particularly from those taken with a downward-facing camera. Therefore, specimens identified from imagery are usually classified based on taxonomy as well as conspicuous morphological attributes (Durden et al., 2016), often using a mixture of taxonomic keys, reference image catalogues, and visible features defined by the image analyst (e.g. Alt et al., 2019; Simon-Lledó et al., 2019a). The level of taxonomic resolution that can be achieved with such an approach depends on the properties of the images obtained (e.g. image resolution, camera orientation) as well as annotator circumstances (e.g. level of expertise, access to physical and image reference material), and therefore can vary considerably between studies. Howell et al. (2019) outlined the challenges associated with the standardisation of image-based identifications, highlighting incomparable naming conventions and missing details about the visual characteristics used to separate morphospecies as key reasons that impede data comparability. They recommend the development of standard regional reference image catalogues and associated metadata databases, easily accessible and curated by experts, in an effort to improve taxonomic identification, consistency between annotators, and ultimately comparability of data.

There can be considerable variability in the fraction of megabenthos sampled between surveys as a result of sampler biases. For example, towed bottom gear is strongly biased by organism size and mobility: otter trawls tend to sample a higher proportion of larger invertebrates and highly mobile demersal fish (Clark et al., 2016; Tecchio et al., 2011), while Agassiz trawls are typically used to catch epibenthic invertebrates, and beam trawls are more effective at sampling smaller invertebrates and slow-moving fish (Clarke et al., 2016). Weather conditions and towing speed can also profoundly affect the catch efficiency of both trawls (Clark et al., 2016) and epibenthic sledges (Kaiser and Brenke, 2016). The detectability of specimens in underwater images depends inherently on camera distance to the seabed, which in turn is affected by operational conditions and can also differ largely between imaging platforms. These sampling biases make a formal size-based categorisation of megabenthos challenging (Bett, 2019). In deep-water image-based studies, the megabenthos is typically defined as organisms readily visible in photographs (sensu Grassle et al., 1975). In practical terms, the cut-off of the smallest organism identifiable has to be set by the annotator and should enable consistent detection and

identification of organisms across the image data set analysed. A minimum dimensions of > 1 cm is often applied in photographic megafaunal studies although there are also several examples where a larger size cut-off had been selected either to ensure consistency in detection and identification (e.g. Jones et al., 2007) or to address specific objectives that did not require quantification of smaller organisms (e.g. Lacharite and Metaxas, 2017). While such an approach ensures consistency at study level, it introduces challenges when assessing broader ecological patterns at basin or global scale that rely on comparing faunal parameters among studies.

## 1.3 Patterns and controls of margin biodiversity

### 1.3.1 Measures

Quantifying species diversity and community composition is of long-standing interest to community ecologists. It forms an important step in the development of ecological and evolutionary theories (Gotelli and Colwell, 2011) as well as the understanding of community processes and functioning (Levin, 1992; Storch and Gaston, 2004). It also provides information critical for conservationists to formulate clearly defined conservation targets, to design effective networks of Marine Protected Areas, and to monitor trends in habitat condition (Blackburn and Gaston, 2003; Magurran, 2004). Likewise, in order to assess the likely environmental impacts of human activities we must have knowledge of species identities and their distributions and environmental tolerances (Glover et al., 2018).

Basic parameters of community standings stocks are abundance and biomass, which for many years have been investigated for potential information about faunal-environment relationships (e.g. Durden et al., 2020; Gunton et al., 2015), population dynamics (e.g. Huffard et al., 2016; Ruhl and Smith, 2004), food web interactions (e.g. von Oevelen et al., 2012), and the environmental impacts of human activities (e.g. Bailey et al., 2009; Jones et al., 2006). For the assessment of species diversity and composition, a diverse range of measures exists, which have traditionally been divided into two broad groups: (1) measures that quantify the number of species and their relative proportion within a given sampling unit, and (2) measures that reflect the extent of change in species numbers and proportions among sampling units (Magurran, 2004; Whittaker, 1960). The first group is

usually partitioned into measures of α-diversity and γ-diversity, with α-diversity representing diversity occurring at smaller spatial scales, for example within a sample, sampling site or habitat, and γ-diversity describing the diversity observed at broader scales, for example across large topographic features, such as mountains or submarine canyons, or across continents and within ocean basins. The variation in diversity among sampling units is generally termed β-diversity (Anderson et al., 2011; Whittaker, 1960). While β-diversity is a widely used concept in ecological studies, there still remains considerable debate about the term's definition (e.g. Jurasinski et al., 2009; Tuomisto 2010a, 2010b), and several different measures have been proposed for its assessment (Anderson et al., 2011). This includes measures to assess the variation in species diversity across spatial scales, such as the relationship between local and regional species richness (Tuomisto, 2010a), and measures to quantify the variation in assemblage composition along geographic and environmental gradients, or between experimental treatments (Anderson et al., 2011).

### 1.3.2 Broad-scale patterns

Traditionally, research into the spatial structure of deep-water benthic assemblages has focussed on assessing trends in standing stocks, α-diversity (primarily changes in species richness), and faunal turnover along geographic and bathymetric gradients (Carney, 2005; McClain et al., 2009). Less information is available about deep-sea γ-diversity, and associations between local and regional diversity, mainly owing to restricted sampling within most ocean basins and limited taxonomic information for many faunal groups (Levin et al., 2001).

Bathymetric trends in α-diversity across margins have been well documented, but unlike changes in standings stocks, they appear to be much more variable among taxonomic groups and between ocean basins (McClain et al., 2009). At larger scales, several studies have recorded a unimodal distribution of richness with water depth, including invertebrate megafauna in the western North Atlantic (Wei and Rowe, 2009), mussel-bed associated communities in the Gulf of Mexico (Cordes et al., 2010), brittle stars on a global scale (Woolley et al., 2016), bivalves in the western North Atlantic (Brault et al., 2013a), isopods in the Norwegian Sea (Svavarsson, 1997), and polychaetes in the eastern North Atlantic (Paterson and Lambshead, 1995). The shape of the distribution and the location

of the diversity peak vary among basins and taxonomic groups, although the number of species is generally largest at mid-slope depths and decreased towards the continental shelf edge and abyssal plain. The unimodal trend is not universal for all faunal groups and deep-sea basins, suggesting that bathymetric trends in α-diversity are taxon-specific and exhibit inter-basin variation (Rex and Etter, 2010). Example for non-parabolic patterns include isopods in the western North Atlantic (Rex and Etter, 2010) and bivalves in the eastern North Atlantic (Brault et al., 2013a), where diversity has been found to peak at abyssal depths, and the macrofauna in the Mediterranean, where a linear decrease in the number of macrofaunal species has been observed along slopes of the South Aegean Sea (Tselepides, 2000). Decreasing richness in invertebrate megafauna was found across the mid-bathyal to lower bathyal in the Faroe-Shetland Channel (Jones et al., 2007). In some cases, the observed differences in richness patterns will have been caused by differences sampled depth ranges.

The few studies that have examined large-scale latitudinal trends in α-diversity suggest large differences in patterns between basins and faunal groups. In the Norwegian Sea and along the margins of the eastern and western North Atlantic gastropods, bivalves and isopods exhibit strong trends of decreasing species richness towards higher latitudes. In contrast, in the South Atlantic relationships of gastropod and bivalve richness with latitude were much weaker within the basins sampled, while the number of isopod species showed no correlation with latitude (Rex and Etter, 2010). In a recent global study assessing the distribution of brittle stars diversity peaks were depth-dependent, with richness in upper to mid bathyal depths (200-1200 m) peaking in the tropics, while at lower depths bimodal maxima at temperate latitudes were observed (Woolley et al., 2016). At smaller regional-scales, along-slope variation in megafaunal diversity are present at the West Shetland Slope (Jones et al., 2007).

Extensive earlier work across the eastern and western North Atlantic (reviewed by Carney, 2005; Levin and Gooday, 2003) has established that the composition of deep-water benthic communities on continental margins, including that of the megabenthos, changes strongly with water depth, similar to compositional changes in flora and fauna found across elevation gradients on land. Since then, bathymetric changes have been well documented for megabenthic communities from around the globe, including scavengers in the northern Pacific (Yeh and Drazen, 2009) and eastern tropical South Atlantic (Jamieson et al., 2017),

molluscs (Olabarria, 2005), sea stars (Howell et al., 2002), echinoderms (Gage 1986), and fish (Eerkes-Medranoa et al., 2019; Priede et al., 2010) on the North Atlantic margin, benthic invertebrates on the Australian slope (Williams et al., 2010), in the Caribbean (Hernández-Ávila et al., 2018), and in the western North Atlantic (Wei and Rowe, 2009), mobile megafauna in the Mediterranean (Fanelli et al., 2018), and for the whole megafauna community in the Arctic Basin (Jones et al., 2007; Soltwedel et al., 2009). Similar widespread bathymetric zonation across margins has been reported for benthic macro- and meiofauna communities (McClain et al., 2009; Rex and Etter, 2010). Faunal turnover is for large parts gradual, interspersed with areas of larger change, with the latter shown to vary among regions (Carney, 2005). More sharp faunal boundaries occur in areas characterised by rapid changes in environmental conditions, such as zones of water mass convergence that are subject to strong gradients in water temperature (Bett, 2001), submarine canyons (e.g. De Leo et al., 2010), and Oxygen Minimum Zones (e.g. Hunter et al., 2011; Wishner et al., 1990). Relative rates of faunal change also vary among faunal groups, as shown, for example, in the western North Atlantic, where the faunal composition of megafaunal species changes more rapidly with depth than the faunal make-up of macrofaunal species (Rex and Etter, 2010). Combining information on species' physiological tolerances in deep-waters with those of faunal zonation patterns across margins, Carney (2005) suggested species may belong to one of three broad faunal groups: (1) species that extend down from the shelf, (2) species that extend upward from the abyss, and (3) species that are restricted to the slope.

Recent studies argue that two phenomena should be considered when investigating bathymetric changes in faunal composition: spatial turnover of species resulting from the replacement of species between sampling areas, and nestedness caused by species loss (Baselga, 2010; Brault et al., 2013a). Investigations into large-scale β-diversity patterns of benthic deep-sea assemblages that partition the two components are limited (McClain and Rex, 2015), but available studies indicate that the relative importance of both varies with water depth, among faunal groups, and among ocean basins. For example, in the West European Basin of the eastern Atlantic, neogastropods exhibit species replacement from bathyal to abyssal depths, while in the North American Basin of the western Atlantic both turnover and nestedness contribute to bathymetric faunal change for this group, with increasing importance of nestedness towards abyssal depths (Brault et al., 2013b). Among

the megafauna, asteroids and holothurians in the eastern North Atlantic showed changes in species composition driven predominantly by turnover from upper bathyal to abyssal depths (Wagstaff et al., 2014).

### 1.3.3 Controls and mechanisms

It is now widely argued that present-day patterns of diversity and species distributions, both in terrestrial and aquatic systems, reflect historical-evolutionary influences as well as contemporary environmental and biotic processes (e.g. Levin et al., 2001; Soberón, 2007; Ricklefs and Jenkins, 2011; Wiens, 2011). Historical influences include speciation and extinction rates, taxon-specific physiological adaptations and genetic differentiation, and long-distance dispersal capabilities (Connallon and Sgrò, 2018; McClain and Hardy, 2010; Wiens, 2011). Such processes typically operate over longer time-scales and larger spatial distances from regional to global extents (Lambshead and Boucher, 2003). On the other hand, contemporary environmental processes are thought to be more important over smaller spatial scales (Lambshead and Boucher, 2003), affecting the distribution of individuals within a species' range limits through the joint effects of environmental conditions, resource availability and biotic interactions (Soberón, 2007; Wiens, 2011). The relative importance of individual processes has proven to be highly scale-dependent (Gage, 2004; Levin et al., 2001; McClain et al., 2009).

Ecological factors linked to observed broad-scale species macrofaunal and megafaunal richness patterns include energy availability (e.g. McClain et al., 2012; Soltwedel et al., 2009; Tittensor et al., 2011; Woolley et al., 2016), temperature (e.g. Bett, 2001; Williams et al., 2010), current regime (Paterson and Lambshead, 1995; Gage et al., 2000), dissolved oxygen concentrations (e.g. Levin, 2003; Mosch et al., 2012), and sediment heterogeneity (e.g. Etter and Grassle, 1992; Jones et al., 2007; Levin et al., 2010). Among those, energy gradients are widely hypothesised to be one of the most important factors influencing species diversity patterns in deep-sea water systems (e.g. McClain et al., 2012; Woolley et al., 2016).

Hypotheses relating energy to deep-water diversity patterns consider the influences of two broad forms of energy (McClain et al., 2012; Rex et al., 2005a). The first group includes hypotheses concerned with the effects of kinetic, or thermal, energy in the form of ambient temperature on biochemical and physiological processes and their consequences on

ecological attributes such as species' range distributions, body size, metabolic rates or standing stocks (e.g. McClain et al, 2012). For instance, over long evolutionary time-scales, gradients in water temperature, in combination with gradients in pressure, are suggested to have contributed to bathymetric diversity patterns by influencing rates of diversification via effects on species range distributions, mutation rates and generation times (Brown and Thatje, 2014; Carney, 2005).

The second group of hypotheses deals with the importance of chemical energy in the form of nutrient / food availability in influencing, for example, species growth rates, range distributions and population dynamics, including reproductive capacity and competitive interactions (e.g. McClain and Schlacher, 2015; Rex et al., 2005a). For instance, depressed species diversity at lower bathyal and abyssal depths have been proposed to result from decreased population densities and increasing rates of local extinction with increasing depth (Rex and Etter, 2010), in accordance with the more-individual hypothesis of the species-energy theory (e.g. Wright, 1983). The hypothesis predicts that as population densities decline, the likelihood of sustaining reproductive viable populations decreases, resulting in the rarest species being more likely to experience local extinctions. As a consequence species richness decreases in areas of low organic input, such as at lower bathyal and abyssal depths. This model led, together with observations that some macrofaunal taxa show a high degree of nestedness at abyssal depths, to the proposition of a source-sink hypothesis for abyssal biodiversity (Rex et al., 2005b). The hypothesis predicts that many abyssal populations may represent sink populations, where local extinctions owing to low population abundances are compensated for by the colonisation by individuals from more abundant bathyal source populations (Rex and Etter, 2010; Rex et al, 2005b). However, as Carney (2005) pointed out, source-sink dynamics may be highly taxon-specific, as many species in the abyss have been shown to be reproductively active.

The decline of species richness towards the shelf edge has been linked to shifts in assemblage composition from more evenly distributed assemblages to those dominated by a few opportunistic species (Levin et al., 2001; Menot et al., 2012). High levels of organic carbon input are thought to facilitate competitive exclusion, favouring species capable of taking better advantage of the higher, and often periodic, inputs of organic matter found at upper bathyal depths (Levin et al., 2001). No study has examined whether this hypothesis can explain bathymetric α-diversity patterns at larger spatial scales (Rex et al.,

2005a), but at smaller scales deep-sea assemblages can exhibit depressed diversity owing to low species richness and evenness in areas of high organic input (Billet et al., 2010; Levin et al., 2001; Levin and Sibuet, 2012;). Alternative explanations for declining diversity in upper bathyal depths include depressed diversity values owing to increased stochasticity under more variable levels of surface production experienced at upper bathyal depth (Levin et al., 2001), and hypotheses based on productivity-driven environmental stability and predator-prey interactions (Rex et al., 2005a).

Like with α-diversity and standing stock, gradients in energy availability are viewed to be a key driver for shaping broad-scale vertical β-diversity patterns (McClain and Rex, 2005). For instance, nested patterns of β-diversity in abyssal macrofaunal mollusc assemblages in the western North Atlantic have been attributed to source-sink dynamics driven by low POC fluxes to abyssal depths (Brault et al., 2013b). Comparisons of standing stock and trophic composition of assemblages suggests that taxon-specific differences in the rate of faunal change may result from differences in trophic position (Rex and Etter, 2010) and energy demands related to body size (McClain and Rex, 2015). Environments with higher energy availability are predicted to support greater trophic complexity (McClain and Rex, 2015) and rates of faunal change are likely to be greater in taxa occupying higher trophic levels (Brault et al., 2013a).

## 1.4 Management and conservation of Angola's deep water environment

At a regional level, the principles guiding the conservation and management of Angola's marine resources are set out in the Benguela Current Convention (BCC), a formal treaty between the three coastal states bordering the Benguela Current Large Marine Ecosystem (BCLME), Angola, Namibia and South Africa (de Barros Neto et al., 2016). Established in 2007 and ratified in July 2014 (Finke et al., 2020), the BCC closely follows international development goals such as commitments under the Convention on Biological Diversity (CBD) by promoting ecosystem-based management (EBM) of the BCLME that balances economic and social provisions with environmental objectives to move towards long-term conservation and sustainable use of the area (Kirkman et al., 2016; Hamukuaya, 2020). With regards to the conservation of marine and coastal ecosystems, the treaty mandates measures to mitigate against adverse impacts from human activities as well as mechanisms

to protect vulnerable species and biological diversity, and where possible to prevent habitat alteration and destruction (Article 4(2), Benguela Current Convention, 2013). Management measures should be based on best available scientific knowledge and, where applicable, be underpinned by Environmental Impact Assessments (EIAs).

At the national level, Angola's commitment to nature is recognised in the Republic's constitution, which stipulates that "The state shall take the requisite measures to protect the environment and species of flora and fauna throughout the national territory, maintain the ecological balance, ensure the correct location of economic activities and the rational development and use of all natural resources, within the context of sustainable development, respect for the rights of future generations and the preservation of species" (Article 39(2), Republic of Angola, 2010). The government's strategic approaches for safeguarding the environment are included in Angola's National Development Plan (2018-2022) (Governo de Angola, 2021) and are closely linked to the country's ongoing efforts towards reaching the 17 Sustainable Development Goals (SDGs) of the United Nations Agenda 2030 (United Nations Country Team Angola, 2019). National objectives and proposed actions for the conservation and protection of Angola's biodiversity are established in the National Biodiversity Strategy and Action Plan (2019-2025), which among other things calls for the designation of at least two Marine Conservation Areas by 2025 (Governo de Angola, 2019).

To implement ecosystem-based management across the BCLME, Marine Spatial Planning (MSP) is being pursued at both national and regional level (Finke et al, 2020). MSP has become a key tool for many ocean nations to deal with the growing use of marine resources and to achieve sustainable blue economies (Douvere, 2008). It provides a mechanism for an integrated and adaptive marine planning and management system that accounts for activities across multiple sectors and their cumulative threats to the environment (Douvere, 2008). Anticipated benefits associated with the MSP approach include (1) better and safer use of ocean space and resources by integrating marine activity information and identifying and managing potential competing demands among sectors, (2) a more efficient and transparent licensing system through consideration of different policies and objectives and by encouraging closer cooperation between government bodies and among ocean users and regulators, and (3) increased capability of identifying potential damaging activities to the environment through improved assessment of cumulative effects and more

strategic selection of development sites (Douvere, 2008; Gilliland and Laffoley, 2008; Finke et al., 2020).

Across the Benguela Current Region, the development of MSP is being promoted through a combination of national programmes, work undertaken by a Regional MSP Working Group, and international partnerships such as the Benguela Current Marine Spatial Management and Governance (MARISMA) project (Finke et al., 2020). To date, these initiatives have produced a regional MSP strategy and national baseline reports of key maritime resources and activities (Finke et al., 2020). Draft Marine Spatial Plans covering selected coastal areas are available for Namibian and Angolan waters, and are under development for South African waters (Federal Ministry for the Environment, Nature Conservation and Nuclear Safety, 2021).

The development of the MSP strategy for the Benguela Current Region has been closely linked with the region's marine conservation planning process (Finke et al., 2020), specifically through the identification of Ecologically or Biologically Significant Areas (EBSAs) in fulfilment of commitments made under the CBD. EBSAs are considered marine areas of ecological or functional importance, for example by providing comparatively high levels of natural biodiversity and productivity, or by harbouring habitats and species highly sensitive to the degradation or depletion by human activities (CBD, 2008). The delineation of EBSAs is not accompanied with any obligations for protection or management, albeit the data supporting their selection may inform the need for spatial measures, such as the location and extent of Marine Protected Areas or the placement of activity exclusion zones (Dunn et al., 2014).

As of September 2021, Angola has identified seven EBSAs awaiting submission to the CBD (described in MARISMA EBSA Workstream, 2020a). Three of them are exclusively coastal while the remaining four expand beyond the shelf break into deeper waters. Nominated benthic deep-water features include shelf-incising canyons, offshore seamounts, and several areas along the upper and lower slope. Information on the distribution of habitats across these features and their associated benthic communities remain severely limited with their importance to the functioning of Angola's deep-water systems largely being predicted from similar features studied in other ocean basins. Canyons and seamounts, for example, are thought to enhance local productivity and to

support elevated levels of biodiversity and sensitive habitat-forming species such as sponges and cold water corals (MARISMA EBSA Workstream, 2020a).

The main activities exerting pressures on Angola's benthic deep-water systems are demersal trawling and hydrocarbon exploration and production (MARISMA EBSA Workstream, 2020b). Commercially important bottom-dwelling species found on the slope include the Benguela hake *Merluccius polli*, the deep-water red crab *Chaceon maritae*, and various shrimp species such as the striped red shrimp *Aristeus viridens*, the deep-sea rose shrimp *Parapenaeus longirostris*, and the scarlet shrimp *Plesiopenaeus edwardsianus* (Kirkman et al., 2016; Saetersdal et al., 1999). Trawlable grounds occur along most of slope, except in localised steep-sloping areas within the southern parts of the margin (Saetersdal et al., 1999).

Angola's petroleum sector is the second largest in West Africa and accounts for over 90% of the country's current export, with the majority of hydrocarbons coming from offshore reservoirs (ANPG, 2021). The search for offshore fields started in the 1960s (Dolan et al., 1999) and increased substantially since the 1990s following the discovery of the first fields in deep waters (< 500 m, Zhang et al., 2019). Infrastructure developments and hydrocarbon extraction are currently concentrated along the northern parts of the Angolan margin and to a lesser degree across the central regions (Brownfield and Charpentier, 2006) though the search for new profitable offshore reserves is ongoing, which includes prospecting across several newly licenced Blocks in the southern regions of the margin (ANGP, 2021).

Relevant national legislation related to the management of oil and gas exploration and production in Angolan waters include Presidential Decree No. 39/00 on Environmental Protection for the Petroleum Industry (Governo de Angola, 2000) and Decree No. 117/20 on the General Regulation for Environmental Impact Assessment and the Environmental Licensing Procedure (Governo de Angola, 2020). The latter sets out the general legal and procedural framework related to the licensing of public and private projects in Angola and the associated EIA process. Decree 39/00 establishes sector-specific environmental protection and management instruments for Angola's onshore and offshore petroleum industry. It mandates an EIA for all oil and gas projects that are likely to have significant environmental effects (Article 6). Each EIA requires the submission of an Environmental Impact Study (EIS) prepared by independent experts, which must contain a description of

the activities to be undertaken, a characterisation of the current environmental conditions across the development area, an assessment of any positive and negative environmental effects that the proposed activities are likely to cause, and a list of measures to mitigate against any potential significant negative effects. Decree 39/00 is complemented by several legal statutes that set out more detailed measures to be adopted in the management of operational waste and oil pollution (ECOLEX, 2021). For example, the Operational Discharge Management Regulations (Decree No. 97/14) stipulate regular monitoring of areas likely to be affected by oil and gas exploration and production activities, both throughout the lifetime of the activities and prior to their commencement to provide baseline data for the EIS (Governo de Angola, 2014).

## 1.5 Thesis outline

### 1.5.1 Thesis aims and structure

The aim of this study is to further understanding of megabenthic ecology along the Angolan continental slope by characterising present-day spatial patterns of assemblage standing stocks, diversity and composition. The research draws on data collected by BP plc across four main deep-water oil and gas provinces along the northern and central parts of the Angolan margin (Figure 1.1). The offshore areas of Angola constitute one of the world's most prolific deep-water petroleum provinces (da Costa et al., 2001; Fraser et al., 2005), and BP are among several hydrocarbon-producing companies in the region. To plan their subsea developments and obtain baseline environmental data for impact assessments and future environmental monitoring, BP have carried out a series of geophysical, geotechnical and ecological surveys off Angola. An extensive set of macrofaunal samples and photographic material was collected as part of the ecological survey programme and made available to the deep-sea ecology team of the National Oceanography Centre, Southampton, UK for scientific studies. Parts of the macrofaunal material is currently subject to taxonomic and genetic analyses to assess the biodiversity of peracarid crustaceans. In addition, parts of the photographic material has previously been analysed to quantify the diversity of bait-attending mobile scavengers (Jamieson et al., 2017), and to examine the morphological and ecological characteristics of asphalt mounds (Jones et al., 2014). The present study has been developed to expand the characterisation of benthic habitats and their associated megafauna. It uses the photographic material to quantify the

spatial structure of epibenthic megafaunal communities and a number of acoustic, sedimentary and hydrographic data sets to assess how faunal patterns relate to the environmental conditions of the area under study.

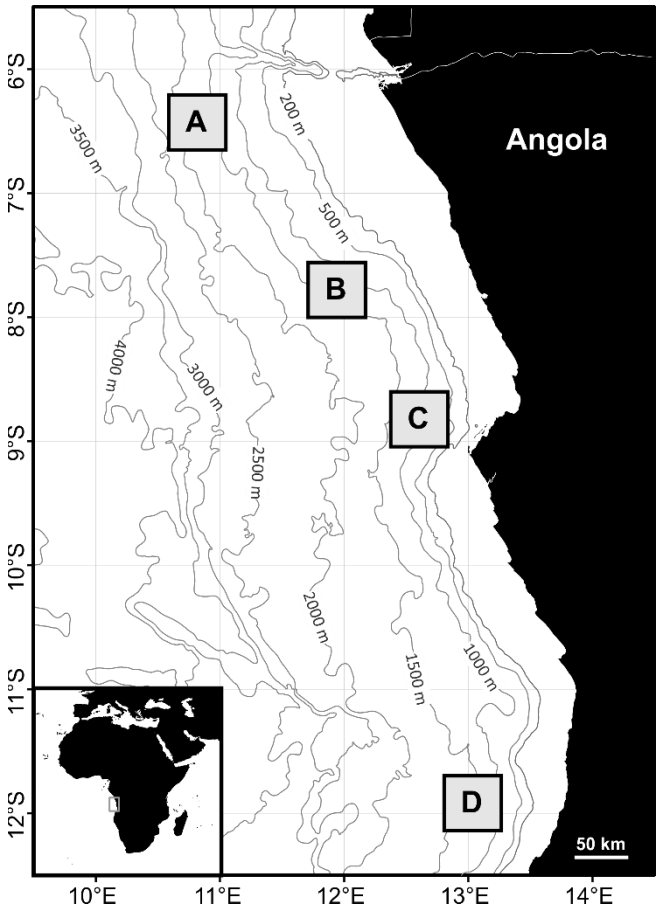


**Figure 1.1** Map of the northern and central Angolan continental margin, marked with the positions of the four oil and gas provinces under study. The four study areas correspond to the Angolan offshore Petroleum Licence Blocks 31, 18, 19 and 24 (from north to south). Inset shows the position of the study region in the southeast Atlantic Ocean. Bathymetry is shown as simplified contours based on GEBCO (General Bathymetric Chart of the Oceans) data (GEBCO Compilation Group, 2019).

The seabed imagery analysed as part of this study was collated during three cruises between 2005 and 2014. All three surveys employed two kinds of sampling: (1) random sampling of open slope sedimentary habitats based on a stratified sampling design using depth as stratum, and (2) targeted sampling of seafloor habitats and geomorphological features identified as being of particular interest, such as salt diapirs, cold-water coral reefs, and potential cold seeps. Subsets of the photographic material were selected to examine different aspects of megafaunal ecology, as outlined below.

**Chapter 2** has been prepared as a review chapter, summarising the current understanding of deep-water benthic ecology along the Angolan continental slope and rise, along with knowledge about the geological, sedimentological and oceanographic conditions that have

contributed to the broad-scale distribution and composition of present-day benthic habitats and faunal assemblages.

**Chapter 3** aims to analyse the ecology of megabenthic soft bottom assemblages based on photographic data collected across all four study areas. The analysis focusses on assessing bathymetric and geographic patterns in standing stocks, alpha diversity, and assemblage composition at larger spatial scales using standard univariate and multivariate analyses approaches. By examining the sedimentological and oceanographic context of the study region, factors that may control faunal patterns are assessed.

**Chapter 4** documents the presence and general structure of cold-water coral reef complexes along the central part of the upper Angolan continental slope (study area C). Using photographic material the structure of associated metazoan megafaunal assemblages is analysed and compared to that found on adjacent coral-free soft substratum.

**Chapter 5** aims to document the structure of epibenthic megafaunal communities associated with different seafloor morphologies on the lower Angolan continental slope in study area A.

**Chapter 6** summarises the results of Chapters 2 to 5, provides conclusions, and presents proposals for future work.

Chapters 3 to 5 are organised as stand-alone chapters with associated supplementary tables and figures included at the end of each chapter. A detailed account of the image processing steps is given in Appendix A. Appendix B provides a reference image catalogue showing representative photographs of all morphospecies that were recognised for the faunal analyses conducted in Chapters 3 to 5. Supplementary information on the environmental data sourced from BP plc is given in Appendix C.

### 1.5.2 Publication of portions of the thesis

The thesis has been prepared as a Three-Paper Thesis. In accordance with the University of Southampton Three-Paper Thesis format requirements, the contents of Chapters 2 to 5 are presented verbatim, as they are in the process of being prepared for publication.

Therefore, each chapter contains information on data sources and methods used with some repetition between chapters.

**Chapter 2**: The manuscript is currently being finalised for submission to *Frontiers in Marine Science* as **Pfeifer S.**, Bett, B.J., Clare, M., and Jones, D.O.B., in prep, Environmental context of the Angolan deep continental margin.

Author contributions: S. Pfeifer conducted the literature review, prepared the figures and wrote the manuscript as it appears within the thesis. D. Jones provided comments on earlier drafts of the manuscript. All co-authors provided assistance with the literature search.

**Chapter 3**: The manuscript is currently being finalised for submission to *Progress in Oceanography* as **Pfeifer, S.**, Bett, B.J., and Jones, D.O.B., in prep., Megafaunal assemblages associated with sedimentary habitats across the Angolan continental slope.

Author contributions: S. Pfeifer annotated the photographs, analysed the data, and wrote the manuscript. My thesis supervisors B.J. Bett and D.O.B. Jones advised on image analysis techniques and provided guidance and assistance with data analysis and interpretation. D.O.B. Jones provided comments on earlier drafts of the manuscript.

**Chapter 4**: The manuscript is currently being prepared for submission to *Deep Sea Research Part 1* as **Pfeifer, S.**, Bett, B.J., and Jones, D.O.B., in prep. Cold-water coral habitats on the upper Angolan continental slope, SE Atlantic.

Author contributions: S. Pfeifer annotated the photographs, analysed the data, and wrote the manuscript. My thesis supervisors B.J. Bett and D.O.B. Jones advised on image analysis techniques and provided guidance and assistance with data analysis and interpretation. D.O.B. Jones provided comments on earlier drafts of the manuscript.

**Chapter 5**: This chapter requires further work. Work to finalise the manuscript is underway for submission to *Deep Sea Research Part 1* as **Pfeifer, S.**, Bett, B.J., and Jones, D.O.B., in prep. Megafaunal assemblages in a highly complex topographic setting from the lower continental slope off Angola, SE Atlantic.

Author contributions: S. Pfeifer annotated the photographs, analysed the data, and wrote the manuscript. My thesis supervisors B.J. Bett and D.O.B. Jones advised on image

analysis techniques and provided guidance and assistance with data analysis and interpretation. D.O.B. Jones provided comments on earlier drafts of the manuscript.

# Chapter 2

# Environmental context of the Angolan deep continental margin

## Abstract

The deep-water environment off Angola forms part of the West African passive margin and is extremely varied. In this review, we summarise the current understanding of deep-water benthic ecology along the Angolan continental slope and rise, along with knowledge about the geological, sedimentological, and oceanographic conditions of the region. Geologically, the Angolan Margin has largely been shaped by the subsurface movement of Aptian salt deposits, associated faulting, and by the formation, migration and release of hydrocarbons. The region is subject to extensive hydrocarbon exploration and exploitation operations. The same geological complexity has created a diverse seabed environment of sedimentary habitats interspersed with features that include salt diapirs, pockmarks, cold seeps, asphalt mounds, and submarine channels. The large Congo submarine canyon is a key topographic feature, and the extensive sedimentary lobe system at the foot of the canyon is one of the world's largest active deep-sea fans. Seasonal coastal upwelling, organic input from the Congo River, and river-induced upwelling combine to increase the region's surface productivity. The water masses impinging on the upper slope experience permanent hypoxic conditions. Despite this large environmental heterogeneity, knowledge of the region's deep-water ecology remains limited, particularly in comparison with the extensive geological investigations associated with petroleum exploration. We highlight the unusual combination of major deep-water habitats, which provides unique opportunities to study habitat spatial distribution, potential connections between neighbouring communities and regional biodiversity - all areas of great importance to deep-sea ecology. Improved understanding of this exceptional and increasingly exploited benthic environment is urgent in order to support spatial management and environmental protection measures.

## 2.1 Introduction

This Chapter describes the environmental settings of the Angolan deep continental margin with emphasis on those aspects that are likely to have shaped the broad-scale distribution and composition of present-day benthic habitats and faunal assemblages. The information included in the review was derived from peer-reviewed articles and publicly available data sources. The review focusses on the region extending from the northern boundary of Angola at about 6°S to the Angola-Benguela Frontal Zone at about 15°S, which marks the transition from tropical waters into the subtropical region of the Benguela Upwelling System.

## 2.2 Physiographic settings

The Angolan margin is part of the Angola Basin, which is bounded to the east by the flanks of the Mid-Atlantic Ridge, to the north by the northeast-southwest trending Guinea Ridge and adjoining Cameroon Volcanic Line, and to the south by the northeast-southwest trending Walvis Ridge (Figure 2.1). Geologically, four sedimentary basins are recognised along the margin, which evolved during the Mesozoic rifting between the South American and African continents (Karner and Gambôa, 2007). The basins are separated by pre-rift basement highs or east-west trending syn-rift fault systems (Anderson et al., 2000; Séranne and Anka, 2005) and stretch beneath present-day onshore, shelf and slope areas. The northern section of the Angolan margin to about 8°S belongs to the Lower Congo Basin, which is delimited from the Gabon Basin in the north by the Casamaria High and from the Kwanza Basin in the south by the Ambriz Arch (Anderson et al., 2000; Moulin et al., 2005). The adjoining Kwanza Basin extends southward up to the Sumbe volcanic chain (von Nicolai et al., 2013), which comprises a series of northwest-southeast trending seamounts and volcanic rocks between 10-12°S (Guiraud et al., 2010), which are interpreted to have originated during the Cenomanian about 95 Ma (Marzoli et al., 1999). The two southernmost basins are the Benguela and Namibe Basins (Davison et al., 2007).

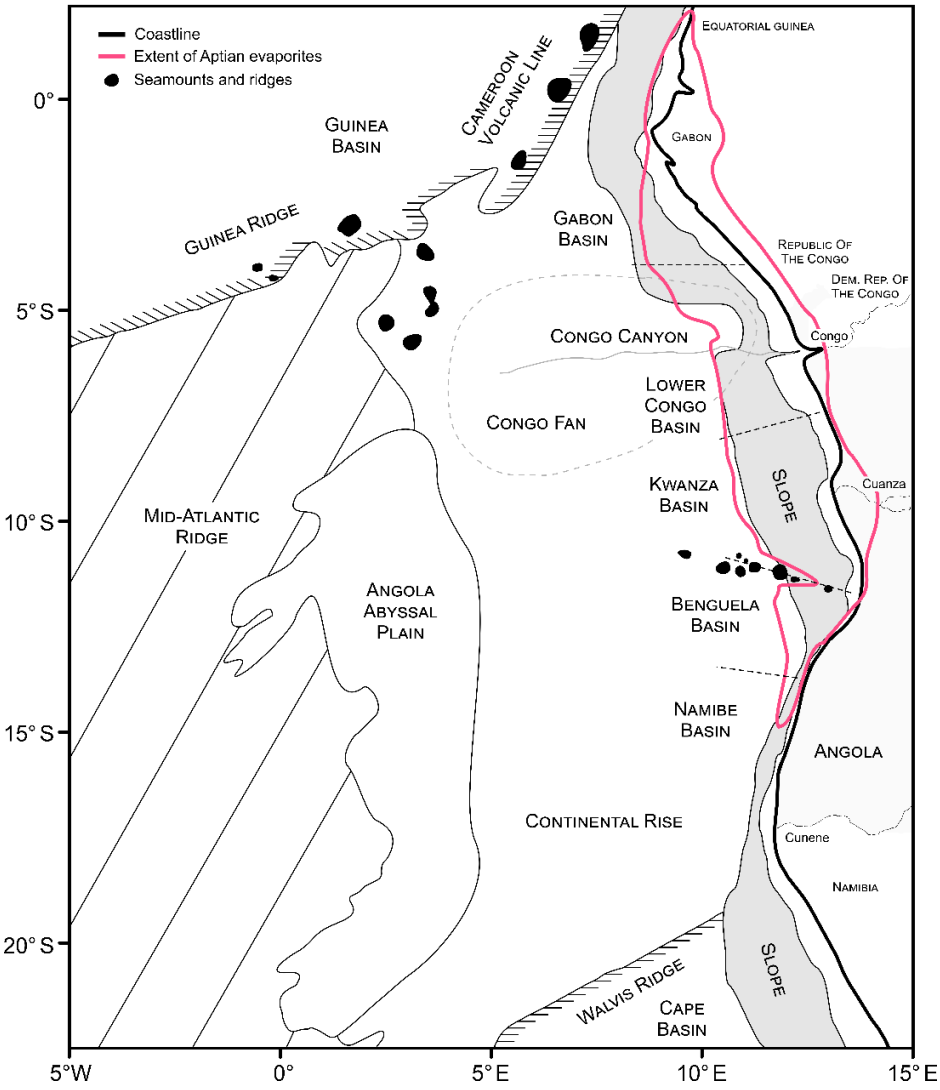


**Figure 2.1** Regional overview map of the eastern tropical South Atlantic, showing main physiographic zones of the Angola Basin and its bounding features (modified from Uchupi, 1992). The dotted lines indicate the approximate seaward boundaries between the sedimentary basins and were adopted from Brownfield and Charpentier (2006) and Marton et al. (2000). The areal extent of the Aptian salt deposits is based on interpretations by Pautot et al. (1973).

The modern Angolan coastline extends some 1200 km from about 5°S to 17°20´S, where the Kunene River marks the border of Angola with Namibia (Figure 2.1). The shelf break is typically located at depths of between 100-200 m, but shows considerable variation in its distance from the coast (Figure 2.2a). The predominantly flat shelf is widest along its northern sections down to about 7°8´S with widths of about 60-90 km. The adjacent upper slope declines at angles of 0.5-3° (Figure 2.2b). Further south to about 12°S, the shelf is generally 20-40 km wide, except for a short section off Luanda, where a change in the orientation of the shoreline is associated with a marked increase in seabed slope close to the coast. The waters between Benguela and Namibe are characterised by a predominantly

narrow shelf, with the 200 m isobath situated locally less than five km from the coast and considerably steeper upper slope sections with gradients up to 15°. The truncated shelf and steep slope topography have been linked to a much greater historic uplift of the southern Angola margin segments, which is also reflected in a much steeper onshore relief (Guiraud et al., 2010). South of Namibe the shelf widens again, reaching widths of up to 50 km. The adjoining continental slope is relatively narrow with upper slope gradients typically ranging from 3° to 6°. The continental slope extends to about 3000-3200 m depth, where a change in seabed slope to < 0.5° marks its transition into the continental rise (Séranne et al., 1999).

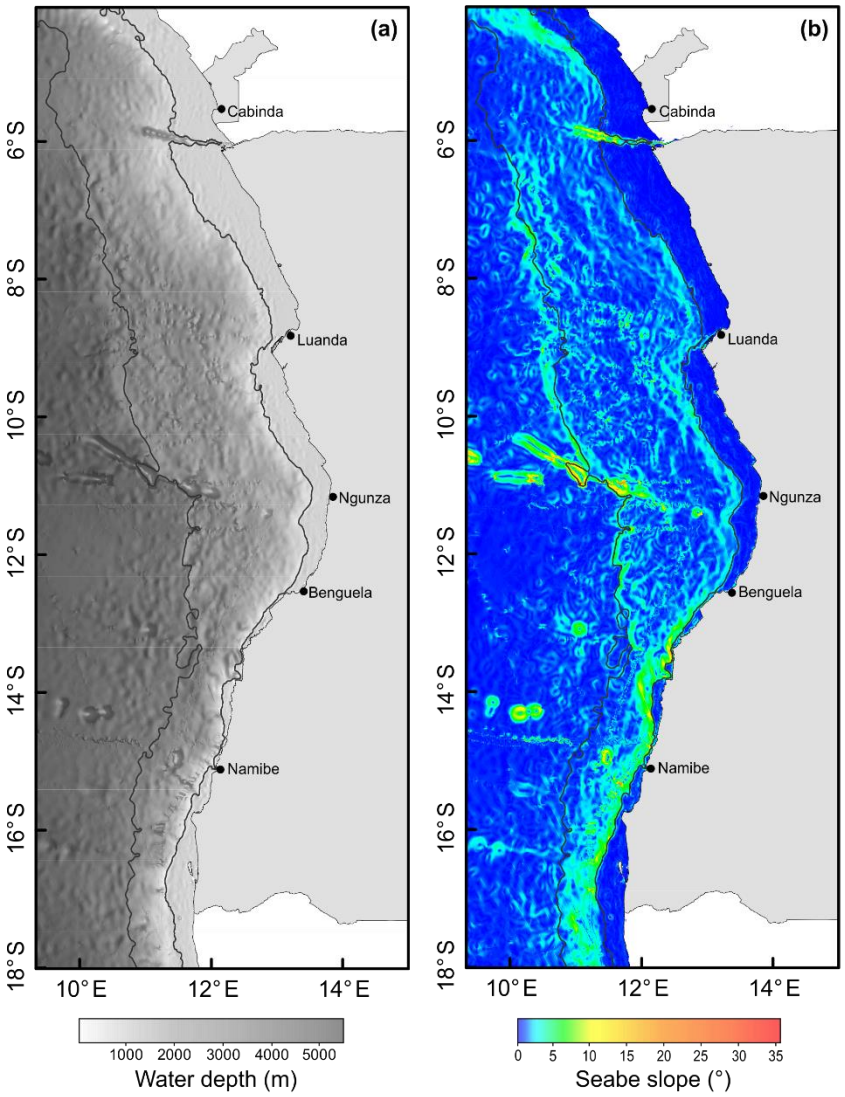


**Figure 2.2** Shaded relief bathymetry **(a)** and derived seabed slope **(b)** of the Angolan continental shelf and slope. Bathymetry is based on GEBCO data at 15 arc second spatial resolution (GEBCO Compilation Group, 2019). Dark grey lines show the 200 m and 3000 m contour lines.

The most prominent morphological feature on the upper Angolan margin is the Congo submarine canyon, which cuts through the shelf and slope in a westward direction at about 6°S. The canyon is directly incised into the Congo River about 30 km upstream from the river mouth (Jansen, 1984), and as such it provides a direct pathway for fluvial sediments into the deep basin (Droz et al., 2003). The canyon has a V-shaped profile and is up to 15 km wide and 1300 m deep (Babonneau et al., 2002; Savoye et al., 2009). Near the base of the continental slope at about 2000 m, the canyon extends into the large active Congo deep-sea fan, which stretches westward over a distance of at least 800 km into abyssal depths of more than 5000 m (Droz et al., 2003; Jansen, 1984; Savoye et al., 2009). At present, the fan is the main sediment depocenter in the Angola Basin and, after the Niger River fan, the second largest depocenter in the eastern South Atlantic Ocean (Savoye et al., 2009), covering a surface area of approximately 330 000 $km^2$ and comprising a volume of at least 0.7 $Mkm^3$ (Anka and Séranne, 2004).

Considerable progress in understanding the morphology and evolution of the large fan system has come through analysis of multi-beam and seismic-reflection data collected during French led research programmes. The first high-resolution maps of the canyon and upper fan were published by Droz et al. (1996), based on acoustic data collected during GUINESS cruises in 1992-1993. Subsequent acoustic and geological investigations made during the ZaïAngo (Savoye et al., 2009) and Congolobe (Rabouille et al., 2017; Olu et al., 2011) cruises provided comprehensive insights into the fan's architecture and evolution. The morphology and sedimentary facies of the Congo deep-sea fan (e.g. Babonneau et al., 2002, 2004, 2010; Droz et al., 2003; Marsset et al., 2009; Picot et al., 2006) extend up to 400 km from north to south (Droz et al., 2003) and consist of several stacked meandering channel-levee systems and distal lobe complexes, which are predominantly composed of turbidite sediments interlaced with hemipelagic sequences (Droz et al., 2003; Savoye et al., 2009). Based on their sedimentary evolution, the channel-levee systems have been grouped into three individual successive fans, the older, inactive Northern and Southern Fans, and the more recent, presently active Axial Fan, which is fed by the modern Congo canyon (Droz et al., 2003; Savoye et al., 2009) and covers an area of about 21400 $km^2$ (Baudin et al., 2020). The processes controlling the sedimentary evolution of the Axial Fan are examined by Picot et al. (2016). Dennielou et al. (2017) present a detailed study into the morphology and composition of the distal part of the

presently active channel-levee complex; and Marsset et al. (2009) provide an analysis of the temporal evolution of the whole fan system and its relation to climate.

## 2.3 Oceanographic conditions

### 2.3.1 Water masses

The hydrographic regime across the Angolan margin forms part of the tropical eastern South Atlantic and is characterised by four principle water masses (Stramma and Schott, 1999). Warm Tropical Surface Water (TSW) extends from the surface to a depth of about 100 m, beneath which it is replaced by Central Water (Stramma and England, 1999). Below this, low-salinity Antarctic Intermediate Water (AIW) is located between about 500 to 1200 m depth, overlaying North Atlantic Deep Water (NADW). At the adjacent abyssal plain, Antarctic Bottom Water (AABW) is present at the deepest parts of the Angola Basin below about 4000 m (Shannon and Chapman, 1991; Stramma and Schott, 1999).

The TSW off Angola is characterised by a relative shallow thermocline of less than 30 m (Lübbecke et al., 2010). A layer of highly saline water can often be recognised just above its lower boundary (Stramma and Schott, 1999), while pools of low saline freshwater discharges from the main rivers occur at the shallow subsurface along the shelf, being most prominent off the Congo River (6°S), the Kwanza River (9°20 S), River Cuvo (10°53 S), and the Kunene River (17°1S) (Axelsen et al., 2004).

The influence of the underlying Central Water is recognisable in a distinctly linear Temperature-Salinity (T-S) relationship (Stramma and Schott, 1999; Figure 2.2). The CW across the eastern tropical South Atlantic is composed of Western South Atlantic Central Water (WSACW) and Eastern South Atlantic Central Water (ESACW) with minor contributions from North Atlantic Central Water (Poole and Tomczak, 1999). The WSACW and ESACW originate, respectively, in the Subtropical Convergence of the south-western South Atlantic and the Indian Ocean (Stramma and Schott, 1999; Poole and Tomczak, 1999), from where they are transported through the South Atlantic to the equator and further into the equatorial circulation system, which eventually transports them into the eastern tropical South Atlantic (Stramma and Schott, 1999). A permanent layer of oxygen-depleted water with dissolved oxygen concentrations of less than 1 ml $l^{-1}$ is present across large parts of the Angolan margin at depths between 300-500 m, extending

westward across the entire region to about 0° longitude (Chapman and Shannon, 1987). Locally, hypoxic conditions of < 0.5 ml $l^{-1}$ (Helly and Levin, 2004) occur. Hydrographic profiles taken across the region indicate strong seasonal shifts in both the latitudinal and longitudinal extent of this low oxygen zone (Chapman and Shannon, 1987). The main processes responsible for these shifts, and the origin of the low oxygen water in general, remain a matter of debate. Poole and Tomczak (1999) argue that constant remineralisation of organic matter in the Central Water masses along their way into the eastern tropical South Atlantic combined with low advective mixing are, at least partly, responsible for the observed reduction in dissolved oxygen concentrations. Other key processes are enhanced remineralisation of organic matter at upper and mid-water depths driven by high oxygen consumption in the lower part of the euphotic layer, and seasonal upwelling of nutrient rich waters within offshore gyres (Chapman and Shannon, 1987, Mohrholz et al., 2008).

The AIW underlying the CW is characterised by temperatures of 2-6°C, and a distinct salinity minima, which increases northward while its depths shallows (Van Bennekom and Berger, 1984). Along the Angolan margin, Van Bennekom and Berger (1984) report a salinity minima of 34.5 at 730 m at the entrance of the Congo canyon. The AAIW is derived mainly from surface waters in the circumpolar layer of the Southern Ocean (Stramma and England, 1999).

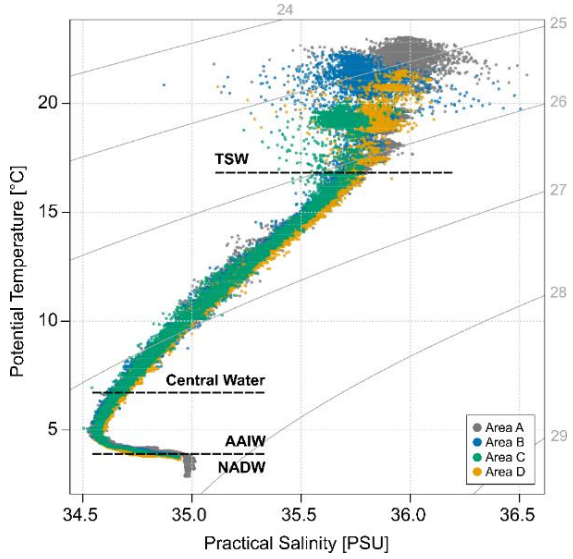


**Figure 2.3** Temperature-Salinity-Density curves from CTD casts obtained across the Angolan continental shelf and slope down to about 2400 m in July and August 2014, keyed to study area (A-D, see Figure 1.1) and marked with the four principle water masses present in the study region. AAIW = Antarctic Intermediate Water, NADW = North Atlantic Deep Water, TSW = Tropical Surface Water. Grey lines represent isopycnals.

### 2.3.2 Regional circulation patterns

A thin layer of surface water (10-20 m) flows to the north to north-east (Stramma and Schott, 1999) driven by the prevailing southerly to south-easterly trade winds (Peterson and Stramma, 1991). Wind stress off Angola varies semi-annually, being minimal in February and intensifying from May through June and again in November (Veitch, 2004). However, wind stress variability over the Angolan margin is relative weak compared to the Namibian and South African margins (Chapman and Shannon, 1987; Picaut, 1983).

The Surface and Central Waters are brought into the region by the eastward flowing components of the equatorial circulation system, namely the Equatorial Undercurrent (EUC), the South Equatorial Undercurrent (SEUC), and the South Equatorial Countercurrent (SECC) (Figure 2.3). Across the Angolan margin, TSW and the upper portions of the CW masses are transported within the Angola Current (AC) (Dias, 1983; Kopte et al., 2017; Moroshkin et al., 1970), which transports warm, oligotrophic tropical waters to about 15°S to 17°S (Mohrholz et al., 2008), where it converges with cooler, nutrient-rich waters of the northward flowing Benguela Current (Lass et al., 2000). At the convergence zone a permanent front called the Angola-Benguela Frontal Zone (ABFZ) occurs with a west to northwesterly orientation and sharp meridional changes in temperature and salinity (Shannon and Nelson, 1996). Location, strength, and extent of the ABFZ migrates seasonally in response to changes in wind stress (Shannon et al., 1987, being furthest north during austral winter (July to August) and furthest south during austral summer (January to March) (Hagen et al., 1981; Meeuwis and Lutjeharms, 1990). The hydrographic properties across the ABFZ are well described in the literature (e.g. Kostianoy and Lutjeharms, 1999; Meeuwis and Lutjeharms, 1990; Shannon and Nelson, 1996).

To the north of the ABFZ, the AC has been linked to the Angola Gyre (e.g. Gordon and Bosley, 1991; Mercier et al., 2003; Reid, 1989), a basin-wide cyclonic geostrophic gyre fed at the north and west by tropical waters via the equatorial circulation system, and with the AC representing its eastern branch (Figure 2.3). The circulation paths within the gyre and its extent are yet to be fully understood (Waconge and Piton, 1990). Using dynamic heights, Gordon and Bosley (1991) estimated the horizontal extent of the gyre to be about

2000 km with its centre located near 13°S, 5°E and cyclonic motion to be most pronounced in the upper 300 m.

Records of currents velocities in the region are sparse. For the shelf and upper slope, recent multi-year upper-ocean velocity profiles taken between 45-450 m depth near 11°S showed a highly variable alongshore flow of the AC, characterised by periodically changing southward and northward currents of up to 40 cm $s^{-2}$ and with maximum southward flows occurring during March/April and September/October (Kopte et al., 2017). These records also indicated a weak residual current directed towards the south for the upper 160-200 m with maximum southward velocities of 5-8 cm $s^{-1}$ at about 50 m depth.

Current meter measurements obtained from the two fixed observation platforms of the Deep-ocean Environmental Long-term Observatory Systems (DELOS) located at about 1400 m depth near 7°53'S and 7°57'S showed a predominantly alongslope bottom flow along isobaths with semi-diurnal tidal oscillations and spring-neap cycles (Vardaro et al., 2013). Current velocities were similar between the two sites with mean flows of 4.81 ± 2.78 cm $s^{-1}$ and 4.18 ± 2.95 cm $s^{-1}$, and maximum speeds of 19.86 cm $s^{-1}$ and 19.66 cm $s^{-1}$. Time series current meter readings taken over a period of three years at similar depths (1300 m) near 7°20'S also evidenced semi-diurnal current oscillations together with inertial cycles (4 to 5 days) and biweekly oscillating currents, the latter with a peak-to-peak amplitude of 20-30 cm $s^{-1}$ at 30 m above the seabed (Vangriesheim et al., 2005, 2009). Numerical modelling suggests that the biweekly oscillations could be remotely forced by varying surface winds in the equatorial Atlantic, which generate deep Yanai waves that spread eastward to the African continent, from where they propagate poleward along the African coastlines as coastally trapped waves (Guiavarc'h et al., 2008). The currents were directed mainly along the isobaths, with a weak southward mean flow of 1-2 cm $s^{-1}$ at 30 metre above the bottom (Vangriesheim et al., 2005).

Temporal variable flows with inertial, semi-diurnal, and bi-weekly cycles were also observed for bottom currents at about 4000 m near 7°40'S and at various locations along the Congo submarine channel between about 3150 and 4800 m water depth (Vangriesheim et al., 2009). Near 7°40'S, mean velocities were 3 cm $s^{-1}$ at 30 m above the bottom, and maximum speeds were 11 cm $s^{-1}$ with current speeds of < 5 cm $s^{-1}$ representing 85% of the total multi-year record. The residual current was directed towards the SE, like those observed

at mid-slope depths. By contrast, the residual current at 30 m above the seabed near the Congo submarine channel at similar depths (4000 m) was directed upslope towards the north-east. The mean velocity was 3 cm $s^{-1}$ and the maximum velocity was 9.7 cm $s^{-1}$. Further upslope at about 3150 m, the residuals current 15 m above the seabed had a southeastward orientation. The mean flow was 4.1 cm $s^{-1}$ and the maximum measured velocity was 12.3 cm $s^{-1}$. At the deepest site sampled (4800 m), the average recorded current speed at 60 m above the bottom was 3.4 cm $s^{-1}$ with a maximum of 8.4 cm $s^{-1}$ and a weak residual current directed towards the northwest (Vangriesheim et al., 2009).

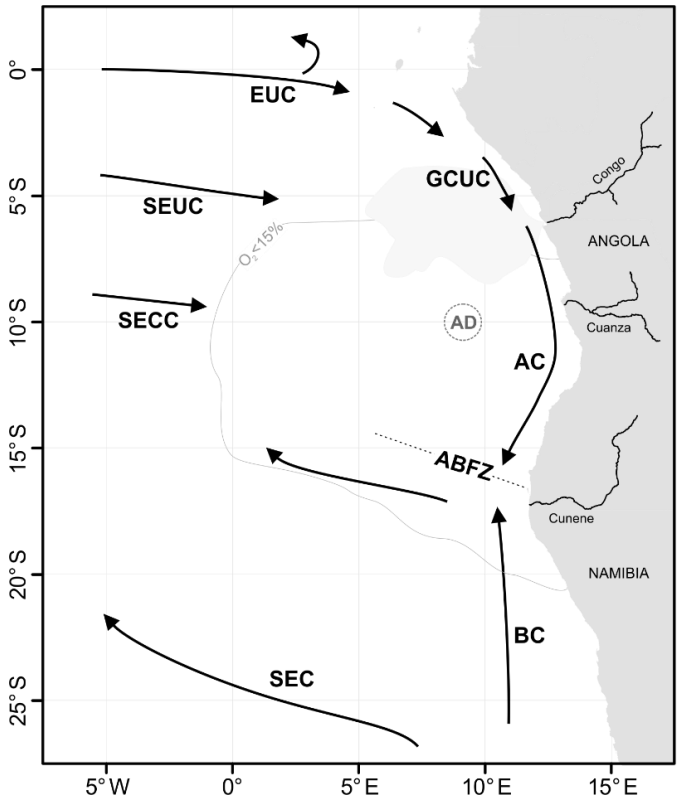


**Figure 2.4** Schematic showing the main surface and shallow subsurface currents in the south-east Atlantic (modified from van Bennekom and Berger, 1994, and Waconge et al., 1992). ABFZ = Angola-Benguela Frontal Zone, AC = Angola Current, AD = Angola Dome, BC = Benguela Current, GCUC = Gabon-Congo Undercurrent, EUC = Equatorial Undercurrent, SEC = South Equatorial Current, SECC = South Equatorial Countercurrent, SEUC = South Equatorial Undercurrent. The maximum extent of the Congo River plume is shown in grey (taken from van Bennekom and Berger, 1984). The maximum extent of waters with oxygen concentrations < 1 ml $l^{-1}$ at 300-400 m water depth is indicated, based on interpretations by Chapman and Shannon (1987).

## 2.4 Nutrient distribution and primary productivity

Nutrient availability and primary production dynamics off Angola are strongly influenced by changes in sea surface temperature (Berrit and Dias, 1977), the Congo River outflow (Da Cunha and Buitenhuis, 2013; Schneider et al., 1994; van Bennekom et al., 1978) as well as coastal (e.g. Ostrowski et al., 2009; Kopte et al., 2017) and oceanic (Mazeika, 1967) upwelling events. Sea surface temperature undergoes a distinct seasonal cycle, with an annual amplitude of about 10°C (Berrit and Dias, 1977) spread over a short cold season from July to September, and a warmer season from October through June with maximum temperatures generally recorded in March/April (Hopkins et al., 2013; Kopte et al., 2017; Van Bennekom and Berger, 1984).

The Congo River is the world's second largest river in terms of freshwater discharge with an estimated average outflow of about 45000 $m^3$ $s^{-1}$ (Eisma and van Bennekom, 1978). Discharge varies seasonally, with the highest outflow occurring between November and December during the wet season in the northern hemisphere and a secondary peak from April through May (Eisma and van Bennekom, 1978; Hopkins et al., 2013). The generated freshwater plume has been traced up to 800 km from the river mouth (van Bennekom and Berger, 1984), attaining its maximum extension between December and April (Hopkins et al., 2013; van Bennekom and Berger, 1984). Near the river mouth, the plume propagates in a WNW direction, while further offshore its direction shifts seasonally in response to changes in the local wind field and current strengths (Eisma and van Bennekom, 1978). In February and March it is deflected mainly towards the south-west, changing to a mainly westward-directed plume from April through August, and a predominant north-westward orientation throughout October and November (Hopkins et al., 2013; van Bennekom and Berger, 1984). Comparisons of nutrient concentrations in sediment cores (Schneider et al., 1997) and surface waters (Van Bennekom et al., 1978) near the river mouth with primary productivity estimates have indicated that surface production near the Congo river mouth is largely driven by nutrients supplied by upwelled subsurface oceanic waters as opposed to river-borne nutrients (Schneider et al., 1994; Van Bennekom and Berger, 1984). Recent biogeochemical modelling (Da Cunha and Buitenhuis, 2013) corroborates these findings, showing that riverine concentrations of nitrate and phosphate are too low to maintain levels of present-day marine coastal productivity. The upwelling near the Congo River is

thought to be caused by the rapid outflow of freshwater across the narrow estuary (Schneider et al., 1994; Van Bennekom and Berger, 1984).

Coastal upwelling has been reported for large parts of the Angolan shelf and upper continental slope during austral winter from June through August with a second weaker upwelling period recorded from December through January (Berrit and Dias, 1977; Kopte et al., 2017; Ostrowski, 2009). During upwelling, the thermocline shoals to less than 20 m depth, bringing cold, nutrient-rich and oxygen depleted Central Water to the shallow subsurface (Ostrowski et al., 2009). Downwelling occurs mainly from March through April and to a lesser degree in October and November (Kopte et al., 2017; Ostrowski et al., 2009), and is characterised by an intensification of the poleward alongshore transport of tropical warm, low saline water in the shallow subsurface of the Angola Current (Bachèlery et al., 2016; Bachèlery et al., 2020) and a corresponding deepening of the thermocline depth (Kopte et al., 2017). The oscillation between upwelling and downwelling events has been linked to seasonally changing zonal trade winds in the western equatorial Atlantic and the associated transmission of coastally trapped waves along the south-western African coastline (e.g. Bachèlery et al., 2020; Hardman-Mountford et al., 2003; Lazar et al., 2006; Ostrowski, 2009; Picaut, 1983). Abrupt changes in wind stress instigate Kelvin waves that spread eastward along the equatorial waveguide until the coast of Africa, from where part of the wave energy continues southward (Bachèlery et al., 2020), inducing vertical shifts of the isotherms (Lazar et al., 2006). A relaxation of zonal wind stress has been associated with high-pressure downwelling waves, while a strengthening is thought to generate upwelling waves (Lazar et al., 2006). Changes in the local wind fields off Angola were found to have a weak influence on nearshore sea surface temperatures, and are therefore thought to only play a minor role in controlling coastal upwelling dynamics (Berrit, 1976; Picaut, 1983). This is contrary to the Benguela current system off Namibia and southern Angola, where permanent coastal upwelling is caused mainly by south-easterly trade winds (Mohrholz, et al., 2008).

Superimposed on the seasonal dynamics of upwelling and downwelling, the Angolan margin experiences intermittent periods of extreme warming and cooling (e.g. Florenchie et al., 2003; Lübbecke et al., 2010; Hardman-Mountford et al., 2003; Rouault et al., 2007), referred to as Benguela Niño and Benguela Niña, respectively, in reference to the Pacific El Niño phenomenon (Shannon et al., 1986). These events express themselves as extreme

surface and subsurface temperature anomalies (Bachèlery et al., 2020; Lübbecke et al., 2010). Using a coupled physical/biogeochemical regional model, Bachèlery et al. (2016) predicted strong declines of nutrient availability and primary productivity along the entire Angolan margin during extreme warm events, with reductions in nitrate concentrations and primary production of up to 60% and 30%, respectively, compared to mean levels between 2000-2008. Changes in nitrate were most pronounced across the area off the Congo River outflow and over the shelf and upper continental slope, decreasing westward. Nearshore primary production anomalies increased southward from about -15% at the Congo River outflow to about -25 to -30% between 9°S and 16°S.

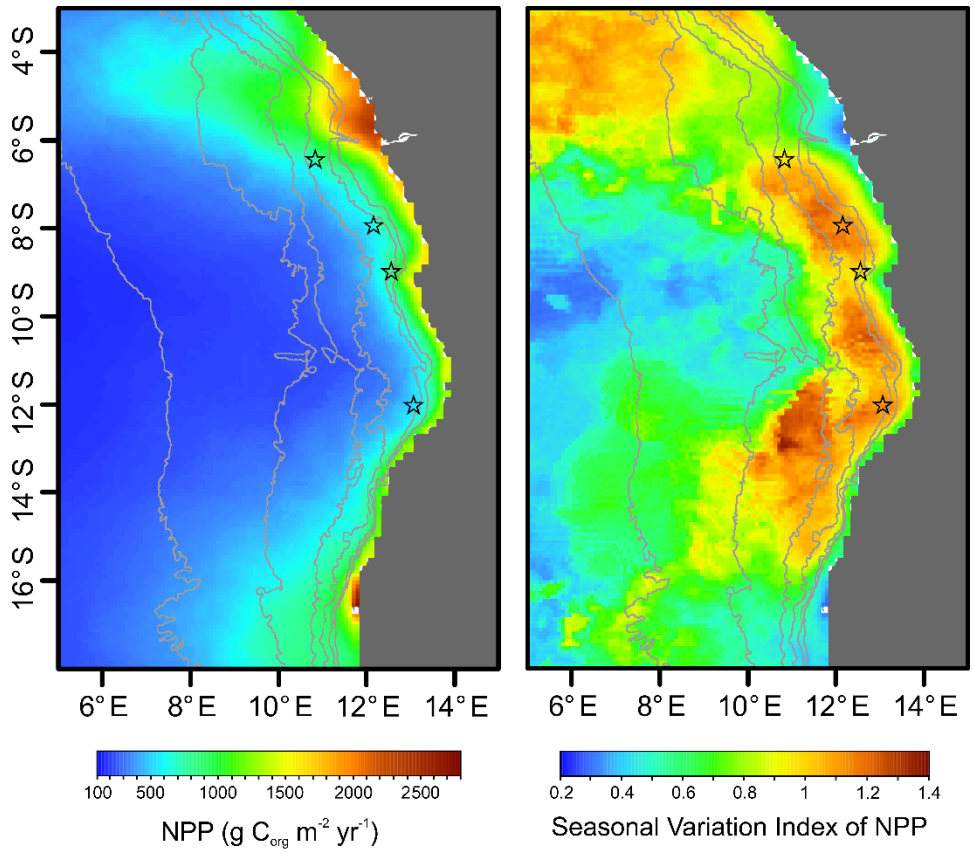


**Figure 2.5** Variation in estimated primary productivity off Angola expressed as annual mean net primary production (NPP, g $C_{org}$ $m^{-2}$ $yr^{-1}$) (left panel), and mean seasonal variation index (SVI) of NPP (right panel). Annual mean primary production estimates were calculated from 15 years (2003-2017) of monthly NPP data downloaded from the Oregon Ocean Productivity website. NPP is based on the standard Vertically Generalized Production Model (VGPM) of Behrenfeld and Falkowski (1997), computed on a 1/12° grid using MODIS R2018 surface chl-a, MODIS 4-micron SST, MODIS cloud-corrected incident daily PAR, and euphotic depths estimated from a model developed by Morel and Berthon (1989). SVI was calculated as the ratio of standard deviation and mean monthly NNP, averaged for the period from 2003 to 2017. Stars represent the approximate centre location of the four deep-water areas under study. Grey lines show contours at 500 m, 1000 m, 2000 m, 3000 m, 4000 m and 5000 m water depth.

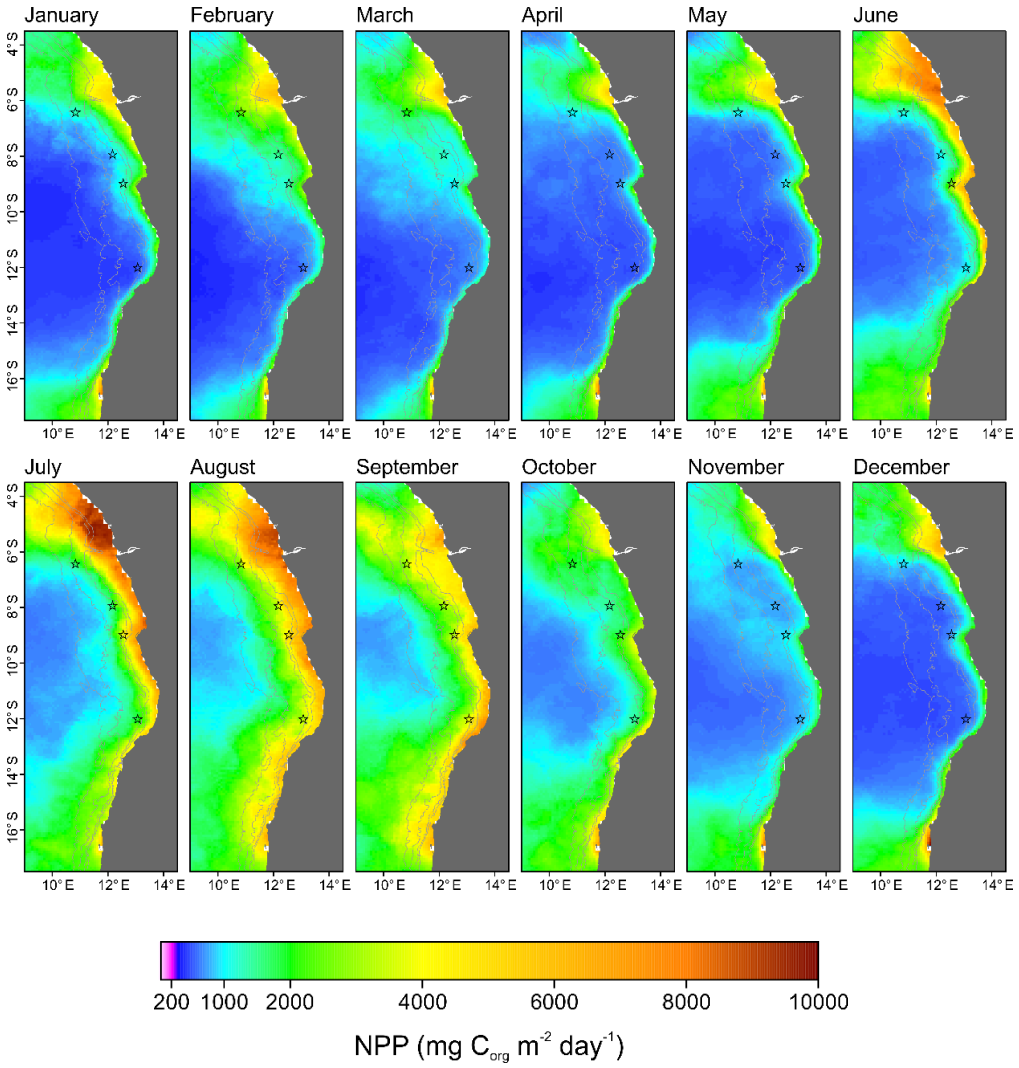


**Figure 2.6** Mean monthly distribution of net primary production (mg $C_{org}$ $m^{-2}$ $d^{-1}$) off Angola using VGPM NPP estimates, averaged for the period from 2003 to 2017. For information about VGPM data refer to Figure 2.5. Stars represent the approximate centre location of the four deep-water areas under study. Grey lines show contours at 500 m, 1000 m, 2000 m and 3000 m water depth.

Wasmund et al. (2005) provided estimates of mean daily gross primary production rates of 1307 ± 699 mg C $m^{-2}$ $day^{-1}$ for shelf waters between about 9-14°S, based on simulated *in situ* values taken in April/May and August/September. Further offshore, production rates decreased to 736 ± 481 mg C $m^{-2}$ $day^{-1}$. These values are somewhat lower than net primary production rates predicted from satellite-derived Chlorophyll-a estimates based on the standard Vertically Generalized Production Model (VGPM) of Behrenfeld and Falkowski (1997; Figure 2.5). However, satellite-derived Chlorophyll-a values tend to be overestimated in highly turbid waters, such as those found near the Congo River mouth, and absolute VGPM values must therefore be interpreted with caution. Nevertheless,

VGPM-based NPP estimates off Angola show evidence of strong along-slope differences in total annual production (Figure 2.5) and seasonal variation in productivity (Figure 2.6) for waters overlying the continental slope and upper rise.

## 2.5 Geological history and seabed morphology

The geological history of the Angolan margin has created a broad range of ecological settings with a variety of distinct seabed features, such as mounds and ridges (e.g. Serié et al., 2012), fault scarps (BP Exploration, 2017), seafloor troughs (Hill et al., 2011a) and furrows (Gay et al., 2004), carbonate (e.g. Haas et al., 2010; Olu et al., 2007a) and asphalt (Jones et al., 2014) mounds, shallow gas hydrates (e.g. Ondréas et al., 2005; Sahling et al., 2008), pockmarks (e.g. Andresen and Huuse, 2011; Gay et al., 2003, 2006a, 2006b; Olu-Le Roy et al., 2007; Sahling et al., 2008; Unterseh, 2013), and reducing environments in the form of cold seeps (e.g. Jones et al., 2014; Olu et al., 2009; Sibuet and Vangriesheim, 2009; Unterseh, 2013; Wenau et al., 2015a,b). The formation and distribution of many of these features are best understood in the context of both the intensive salt tectonics experienced by the region, which to this day influences seafloor topography, and the flow of hydrocarbons from underlying deposits, which give rise to a diverse range of geomorphologic and geochemical conditions on the seabed that form the basis of different benthic habitats. The sub-surface geological and geophysical processes of the Angolan margin appear to be relatively well known, especially for the Lower Congo and Kwanza basins where extensive seismic mapping and geotechnical investigations have been taken place in response to their geological complexity and enormous petroleum potential. A brief overview of the geologic evolution and architecture of the Angolan margin is given below to provide context for the variation in modern seabed habitat types.

### 2.5.1 Geological evolution

The geological development of the Angolan margin may be separated into three main evolutionary phases: (1) a pre-salt phase marking the formation of the South Atlantic basin and its passive margins; (2) a salt phase, characterised by the deposition of large amounts of evaporites; and (3) a post-salt phase dominated by the deformation of the evaporitic layer and their overlaying strata as a result of gravitational tectonics (Marton et al., 2000; Séranne and Anka, 2005; Uchupi, 1992). The South Atlantic started to form around 150

million years ago with the break-up of the Gondwana super-continent during the Upper Jurassic to Lower Cretaceous (Duval et al., 1992) and concomitant rifting between the African and South America continents from Late Jurassic (Tithonian) through to Lower Cretaceous (Barremian to Albian) time (Marton et al., 2000). Continental break-up began in the south propagating northwards (Hudec and Jackson, 2002), with the separation of the Angolan margin from its conjugate sections of the Brazilian margin being dated back to Berriasian through to late Barremian-early Aptian time (Brice et al., 1982; Hudec and Jackson, 2002; Karner and Driscoll, 1999). During the mid and late Aptian (Bolli et al., 1978; Karner and Gambôa, 2007; Moulin et al., 2005), large volumes of evaporites precipitated in the early rift basins of the West African margin (Aptian Loeme Formation; Figure 2.1), forming an area with relative continous salt coverage between the Ascension Fracture Zone and southern Angola commonly referred to as the West African salt basin (Davison, 2007; Patout et al., 1973). Along the Angolan margin, the eastern edge of the salt layer is located mostly onshore, while the current seaward limit runs roughly beneath the base of the continental slope in water depths between about 2500 to 3000 meters (e.g. Marton et al., 2000; Pautot, 1973; Uchupi, 1992).

During the post-salt phase from late Aptian onwards, the salt deposits and their overlying post-salt sequences underwent intensive displacement and deformation owing to a complex interplay of gravity-driven raft (e.g. Duval et al., 1992; Lundin, 1992; Mauduit et al., 1997; Valle et al., 2001) and salt (e.g. Brun and Fort, 2004; Fort et al., 2004; Marton et al, 2000; Quirk et al. 2012; Séranne and Anka, 2005) tectonics. Seismic studies (e.g. Cramez and Jackson, 2000; Fort et al., 2004; Hudec and Jackson, 2004; Marton et al., 2000; Spathopoulos, 1996; Valle et al., 2001) have established the presence of distinct tectonic provinces arranged parallel to the basin margin (Hudec and Jackson, 2004) with a gradual downward succession from mostly extensional to compressional regimes. Across the shelf and upper slope increased sedimentary loadings (e.g. Hudec and Jackson, 2002; Séranne and Anka, 2005), combined with tilting of the margin owing to thermal subsidence and continental uplift (e.g. Duval et al., 1992; Hudec and Jackson, 2002, 2004; Jackson et al., 2005) led to faulting and dissection of the post-salt deposits into partially (pre-rafts) or completely (rafts) separated sediment blocks (e.g. Valle et al., 2001) bounded by extensional growth faults (Hudec and Jackson, 2004; Séranne and Anka, 2005). Movement of these blocks downslope along the ductile salt layer has created elongated

intervening troughs (grabens) filled with Tertiary sediments (Lundin, 1992), while the underlying evaporitic layer has become progressively thinner as salt has been transferred down slope (e.g. Marton et al., 2000; Quirk et al., 2012; Spathopoulos, 1996). The extensional processes upslope are accommodated by contractional deformations along the downslope parts of the margin in the form of thrust and fold belts (Cramez and Jackson, 2000), and complicated salt structures (Marton et al., 2000), such as salt anticlines, salt pillows, laterally compressed diapirs, salt canopies and large inflated salt sheets (e.g. Fort et al., 2004; Marton et al., 2000). The general succession of the different structural domains is illustrated in Figure 2.3 by means of two cross-sections through the Lower Congo Basin. Extent and characteristics of each domain vary notably along the margin, reflecting differences in basin geometry, sedimentation patterns, uplift history and base-salt volumes (Hudec and Jackson, 2004; Marton et al., 2000; Spathopoulos, 1996). For example, the original amount of salt deposited shows a strong regional increase from north to south (Evans and Jackson, 2020; Marton et al., 2000).

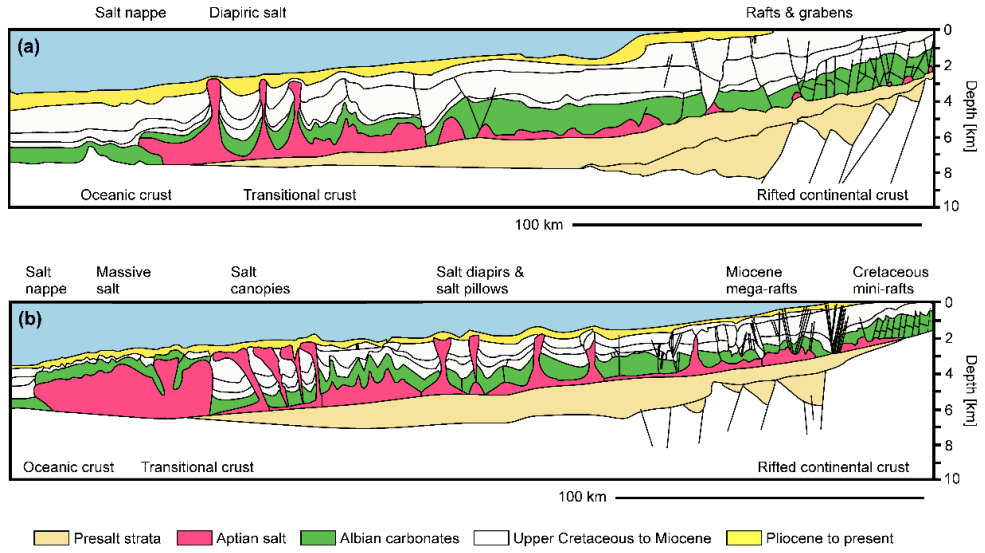


**Figure 2.7** Schematic cross-sections through **(a)** central Lower Congo Basin, north of the Congo canyon at about 6°S, and **(b)** southern Lower Congo Basin at about 9°S based on seismic reflection data, illustrating typical structural domains on the Angolan Margin (redrawn from Marton et al., 2000). Generally, the margin architecture is characterised by an oceanward transition from extensional to compressional structures created by raft and salt tectonics. Small to large tilted blocks and associated grabens and growth faults characterise the extensional zone on the shelf and upper slope. Here, Aptian salt is thin or absent owing to its gravitational displacement downslope. Thin to moderately thick salt in the form of salt pillows and diapirs define the transitional zone along the mid to lower slope. The compressional domain towards the base of the slope contains allochthonous salt canopies and tectonically thickened salt masses to the west. A salt nappe extruding above younger sequences marks the current seaward limit of the Aptian salt (e.g. Cramez and Jackson, 2000; Fort et al., 2004; Lundin et al., 1992; Marton et al., 2000). The absence of canopies and outer massif salt across the central Lower Congo Basin (a) has been linked to a general northward decrease in the amount of original salt deposited and spatial differences in sedimentary overburden (Marton et al., 2000). Both cross-sections run ENE to WSW.

### 2.5.2 Modern seafloor topography and geomorphology

The intensive salt tectonics have provided an important source of variability in modern seafloor topography, in particularly along the middle and lower slope sections above the transitional and compressional domains. Here, active doming of salt structures has formed a highly irregular seabed topography with elevated terrain in the form of broad bathymetric highs (Serié et al., 2012, 2017), elongated diapiric ridges (van Weering and van Iperen, 1984; Wenau et al., 2015a), and isolated seafloor mounds (Hill et al., 2011a). The seaward limit of salt-induced deformations is marked by a steep up to 800 m high bathymetric feature, the Angola Escarpment, which stretches along the base of the continental slope (Cramez and Jackson, 2000).

Besides its direct influence on seafloor morphology, salt tectonism has had a marked effect on the location of subsurface hydrocarbon accumulation and migration. Deformation and migration of salt bodies, together with sedimentary compaction, has led to the formation of faults, cracks, and tilted sedimentary layers, which provide efficient pathways for hydrocarbon migration (e.g. Gay et al., 2007; Wenau et al., 2017). Hydrocarbon migration in turn provides mechanisms for the occurrence of fluid flow phenomena in the shallow subsurface in the form of seismic chimneys and pipes (e.g. Gay et al., 2003; Ho et al., 2012; Wenau et al., 2017), gas hydrates (e.g. Charlou et al., 2004; Sahling et al., 2008), and associated zones with free gas (e.g. Anka et al., 2013; Gay et al., 2006a). On the seafloor, fluid expulsion is manifested in hydrocarbon escape features such as pockmarks (e.g. Andresen et al., 2012; Gay et al., 2006a, 2006b, 2007; Serié et al., 2017), asphalt mounds (Jones et al., 2014; Jatiault et al., 2019a), and cold seeps (e.g. Sahling et al., 2008; Wenau et al., 2015a).

Seafloor pockmarks have been described from the upper to lower slope (Gay et al., 2007), where they occur as cone-shaped circular to elliptical depressions from 100 m up to 1000 m wide and up to several tens of meters deep (e.g. Gay et al., 2003, 2007; Sahling et al., 2008; Ondréas et al., 2005). A protracted history of past fluid escape is evidenced by the presence of abundant buried paleopockmarks for the Lower Congo Basin (e.g. Andresen and Huuse, 2011; Anka et al., 2013; Ho et al., 2018) and the Kwanza Basin (Serié et al., 2017). Pockmarks are usually formed in fine-grained substratum following the release of over-pressurised fluids from the sediment (Hovland et al., 2002). On the Angolan margin, this process has been associated with the expulsion of excess pore water during early-stage

sediment burial and compaction, the flow of biogenic methane formed during the microbial decomposition of organic matter, the migration of dissolved gas hydrates, and the vertically ascent of thermogenic hydrocarbons from deeper reservoirs (e.g. Andresen, 2012; Andresen and Huuse, 2011; Gay et al., 2006b, 2007; Serié et al., 2017; Wenau et al., 2015a). Geophysical investigations have shown a close link between the source of fluids, stratigraphic and structural components in the sedimentary succession, and the geometry and spatial arrangement of pockmarks on the seafloor (e.g. Andresen 2012; Anka et al., 2013; Gay et al., 2007; Serié et al., 2017). For example, widely distributed pockmarks in salt minibasins are thought to result from sediment dewatering and biogenic gas seepage (e.g. Andresen et al., 2011; Serié et al., 2017) with gas migration through the sediment possibly being facilitated by shallow polygonal dewatering faults (e.g. Gay et al., 2006a, 2007, Andresen and Huuse, 2011). Pockmarks aligned with structural components such as salt-induced faulting, salt diapirs, clustered pipes, and seismic chimneys have been linked to deep-rooted plumbing systems that promote focussed hydrocarbon flow from deeper reservoirs (e.g. Andresen et al., 2012; Gay et al., 2007; Jatiault et al., 2019a, 2019b; Serié et al., 2017; Wenau et al., 2017).

Active seepage of methane-rich fluids has been documented in several pockmarks based on visible gas bubbles in the water column, acoustic signatures, and chemical analyses of water samples (Charlou et al., 2004; Gay et al., 2007; Ondréas et al. 2005; Pierre and Fouquet 2007; Sahling et al., 2008; Wenau et al., 2017). Cold seep conditions have also been found on the crest of seafloor ridges located above the seaward limit of the Aptian salt (Wenau et al., 2015a). Here, gas bubble trains identified from echosounder anomalies were detected up to 1900 m above the seafloor. In many cases, the seeps were associated with methane-derived authigenic carbonates (e.g. Ondréas et al. 2005; Sahling et al., 2008; Wenau et al., 2015a) formed through the anaerobic oxidation of methane and associated sulphate reduction (Feng et al., 2010; Pierre et al., 2012). Carbonates were present on the seafloor, often as massive crusts up to several metres long (e.g. Ondréas et al., 2005), and in the upper sediment layers, where they formed small nodules or thin discontinues layers of semi-cemented sediment (Pierre and Fouquet, 2007; Pierre et al., 2012). Nodule shape varied widely and included plate-like, contorted and tubular forms, which are thought to represent cemented cracks, small conduits, and faunal burrows (Pierre et al., 2012; Sahling et al., 2008). Across Licence Block 31 on the lower Angolan slope, aggregations of

carbonate nodules and discontinuous beds of carbonate claystones between 0.1-0.7 m thick have been identified in the top 30-40 m of sediment, based on samples in sediment cores and interpretations of sub-bottom profiler data (Hill et al., 2011a, 2011b).

Recurrent seepage of liquid, thermogenic hydrocarbons has been evidenced for the deeper sections of the Lower Congo Basin based on sea-surface oil slicks mapped using satellite-based Synthetic Aperture Radar (Jatiault et al., 2017, 2018, 2019a). More than one hundred natural seep sites have been identified with an estimated combined release 4380 $m^3$ of oil per year, which ranks the Lower Congo Basin third in terms of naturally expelled oil behind the Gulf of Mexico and the Santa Barbara basin (Jatiault et al., 2017). On the seafloor of the Lower Congo Basin, seeping oil has been observed to form mounds of solidified asphalt ranging from < 0.5 m up to 50 m in diameter (Jones et al., 2014). Distinct extrusive mounds interpreted as mud or asphalt volcanos were documented on the seafloor of the deep Kwanza Basin based on high-resolution 3D seismic data (Serié et al., 2017). Moreover, Serié et al. (2012) identified small circular to elliptic seafloor mounds between 80-300 m wide, up to 40 m in height, and with reliefs of 3-16° on the slopes of the Kwanza Basin, and interpreted these to relate to gas hydrate pingoes associated with the formation and dissociation of massive gas hydrate in the shallow subsurface.

## 2.6 Sedimentology and sedimentary processes

### 2.6.1 Historic sedimentary regime

The Precambrian basement is overlain by pre-rift fluviolacustrine sandstones and shales (Brice et al., 1982; Uchupi, 1992) that grade upward into syn-rift fluvial and lacustrine Neocomian to Barremian sequences of organic-rich shale, sandstones and carbonates interbedded with volcanics, which were deposited in lacustrine lakes during the initial phase of rifting (Anderson et al., 2000; Brice et al., 1982; Karner and Driscoll, 1999; Uchupi, 1992). The late syn-rift and early post-rift phase from Barremian to Aptian times marks the onset of restricted marine conditions when saline water started to enter the evolving rift basins and initiated the formation of the thick salt deposits along the West African margin (Brice et al., 1982; Séranne and Anka, 2005; Uchupi, 1992). The post-salt sedimentation proceeded from Albian to Upper Cretaceous (Cenomanian / Turonian) deposition of primarily biogenic carbonates (dolomite and dolomitic limestones) that

grade into mudstones and blacks shales to Upper Cretaceous (Senonian) to present day deposition of mainly terrigenous siliciclastics, including organic shales, mudstones, siltstones and sandstones (e.g. Bolli et al., 1978; Anderson et al., 2000; Brice et al., 1982; Marton et al., 2000; Séranne and Anka, 2005; Valle et al., 2001; Uchupi, 1992).

The deposition of pelagic carbonates commenced in the Albian under shallow marine conditions and created a broad and aggrading carbonate platform (Ala and Selley, 1997; Karner and Driscoll, 1997; Séranne and Anka, 2005). Borehole data (Bolli et al., 1978) indicate high planktonic productivity during that time with carbonate sedimentation rates of up to 55 m / my. For the subsequent Upper Cretaceous to Eocene period, interpretations of stratigraphic data suggests slow sediment accumulation rates (e.g. Anderson et al., 2000; Anka et al., 2009; Lavier et al., 2000; Leturmy et al., 2003; Valle et al., 2001) with deposition mainly confined to the shelf (Séranne, 1999). Isopach maps place the main depocenters of the South West African margin during that time at today's outlets of the Kwanza River off Angola in the south and the Ogooué River off Gabon in the north (Leturmy et al., 2003). At the Eocene-Oligocene transition, a period of prolonged submarine erosion at intermediate water depths is documented for much of the South West African margin (e.g. Bolli et al., 1978; Jackson et al., 2005; Karner and Driscoll, 1997; Meyers et al., 1996; Rasmussen, 1996), during which up to 500 m of sediments may have been removed from the outermost shelf and upper slope (Lavier et al., 2000, 2001; Seranne et al., 1992). From the Oligocene onwards, the Angolan margin experienced a substantial increase in the supply of terrigenous sediments from the continent, concentrated around the outlets of the main rivers (e.g. Anderson et al., 2000; Bollie et al., 1978; Leturmy et al., 2003; Séranne and Anka, 1992). The depositional style changed from mostly aggradation across the shelf to progradation of deltaic sediments basinward (Anderson et al., 2000; Séranne, 1999) leading to large changes in margin morphology (Seranne et al., 1992).

The timing of the increased sediment supply coincided with the migration of the main sedimentary depocenters from the mouths of Ogooué and Kwanza Rivers to that of the Congo River (Karner and Driscoll, 1999; Leturmy et al., 2003), and the concomitant initiation of the large Congo turbiditic sedimentation system in early Oligocene (Anka et al., 2009). The mechanisms responsible for the changes in sedimentation patterns remain a matter of debate (Anka et al., 2009). Several authors (e.g. Anderson et al., 2000; Hudec

and Jackson, 2004; Séranne, 1999; Walgenwitz et al., 1992) have suggested enhanced coastal and onshore erosion in response to regional uplift of the inner margin and the southern Africa continent in the Miocene (e.g. Bond, 1978; Walgenwitz et al., 1992) as a possible cause for the surge in terrigenous sediment supply. Others (Lavier et al., 2001; Séranne, 1999; Séranne and Anka, 2005) emphasise the importance of global climate forces, suggesting that a regional shift to more humid and variable climatic conditions across the West African margin commencing in the early Oligocene, together with long-term global sea-level fall (e.g. Bartek et al., 1991) may have enhanced sedimentary loads by increasing riverine runoff and facilitating continental weathering and erosion of exposed shelf and coastal areas. The evolution of the Congo River as a major source of sediment influx is inferred to result from large-scale reorganisation of the Congo drainage system inland (e.g. Karner and Driscoll, 1999; Leturmy et al., 2003; Stankiewicz and de Wit, 2006; Uenzelmann-Neben, 1998). For example, Karner and Driscoll (1999), based on elevation and geological data, suggested the presence of an antecedent Congo river system located north of the current drainage basin, which may have discharged near today's Ogooué River mouth during the late Cretaceous and early Tertiary but was redirected southward in the late Paleogene owing to uplift of the hinterland and changing sediment loadings. By contrast, Stankiewicz and de Wit (2006), based on the comparison of marine fossils and drainage patterns of African river systems, proposed that a paleo-Congo River may have drained eastward towards the Indian Ocean for much of the Cretaceous, before uplift of the East African hinterland in the Eocene or Oligocene diverted the river westward where it merged with smaller rivers to generate the drainage pattern seen today.

Seismic reflection data show the presence of complex networks of channel-lobe systems traversing across the slope throughout the Oligocene and Miocene (e.g. Anderson et al., 2000; Ferry et al., 2004; Gee et al., 2007), indicating that turbidite sedimentation was an important process in the historic transfer and deposition of clastic sediments into deeper waters. Channel morphologies and pathways are closely linked to the complex subsurface architecture, such as the location of salt-related structures (Gee and Gawthorpe, 2006; Oluboyo et al., 2014), or the orientation of growth folds and faults (e.g. Anderson et al., 2000; Broucke et al., 2004; Gee and Gawthorpe, 2006; Mayall and Stewart, 2000; Oluboyo et al., 2014). Combining data on the age and location of historic channel systems, Anka et

al. (2009) proposed that earlier (Oligocene to early Miocene) turbidite sedimentation in the Lower Congo Basin was largely confined to the south-eastern slope sections. A general northwestern shift of the turbidite depocenters occurred during the late Miocene, which was followed by a basinward migration and confinement of the turbidite flow into abyssal depths as a result of the incision of the Congo canyon around the Miocene-Pliocene transition period. Since then, sedimentation across the Angolan slope is dominated by hemipelagic deposition across the shelf and slope, with turbidites originating from the Congo River being transported directly onto the deep-sea fan via the canyon (Anka, 2004).

### 2.6.2 Present sedimentary regime

Modern sediments along the Angolan continental slope and rise are mainly derived from material discharged by the two largest river systems of Angola, the Congo River and the Kunene River (Bornhold, 1973). An additional but small input of Aeolian dust from the Namib desert into the south-eastern Angola Basin by the south-easterly trade winds is reported by Bornhold (1973) and Embley and Morley (1980).

The annual supply of total suspended sediments from the Congo River is estimated at between 30-70 Tg (annual average 55 Tg) (Wetzel, 1993), which is relatively small compared to the river's high average discharge rate of about 45000 $m^3 s^{-1}$ (Eisma and van Bennekom, 1978) and its extensive drainage basin of about 3.7 million $km^2$, which covers a major portion of equatorial Africa (Jansen, 1990). Nevertheless, the contribution of particulate organic matter (POC) is high with an estimated mean of 2 TgC $yr^{-1}$, making the Congo the 5$^{th}$ largest river in terms of annual POC flux to the oceans (Coynel et al., 2005). The sedimentary processes of the Congo canyon and the associated deep-sea fan system have been extensively studied as part of several interdisciplinary research programmes and geoscientific appraisals by the petroleum industry. For example, studies of the Congo River outflow and sediment dispersal patterns by the Netherlands Institute for Sea Research conducted between 1976 and 1980 (e.g. Eisma and Kalf, 1984; van Weering and van Iperen, 1984) recorded total suspended matter concentrations in the Congo River plume of 2 g $m^{-3}$ at the shelf edge decreasing to less than 1 g $m^{-3}$ above the slope and to about 0.03 g $m^{-3}$ in surface waters of the central Angola Basin. Near-bottom suspended matter concentrations were largest at the canyon head with 10-15.6 g $m^{-3}$ decreasing steadily basinward to about 0.1 g $m^{-3}$ before declining rapidly to less than 0.05

g $m^{-3}$ at the transition from canyon to fan system (Eisma and Kalf, 1984). Based on suspended matter distributions in the Congo estuary and adjacent areas, Eisma and Kalf (1984) estimated that about half of the annual surface suspended sediment load is carried by the river plume seaward, from where it is either dispersed over the shelf edge or deposited along the shelf to the north of the river mouth. The remaining half is thought to settle in the Congo estuary along the canyon walls or in the mangrove swamps that border the river mouth. From here, it is thought to be episodically activated and transported down the canyon by gravity processes, such as turbidity currents (Eisma and Kalf, 1984; Vangriesheim et al., 2009).

Active turbidity flows in the Congo canyon were first predicted by Heezen et al. (1964), based on frequent submarine cable ruptures near the canyon between 500 and 2300 m water depths. Since then, mud-rich turbidity currents have been measured by Khripounoff et al. (2003) near 4000 m in March 2001, by Vangriesheim et al. (2009) at three moorings located along the channel from 3420 to 4790 m depth in January 2004, and by Andrieux et al. (2013) and Azpiroz-Zabala et al. (2017) from moorings deployed in the canyon channel at about 2000 m depth at several occasions between December 2009 and March 2010. All studies showed, by comparison with other canyon systems, unusually long turbidity flow periods lasting up to 6-10 days, and exceptionally high peak velocities, which varied between 100 and 250 cm $s^{-1}$ for turbidity flows recorded at 2000 m (Azpiroz-Zabala et al., 2017) and exceeded 121 cm $s^{-1}$ about 150 m above the channel floor during the turbidity flow measured at 4000 m in 2001. For the turbidity event in January 2004, Vangriesheim et al. (2009) reported a mean velocity of 350 cm $s^{-1}$ between 3420 and 4070 m, decreasing to 70 cm $s^{-1}$ between 4070 and 4790 m. Turbidity data collected above the channel suggests that turbidity flows are likely to be confined to the channel down to about 4000 water depths as the channel depth exceeds the vertical extent of the turbidity flow (Babonneau et al., 2002), which is estimated to reach up to 250-300 m (Vangriesheim et al., 2009). Further downslope, as the channel relief decreases, overspill is likely (Vangriesheim et al., 2009), as has been observed during the 2001 event, when large concentrations of turbiditic particles were collected in sediment traps located 13 km south of the main channel (Khripounoff et al., 2003).

Based on morphological properties, the present Congo turbidite system has been divided into four distinct domains: the submarine canyon down to about 2000 m, the upper-fan

valley down to about 3300 m, the upper and lower channel levee systems, and the distal lobe complex below about 4800 m (Babonneau et al., 2002, 2010). The presently active channel of the upper (c. 3300-4000 m) and lower (c. 4000-4800 m) channel levee systems is about 1.5 km wide and bordered at both sides by mud-rich overspill deposits (Babonneau, 2002; Savoye et al., 2009). The sedimentary processes of the turbidite system have been extensively studied, mainly by the French research community (Rabouille et al., 2017b; Savoye et al., 2009). The key findings of these investigations were synthesised by Baudin et al. (2020) and Rabouille et al. (2017a,b) and are only very briefly summarised here. Core data showed that the sediments of the modern Congo deep-sea fan are dominated by terrigenous clay and silt minerals (up to 80-90%) (e.g. Baudin et al., 2010; Gervais et al., 2001; Jansen, 1990; van Weering and van Iperen, 1984), with coarser fractions generally being restricted to the central axes of feeding channels (Babonneau et al., 2002; Dennielou et al., 2017). Present-day sediment accumulation rates along the turbidite system are high, reaching up to 2.5-22 cm $yr^{-1}$ in the main depositional area of the distal lobes at the end of the currently active turbidite channel (Baudin et al., 2017b; Rabouille et al., 2017b; Stetten et al., 2015) and 0.3-1 cm $yr^{-1}$ on its levees (Rabouille et al., 2009, 2017b), which is about one to three orders of magnitude higher than sedimentation rates at an abandoned lobe 50 km northwest of the active channel (< 0.05 cm $yr^{-1}$; Rabouille et al., 2009). For the upper and lower channel levee systems sedimentation rates of 0.06-0.4 cm $yr^{-1}$ are reported (Baudin et al., 2010). The large sedimentation rates along the turbidite system are reflected in high amounts of organic carbon (Baudin et al., 2017), which values of around 2.5-3% (up to 5.6%) in surface sediments along the lower channel-levee system below about 4000 m depth (Baudin et al., 2010), and between 3-4% (up to 5.2%) in sediments across the terminal lobe complex at c. 5000 m (Baudin et al., 2017b; Stetten et al., 2015). For comparison, organic matter concentrations in surface sediments in the deep Angola Basin (5100-5400 m) are an order of magnitude lower (0.4-0.6%, Kröncke and Türkay, 2003). The organic matter is distributed relatively homogenously along the channel levees (Baudin et al., 2010) and across the distal lobe complex (Stetten et al., 2015), which, together with relative homogenous C:N mass ratios in the channel-levee systems (10.7-15.7) and distal lobe complex (15.4-18.5), points to a homogenous distribution of the particulate organic material supplied through the canyon (Baudin et al., 2017b, 2010; Stetten et al., 2015).

The organic material found in the fan sediments contains a mixture of terrestrial higher-plant debris, degraded organic matter from soils, and remains of freshwater and marine algae (Baudin et al., 2020 and references therein). Elemental, isotopic, and palynological data suggest that terrestrial sources may contribute at least 70-80% to the organic matter observed in sediments along the active turbidite channel (Baudin et al., 2010) and in the distal lobe area (Baudin et al., 2017b; Stetten et al., 2015). Based on a combination of sedimentary short-live radionuclide profiles, organic matter concentrations, and oxygen uptake rates derived from in situ benthic chambers and microprofiler measurements, Rabouille et al. (2009, 2019) estimated that about 22 % (0.42 TgC) of the annual organic carbon discharged by the Congo River (1.9 TgC) reach the distal lobes, of which about 15% (0.07 TgC) are remineralized on the seafloor, while about 85% (0.35 TgC) are buried. Extending these calculations to the entire active turbidite system from the canyon to the distal lobes, Baudin et al. (2020) estimated the annual burial of terrestrial organic carbon to be between 0.53 and 1.11 TgC $y^{-1}$ (average 0.74 TgC $y^{-1}$), which would represent 1.3-2.6% of the terrestrial organic carbon buried annually in the world's ocean (43 TgC; Schlünz and Schneider, 2000). The authors acknowledge that their carbon storage budget remains unbalanced with some riverine organic matter being unaccounted for. However, these calculations nevertheless show that the sediments of the Congo deep-sea fan are an important sink of fluvial organic carbon in today's ocean (Baudin et al., 2020; Rabouille et al., 2019).

## 2.7 Benthic communities

### 2.7.1 Invertebrates

The number of studies that have examined the modern ecology of the Angolan margin remains rather limited compared to the large amount of geological and geotechnical investigations. The first comprehensive investigations into the biodiversity of deep-water benthic systems were conducted as part of the multidisciplinary BIOZAIRE programme led jointly by TOTAL and Ifremer. Eleven contrasting sites were sampled between 2000-2005 within and outside the Congo canyon and submarine fan from the upper slope (330 m) down to the continental rise (4800 m), using a range of sampling gears to quantify the structure of different faunal components from microbial to megafaunal communities and to assess the physico-chemical properties of the water column and underlying sediments

(Sibuet and Vangriesheim, 2009; Vangriesheim et al., 2009). The subsequent French Congolobe cruises (2011-2012) focussed on the biogeochemical characteristics of benthic systems in the terminal lobe complex of the Congo deep-sea fan (Rabouille et al., 2017a, b).

### *Chemosynthetic habitats*

A large part of the ecological investigations conducted during BIOZAIRE, as well as subsequent studies in the region (Table 2.1), focussed on chemosynthetic communities, in particular those found within a large, circular 800 m wide and on average 20 m deep cluster of coalescent pockmarks (named Regab) at 3160 m water depth about 8 km to the north of the Congo submarine channel (Ondréas et al., 2005; Sibuet et al., 2002). Common to deep-water chemosynthetic systems around the globe (e.g. Levin et al., 2016; Sibuet and Olu, 1998), the megafauna at Regab is dominated by patches of symbiont-bearing species, in this case clusters of the vesicomyid clams *Laubiericoncha chuni* and *Christineconcha regab* (Cosel and Olu, 2008, 2009; Krylova and Cosel, 2011), thickets of the siboglinid tubeworm *Escarpia southwardae* (Anderson et al., 2004), and beds of mytilid mussels belonging to the *Bathymodiolus* aff. *boomerang* complex (Olu-Le Roy et al., 2007). Sulfide-oxidising bacteria growing in white mats surrounded by reduced black sediments are also present (Ondréas et al., 2005; Pop Ristova et al., 2012) together with abundant gas hydrates in and on the seabed and methane rich fluids in the water column, indicating widespread and active seepage of gas and gas-rich fluids across the site (Charlou et al., 2004). Microscopic and genetic studies provided evidence of sulfide-oxidising symbionts in the tubeworms (Andersen et al., 2004; Cambon-Bonavita et al., 2009) and vesicomyid clams (Cambon-Bonavita et al., 2009), and sulfide- and methane-oxidising bacteria in the bathymodiolid mussels (Cambon-Bonavita et al., 2009; Duperron et al., 2005). Analysis of lipid biomarkers and stable isotopes in sediment cores taken across the Regab pockmarks showed that the chemosynthetic assemblages are sustained by anaerobic oxidation of methane (AOM) and associated sulfide production, mediated by methanotrophic archaea and possibly sulfate-reducing bacteria (Bouloubassi et al., 2009; Sibuet and Vangriesheim, 2009). Microbially mediated AMO is also thought to be the main process responsible for the formation of abundant authigenic carbonates across the central section of Regab (Charlou et al., 2004; Pierre and Fouquet, 2007), both in the

shallow subsurface and on the seafloor where carbonates form large concretions up to several metres thick (Ondréas et al., 2005).

Data on the composition and distribution of the large symbiont-bearing foundation taxa at Regab were given by Olu-Le Roy et al. (2007) and Ondréas et al. (2005), who showed that the central part of Regab is dominated by high density clusters of mytilid mussels and siboglinid polychaetes interspersed with occassional high density clusters of vesicomyid clams. By contrast, the peripheral areas are populated by scattered, less dense aggregations of dead and live vesicomyid clams. Sedimentary and geochemical characterisation of the Regab site indicated that the spatial distribution of each of the symbiont-bearing species is strongly controlled by the concentration of methane in venting fluids, which peaked in mussel patches (Olu-Le Roy et al., 2007; Pop Ristova et al., 2012), and by the location of carbonate excretions, which is thought to promote the settlement of siboglinids and mytilids (Marcon et al., 2014; Olu-Le Roy et al., 2007; Ondréas et al., 2005). Sediments of clam populated sites were characterised by lower sulphide concentrations as well as lower consumption rates of methane and sulphate (Olu-Le Roy et al., 2017; Pop Ristova et al., 2012). Changes in the location and extent of the symbiont-associated megafaunal taxa in the Regab cold seep communities were relative small between 2001 and 2011 (Marcon et al., 2014), suggesting stable environmental conditions with continuous fluxes of methane and sulfide, which the author relate to the presence of abundant gas hydrates across the site that maintain ongoing seepage activity. Patches with living vesicomyid clams underwent the largest changes, possibly reflecting more transient fluxes within clam populated sediments compared to areas populated by mussels and tubeworms (Marcon et al., 2014).

Spatial gradients in methane and sulfide emissions across Regab shape the structure and dynamics of microbial (Pop Ristova et al., 2012), meiofaunal (Van Gaever et al., 2009), and macrofaunal (Guillon et al., 2017; Menot et al., 2010a) communities. Outside the pockmark area at Regab, macrofaunal densities and community composition resembled those found in typical abyssal sediments, with densities ranging from 1720 to 3909 ind. $m^{-2}$ (Menot et al., 2010a). In seep sediments, total macrofaunal densities were in most cases higher, reaching values of up to 22300 ind. $m^{-2}$. Polychaetes were mainly represented by families rarely seen in background sediments, and richness of polychaete families was reduced compared to the surrounding background sediments. There was also considerable

variation in the composition of polychaete communities between patches populated by the different symbiont-bearing taxa, leading to high beta diversity. Surface-feeders (ampharetids) and small mobile carnivores (dorvelleids, hesionids, and syllids) dominated tubeworm populated patches, while deep-dwelling taxa (capitellids and cossurids) dominated in sediments associated with clam and mussel patches (Menot et al., 2010a). The higher proportion of subsurface feeding polychaetes in clam beds is thought to reflect better bioturbated sediments resulting from the burrowing activity of the clams and an abundant microbial community of free-living chemoautotrophic bacteria, which may provide a rich food source for deep-dwelling taxa.

Epibenthic megafaunal communities associated with aggregations of symbiont-bearing species at Regab resembled those found at cold seeps in the western Atlantic (Olu et al., 2009) and included alvinocarid shrimps, galatheid crabs (*Munidopsis geyeri* and *Munidopsis hirtella*), several species of gastropods including ten species new to science (Warén and Bouchet, 2009), holothurians of the genus *Chiridota*, irregular echinoids, and several fish species, including Zoarcidae and Ophidiidae (Olu et al., 2009; Olu-Le Roy et al., 2007). The highest densities and biomass of associated megafauna were found within the mytilid beds (Olu et al., 2009).

Besides Regab, chemosynthetic communities have been identified at several other locations on and near the Angolan margin, including in the Kouilou pockmark field in the northern Congo deep-sea fan (c. 3100 m; Sahling et al., 2008), in the Astrid pockmark off Congo about 100 km to the northeast of Regab (2820 m; Cosel and Olu, 2009), in the Guiness pockmarks on the upper slope of the Gabonese margin (580-670 m; Olu et al., 2010; Sibuet and Vangriesheim, 2009), on the lower Angolan slope about 100 km to the south of the Congo canyon (c. 1500 m; Jones et al., 2014), and in the organic-rich sediments found across the distal lobe complex of the Congo deep-sea fan (c. 4750-5070 m; Khripounoff et al., 2005; Rabouille et al., 2017; Sen et al., 2017). The Kouilou pockmarks (Hydrate Hole, Worm Hole, and Black Hole) are circular or oval and between 10-20 m deep (Sahling et al., 2008). Like Regab, they appear to be coalescent features composed of several up to 1000 m wide distinct depressions with patchily distributed fluid seepage, and abundant authigenic carbonates of various sizes and shapes at and below the sediment surface. Gravity cores revealed the presence of up to 2 cm thick gas hydrate accumulations in the sediment at depths below 50 cm down to at least 12 m. Small clusters

of live and dead vesicomyid clams occur in soft sediments and vestimentiferan tubeworms are common in close proximity to carbonate excretions on the seafloor (Sahling et al., 2008). Data for the Astrid pockmark are sparse, but show the presence of live vestimentiferan and empty vesicomyid shells (Cosel and Olu, 2009). Seafloor images from the Guiness pockmarks revealed the presence of isolated authigenic carbonates, bacterial mats, Lucinidae, and small (about 1 m in diameter,) but dense clusters of vesicomyid clams, mostly *Calyptogena valdiviae* (Cosel and Olu, 2009; Sibuet and Vangriesheim, 2009). Several of the Guiness pockmarks appear to be inactive (Cosel and Olu, 2009), and fluid flow across the active pockmarks is thought to be low and dispersed (Sibuet and Vangriesheim, 2009). Using molecular analysis, stable isotopes, and fluorescence in situ hybridization, Duperron et al. (2012) investigated microbial communities in five metazoan species collected at the Guiness site: the bivalves *Acharax* sp. (Solemyidae), *Thyasira* sp. (Thyasiridae), *Elenaconcha guiness*, and *C. valdiviae* (Vesicomyidae), and the siboglinid tubeworm *Lamellibrachia* sp. They found that all five species host abundant chemosynthetic, sulfur-oxidizing bacteria, which provide a major source of energy for the host's nutrition. Sulfur-oxidizing endosymbionts were also detected in the smaller vesicomyid *Isorropodon bigoti* (Rodrigues et al., 2012). The chemosynthetic communities recorded on the lower Angolan slope comprised dense, up to 1 $m^2$ large patches of bathymodiolin mussels and vesicomyid clams, and dense fields (< 0.25 $m^2$) of siboglinid polychaetes (Jones et al.. 2014). Carbonate concretions were also present, occasionally in association with asphalt mounds, which are abundant in the study region (see below). The chemosynthetic communities in the terminal lobes of the Congo deep-sea fan are composed of microbial mats, possibly formed by large sulphur-oxidising bacteria of the *Beggiatoa* type, and scattered clusters of the vesicomyid clams *Christineconcha regab* and *Abyssogena southwardae*, which are often associated with black reduced sediments (Sen et al., 2017). Clam patches were mostly found along channel flanks and their levees, but were scarce across main deposition zones and within the centre of active feeding channels, likely owing to the frequent disturbances in these areas caused by high velocity turbidity currents (Sen et al., 2017). The chemosynthetic communities across the Congo lobe complex are thought to be sustained by the microbial decomposition of organic material supplied via the Congo submarine canyon (Pruski et al., 2017; Rabouille et al., 2017a; Sen et al., 2017). High total oxygen uptakes and high concentrations of methane and sulphate

were identified in sediments underlying clams, microbial mats and reduced surfaces, pointing towards anaerobic mineralisation processes of organic matter, such as dissimilatory sulphate-reduction and methanogenesis (Pastor et al., 2017; Pozatto et al., 2017). In addition, the sediments were characterised by highly diverse microbial communities including archaea and sulphate-reducing bacteria, indicating AOM with sulphate reduction as possible source for sulphides used by sulphide-oxidizing symbionts inhabiting the clams (Decker et al., 2017; Pastor et al., 2017). No authigenic carbonates are present in lobe sediments, which is thought to explain the absence of bathymodiolin mussels and vestimentiferan tubeworms (Sen et al., 2017). Furthermore, the patchily distributed and temporally variable fluid emissions in the lobe sediments are hypothesised to favour the mobile vesicomyid clams, as they may be able to move away from unfavourable sedimentary conditions (Sen et al., 2017). The structure of macrofaunal communities in lobe sediments associated with microbial mats, black reduced substratum, and clam aggregations resembled those found at cold seep habitats, exhibiting low diversity, high proportions of sulfide-tolerant polychaetes and gastropods, and high beta diversity owing to large variations in community composition among the different chemosynthetic habitat types (Olu et al., 2017). Macrofaunal densities were highly positively correlated with total oxygen uptake, reaching 65699 ind. $m^{-2}$ in black reduced sediments and 42525 ind. $m^{-2}$ in microbial mats, compared to 3795-8713 ind. $m^{-2}$ in vesicomyid bivalve assemblages, and 1001 ind. $m^{-2}$ in sediments of an abandoned lobe outside the influence of modern turbidite deposition (Olu et al., 2017).

Analysis of faunal similarities between cold seep communities along the Atlantic Equatorial Belt (AEB) from the Gulf of Mexico to the Gulf of Guinea suggested that the composition of seep invertebrate megafauna is strongly influenced by depth, and to a lesser degree by geographic location (Olu et al., 2010). Almost 30% of the seep species analysed by Olu et al. (2010) showed an amphi-Atlantic distribution, which is hypothesized to indicate recent and large scale connectivity among these species across the Atlantic (Olu et al., 2010). Recent molecular analyses by Teixeira et al. (2013) corroborate this hypothesis for selected seep vesicomyid bivalves and Alvinocarididae shrimp, which showed low genetic divergence among populations from both sides of the AEB. The processes maintaining the connectivity between populations across the Atlantic remain unknown. It is argued that they possibly include long-distance dispersal of propagules by

ocean currents (Olu et al., 2010; van Dover et al., 2002) potentially coupled with prolonged larval developments and possibly with hydrothermal vents located along the Mid-Atlantic Ridge acting as a stepping stone for some taxa (Olu et al., 2010, Teixeira et al., 2013, van Dover et al., 2002). In addition, currently unknown habitats favourable for hosting common seep species may facilitate the high connectivity of seep species across the AEB (Teixeira et al., 2013).

### *Non-chemosynthetic habitats*

As part of the BIOZAIRE programme, benthic meio- and macrofaunal communities were studied at several sites along the Congo sub-marine channel: at the base of the continental slope in sediments surrounding the Regab pockmark (c. 3160 m, site Regab), inside the channel at about 4000 m (site Channel), in the lower channel levee system about 15 km south of the channel (c. 4000 m, site ZD), and in the distal lobe complex at about 4800 m (site Lobe). In addition, two sites on the open slope about 150-200 km south of the Congo submarine channel outside the influence of turbidite deposition were sampled, one located at mid-slope depths at about 1300 m (site ZA), and one located on the continental rise at about 4000 m (site ZC) (Sibuet and Vangriesheim, 2009). The macrofaunal community (*senso strictu*, > 250 μm) at Regab, and sites ZC and ZD was dominated by polychaetes with isopods, tanaidaceans, and bivalves also regularly being present in larger proportions (Galéron et al., 2009). Sediments at Regab had larger proportions of nemerteans, bivalves, and holothurians, as well as spionids, lumbrinerids, and ophellids compared to the deeper sites ZC and ZD, while nereids and syllids were mostly absent. Polychaete assemblages at site ZD differed from those at site ZC by higher densities of paraonids and pilargids, while at ZC cirratulids, hesionids, and ampharetids were more abundant. Mean macrofaunal densities at the two deeper sites (ZC and ZD) ranged between 1308-1524 ind. $m^{-2}$ during the first two years of sampling, but increased significantly during the third year to 2808 ind. $m^{-2}$ at ZC and 1744 ind. $m^{-2}$ at ZD. The lower densities on the Congo levees (ZD) were hypothesized to be caused by lower energetic value of organic material at ZD, which originates mainly from terrestrial sources, compared to the open slope site where sedimentary organic material is predominantly of marine origin.

The open slope (ZC) also supported higher meiofaunal abundances compared to sediments on the Congo levees at similar depths (ZD), with mean densities of 1005 ± 78

ind. 10 $cm^{-2}$ at ZC and 506 ± 100 ind. 10 $cm^{-2}$ at ZD (Van Gaever et al., 2009). Slightly larger mean densities of 1320 ± 460 ind. 10 $cm^{-2}$ were present at mid-slope depths of the open slope at site ZA. The meiofaunal community at all three sites (ZA, ZC, and ZD) was dominated by nematodes (> 90%), followed by copepods and nauplii (Van Gaever et al., 2009). Among the nematodes, *Thalassomonhystera* (21.5%) and *Acantholaimus* (18.4%) dominated the levee sediments of site ZD, while site ZC was characterised by larger proportions of *Leptolaimus* (13.2%) and *Thalassomonhystera* (9.7%). At site ZC, specimens of the opportunistic *Microlaimus* were dominant (33.6%). Sediments sampled inside the channel and in the distal lobe had very low meiofaunal densities (channel 3 ± 3 ind. 10 $cm^{-2}$, lobe 15 ± 9 ind. 10 $cm^{-2}$, which was attributed to unstable sedimentary conditions caused by high-velocity bottom currents and turbidite deposition (Van Gaever et al., 2009).

Low densities (398-607 ind. 10 $cm^{-2}$, 30-4474 m depth) and lack of depth trend were documented near the Congo canyon (about 6°2'S, Soltwedel, 1997). Further south (11°45′S), and presumably outside the area of influence of the Congo canyon, total meiofaunal densities followed the general basin-wide trend of declining standing stocks with increasing depth, with densities of 1954 ind. 10 $cm^{-2}$ at 73 m, 1389 ind. 10 $cm^{-2}$ at 1638 m, and 733 ind. 10 $cm^{-2}$ at 4530 m water depth (Soltwedel, 1997). These densities were among the highest recorded in the tropical East Atlantic between Guinea (10°N) and Angola (18°S; Soltwedel, 1997). However, they appeared relative low when compared to concentrations of sediment-bound chloroplastic pigments, particularly in the shallower sites. It is hypothesised that this may indicate the presence of fractionated, lower energy organic matter, which has been transported to the site over long distances by subsurface currents (Soltwedel, 1997).

Asphalt mounds were recently documented (Jones et al., (2014) on the lower Angolan slope across Licence Block 31, the first description of these features from the eastern Atlantic continental margin. Side-scan sonar interpretations predicted the presence of 2254 distinct mound features, covering an area of 3.7 $km^2$ across the study area of 5349 $km^2$. Seafloor photographs showed a diverse range in the form and size of mounds, including single mounds < 0.5 m in diameter, small coalescent features, and large extensive mounds < 50 m in diameter. The mounds hosted diverse heterotrophic epilithic communities with megafaunal poriferans, anthipatharians, actinians and alcyonaceans, and smaller-sized

polychaetes, ophiuroids and unidentified arborescent structures being the most commonly observed species. They range from providing minor habitat within areas of active methane seepage, chemosynthesis and authigenic carbonate to discrete non-chemosynthetic habitats. Like the chemosynthetic habitats observed in the region, asphalt mounds elevate habitat heterogeneity and with it biodiversity on the West African margin (Jones et al., 2014).

Frame-work building deep-water Scleractinian reefs are documented from the upper slope between about 250 to 500 m water depth, with the first record being from the 1950 *Galathea* cruise, which documented the presence of the reef-forming coral *Desmophyllum pertusum* at 380 m near the Congo submarine canyon (Le Guilloux et al., 2009; Zibrowius, 1980). First insights into the structure and ecology of Angolan deep-water reefs were given by Le Guilloux et al. (2009), who studied a small cluster of mostly elongated coral mounds at c. 400 m water depth on the northern margin (c. 7°18'S) as part of the BIOZAIRE programme. The mounds are about 30 m high, and up to 300 m wide and 1.5 km long. Their orientation appear to follow the direction of underlying faults originating from salt tectonic processes. Common megafaunal species associated with the reefs included macrourids and scorpaenid fish, gorgonians, echinoids, and the glass sponge *Aphrocallistes* sp. Reduced sediments with bacterial mats and Lucinid bivalves (*Graecina karinae* n. sp., *Lucinoma myriamae* n. sp., *Joellina dosiniformis* n. sp.; Cosel, 2006) were recorded at sites surrounding the reefs, suggesting active fluid escape across the study area.

Recent acoustic mapping and ROV investigations along the central Angolan slope (c. 9°40'S - 9°50'S; Hebbeln et al., 2016)) found dense living reefs on up to 100 m high mounds, which occurred either isolated or as long ridges (Hanz et al., 2019). U series dating of coral bearing sediment cores from one of these mounds indicates coral presence for at least 34000 years with coral growth occurring during glacial and interglacial periods (Wefing et al., 2007). Coral aggregations were, like those located further north, formed mainly by *D. pertusum* interspersed with some colonies of *Madrepora oculata* (Hebbeln et al., 2016). The largest aggregations were recorded at depths between 330-470 m (Hebbeln et al., 2020), coinciding with the core of the OMZ where dissolved oxygen concentrations were as low as 0.5 ml $l^{-1}$ (Hanz et al., 2019). These oxygen concentrations are well below levels documented across living CWC reefs in other ocean basins, raising

new questions on how coral populations can adapt to local environmental conditions (Hanz et al., 2019; Hebbeln et al., 2020; Orejas et al., 2021). Sediment trap and current meter data revealed the presence of a 100 m thick nepheloid layer located just above the coral mound zone, containing high concentrations of suspended particulate organic matter of both marine and terrestrial origin (Hanz et al., 2019). Vertical mixing caused by internal tidal movements suggests enhanced transport of organic material to the corals below, which in turn is hypothesised to offset potential physiological stresses caused by the ambient hypoxic conditions (Hanz et al., 2019; Hebbeln et al., 2020).

Information about the diversity and taxonomy of species associated with the Angolan cold-water coral reefs and their genetic relations remain very scarce, but is likely to increase as recently acquired specimens and image material (Hebbeln et al., 2016) are being processed. Novel species are likely to be found, as illustrated by a newly described caprellid amphipod collected from the mound complex on the central slope (Zettler et al., 2018).

The abyssal plain outside the direct influences of the Congo deep-sea fan was studied in the German-led DIVA-1 programme, conducted in 2000, which sampled six sites along a 700-mile long transect crossing the southern part of the Angolan Basin (c. 16-22°S) using an Agassiz trawl, an epibenthic sledge, and a box corer (Arbizu and Schminke, 2005; Kröncke and Türkay, 2003). Numerous new meiofaunal, macrofaunal, and megafaunal species were described (Special volume of Organisms, Diversity & Evolution Volume 5, Supplement 1, Arbizu and Schminke, 2005). There were differences the structure and distribution of macro- and megafaunal communities along a latitudinal gradient that appeared to be associated with differences in the productivity of overlying water masses (Kröncke and Türkay, 2003). Clear latitudinal patterns were also seen in assemblages of sipunculans and echiurans (Saiz-Salinas, 2007), harpacticoid copepods (George et al., 2014), and polychaetes (Fiege et al., 2010).

### 2.7.2 Ichthyofauna

The demersal fish fauna of the upper Angolan slope down to about 800 m has become relatively well known through extensive trawl surveys, particularly those conducted under the Dr Fridtjof Nansen Survey Programme, which has been operating in the region since 1985 (Strømme and Sætersdal, 1986). The resulting data have mainly been used to monitor

fish stock dynamics and to inform advice on fisheries management (Bianchi et al., 2016), though a range of studies have also been conducted (Table 2.1) that have led to useful ecological and taxonomic insights. For example, these data showed strong bathymetric changes in faunal composition on the shelf and upper slope (down to about 750 m) with three main groups recognised across the study area (between 5 and 17°S): (1) a shallow water and intrathermocline demersal fish assemblage down to about 50 m, (2) a subthermocline shelf assemblage from 50-200 m, and (3) an upper slope assemblages below 200 m, the latter characterised by the Benguela hake *Merluccius polli*, macrourids, codlings of the genus *Laemonema*, and several nematocarcinid, panaeid and aristeid deep-water shrimp species (Bianchi, 1992). Within these major bathymetric groupings, thermal stratification and bottom type were also important in driving community changes. A major transition in the composition of the subthermocline fish assemblage occurred south of 16°S, possibly driven by changes in hydrographic conditions across the Angola-Benguela Frontal system (Bianchi, 1992). A similar shift in assemblage composition across the Angola-Benguela frontal zone was noted for grenadier species (Sobrino et al., 2012), based on the analysis of demersal trawl data collected along the West African coast from Morocco to Namibia. The composition of grenadier assemblages off Angola (sampled to depths of about 750 m) resembled that of assemblages caught off neighbouring Gabon and Bissau to the north, but was distinct from assemblages recorded in Namibian waters to the south.

Another useful outcome from the Nansen survey data include an extensive list of fish species for the Angolan shelf and upper slope down to about 800 m water depth (Tweddle and Anderson, 2008), thereby updating existing species lists for the eastern central (e.g. Fisher et al., 1981) and tropical (Quero et al., 1990) Atlantic. More recently, complex climate related patterns in both pelagic and benthic fish species in the Benguela Current Large Marine Ecosystem have been elucidated from integrations of Nansen data from Angola, Namibia and South Africa (Jarre et al., 2015; Yemane et al., 2014).

Patterns of demersal fishes along the deeper sections of the Angolan slope and the adjacent continental rise and abyssal plain are less known. The first insight into the spatial distribution and foraging behaviour of bait-attending benthopelagic species was provided using baited landers deployed at the northern and central parts of the Angolan slope in water depths between 1300-2450 m (Jamieson et al. 2017). Among the 31 species

recorded, the Portuguese dogfish *Centroscymnus coelolepsis*, blue hake *Antimora rostrata*, and the synaphobranchid eels *Simenchelys parasitica* and *Synaphobranchus* cf. *kaupii* were the most frequently encountered scavenging species. An unusually high number of grenadiers and patchy aggregations of the eelpout *Pachycara crassiceps* were also noted. Fish communities observed from ROV video footage at whale shark and manta ray carcasses at depths of about 1200 m depth at the northern slope were dominated by Zoarcids (Higgs et al., 2014), which, in line with observations by Jamieson et al. (2017), were mainly seen roosting near the carcasses with limited or no active feeding. From the approximated carcass mass, the authors estimated that the food falls may account for 4% of the normal POC flux to the seabed. More recently, strong seasonal cycles, with recurrent peaks in late November and in June (Milligan et al., 2020) have been documented in the abundance of demersal fishes at two mid-slope sites (c. 1400 m) on the central Angolan slope. The time series of fish densities, based on photographic data collected over 7.5 years from the Deep-ocean Environmental Long-term Observatory Systems (DELOS; Vardaro et al., 2013), was significantly correlated with estimated POC flux to the seabed at lags of 4 and 5 months. Bottom-up trophic controls driven by secondary benthic production and the availability of carrion from large food falls (e.g. Higgs et al., 2014) may underlie these fluctuations and may lead to region-wide seasonal migrations of large parts of the demersal fish assemblage (Milligan et al., 2020).

**Table 2.1** Summary of research programmes and individual studies with focus on deep-water benthic systems across or near the Angolan continental margin and abyssal plain.

| Study | Date | Study area and main purpose | Example references |
|---|---|---|---|
| **Historic research expeditions covering the tropical eastern South Atlantic** | | | |
| Challenger Expedition | 1872-1876 | Global expedition including northern West Africa to examine the physical and biological conditions of the deep ocean | Thomson and Murray (1895); Murray and Hjort (1912) |
| Atlantide Expedition | 1945-1946 | Danish Expedition to the Coasts of Tropical West Africa | Marshall (1952); Atlantide report series, e.g. Mortensen (1951) and Nørvang (1961) |
| Galathea II Deep Sea Expedition | 1950-1952 | Global expedition to study the oceanography and fauna of the deep ocean | Bruun (1957); Bruun et al. (1956); Galathea report series (1956 to present) |
| **Recent research programmes** | | | |
| 'Meteor' Expedition DIVA I | 2000 | Benthic sampling (trawls, sledge and cores) in the Angola Basin at depths of about 5500 m to examine the ecology of abyssal assemblages. Part of wider study to examine latitudinal gradients in biodiversity in the deep Atlantic. | Overview: Arbizu and Schminke (2005)<br>Community ecology: Fiege et al. (2010); George et al. (2014); Kröncke and Türkay (2003); Saiz-Salinas (2007)<br>Taxonomy and morphology: Publications presented in special issue of Organisms Diversity & Evolution, 2005, Volume 5, Supplement 1; Brix (2007, 2015, Isopoda); Gil-Mansilla et al. (2008, Solenogastres); Mühlenhardt-Siegel (2003, Cumacea); Mursch et al. (2008, Munnopsidae); Seifried et al. (2007, Copepoda); Wittmann (2020, Lophogastrida and Mysida) |
| BIOZAIRE | 2000-2005 | Multidisciplinary research programme led by TOTAL and Ifremer to study deep-sea benthic ecosystems on the Congo-Angola margin in the Gulf of Guinea. Eleven contrasting sites were selected for ecological, physical, and chemical studies based on sedimentological and geophysical data collected during the ZAIANGO project (Savoye et al., 2000, 2009). | Overview: Sibuet and Vangriesheim (2009); Vangriesheim et al. (2009)<br>Results of individual studies are presented in a special issue of Deep Sea Research, Volume 56(23), titled "Deep-Sea Benthic Ecosystems of the Equatorial African Margin: The Multidisciplinary BIOZAIRE Program - A Contribution to Census of Marine Life"<br>Chemosynthetic habitats: Cambon-Bonavita et al. (2009); Cosel (2006); Galéron et al. (2009); Krylova and Cosel (2011); Menot et al. (2010a); Olu et al. (2009, 2010); Olu-Le Roy et al. (2007); Ondréas et al. (2005); Sibuet et al. (2002); Cosel and Olu (2008, 2009); Van Gaever et al. (2009); Warén and Bouchet (2009)<br>Non-chemosynthetic habitats: Brind'Amour et al. (2009); Galéron et al. (2009); Le Guilloux et al. (2009); Menot et al. (2009); Van Gaever et al. (2009) |
| West African Cold Seeps and Congolobe cruises | 2011-2012 | Multidisciplinary project to examine the ecological and geochemical properties of the Congo deep-sea fan lobe complex. Data were collected during two cruises: (1) the West African Cold Seeps (WACS) cruise in February 2011 (Olu, 2011), and (2) the Congolobe cruise from December 2011 to January 2012 (Rabouille, 2011) | Overview: Rabouille et al. (2017a,b)<br>Results of individual studies are presented in a special issue of Deep Sea Research, Volume 142, titled "Organic carbon transfer and ecosystem functioning in the terminal lobes of the Congo deep-sea fan: The Conglobe multidisciplinary study"<br>Ecology and physiology: Bessette et al. (2017); Decker et al. (2014, 2017); Duperron et al. (2012); Gaudron et al. (2017); Guillon et al. (2017); Marcon et al. (2014); Olu et al. (2017); Rodrigues et al. (2012); Sen et al. (2016, 2017) |
| R/V "Goa" programme by the Fisheries Research Institute of Angola | 1986-1991 | Series of trawl surveys to characterise the distribution and abundance of the most important demersal fish species off the Angolan coast from 25 to 150 m water depth | Constança (1995) |

**Table 2.1** continued

| | | | |
|---|---|---|---|
| Dr Fridtjof Nansen Survey Programme; global survey initiative aimed at providing developing countries with fisheries resource data | 1985-present | Series of trawl and echosounder surveys to monitor the demersal and pelagic fish resources along the Angolan continental shelf and upper slope to about 800 m water depth. | Axelsen et al. (2004); Bianchi (1992); Jarre et al. (2015); Kirkman et al. (2013); Sætersdal et al. (1999); Strømme and Sætersdal (1986); Strømme and Sætersdal (1991); Tweddle and Anderson (2008); Yemane et al. (2014) |
| **Individual studies** | | | |
| Higgs et al. (2014) | Observations of large food falls (whale shark and rays) on the northern Angolan slope (c. 1200 m) | | |
| Jamieson et al. (2017) | Diversity and composition of scavengers using baited cameras (1200-2500 m) | | |
| Jones et al. (2014) | Structure and associated megafaunal assemblages of asphalt mounds in the Lower Congo Basin | | |
| Kröncke et al. (2013) | Macro-and megafauna communities in the eastern and western Guinea Basin, and northern Cape and Angola Basins (5040-5670 m) | | |
| Lange and Zettler (2014) | Diversity of macrofaunal communities on the Angolan shelf (19-340 m, c. 7°S to 17°S) | | |
| Milligan et al. (2020) | Long-term study into seasonal cycles in demersal fish abundances off Angola (c. 1400 m) | | |
| Sahling et al. (2008) | Acoustic, sedimentological and photographic investigations of three pockmarks (Hydrate Hole, Black Hole, and Worm Hole) in the northern Congo fan area (c. 3100 m, 4°46'S to 4°49'S). | | |
| Sobrino et al. (2012) | Geographic and bathymetric distribution of grenadiers from the African Atlantic Coast. | | |
| Soltwedel (1997) | Meiobenthos distribution pattern in the tropical East Atlantic between Guinea and Angola (30-4500 m). | | |
| Pop-Ristova et al. (2012) | Benthic bacterial diversity and biogeochemistry of different chemosynthetic habitats across the Regab pockmark (3160 m) | | |
| Vardaro et al. (2013) | Overview of and first results from the Deep-ocean Environmental Long-term Observatory System (DELOS) located off Angola (c. 1400 m) | | |

## 2.8 Frontiers in Angolan Deep-Sea Research

The Angolan Continental Margin is a place of remarkable heterogeneity. Geological and hydrological processes, principally, have led to variability on a wide range of scales from very broad scale organic input from the Congo River to localised fluid flow habitats less than a meter across. A large body of literature on margin geology and evolution has illustrated a complex system of salt tectonic features, which resembles that found on other major salt margins, such as the Gulf of Mexico (e.g. Mohriak et al., 2004; Peel et al., 1995) and the Brazil margin (e.g. Mohriak, 1995, 2012). Key insights into the process of gravity-driven salt tectonics have been gained from studies of the Angolan sedimentary basins and their conjugate basins on the eastern Brazil margin, i.e. the Espírito-Santos, Campos and Santos Basins (Quirk et al., 2012). The palaeo-connection between the South Atlantic conjugate margins of Angola and Brazil remains of interest for interpreting the history of Aptian salt deposition and the opening of the South Atlantic Ocean (e.g. Torsvik et al., 2009). There is also emerging evidence of a widespread hydrocarbon migration system with gas hydrates and cold seeps. Although these features are common on many margins (Gay et al., 2007), gaining a better understanding about their regional distribution off

Angola may prove useful to improve estimations of oceanic greenhouse gas emissions and their contribution to global carbon budgets (e.g. Riedel et al., 2018).

Other environmental aspects, such as oceanographic properties are much less well known. Similarities exist with other eastern boundary marginal systems in the tropical Pacific and Atlantic Oceans in the presence of mid-water oxygen minima formed through weak water mass renewal of Central Water layers and oxygen consumption in the upper ocean (Karstensen et al., 2008). The co-location of permanent thermocline domes with the OMZs has been noted off Angola, Guinea and Costa Rica; however the relationship between these two features remains unclear (Karstensen et al., 2008). The remotely forced seasonal upwelling dynamics off Angola contrast with the dynamics of the Benguela Upwelling System off Namibia and South Africa where upwelling is forced by locally strong winds (Bachèlery et al., 2020).

Major gaps in understanding exist in the biology of Angola's deep-water area. Mapping, even at a broad scale, has revealed major features that have not been investigated from a biological perspective, such as the majority of canyons that incise the slope and the topographic highs and lows formed by underlying salt tectonics. Most of the sampling done to date, with the exception of the deepest studies in the Angolan Basin, have concentrated on relatively unusual chemosynthetic habitats or those associated with the Congo fan.

Offshore pelagic communities, outside commercially-important fishes, are virtually unstudied. Similarly, the most widespread benthic deep-water habitat, of soft sediments, is largely unsampled and not well understood. The samples that have been taken tend to show high diversities and high proportions of undescribed species. Taxonomic and autecological investigations of Angolan fauna are important in their own right but also needed to support ecological investigations. This is particularly lacking in non-chemosynthetic hard substratum, which is commonly found, for example associated with topography and salt tectonic processes, but challenging to sample. Likewise, the influence of the large terrain variability observed at lower slope depths on habitat and species diversity remains unknown. The potential importance of seafloor topography in regulating deep-water benthic standing stocks and diversity has been highlighted in recent studies (e.g. Durden et al., 2015, 2020; Jones et al., 2013; Stefanoudis et al., 2016). The highly

heterogenous area of the lower Angolan continental slope provides great possibilities to conduct further ecological studies into this topic.

The controls on biodiversity and faunal patterns are also poorly known. Links between oceanography, geology, biogeochemistry, surface ocean processes and the current and paleo fauna are largely unknown. Temporal patterns with important implications are starting to emerge, particularly from long-term observatories such as DELOS. There is almost no knowledge on biological controls or the interactions between species or functional components of communities. Biogeographic and regional scale faunal patterns are unknown for many taxonomic groups.

Further sampling should be encouraged to fill knowledge gaps pertaining to population genetics and species identities, range distributions, and diversity. Such information remains central to answer long-standing questions about ecological patterns and processes in contintental margin settings, and beyond (McClain and Schlacher, 2015). Off Angola, the combination of a mid-water oxygen minimum zone with spatio-temporal variable surface production offers great opportunities to test how multiple abiotic influences such as resource availability and oxygen limitations interact to shape faunal distributions and community dynamics. The effects of the Benguela Niño and Niña events on faunal distributions and standing stocks also warrants further investigation to improve understanding of long-term faunal dynamics on continental slope settings in response to changing surface temperatures and ocean production.

There is emerging evidence of widespread flourishing Scleractinian cold-water coral reefs on the upper Angolan continental slope. Their unique occurrence within oxygen-depleted waters provide new avenues for further studies into the physiological tolerance of reef-forming taxa and their ability to adapt to climate related changes in the deep ocean (Hebbeln et al, 2020). Ecological, taxonomic and genetic comparisons with Atlantic and NW African coral reefs may offer new insights into population-specific genetic and phenotypic adaptations (Orejas et al., 2021), and may also allow for a deeper understanding of how local oceanographic characteristics influence reef formation and stability.

There is also some evidence of large-scale connectivity pathways between the Angolan Margin and other habitats around the Atlantic that should be better explored, such as the

hypothesised links between the seep fauna off Angola and the Gulf of Mexico. Knowledge of species composition and basic functional attributes is lacking as are the broader functions provided by the Angolan Margin's ecosystems.

The Angolan Margin offers many important ecosystem services, it supports major hydrocarbon activities and vital fisheries. Anthropogenic activities, both local and more widespread impacts such as those caused by climate changes, are increasing and may already be having broad scale effects. Limited knowledge of Angola's deep-water diversity and functioning remains a main barrier to effective conservation and management. Management of activities is increasingly important to Angola and regional-scale syntheses of information are greatly valuable to inform appropriate actions and encourage additional research.

# Chapter 3

# Epibenthic megafauna associated with sedimentary habitats on the Angolan continental slope

## Abstract

The increasing exploitation of marine resources from deep continental margins has reinvigorated interest in spatial patterns of bathyal habitat and species distributions, and the processes that control these patterns. Here we use an extensive set of still images to quantify the bathymetric and geographic variation in biodiversity, standing stocks, and composition of epibenthic megafaunal assemblages associated with the wider sedimentary environment of the poorly studied Angolan margin. A total of 42 photographic transects obtained between 2008 and 2014 from four locations along the northern and central parts of the continental slope in water depths between 480 and 2400 m were studied. Megafaunal invertebrate density declined with increasing depth from 102100 ind. $ha^{-1}$ at 480 m to 730 ind. $ha^{-1}$ at 1870 m. Deeper than 1900 m, densities of up to 19210 ind. $ha^{-1}$ were observed, caused by high densities of the irregular urchins *Pourtalesia* sp. A corresponding peak in invertebrate biomass of up to 56 g fwwt $m^2$ was observed at the deeper sites. Invertebrate richness remained low on the upper slope, then increased peaking at depths between 1100 and 1900 m. Invertebrate assemblage composition changed gradually with depth as a result of morphospecies replacement. The density of benthic and benthopelagic fish declined exponentially with increasing depth from 2305 ind. $ha^{-1}$ at 480 m to between 13-54 ind. $ha^{-1}$ at depths below 2000 m. The composition of fish assemblages changed from a dominance of smaller, benthic taxa to larger benthopelagic morphospecies with increasing depth. Small branching protists, possibly belonging to the genus *Schizammina*, were widespread along the upper and middle slope. By comparison with local and regional differences in sediment characteristics,

oceanographic conditions, and overlying production, the factors that may control megafaunal distributions are discussed.

## 3.1 Introduction

The deep-waters off Angola are characterised by a broad range of environmental settings. Oceanographic and hydrological processes, for instance, have led to the formation of permanent oxygen depleted waters and broad scale variability in surface production substantially regulated by the Congo River outflow and coastal upwelling. On the seafloor, a long history of salt tectonics and hydrocarbon formation and migration has created a variety of geomorphological and geochemical features on a wide range of scales from broader-scale canyon systems, bathymetric highs and diapiric ridges to localised fluid flow features less than a meter across (reviewed in Chapter 2). In addition, the Angolan margin contains substantial petroleum resources and is subject to ongoing deep-water hydrocarbon exploration and production (Burwood, 1999).

Knowledge about the biodiversity and ecology of the Angolan margin remains limited. This includes the deep-water benthic megafauna, which constitutes a major component of benthic systems (Gage and Tyler, 2010). The megafauna contributes substantially to benthic biomass (e.g. Haedrich and Rowe, 1977; Lampitt et al., 1986; Smith and Hamilton, 1983) and many ecosystem processes and characteristics, such as community respiration (Smith, 1983), nutrient cycling (Miller et al., 2000), and environmental heterogeneity (e.g. Beaulieu, 2001; Buhl-Mortensen et al., 2010, Gates et al., 2017; Levin et al., 1986; Smith et al., 1983). Previous studies investigating invertebrate megafaunal communities off Angola have focussed mainly on discrete habitats provided by cold seeps (e.g. Macron et al., 2004; Olu-Le Roy, 2007; Ondréas et al., 2005; Sahling et al., 2008), asphalt mounds (Jones et al., 2014), large food falls (Higgs et al., 2014), and organic rich sediments found across the terminal lobes of the Congo deep-sea fan (e.g. Sen et al., 2016, 2017). A rich scavenging megafauna has been described by Jamieson et al. (2017) for the middle and lower slope (c. 1300-2500 m). At mid-slope depths (c. 1400 m), recent analysis of photographic time series data collected from the Deep-ocean Environmental Long-term Observatory Systems (DELOS; Vardaro et al., 2013) has shown strong seasonal cycles in the abundance of demersal fishes (Milligan et al., 2020).

Faunal distributions are controlled by multiple biotic and abiotic processes that act on different spatial and temporal scales (Levin, 2001). At broader spatial scales, benthic margin communities are strongly structured by water depth (Gage and Tyler, 2010), which is likely to reflect the combined influences of evolutionary history and contemporary abiotic and biotic processes such as those driven by the strong bathymetric gradients in hydrographic and physico-chemical conditions (e.g. Levin et al., 2001; Wiens, 2011; Ricklefs, 1987). Metazoan densities generally decreases with increasing water depth (e.g. Billet et al., 1986; Hughes and Gage, 2004; Duineveld et al., 1997; Merrett and Marshall, 1981), which is thought to reflect the decline in organic matter supply (e.g. Rex et al., 2006; Wei et al., 2010). Trends can vary among regions, which has been related to large-scale variations in surface production (e.g. Merrett and Marshall, 1981) and phytodetrital flux (Thurston et al., 1994). Finer scale variations in megafaunal standing stocks have been linked to a range of, often interacting, factors, such as variations in local topography and geology (e.g. Hecker et al., 1990; Jones et al., 2012), sediment grain size distributions (e.g. Durden et al., 2015), and resource availability (e.g. Duineveld et al., 1997; Morris et al., 2016).

The composition of metazoan assemblages has long been known to vary continuously along the depth gradient (Carney, 2005). These changes are for large parts gradual, interspersed with zones of larger faunal turnover with the latter shown to vary among regions (Carney, 200; Menot et al., 2010b). More sharp faunal boundaries have been reported from areas with rapid changes in environmental conditions, such as found across oxygen minimum zones (OMZ) (e.g. Gooday et al., 2009). Broad-scale variations in species richness along the depth gradient are also commonly observed, though most studies have involved the macrofauna (Rex and Etter, 2010; Menot et al. 2010b). Several studies have recorded a parabolic trend with peaks occurring at mid slope depths (Menot et al., 2010b; Rex and Etter, 2010). However, deviations from the unimodal trend have been reported, suggesting that, compared to changes in faunal density and composition, richness patterns may more variable among taxonomic groups and ocean basins (McClain et al., 2009).

In this study, we use photographic data collected from the upper to lower Angolan continental slope to gain a better understanding of broad-scale spatial patterns of epibenthic megafaunal communities associated with widespread soft-bottom habitats.

Such knowledge is central to the conservation and management of natural resources and to address fundamental ecological questions about species distributions and their underlying causes (Levin and Dayton, 2009). We hypothesise that water depth and associated gradients in organic matter flux, dissolved oxygen concentrations, and sediment characteristics will strongly influence the density, biomass, and composition of epibenthic megafauna. Specifically, we aim to test whether (1) metazoan standing stocks show bathymetric and geographic trends in relation to gradients in organic matter input, (2) metazoan composition changes continuously along the depth gradient and varies geographically along the slope, and (3) megafaunal species richness displays any trend with water depth.

## 3.2 Materials and methods

### 3.2.1 Data sources and study sites

The photographic data used to examine the megabenthic ecology was acquired during three surveys: in austral spring of October/November 2005 on the MV *Ocean Endeavour* (Bett, 2007), in late austral summer of March/April 2008 on MV *Sea Trident* (Hughes and Hunt, 2008), and in austral winter of late July to early September 2014 on MV *Ocean Discovery* (IMAR Survey, 2015a). All surveys were commissioned by BP plc to inform planning of their deepwater hydrocarbon exploration and production programme in Angola. The environmental investigations targeted four areas (A to D) in the upper and lower bathyal along the northern and central parts of the Angolan continental slope, extending from about 6° to 12°S and 10° to 13°E and covering water depths between about 480 m to 2400 m (Figure 3.1).

Study area A extends from about 6°S to 6.8°S, with photographic sites spanning water depths between 1400 to 2400 m (Figure 3.2a). The seafloor of the shallower sections down to about 1600 m has a relative uniform topography with slope angles of between 0.5-3°. Across the deeper parts, the uplift of subsurface salt structures combined with the migration of hydrocarbons has created a less regular terrain with numerous topographic features, such as small seafloor mounds, pockmarks, narrow troughs, and long ridges with reliefs of up to several 100 metres and locally steep slopes of greater than 15° (Gay et al., 2007; Hill et al., 2010). Study area B (7.8-7.9°S, 1160-1650 m, Figure 3.2b) has a relative

smooth topography down to about 1400 m with slope angles of between 0.7-1.5°. Below this point, the seafloor is interspersed with pockmarks and small furrows. A similar morphology is observed in Area D (11.8-12.2°S) although pockmark fields are present across the whole depth range sampled (780-1750 m, Figure 3.2d). The seafloor in Area C (8.8-9.2°S, 480-1430 m) is characterised by a large sinous submarine canyon and several associated channel complexes, which dissect the slope in a predominantly southeast to northwest direction (Figure 3.2c). In addition, bathymetric data indicate the presence of numerous downslope trending gullies along the upper and middle slope in the southern portion of the study area. Across the lower slope sections, deeper than 1000 m, seafloor ridges formed by salt uplift (BP, 2013) are prominent.

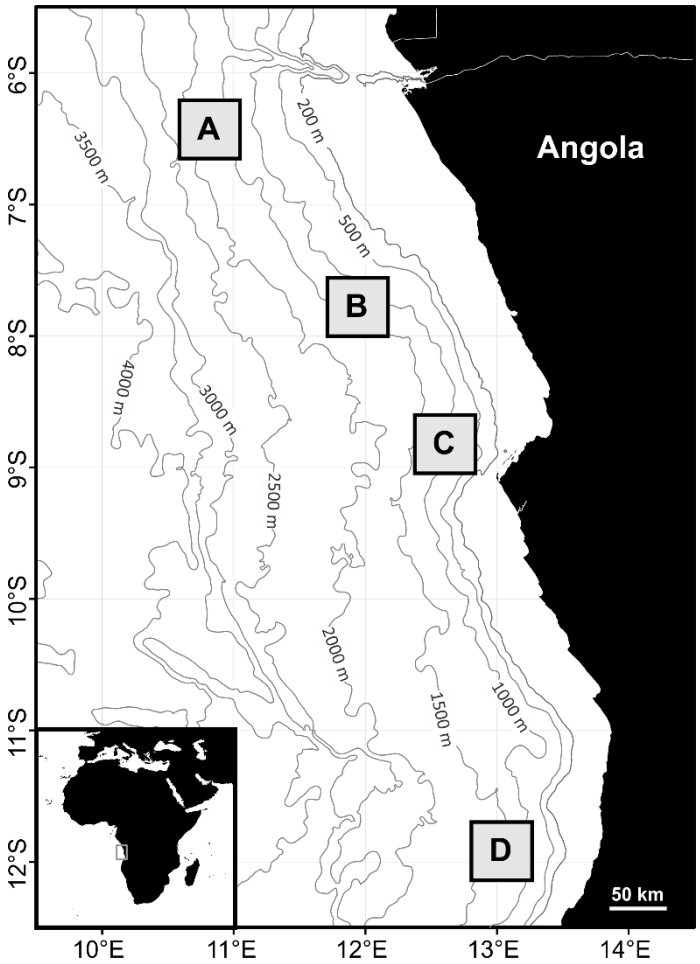


**Figure 3.1** Map of the northern and central Angolan continental margin showing the positions of the four areas under study. Inset shows the location of the study area in the southeast Atlantic Ocean. The four study areas correspond to the Angolan offshore Petroleum Licence Blocks 31, 18, 19 and 24 (from north to south). Bathymetry is shown as simplified contours based on 30 arc-second interval GEBCO (General Bathymetric Chart of the Oceans) data (GEBCO Compilation Group, 2019).

The overlying waters off Angola show high primary productivity governed by an interplay of the large Congo River outflow and associated river-induced upwelling (Da Cunha et al., 2013; Schneider et al., 1994; van Bennekom and Berger, 1978), and seasonally varying coastal (e.g. Ostrowski et al., 2009; Kopte et al., 2017) and oceanic (Mazeika, 1967) upwelling events. The seafloor along the continental slope and rise is influenced by three water masses. Between about 100 m to 500 m water depth, Central Water originating in the Indian and south-western South Atlantic Oceans (Stramma and Schott, 1999; Poole and Tomczak, 1999) is fed into the region by the eastward flowing components of the equatorial circulation system (Stramma and England, 1999). Its upper portion down to about 400 m is transported within the Angola Current (Dias, 1983; Moroshkin et al., 1970), which is characterised by periodically changing southward and northward currents of up to 40 cm $s^{-2}$ and a weak residual southward flow of up to 5-8 cm $s^{-1}$ in the upper 160-200 m (Kopte et al., 2017). A permanent layer of oxygen-depleted water (< 1 ml $l^{-1}$) is present at depths between 300-500 m (Chapman and Shannon, 1987), locally with dissolved oxygen concentrations of < 0.5 ml $l^{-1}$ (Helly and Levin, 2004). Below Central Water, Antarctic Intermediate Water derived mainly from surface waters in the circumpolar layer of the Southern Ocean is located between about 500 to 1200 m depth, while the lower slope sections and the continental rise are affected by North Atlantic Deep Water (Stramma and England, 1999). Current meter readings evidenced semi-diurnal, inertial (4 to 5 days) and biweekly current oscillations at locations on the middle (Vangriesheim et al., 2005; Vardaro et al., 2013) and lower slope (Vangriesheim et al., 2009). Present-day sedimentation across the slope is dominated by fine-grained hemipelagic inputs supplied by the Congo River (Anka et al., 2009; Eisma and Kalf, 1984). Transport of coarser fluvial sediments is restricted to the large Congo submarine canyon, which dissects the slope in a westward direction at about 6°S.

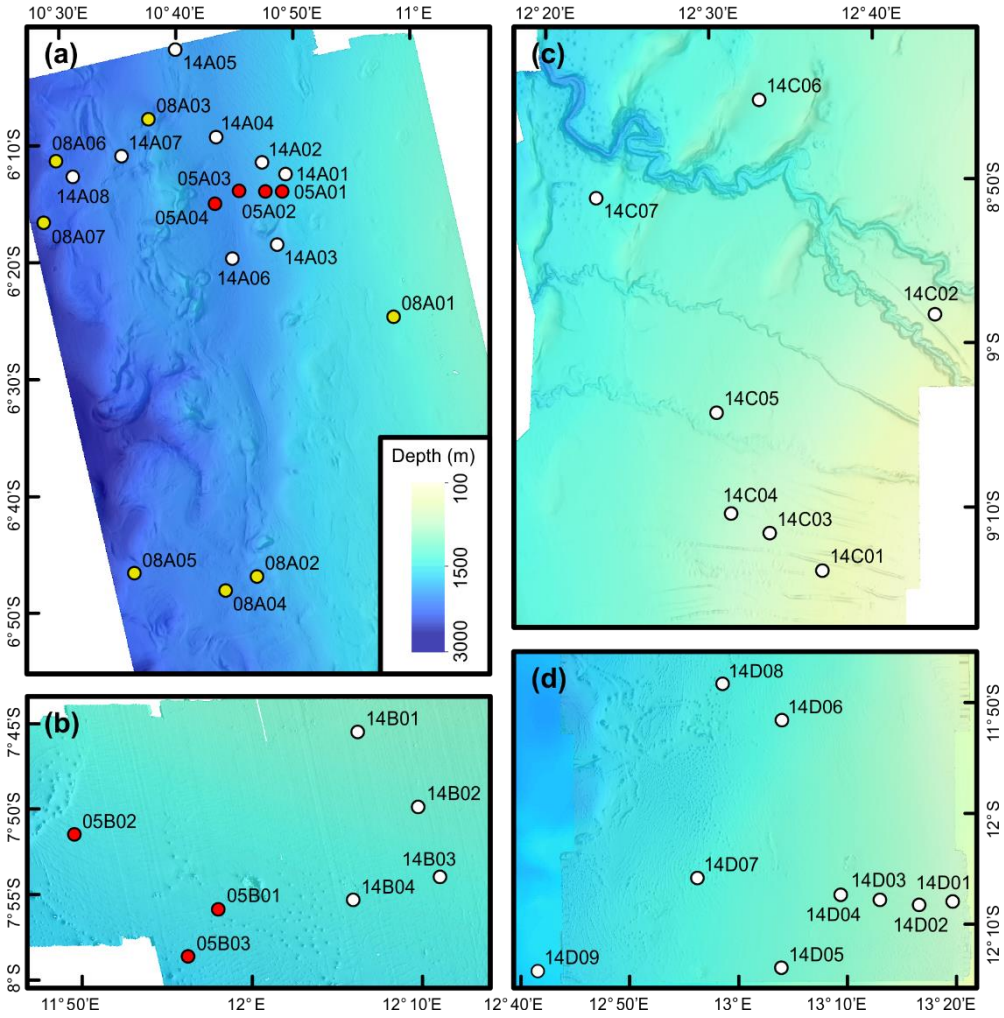


**Figure 3.2** Shaded relief bathymetry maps for the four areas under study, marked with the centre locations of the camera deployments undertaken in 2005 (red symbols), 2008 (yellow symbols) and 2014 (open symbols). Bathymetric data are based on large scale seismic data and were supplied by BP processed to 25 x 25 m resolution for study areas A **(a)**, B **(b)** and C **(c)**, and 13 x 13 m for Area D **(d)**. Shaded reliefs were derived from multidirectional hillshading as implemented in ArcGIS v10.5 and are vertically exaggerated by a factor of two.

### 3.2.2 Collection of photographic data

All photographic data were collected with towed-camera platforms across areas of comparatively featureless soft substratum of low relief, which had been identified prior to each survey from acoustic data interpretations. Transect locations were all randomly placed within depth bands (100 or 200 m wide) following a stratified random sampling approach. The location and spatial extent of the four sampling areas was driven by BP's hydrocarbon interests in the region, and therefore the number of transects per area and depth stratum was not spatially balanced (Table 3.1).

**2014 survey** (Area A, B, C and D): The majority of the photographic data was collected in 2014 when 28 transects were completed, ranging in length from approximately 600 to 2700 m (Figure 3.2a-d). Video was continuously recorded with a wide angle high-definition video camera (SubCControl 1Cam) (IMAR Survey, 2015a), while digital stills were taken every 15 seconds with a vertically mounted downward facing 14 megapixel Imenco TigerShark SDS1210 camera (4320 x 3240 pixels), which was later replaced with a 5 megapixel Kongsberg OE14-208 camera (2592 x 1944 pixels). Two sets of parallel lasers (7 and 10 cm apart) provided capabilities for scaling. Positional information was recorded every 3 seconds with an ultra-short base line (USBL) beacon linked to the ship's Sonardyne acoustic tracking system.

**2008 survey** (Area A): During the 2008 survey, seven transects between approximately 430 and 650 m long were sampled across six depth strata in Area A (Figure 3.2a) using the Seatronics DTS 6000 Mini Multiplexer camera platform. Still images were typically taken every 10 seconds with a Kongsberg OE14-2008 camera (2592 x 1944 pixels), which was triggered manually to account for varying flash recharge times and movements of the camera frame caused by swell of the towing vessel (Hughes and Hunt, 2008). A pair of parallel point lasers spaced 38 cm apart was used for scaling, and camera positions were logged with an USBL transponder beacon.

**2005 survey** (Area A and B): In 2005, seven sites were surveyed, four in Area A and three in Area B, using the National Oceanography Centre's (NOC) Wide-Angle Seabed Photography (WASP) system, which was fitted with a Simrad Mesotech 200 kHz altimeter to record camera height above the seabed, an active transmitter (10 kHz) for telemetry, a vertically mounted OceanCam6000V video camera, and a vertically mounted OSIL (Ocean Scientific International Limited) Mk7 film camera (Bett, 2007). Still images were taken automatically every 12 seconds and recorded onto 35 mm Kodak Vision 250D film along with frame identification number and camera altitude. Transect lengths varied from approximately 160 to 770 m. Further details for each camera deployment including transect locations are reported in the Supplementary Information (Section 3.6, Table S3.1).

**Table 3.1** Number of photographic sites and associated depth strata surveyed in 2005, 2008 and 2014 to characterise megafaunal soft sediment assemblages along the Angolan continental slope. Area letters as shown in Figure 3.1. Numbers in brackets represent the number of transects per sampled depth band.

| Area | Sites | Depth strata |
|---|---|---|
| MV *Ocean Endeavour* 13/10-06/11 2005 | | |
| A | 4 | 1700-1800 (1), 1800-1900 (1), 1900-2000 (1), 2000-2100 (1) |
| B | 3 | 1500-1600 (2), 1600-1700 (1) |
| MV *Sea Trident* 28/03-23/04 2008 | | |
| A | 7 | 1400-1500 (1), 2000-2100 (2), 2100-2200 (1), 2200-2300 (1), 2300-2400 (1), 2400-2500 (1) |
| MV *Ocean Discovery* 04/07-11/09 2014 | | |
| A | 8 | 1600-1800 (1), 1800-2000 (3), 2000-2200 (3), 2200-2400 (1) |
| B | 4 | 1100-1200 (1), 1200-1300 (1), 1300-1400 (1), 1400-1500 (1) |
| C | 7 | 400-500 (1), 600-700 (2), 800-900 (1), 1000-1100 (1), 1200-1300 (1), 1400-1500 (1) |
| D | 9 | 600-800 (1), 800-1000 (2), 1000-1200 (1), 1200-1400 (2), 1400-1600 (2), 1600-1800 (1) |

### 3.2.3 Analysis of photographic data

Faunal patterns were quantified based on analysis of the still images, while the video footage was used to get a general understanding of the seabed environment and to complement taxa identifications. Photographs that were overexposed, out of focus, or where suspended matter obscured view of most of the seabed were excluded. To maximise the number of suitable images, photographs whose edges were affected by backscatter or vignetting were cropped, either to pre-defined sizes using the batch processing tool in Adobe Photoshop CS6 or, in the case of the films, by identifying unsuitable areas as part of the annotation process. Image vignetting in the photographs from 2014 was further reduced through flatfield corrections using MATLAB (R2015a) as described by Morris et al. (2014). The seabed area covered by an image was calculated based on camera acceptance angles and image altitude (2005 data) as described by Jones et al. (2009) or, when camera height was unknown (2008 and 2014 data), by using the scale provided by the laser markers following the trigonometric approach outlined in Durden et al. (2016). Scaling measurements were made using the ImageJ software (Schneider et al., 2012). To ensure only non-overlapping images were retained, image footprints were mapped based on image position, image size, and if known, camera heading, using multiple functions from the 'stringi' (Gagolewski et al., 2019), 'sp' (Pebesma and Bivand, 2005) and 'rgdal' (Bivand et al., 2019) packages in R (R Core Team, 2020). In the case of the films, where

positioning information could not reliably be matched to individual frames, potential overlaps were first estimated from calculated vessel speeds, and then verified during the annotation process.

Annotation of the digital images collected in 2008 and 2014 was carried out with the image analysis software Image-Pro Plus v7.0 (MediaCybernetics). To detect specimens, we used a constant maximum magnification, while taxonomic identification and measurements of physical dimensions were made, if required, at higher magnification. The photographic films collected in 2005 were annotated with a Carl Zeiss Jena DLZ Dokumator film viewer, set to a constant 9x zoom for specimen detection. In each photograph, all fauna was recorded and measured using a standard dimension pre-defined for each expected faunal class. We included partially buried megafaunal specimens with body parts extruding above the sediment, such as ophiuroids and asteroids. Surface dwelling specimens, epibenthic gastropods, and mobile tubicolous polychaetes (quill worms) were recorded when trails behind the specimen indicated recent movement or when parts of the organism's soft tissue were visible. Sediment tubes extruding from the seabed were not counted as it was not possible to determine whether they were inhabited.

Specimen identification was based on morphology visible in images and facilitated through a morphospecies image catalogue (Appendix B), which was developed with help from taxonomic experts and by reference to deep-water taxonomic literature, identification guides as well as published image-based morphospecies lists from the region (Jamieson et al., 2017; Jones et al., 2014; Vardaro et al., 2013). Owing to the variation in image altitudes and the angle at which specimens were photographed some morphospecies could not consistently be identified to the same taxonomic level. For statistical analyses, these morphotypes were aggregated to the lowest taxonomic rank that allowed consistent identification across all processed photographs.

Finally, we estimated the biomass of all metazoan specimens by applying the generalised volumetric method of Benoist et al. (2019), which uses biovolume as predictor for body mass. Details of the morphometric measurements taken to calculate biovolume are given in the Supplementary Information (Section 3.5.3.1). The estimated volume of each metazoan megafauna was converted to fresh body mass (g fresh wet weight [fwwt]) assuming a volumetric mass density of 1 g $cm^{-3}$. Foraminifera were omitted from biomass estimations since it could not be determined whether they were alive.

### 3.2.4 Data analyses

Preliminary analysis of the image data indicated a decrease in the detectability of smaller morphospecies with increasing image altitude (for details see Section A7 in Appendix A). Therefore, faunal analyses were limited to images taken between 0.8 and 3.5 m above the seabed and specimens > 1 cm in maximum dimension. Images collected at sites 14D01 (Area D, 780 m) and 14D03 (Area D, 1104 m) were only used to quantify faunal density and biomass owing to lower image quality, which impeded morphospecies identification to the same detail as for the remaining transects. The majority of images taken at 14D03 were slightly out of focus, while images from 14D01 site showed high loads of resuspended sediments, likely from demersal fishing activities that had been observed in the area prior to the camera deployment (IMAR Survey, 2015a).

Also omitted from analysis were ectoparasites and any invertebrate morphotype recorded exclusively off-bottom, i.e. chaetognaths, Scyphozoa, Ctenophora, Copepoda, and specimens of the elpidiid holothurian *Peniagone* msp-2. The latter morphospecies resembled the planktonic holothurian *Peniagone diaphana* recorded by Barnes et al. (1976) off Southern California. Off Angola, it occurred in high abundances above the seabed at several locations in Areas A and B, which was most noticeable in the video footage. However, these small, semi-transparent specimens were either not present or not detectable on or just above the substrate and were therefore omitted from analysis. Among the retained megabenthic specimens, all were included in the quantification of standing stocks, while specimens that could only be assigned to general groups (e.g. Cnidaria spp. indet.) were excluded when analysing patterns in diversity and faunal composition. The structure of invertebrate assemblages was examined separately from the ichthyofauna as the latter commonly contains a mixture of both benthic and benthopelagic species. Likewise, the distribution of protists was assessed separately from metazoan megafauna as it could not be determined from the imagery whether they were alive.

#### 3.2.4.1 Standing stocks

Comparisons of megabenthic standing stocks were performed at transect level, with specimen counts and biomass estimates standardised for each transect to the total seabed area analysed. To obtain variance estimates for each parameter, we applied a modified form of non-parametric bootstrapping (Davison and Hinkley, 1997; Puth et al., 2015). For each transect, the analysed image data set was first randomly resampled 1000 times with replacement. Invertebrate and fish numerical density and biomass were then computed for each of the 1000 bootstrapped samples, from which mean density and median biomass were subsequently derived. Corresponding 95% confidence intervals for the parameter estimates were approximated using the simple percentile method, with the upper and lower confidence bounds expressed as the 2.5% and 97.5% percentile of the bootstrapped replicates (Davison and Hinkley, 1997). Given the relatively low number of individuals and morphospecies sampled in 2005 and 2008, estimation of confidence intervals using bootstrapping was only conducted for the 2014 image data set.

In addition to the variation in density and biomass estimates between transects, the distribution of numerical density among invertebrate morphospecies and the distribution of invertebrate biomass was compared graphically for each transect sampled in 2014 using the Abundance-Biomass Comparison (ABC) method (Warwick, 1986), which is based on the comparison of morphospecies density and biomass k-dominance curves. Differences between abundance and biomass dominance patterns have traditionally been employed to detect pollution-induced disturbances of marine benthic communities in shallow waters (e.g. Agard et al., 1993; Warwick, 1986) and were here used more generally as a potential proxy for the degree of environmental perturbation. Following Clarke (1990), we subsequently calculated the W-statistic from each ABC plot to facilitate the analysis of spatial trends. The W-statistic quantifies the difference between the respective density and biomass k-dominance curves as a single value. It is constraint between -1 and 1, with negative values being hypothesised to indicate disturbed environments with an immature successional stage where the density curve lies above the biomass curve, and vice versa positive values being indicative of assemblages exposed to less environmental stress potentially representing more mature conditions where the density curve is located below the biomass curve (Clarke, 1990). All calculations concerning faunal density and biomass

and the construction of the k-dominance curves were performed in R (R Core Team, 2020) using a series of custom scripts.

#### 3.2.4.2 Alpha diversity

Patterns in alpha diversity were assessed based on the effective number of species (i.e. Hill numbers, *sensu* Hill, 1973), expressed as (1) morphotype richness $^{0}D$, (2) the effective number of common morphotypes (exponential form of Shannon entropy exp $H'$ or $^{1}D$), and (3) the effective number of dominant morphotypes (reciprocal of Simpson's concentration index 1/D or $^{2}D$). To account for sample size dependencies on the number of taxa encountered (e.g. Gotelli and Colwell, 2001), comparisons of diversities among transects were based on diversity estimates at equivalent sample sizes, which we determined from rarefaction and extrapolation curves. For morphospecies richness, sample-based rarefaction and extrapolation curves with unconditional variance estimates were constructed based on the analytical method of Colwell et al. (2012), as implemented in EstimateS v9.1 (Colwell, 2013), using individual photographs as sampling units. For $^{1}D$ and $^{2}D$, sample-based rarefaction and extrapolation curves with associated 95% confidence intervals were computed by resampling using the formula of Chao et al. (2014), implemented in the R package iNEXT (Hsieh et al., 2016) and based on 100 random permutations, again using individual photographs as sampling units. Additionally, coverage-based rarefaction and extrapolation (Chao and Jost, 2012; Chao et al., 2014) was applied to examine morphospecies richness patterns. This approach allows rarefied and extrapolated richness to be compared based on equal levels of sample completeness rather than equal sample sizes. Sample coverage was computed based on the method of Chao and Jost (2012), as implemented in the R package iNEXT. Following the recommendation of Colwell et al. (2012), we extrapolated diversity measures to double the number of sampling units (images) annotated for each transect. For transect-level comparisons of morphospecies richness, the effective numbers of morphospecies were standardised to the number of accumulated individuals or sample coverage, while morphospecies density was assessed based on diversity standardised to the seabed area sampled. Linear interpolation between rarefied or extrapolated values of consecutive samples was used to approximate diversity values for a common sample size (number of individuals, area sampled, and sample coverage), using the 'approx' command in R (R Core Team 2020). Non-

overlapping 95% confidence intervals were taken as indicative of significant differences at a level < 5%. In addition to Hill numbers $^0D$ to $^2D$, we assessed assemblage evenness using Pielou's evenness index J' (Pielou, 1966), expressed as = ln $^1D$ / ln $^0D$ (Jost, 2010). Contrary to the diversity measures, we computed evenness for the observed number of morphospecies given the strong dependence of evenness on species richness (Jost, 2010).

Owing to the relatively low number of fish and protist morphospecies as well as the comparatively low number of images obtained in 2005 and 2008, and the resulting low numbers of recorded individuals and morphospecies (Table S3.1), alpha diversity patterns were only assessed for the invertebrate metazoan morphospecies recorded in 2014. The relationships between the different diversity metrics and the presence of bathymetric trends was assessed using Spearman's rank correlation method, as implemented in R, with significant trends reported at the 1% and 5%. To control the rate of false positives (type I error rate) in multiple significance testing, threshold levels for significance were adjusted using Holm's sequential Bonferroni procedure (Holm, 1979; Rice, 1989). Noticeable along-slope variations in parameter estimates were described but not formally tested as factorial analysis was not possible with the uneven spatial distribution of the photographic transects.

#### 3.2.4.3 Assemblage composition

Spatial trends in invertebrate assemblage composition were examined with classification and unconstrained ordination methods, both implemented in R using functions from the 'vegan' (Oksanen et al., 2019), 'cluster' (Maechler et al., 2019) and 'stats' (R Core Team, 2020) packages. Non-metric multi-dimensional scaling (NMDS) was applied to visualise assemblage similarities in two dimensions, using the 'metaMDS' command. In addition, we carried out hierarchical agglomerative clustering on the pairwise faunal dissimilarities using the between-group average linkage (UPGMA) method for comparison with any assemblage groupings identified from the ordination. Clustering and ordination were carried out for both the 2014 invertebrate data set and the combined invertebrate data set (all years) using Bray-Curtis dissimilarities (Bray and Curtis, 1957) computed on the fourth-root transformed standardised invertebrate densities. The fourth-root transformation was chosen to examine compositional differences in both common and rarer morphospecies (Clarke and Warwick, 2001). The silhouette method (Rousseeuw,

1987) was applied to assess how well sites were matched to their assigned clusters. The cluster groupings that best partitioned the data were subsequently used to identify those invertebrate morphospecies typical of main faunal groups (1) by comparing the proportional contributions of the five most abundant morphotypes of each photographic site, and (2) by applying the 'species indicator values' method (Dufrêne and Legendre, 1997) to the fourth-root transformed densities using the 'indicspecies' package (De Caceres and Legendre, 2009) in R.

To assess the rate of faunal change along the studied depth gradient, a modified form of Cody's beta diversity index $\beta_c$ was computed for the 2014 data set (Cody, 1975; Magurran, 2004), expressed as $\beta_c = (g_s + l_s) / 2$, where $g_s$ denotes the number of morphospecies gained along the bathymetric gradient and $l_s$ represents the number of morphospecies lost. Following previous work applying $\beta_c$ (e.g. Gooday et al., 2010), gained morphospecies were subtracted from the shallowest site sampled and lost morphospecies doubled to compensate, while for the maximum depth sampled lost morphospecies were discounted and arrivals doubled. Finally, we adopted the approach of Baselga (2010), as implemented in the R package 'betapart' (Baselga et al., 2018), and partitioned the total Sørensen index of dissimilarity ($\beta_{SOR}$) for all photographic sites sampled in 2014 into its nestedness ($\beta_{NES}$) and spatial turnover ($\beta_{SIM}$) components to evaluate their respective contributions to bathymetric and geographic differences in invertebrate assemblage composition.

#### 3.2.4.4 Environment-Faunal relationships

To examine the influence of environmental conditions on patterns in megabenthic assemblage structure, a set of environmental data was collated from both publicly available sources and unpublished data supplied by BP. This information was assessed in two stages: First, the environmental data were examined for any broad-scale patterns and differences among the four areas studied. Second, environmental data were extracted for each of the photographic sites to formally test their relationships with ecological descriptors.

Mean water depth for each phototransect was computed from the USBL positioning data, and cross-checked with multibeam bathymetry data supplied by BP for each of the four sampling areas (as shown in Figure 3.2). Oceanographic properties (temperature, salinity and dissolved oxygen concentrations) were examined from twenty CTD casts (Appendix

C, Table C.1) that were obtained with a Valeport 606+ multiparameter instrument across the four study areas during the 2014 environmental survey (IMAR Survey, 2015a).

Data on surficial (top 3-5 cm) sediment properties (particle size distributions, and nitrogen and organic carbon contents) were sourced from unpublished BP reports (Bett, 2007; ERT, 2006, 2008; Hughes, 2008; IMAR Survey, 2015a-e). They were based on megacore samples (10 cm internal diameter) taken across relative featureless areas of fine-grained substratum during the cruises conducted in 2005, 2008 and 2014. Megacore sampling followed a stratified random design with two to four core stations per 100 m depth interval. A description of the analytical methods employed by BP to measure the sediment parameters are presented in Appendix C (Section C.2). In summary, grain size distributions were quantified by dry sieving (coarse fractions) and laser diffraction (fine fractions) after removal of organic material with hydrogen peroxide. Concentrations of total organic carbon (TOC) and total nitrogen (TN) were measured by combustion analysis with automatic elemental analysers. Inorganic carbon was removed from samples prior to TOC measurements using acidification. For statistical analyses, granulometric size fractions were converted to the Wentworth (1922) grain size scale. In addition, grain size distribution statistics (mean grain size, sorting, skewness and kurtosis) were computed with GRADISTAT (version 8.0, Blott and Pye, 2001) for each core sample using Folk and Ward (1957) graphical moment methods. The variability in sedimentological characteristics among core sites was visualised using Principal Component Analysis (PCA), computed in R using the 'rda' routine of the vegan package (Oksanen et al., 2019), based on Euclidean distances between normalised (unit variance and zero means) sedimentological parameters. Centred-log-ratio transformations were applied to the weight percentages of the grain size fractions prior to normalising the data to overcome the closed structure of compositional data (Aitchison, 1982).

To explore patterns in surface production, depth integrated multi-year estimates of Net Primary Productivity (NPP) from the Standard Vertically Generalised Production Model (VGPM) of Behrenfeld and Falkowski (1997), based on MODIS R2018 data, were obtained from http://www.science.oregonstate.edu/ocean.productivity/index.php. A mean annual rate of net primary production (gC $m^{-2}$ $yr^{-1}$), averaged over 15 years (2003-2017), was computed from gridded (1/12°) monthly NPP data and mapped using ArcGIS software (v.10.5) to assess spatial differences in surface production along the Angolan

continental slope. Yearly NPP climatologies (annual mean production in mgC $m^{-2}$ $day^{-1}$ and associated standard deviations) were used to approximate particulate organic carbon (POC) fluxes to the seabed using the Lutz algorithm (Lutz et al., 2007). In addition, we estimated monthly POC flux rates using the algorithm described in Pace et al. (1987) to examine spatial patterns in the seasonal variation of organic matter supply.

The multidimensional spatial relationship among environmental variables was analysed with Principle Component Analysis (PCA) using the 'vegan' package in R. Associations between environmental variables and univariate ecological descriptors were explored using pairwise Spearman rank correlations with significance thresholds adjusted using Holm's (1979) sequential Bonferroni method.

## 3.3 Results

### 3.3.1 Environment and physical settings

#### 3.3.1.1 Regional observations

***Sedimentological characteristics***

Analysis of the sedimentary data collected in 2014 revealed strong variations in sediment properties with water depth and among locations (Figure 3.3). Sedimentary organic carbon content (TOC) varied from 1.3 to 4.5 wt% (Figure 3.3b) and showed a significant monotonic decline with increasing water depth when assessed across all megacore stations and sampling areas ($r_s$ = -0.84, $p < 0.01$; Table S3.2). Likewise, there was a significant negative correlation between TN and water depth ($r_s$ = -0.81, $p < 0.01$), with values ranging between 0.17 and 0.55 wt%. The estimated POC flux to the seabed was significantly ($p < 0.01$) positively correlated with both TOC ($r_s$ = 0.73) and TN ($r_s$ = 0.68). Carbon-nitrogen ratios (TOC/TN) varied from 5.8 to 8.8, except for one sample in Area B (1380 m, TOC/TN = 10.6), indicating that marine algae were the predominant source of the organic matter found in surficial sediments across the background slope environment (Meyers, 1994).

The largest variation in TOC and TN contents as well as in sediment particle size distributions occurred among samples from Area C, where the mud (silt + clay) content ranged from 30.9-96.5% (Figure 3.3a). Sediments were poorly to very poorly sorted with

unimodal or bimodal grain size distributions. Principal Component Analysis performed on the core data indicated that differences in sediment properties were defined most strongly by differences in the relative proportions of grain size fractions (PC1, eigenvalue 8.2) and to some extent by sediment sorting (PC2, eigenvalue 1.7; Figure S3.1e). Specifically, the analysis flags a divide of deeper sites associated with higher proportions of coarse grains (> 63 μm) and low sediment sorting near the canyon system in the north of the study area, and shallower sites linked to high silt and clay contents at the south. A third group associated with coarser better sorter sediments included shallower and deeper sites. Overall this data indicates large variation in sediment properties across Area C at both broader and local scales, which might reflect highly variable hydrodynamic conditions driven by the large heterogeneity in seafloor topography.

Large variation in grain-size distributions were also observed at mid-slope depths in Areas B and D, with silt and clay content varying from 51 to 90% in Area B, and from 54-94% in Area D at similar depths. Grain-size distributions were unimodal and poorly sorted in samples from these areas and also across Area A.

Comparison of the 2014 sedimentary data from Area A with those collected in 2005 and 2008 revealed unexpected area-wide differences in grain-size distributions, with samples collected in 2005 and 2008 containing substantially larger proportions of silt and clay (Figure S3.2), including in samples taken an stations sampled repeatedly over the years for monitoring purposes. Slightly deeper depth horizons were sampled in 2005 (top 4 cm) and 2008 (top 5 cm) compared to 2014 (top 3 cm, Table C.2), which might, at least, partly explain the greater proportion of silt and clay content, assuming an increase in finer material with sediment core depth. A widespread re-distribution of surface material or new large-scale deposition events or analytical differences in grain size measurements might also have contributed to the observed differences.

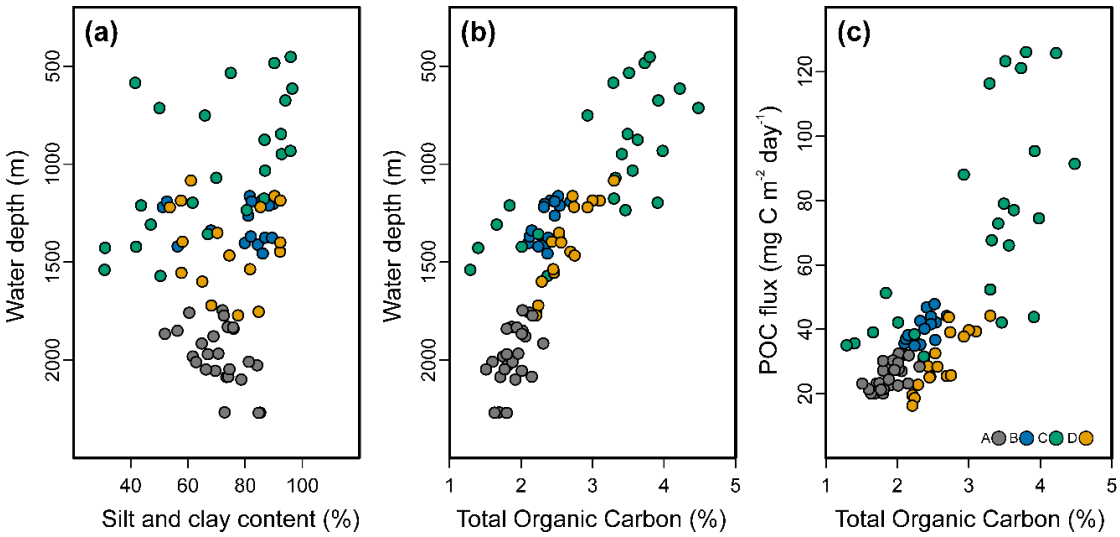


**Figure 3.3** Bathymetric variation in the proportion of mud **(a)** and Total Organic Carbon **(b)** in surficial sediment samples collected along the Angolan continental slope in 2014, keyed to study area (A-D). **(c)** Relationship between sediment TOC content and estimated POC flux to the seabed. POC flux was approximated using the Lutz algorithm (Lutz et al., 2007) and represents mean annual flux rates averaged for the period from 2003 to 2017. NPP estimates used in the flux calculations were derived from 15 years of monthly NPP values based on the Vertically Generalized Production Model of Behrenfeld and Falkowski (1997).

### *Water column characteristics*

Vertical profiles of both salinity and temperature were broadly similar among the four sampling areas (Figure 3.4a and b), showing surface waters characterised by salinities above 35.6 PSU and temperatures between 19-22.6°C, which agrees well with other profiles taken across the Angolan continental shelf and upper slope during austral winter (Kopte et al., 2017; Ostrowski et al., 2007). Below a sharp thermocline (< 20 m), temperature decreased steadily to about 3.1°C at 2200 m with the rate of change declining at about 900 m and again at 1500 m. Salinity exhibited a pronounced minimum of 34.52 to 34.57 PSU near 750-850 m, consistent with the salinity minima that characterises Antarctic Intermediate Water (AAIW) throughout the Atlantic (Stramma and Schott, 1999). Similarly, concentrations of dissolved oxygen showed, in accordance with published profiles from the region (e.g. Chapman and Shannon, 1987; Hanz et al., 2019), a profound minimum in the Central Water mass at depths between about 250-500 m (Figure3.4c). However, in contrast to the temperature and salinity distributions, oxygen profiles varied noticeable among sampling areas. Minimum oxygen concentrations recorded in Areas C and D (cast minima 0.29-0.37 ml $l^{-1}$) were up to three times lower compared to levels recorded in Area B (0.62-0.7 ml $l^{-1}$) and Area A (0.83-0.92 ml $l^{-1}$).

Furthermore, while oxygen levels in Area A displayed a gradual decline from well oxygenated surface waters down to the oxygen minima, oxygen concentrations in Areas B to C fell rapidly within the first 50-100 m then remained relatively constant at 1.3-1.5 ml $l^{-1}$ (Area B) and 0.7-0.9 ml $l^{-1}$ (Areas C and D) down to about 100-230 m depth before declining further to reach minimum levels.

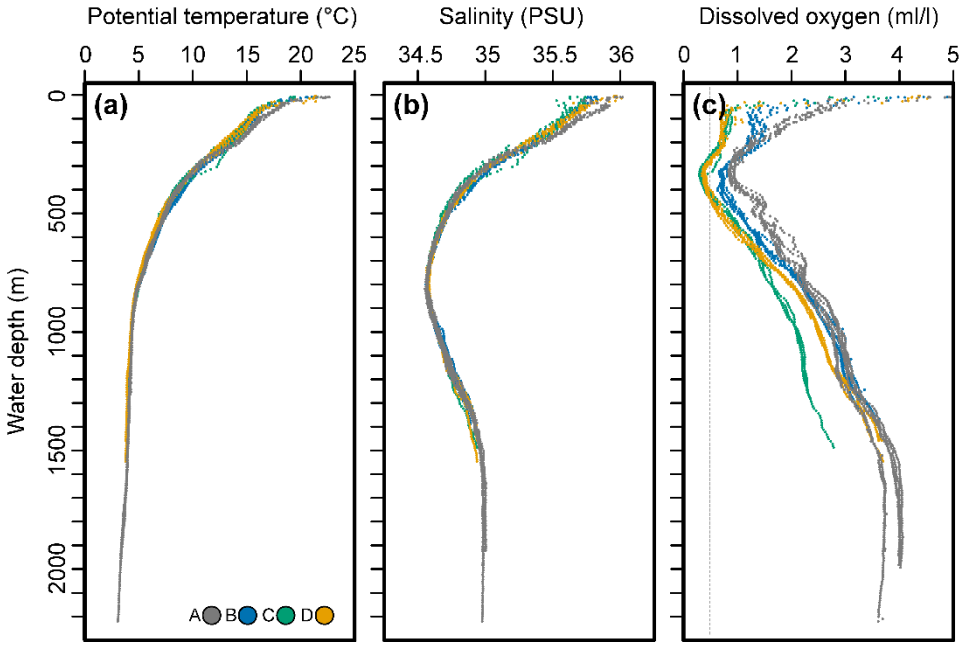


**Figure 3.4** Vertical profiles of **(a)** potential temperature, **(b)** salinity, and **(c)** dissolved oxygen concentrations based on twenty CTD cast obtained in July and August 2014 along the northern and central parts of the Angolan continental slope, keyed to study area (A-D). For each hydrocast, downcast data were averaged over 10db pressure bins. Dashed grey line shows oxygen concentration at 0.5 ml $l^{-1}$ (≈ 20 µmol $kg^{-1}$). Dissolved oxygen concentrations (ml $l^{-1}$) were calculated from measured oxygen saturation levels using the formula of Weiss (1970), and salinity (PSU) and potential temperature (θ) were computed as per Fofonoff and Millard (1983). For cast locations see Table C.1 in Appendix C.

### *Surface production and export flux*

Maps of estimated net primary productivity (Figure 3.5, a-c) indicate large spatial differences in surface production among the four study areas. The most productive waters are located across the upper slope in Area C (Figure 3.5c) and the lower slope sampled in the northern part of Area A (Figure 3.5a), the latter reflecting the influence of the Congo River outflow.

There are also clear geographic differences in seasonal variation in NPP, with waters overlying the lower slope in the northern part of Area A (Figure 3.5d) exhibiting much less monthly variability than do waters located across the mid-slope sections sampled in Area B (Figure 3.5e) and the upper to lower slope in Area D (Figure 3.5f). Similarly,

waters located above the upper to mid-slope sections sampled in Area C showed less intra-annual variation in surface production (Figure 3.5e) than waters above upper and mid-slope depths in Area D (Figure 3.5f).

The distinct differences in NPP seasonality and net production among the sampling areas are reflected in the estimated monthly POC flux rates to the seabed (Figure S3.3), which suggest organic matter supply along the Angolan slope to vary as a function of both depth and geographic location (Figure S3.3). For instance, from January to May, outside the upwelling periods, similar or greater flux rates are estimated for the lower slope areas in Area A compared to the mid-slope sites sampled in Areas B to D, reflecting the comparatively high NPP around the Congo River outflow all year around. Overall, estimated monthly POC flux rates to the seabed peak in the period June-August during the main coastal upwelling event.

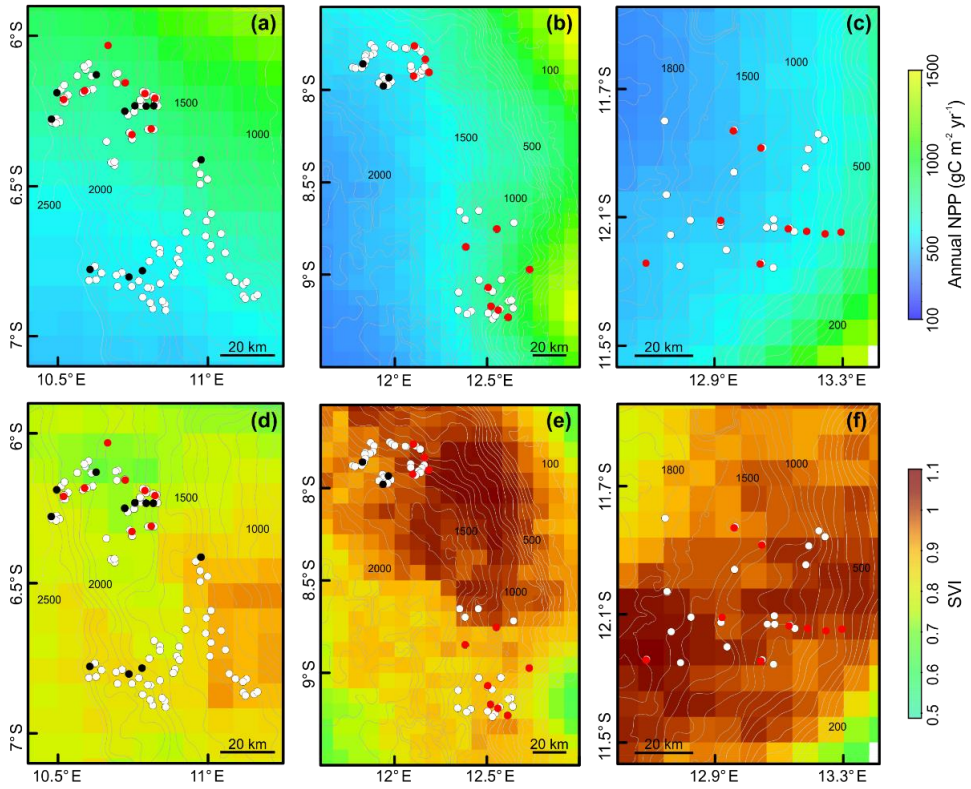


**Figure 3.5** Spatial variation in estimated annual primary productivity and Seasonal Variation Index (SVI) off Angola across study areas A **(a, d)**, B **(b, e: upper part)**, C **(b, e: lower part)**, and D **(c, f)**. Primary productivity is expressed as mean annual net primary production (NPP, g $C_{org}$ $m^{-2}$ $yr^{-1}$), calculated from 15 years (2003-2017) of monthly NPP data downloaded from the Oregon Ocean Productivity website. NPP is based on the standard Vertically Generalized Production Model (VGPM) of Behrenfeld and Falkowski (1997), computed on a 1/12° grid using MODIS R2018 surface chl-a, MODIS 4-micron SST, and MODIS cloud-corrected incident daily PAR. SVI was calculated as the ratio of standard deviation and mean monthly NNP, averaged for the period from 2003 to 2017. Open symbols are the locations of the megacore samples examined to characterise sediment properties. The location of the photographic transects examined in this Chapter are shown in red (2014 survey) and black (2005 and 2008 surveys). Grey lines show simplified contours at 100 m depth intervals.

### 3.3.1.2. Environmental conditions at photographic transects

Visual assessment of the seabed imagery revealed fine sediments to be present at all sites, with light to medium brown sediment dominating. The seafloor at the shallowest site sampled (14C01, 480 m) had noticeable ripples, suggesting strong bottom currents. Seabed surfaces at the remaining upper slope sites as well as in the upper mid-slope region down to about 1300 m were relatively featureless with occassional shallow ovoid depressions present. At depths between about 1300 to 1750 m an increase in the number of ovoid depressions was noted at several sites sampled in Areas A, B and D. By contrast, the substratum at the two mid-slope sites sampled in Area C (14C06, 1217 m and 14C07, 1435 m) appeared to be more compacted compared to those at all other transects. Here, the substratum was overlain with a thin flocculant layer, which was easily suspended following contact of the camera with the seabed. Ordination of the environmental variables (Figure 3.6) confirmed the presence of different grain size distributions at these two sites, characterised by surface sediments with a greater proportion of coarse material (> 63 μm). At the broader scale, differences in environmental conditions among photographic sites mainly reflect large-scale bathymetric changes in water column and sedimentary characteristics (PC1, eigenvalue 7.5). The substratum at the deepest sites (< 2000 m) was mostly flat and shallow depressions were rarely seen. Lebensspuren other than the ovoid depressions were visible across all sites, but were not assessed. Noticeable large amounts of phytodetritus in the form of small reddish pellets were observed at sites 14C04 (698 m) and 14C05 (1047 m), indicating recent deposition events. Remains of vascular plants were seen at most sites, with large quantities observed at the upper slope of Area C at depths between 400 to 900 m (sites 14C01 to 14C4). Trawl marks and elevated levels of resuspended sediments were visible at site 14D01 in Area D (780 m).

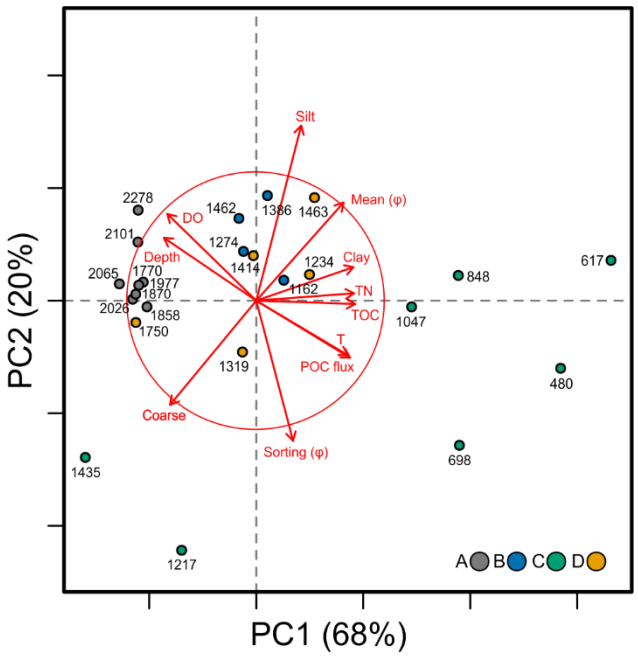


**Figure 3.6** Euclidean distance biplot (scaling type 1) of principal components for normalised (zero mean and unit variance) water column and sedimentary parameters measured at or near image transects sampled along the Angolan continental slope in 2014, keyed to study area (A-D). The coarse sediment fraction combines all particles > 63 µm. Centred-log-ratio transformations were applied to the weight percentages of the grain size fractions prior to normalising the data to overcome the closed structure of compositional data (Aitchison, 1982). Numbers represent mean water depth at image transect. DO - Dissolved oxygen concentration; T - Bottom water temperature; POC flux - estimated annual flux rate to the seabed (mg C $m^{-2}$ $day^{-1}$) approximated using the Lutz algorithm (Lutz et al., 2007) averaged for the period from 2003 to 2017.

### 3.3.2 Ecological characterisation

#### 3.3.2.1 Invertebrate megafauna

***Variations in standing stocks***

In all, 19312 metazoan specimens were included in the analyses from the 25317 $m^2$ of seabed examined (Table S.3.1). Invertebrate numerical density for the 2014 data set was highest at the upper slope, with maximum bootstrapped mean densities observed at the shallowest site 14C01 (480 m, 102100 ind. $ha^{-1}$), followed by site 14C04 in the 800-900 m depth band (848 m, 45700 ind. $ha^{-1}$) (Figure 3.7a). Overall, invertebrate density showed a moderate significant negative correlation with water depth to around 1900 m ($r_{s\ (2014)}$ = -0.70, $r_{s\ (all\ years)}$ = -0.62, $p < 0.05$), with the lowest densities of about 730 ind. $ha^{-1}$ recorded at site 14A03 in Area A. Below 1900 m, higher faunal densities of up to 6724 ind. $ha^{-1}$ were observed at a cluster of sites to about 2100 m, followed by a slight decline in densities at the deepest sites sampled. Differences in invertebrate densities along the slope were evident for several depth bands, being most pronounced at depths between 700-900 m.

Here invertebrate densities at sites sampled in Area D (sites 14D01 and 14D02) were 5 to 15 times lower compared to those found at similar depths in Area C (sites 14C03 and 14C04). At mid-slope depths between 1100 and 1400 m, transects surveyed in Area B (sites 14B01 to 14B03) exhibited consistently lower invertebrate densities compared to sites sampled at similar depths in Areas C and D. Invertebrate densities recorded in 2005 and 2008 largely followed the trends observed in 2014. Precision of invertebrate densities recorded in 2014, as estimated from bootstrapping, was high for all transects, ranging between 2.4 and 13% and showing a significant negative correlation with mean invertebrate density ($r_s$ = -0.76, $p < 0.01$).

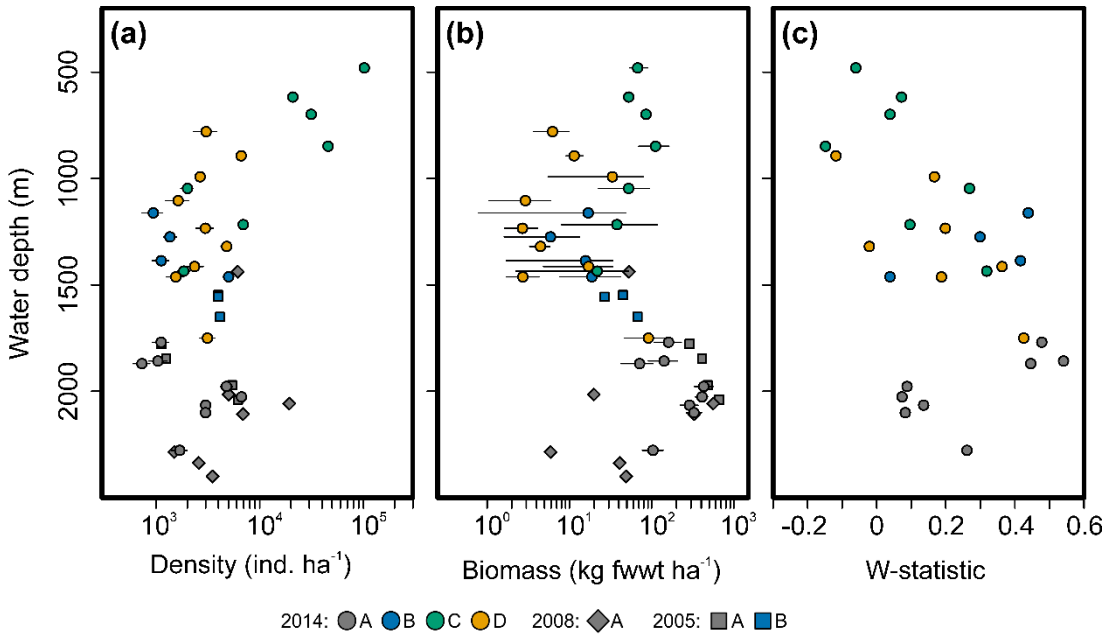


**Figure 3.7** Bathymetric distribution of invertebrate standing stock and W-statistic along the Angolan continental slope, keyed to study area (A-D) and sampling year (2005, 2008 and 2014). **(a)** Invertebrate density **(b**) Invertebrate biomass **(c)** W-statistic (2014 data only). Standing stock estimates for 2014 are shown as transect mean density and median biomass as calculated from bootstrapping (see Methods). Error bars represent 95% confidence intervals. The 2005 and 2008 data are shown as single transect values. The W-statistic was only computed for transects retained in the analysis of alpha diversity and faunal composition (n = 26).

Approximated invertebrate biomass (Figure 3.7b) peaked along the lower slope in Area A at sites sampled between 1700 and 2100 m water depth, reaching bootstrapped median values of up to 430 kg fwwt ha$^{-1}$ in 2014, and 660 kg fwwt ha$^{-1}$ in 2005 and 560 kg fwwt ha$^{-1}$ in 2008. The lowest biomass was recorded in the mid-slope region with minimum values of about 3 kg fwwt ha$^{-1}$. At the upper slope between 700-900 m, the observed 5 to 15 fold lower numerical densities in Area D compared to Area C are echoed in a 7.5 to 18 fold reduction in numerical biomass. In contrast, the high numerical density observed at the shallowest site (14C01) did not translate into high biomass values. However,

biovolume approximation for the site's numerically dominant seapens did not include the buried peduncle, and as a consequence the approximated biomass for site 14C01 is considered an underestimate. At the remaining sites, seapens accounted for 0.1 to 7.8% of the total invertebrate numerical density and the resulting underestimation of sea pen biomass is considered less influential on total biomass.

The comparison of abundance and biomass dominance patterns for the 2014 data, as assessed by the W-statistic, revealed a unimodal pattern of change with water depth (Figure 3.7c): W gradually increased from weakly negative values at the upper slope indicating invertebrate assemblages with relatively more uneven abundance distributions than biomass distributions to strongly positive values in the mid-slope region characteristic of assemblages with more even abundance distributions but larger biomass dominance. At sites below 1900 m low positive W values prevailed indicating assemblages with similar distribution patterns of density and biomass among morphospecies. Complementary comparison of the individual rank density and biomass distribution curves (Supplementary Information, Figure S3.5) revealed strong abundance dominance relative to biomass on the upper slope at site 14C04 (848 m, numerical density dominated by small squat lobsters Anomura msp-01) and to a lesser degree at sites 14C01 (480 m, high densities of seapens) and 14D02 (893 m, density dominated by Anomura msp-1). In contrast, upper slope sites 14C02 (617 m) and 14C03 (698 m) exhibited similar relative rank density and biomass distributions, as indicated by closely spaced k-dominance curves, with strong dominance of medium-sized morphospecies that also dominated biomass (*Nematocarcinus* msp-1 at site 14C02 and Ophiuroidea msp-4 at site 14C03). Similar configurations of the k-dominance curves were found at the five deepest sites sampled in 2014 (Area A, below 1900), where assemblages were dominated by the medium-sized irregular echinoid *Pourtalesia* msp-1 both in terms of numerical density and estimated numerical biomass, accounting between 34 to 69% of the total invertebrate density and between 46 to 89% of total biomass at these sites. In the mid-slope region at depths between 900 and 1500 m, the majority of assemblages showed relative even abundance distributions, whereas biomass distributions were dominated by one or very few large-sized specimens, mainly holothurians, resulting in biomass curves that lie well above the abundance curves. This extreme rarity of large specimens in the mid-slope region is reflected in the low precision of the biomass estimates, as indicated by the large confidence intervals (Figure 3.7b) and

coefficient of variations of the bootstrapped biomass estimates, which ranged from 34% to 78%. While the low precision illustrates the strong dependence of biomass estimates on sampling effort for assemblages with rare large-bodied taxa, it may also in the current case suggest that sampling across these transects has been sufficient to sample the largest taxa of the megabenthic assemblages. By contrast, invertebrate assemblages at mid-slope sites 14D05, 14D06 and 14D08 showed more even biomass distributions and the absence of large specimens, leading to more closely spaced k-dominance curves and seemingly more precise biomass estimates. This may reflect an even larger rarity of large-bodied invertebrates at these sites. Lastly, at depths below 1500 m down to about 1900 m, abundance and biomass rank distributions indicated a shift towards larger numbers of large-bodied taxa, predominantly the synallactid holothurian *Paelopatides* msp-1 (Figure 3.8k), which accounted for 18 to 27% of the total invertebrate numerical density and between 71 to 82% of the total invertebrate biomass at this depth range. Abundance distributions were relative even, leading to widely spaced density and biomass curves and corresponding large values of the W-statistic.

### *Variations in alpha diversity*

For diversity analyses, invertebrates were classified into 160 morphospecies (Table S3.4), of which 18 were recorded in 2005, 28 in 2008, and 157 in 2014. The following results are based on the analysis of 26 photographic sites sampled in 2014 (see Methods). Taxonomic units omitted from diversity analysis (e.g. Decapoda spp. indet) included seven invertebrate groups, which comprised about 1.7% of the 2014 invertebrate count. In terms of occurrence, most morphospecies were rare, with about 41% of morphotypes being present at only one site, and about 76% being recorded at five or less sites. In terms of abundance contributions, about 38% of invertebrate morphospecies were represented by one or two individuals. Cnidaria were the most morphospecies-rich invertebrate phylum (28% of nominal invertebrate taxa), followed by Echinodermata (24%) and Arthropoda (21%). Figure 3.8 shows examples of observed morphospecies, and representative images of each morphotype can be found in the morphospecies image catalogue in Appendix B.

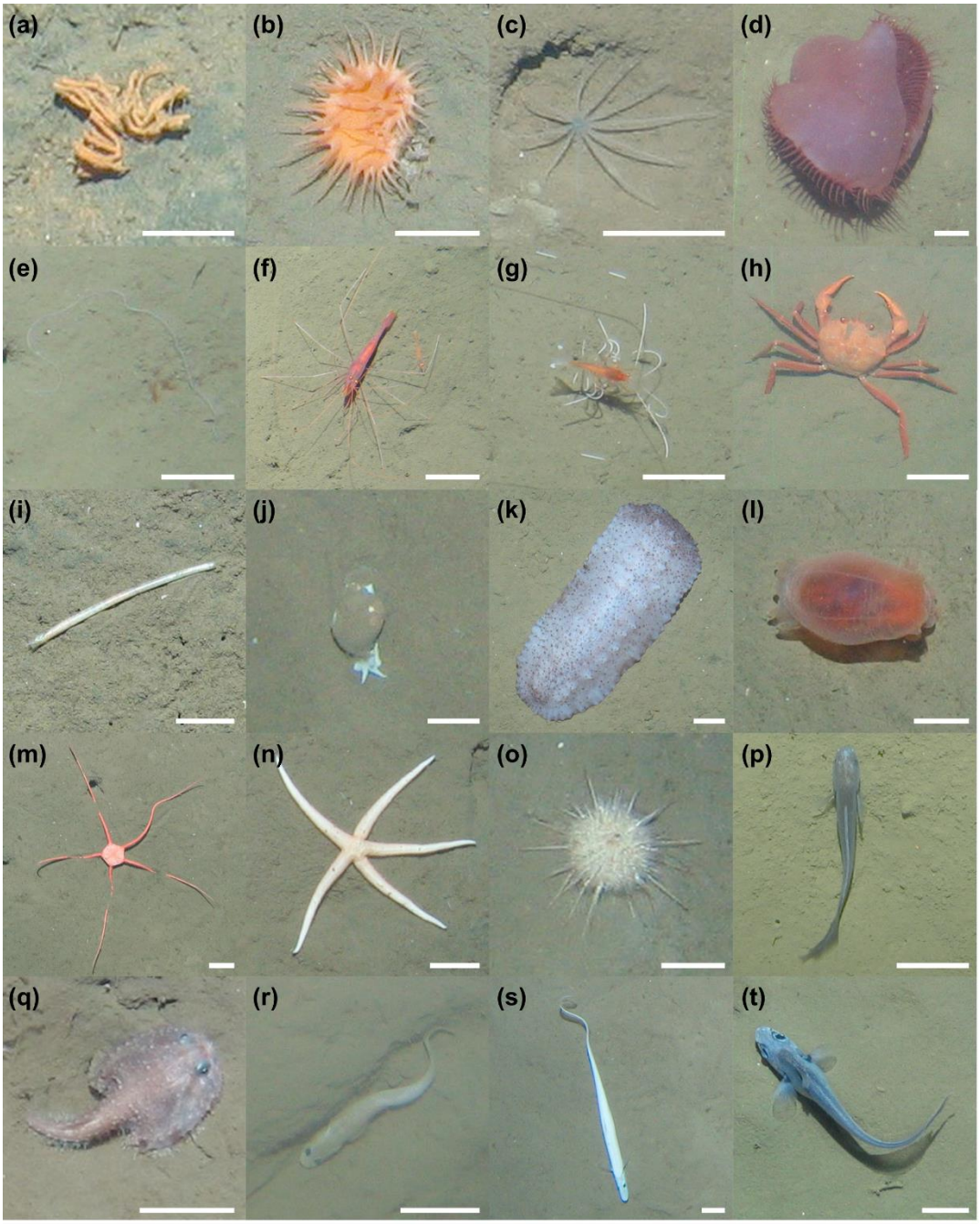


**Figure 3.8** Examples of epibenthic megafauna recorded across sedimentary habitats along the Angolan continental slope. Scale bars represent 5 cm. **(a)** Porifera msp-1 **(b)** Actiniaria msp-6 **(c)** Actiniaria msp-5 **(d)** Actinoscyphia msp-1 **(e)** Nemertea msp-4 **(f)** *Nematocarcinus* msp-1 (left) and Caridea msp-3 (right), the latter often seen buried with only the eyes visible **(g)** Aristeidae msp-2 **(h)** Red crab Geryonidae msp-1 **(i)** Onuphidae **(j)** Gastropoda msp-15 **(k)** *Paelopatides* msp-1, three colour morphs were recorded: white/pale, uniform purple, and speckled purple **(l)** *Peniagone* msp-1 **(m)** Ophiuroidea msp-5 **(n)** Zoroasteridae **(o)** Echinidae msp-2 **(p)** Ophidiiformes msp-1 **(q)** Batfish Ogcocephalidae msp-2 **(r)** Actinopterygii msp-12 **(s)** Halosauridae **(t)** Macrouridae msp-3.

Overall, we consider the number of classified morphospecies to be an underestimation of the true invertebrate richness, owing to the mixed taxonomy applied when delineating morphotypes and the presence of unidentified specimens. Additionally, none of the rarefaction curves evaluating invertebrate morphospecies richness had reached an asymptote (Figure S3.6), indicating that further sampling would detect additional rare morphospecies within the areas sampled. Sites sampled on the upper slope (14C01 to 14C4 and 14D2) showed the closest approach to asymptotic rarefaction curves, reaching sample coverages between 98.0 and 99.5% (Figure S3.8).

Invertebrate morphospecies density showed broadly similar patterns whether examined based on a standardised area of 400 $m^2$ or 800 $m^2$ (Figure 3.9a), declining from the upper slope to the mid-slope region at depths between 480 m down to about 1100 m. After this point, morphospecies density showed no discernible trend. In contrast, invertebrate morphospecies richness estimated by sample-based rarefaction rarefied down to 90 individuals ($ES_{90}$) showed the lowest expected richness at the upper slope at sites above 900 m, with the lowest number of morphospecies expected at site 14C04 (849 m) (Figure 3.9b). The highest invertebrate richness occurred on the middle to lower slope at depths between about 1150-1900 m, with the maximum number of expected morphospecies being up to five times higher than the expected richness below 900 m. Noticeable differences among sampling areas included higher expected richness at Area B between 1100-1300 m compared to similar depths in Areas C and D. This contrasted with a comparatively low expected richness at the deepest site in Area B (1464 m). In Area A, an up to two-fold decline in expected richness was found at several locations below 1900 m compared to the remaining sites sampled in this area. Morphospecies richness estimated based on a sample size of 180 individuals ($ES_{180}$, Figure 3.9b, open symbols) and the richness estimates based on coverage-based rarefaction ($SC_{0.883}$ and $SC_{0.904}$, Figure S3.8) largely followed the trends in $ES_{90}$, showing an overall increase in expected richness with increasing water depth from the upper slope to the middle slope in Areas C and D, comparable high expected richness at mid-slope sites in Areas A and B, and variable expected richness at sites sampled below 1900 m in Area A.

Comparisons of the individual richness rarefaction and extrapolation curves (Figure S3.6) suggests the presence of several intersecting curves (e.g. sites in Area B, and shallower sites in Area C), indicating that ranked differences in expected richness among several assemblages are unlikely to be consistent across different sampling efforts. However, the large scale trend of increasing richness towards mid-slope depths holds. Intersecting curves are likely to reflect differences in invertebrate richness among sites, varying proportions of common and rare morphotypes, and dissimilar morphospecies aggregation patterns, which all will affect species accumulation rates (Chase et al., 2018; Gotelli and Colwell, 2001).

Patterns in Shannon ($^1D$) and Simpson ($^2D$) diversity were broadly concurrent and strongly correlated ($p < 0.01$) whether standardised by the number of individuals ($r_s = 0.96\text{-}0.97$), sample coverage ($r_s = 0.96\text{-}0.97$) or sampled area ($r_s = 0.96\text{-}0.97$) (Table S3.5). They showed an overall regional trend of increasing numbers of common and dominant morphospecies with increasing water depth for sites sampled above 1900 m, followed by a sharp significant decline at the five deepest sites (Figures 3.9c,d and S3.9). As with expected invertebrate richness, local deviations from this trend were present at mid slope depths, with significantly lower numbers of common and abundant invertebrate morphotypes at sites sampled between 1100-1300 m in Areas C and D compared to sites sampled at similar depths in Areas B, as well as low Shannon diversity and high dominance at site 14B04. Overall, the lowest Shannon diversity occurred at the two sites sampled in the 800-900 m depth band, mid-slope site 14B04, and lower slope site 14A01, with the order varying among the applied standardisation method. Dominance was consistently predicted to be highest at site 14B04. Unlike morphospecies richness, the majority of rarefied and extrapolated Shannon and Simpson diversities reached or were approaching asymptotes (Figure S3.7).

The overall curvilinear trend in Shannon and Simpson diversity was echoed in the assemblage evenness, which was strongly and significantly positively correlated with both $^1D$ and $^2D$ for any of two standardised sample sizes and the three standardisation methods ($r_s = 0.918\text{-}0.975$, $p < 0.01$, Table S3.5). As for $^2D$, the lowest evenness was observed at station 14B04, likely as a result of a relative high number of observed invertebrate morphotypes combined with the dominance of a small anthozoan, which accounted for 78.5% of the observed numerical density.

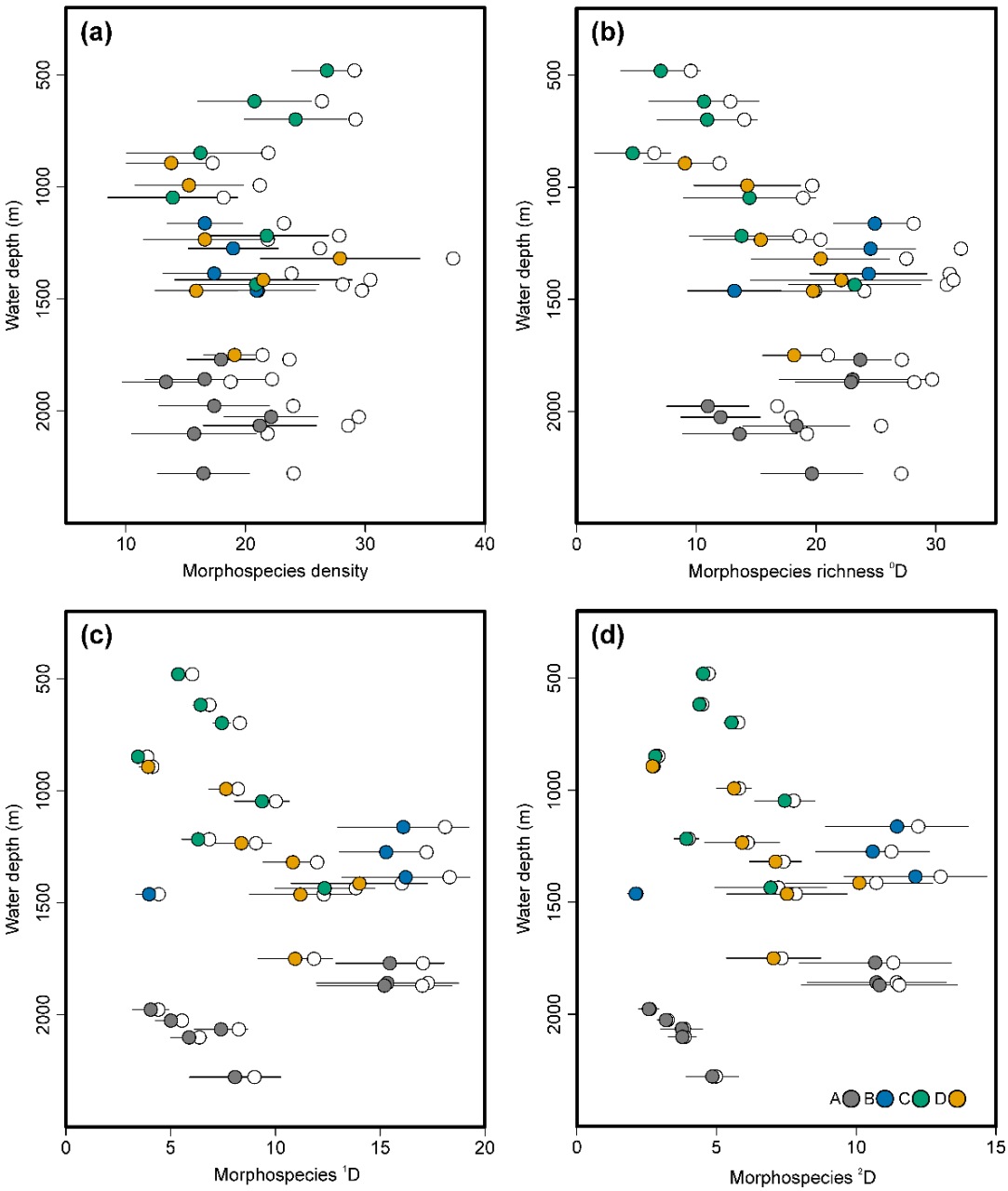


**Figure 3.9** Bathymetric variation in expected invertebrate morphospecies diversity for the photographic transects sampled in 2014 (n = 26), keyed to study area (Area A-D). **(a)** Morphospecies density **(b)** Morphospecies richness ($^0$D) **(c)** Exponential Shannon entropy ($^1$D) **(d)** Inverse Simpson concentration ($^2$D). Filled circles represent rarefied diversity per 400 m$^2$ of seabed sampled for morphospecies density, and per 90 individuals for morphospecies richness, $^1$D and $^2$D. Empty circles show the extrapolated diversities per 800 m$^2$ and 180 individuals, respectively. Error bars represent the 95% confidence intervals for the interpolated diversity values. Confidence intervals of the extrapolated values were omitted for better readability.

### *Variations in faunal composition*

Ordination of the 2014 data set reveals a clear change in invertebrate assemblage composition with water depth (Figure 3.10a). Sites are primarily arranged by depth in a pronounced arch configuration, a distortion commonly seen in ordinations of data sets obtained along strong environmental gradients, which is thought to result from the non-linear increase of sample dissimilarities with increasing differences in assemblage composition (e.g. Gauch, 1973; Swan, 1970). There is strong indication that the invertebrate composition of the shallowest site 14C01 is distinct from the remaining sites but most closely related to the two sites sampled in the 600-700 m depth band. Likewise, there is a clear separation of the deepest sites sampled in Area A from sites on the middle slope. Site 14D09 (Area D, 1750 m) takes an intermediate position between the mid-slope sites and the deep-water sites of Area A, suggesting a change in invertebrate assemblage composition at Area D towards assemblages similar to those recorded in Area A. To better visualise potential differences in faunal composition among sites on the middle slope, an additional MDS analysis without sites from Area A was carried out (Figure 3.10b). The resultant ordination confirms depth-related changes in invertebrate composition in all three areas. Limited overlap between mid-slope sites (1200-1500 m), in particular between sites sampled in Area D and sites in Areas B and C, suggests geographic differences in invertebrate assemblages among sampling areas along the mid-depth sections of the slope.

Average-linkage clustering supports the conclusions from the ordination, dividing sites into three distinctly dissimilar groups on the basis of water depth at an average dissimilarity between clusters of 75-85% (Figure 3.10c). The first division separates the sites sampled below 1700 m from the upper and mid-slope sites sampled in Areas B to D. Comparison of silhouette scores (Table S3.8) showed that all deep-water sites were well matched to the cluster with the exception of site 14D09, which held an intermediate position between the mid-slope sites sampled in Area D and the deeper sites of Area A, confirming the pattern seen in the ordination. The lower slope assemblages in Area A are further partitioned into two bathymetric groups at about 1900 m, which mirrors the recorded trends in invertebrate densities and the diversity of common and dominant morphospecies. The upper slope group (> 700 m) comprised assemblages of the three shallowest sites sampled in Area C, with the two sites sampled at depths between 600-700 m forming a separate sub-grouping. For the mid-slope group, the clustering pattern

indicates the two sites sampled in the 800-900 m depth band to be more similar to each other than suggested by the ordination. The remaining mid-slope sites (1000-1500 m) are further split primarily by geographic location. Among them, site 14D03 (Area D, 992 m) exhibited a low affinity to its assigned cluster group (Table S3.8) showing also some resemblance with the assemblages sampled at similar depths at site 14C05 (Area C, 1047 m), further indicating depth-related changes in environmental conditions as a strong driver of faunal change.

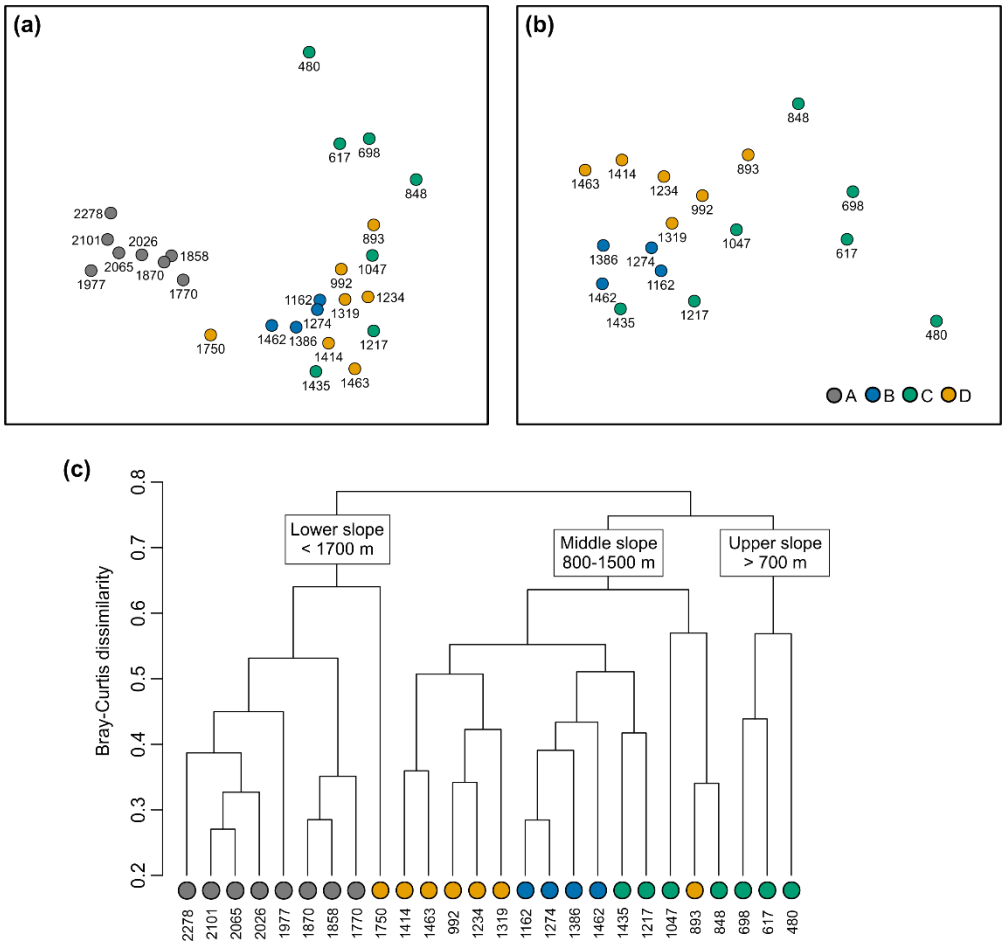


**Figure 3.10** Spatial variation in invertebrate morphospecies composition along the Angolan continental slope, based on the fourth-root transformed invertebrate numerical densities recorded in 2014. **(a)** Two-dimensional NMDS ordination of all photographic sites (MDS stress: 0.107). **(b)** Ordination of upper and middle slope stations sampled above 1500 m (MDS stress: 0.097). **(c)** Between-group average linkage cluster analysis for all sites. Sites are keyed to study area (A-D). The numbers below site symbols represent mean transect depths.

Partitioning of the overall beta diversity $\beta_{SOR}$ of sites sampled in 2014 in its nestedness ($\beta_{NES}$) and turnover ($\beta_{SIM}$) components indicates that compositional differences among invertebrate assemblages were almost completely the result of morphospecies replacement ($\beta_{SOR}$ = 0.913, $\beta_{SIM}$ = 0.897). Variation in Cody's beta diversity $\beta_C$, expressed as

cumulative percentage change, suggests that the bathymetric turnover is more or less gradual with some areas of more rapid changes (Figure 3.11). The greatest rate of change occurred at mid-slope depths between about 1400-1500 m, which largely reflected an increased rate in the number of morphospecies lost. No sites were sampled between 1500-1750 m, which may at least partly explain the enhanced number of lost morphospecies at about 1500 m. A slightly greater turnover was also observed among sites at the upper slope to about 700 m, between the deepest site of Area D (14D09, 1750 m) and the shallowest site in Area A (14A01, 1770 m), and among the lower slope sites sampled in Area A between about 2000-2100 m.

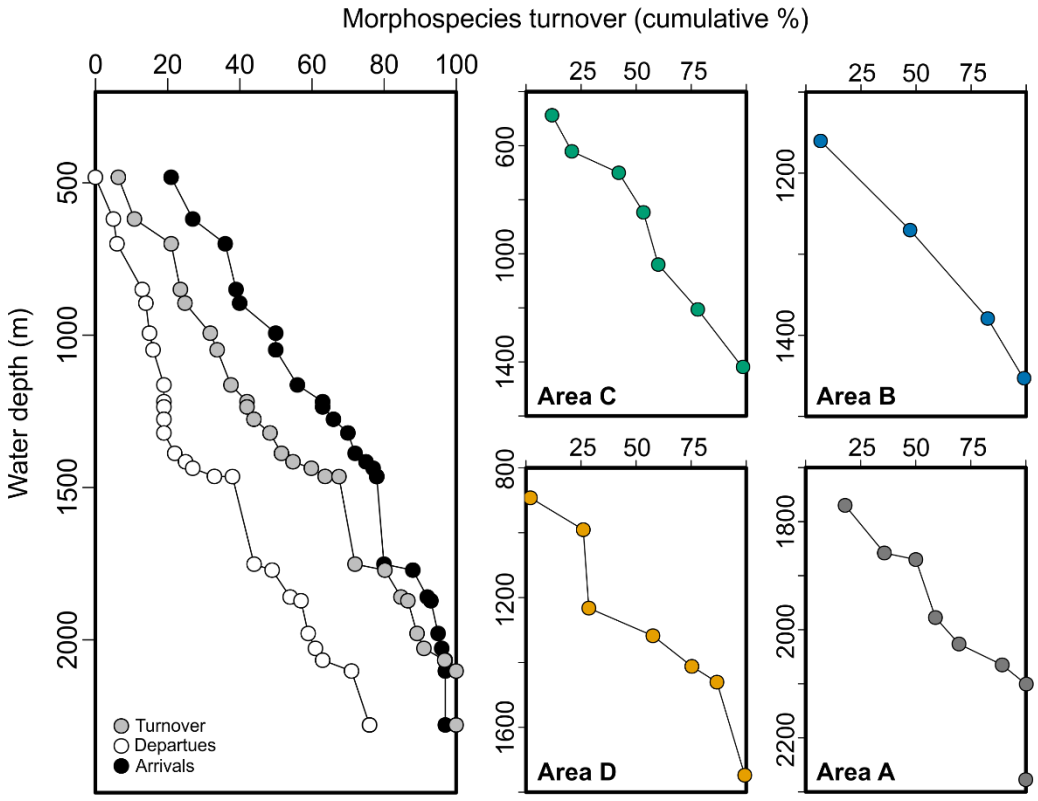


**Figure 3.11** Turnover of invertebrate morphospecies with water depth, expressed as cumulative percentage change in Cody's $\beta_c$, combined for photographic sites sampled in 2014 (left hand side), and separately for each sampling area (right hand side). For the plot combining all sites, the cumulative gain and loss of morphospecies is also shown. Turnover has been computed from a reduced dataset including only invertebrate morphospecies with more than two specimens (n=97). Note that the depth range is different for each plot.

Comparisons of relative morphospecies abundances at higher taxonomic level showed that with few exceptions arthropods (all crustaceans) dominated faunal assemblages at upper and mid-slope depths between about 600-1500 m water depths, whereas echinoderms accounted for the largest portion of invertebrates at the majority of sites below 1500 m (Table S3.7). Among the Arthropoda, caridean shrimp were the most widespread and

proportionally most abundant, representing 55.8-100% of arthropods across all sites, with the exception of the two sites sampled between 800-900 m where squat lobsters were dominant (82.3 and 98.3% of arthropods). Among the echinoderms, ophiuroids showed the widest bathymetric range, being recorded at all sites and representing between 0.1 and 64.8% of observed invertebrate densities. Holothurians were not recorded at sites above 900 m. Below 900 m, they exhibited a unimodal trend in relative densities, reaching maximum proportions (28.2-40% of invertebrate numerical density) at depths between 1750 and 1870 m. Asteroid relative densities also showed a curvilinear trend, peaking at depths between about 1100-1900 m although they were less common with relative densities of up to 11.9%. Likewise, only small numbers of echinoids were observed at most sites (up to 15.4% of invertebrates) except for the five deepest sites where echinoids made up between 35.3-69% of the observed invertebrate numerical density. Sponges had their highest relative densities at mid-slope depths between about 1200-1500 m (up to 52.8% of invertebrate densities), while they were rare or absent at shallower and deeper sites. By contrast, cnidarians (Anthozoa) were found at all sites, reaching locally high relative abundances of up to 82.9%.

At lower taxonomic levels, the progressive change in invertebrate assemblage composition along the bathymetric gradient is reflected in the changing depth of maximum density among the majority of the most dominant morphospecies (Figure 3.12). Few morphotypes showed wide depth ranges, of which the majority are likely to comprise multiple species, potentially with different depth distributions, such as in the case of the natant decapod morphospecies Caridea msp-3 and Caridoid msp-3 as well as the shallow surface dwelling specimens classified as Animalia indeterminate msp-2.

***Upper slope assemblages, 480-700 m**:* The three upper slope sites were typified by the presence of sea pens, small zoanthids and a medium-sized munidid squat lobster with quill worms, burrowing ophiuroids and nematocarcinid shrimp also largely restricted to them (Table S3.9). However, while the overall faunal make up of the sites was similar, the relative abundances of the most dominant morphospecies varied considerably among them. The shallowest site (480 m) was dominated by a light-coloured sea pen, likely a Virgulariidae, representing 66.7 % of the standardised invertebrate megafauna (67840 ind. $ha^{-1}$), followed by a larger, dark-red pennatulid (15.3%, 15554 ind. $ha^{-1}$) and *Nematocarcinus* msp-01 (11.4%, 11587 ind. $ha^{-1}$) (Figure 3.8f). Several gastropod

morphospecies were unique to this site, of which the two most abundant reached densities of 1082 and 1539 ind. $ha^{-1}$. Quill worms and partially buried ophiuroids (both with 144 ind. $ha^{-1}$) and small decapod shrimp species (722 ind. $ha^{-1}$) were less common.

In contrast, the 617 m site was mainly populated by benthic shrimp species (76.3% of invertebrates), with *Nematocarcinus* msp-01 being dominant, accounting for 58.9% of observed faunal density (12229 ind. $ha^{-1}$), whereas burrowing ophiuroids (688 ind. $ha^{-1}$) zoanthids (303 ind. $ha^{-1}$) and cerianthid anemones (292 ind. $ha^{-1}$) reached intermediate densities. At the 698 m site, burrowing ophiuroids were the most abundant invertebrates, making up 64.5% in total density with an estimated 20100 ind. $ha^{-1}$. Benthic shrimp species were common (combined density of 5017 ind. $ha^{-1}$) together with large tube anemones (1773 ind. $ha^{-1}$), munidid squat lobsters (279 ind. $ha^{-1}$), asteroids (100 ind. $ha^{-1}$) and a thin ribbon worm (413 ind. $ha^{-1}$, Figure 3.8e), which was also occasionally recorded at 617 m (23 ind. $ha^{-1}$). Seapens were markedly reduced at the two deeper sites compared to the 480 m site, reaching total densities of only 618 and 1126 ind. $ha^{-1}$, while quill worm densities were about 10 times higher (1260 and 1610 ind. $ha^{-1}$). Rare sightings across all three upper slope sites included small actinian species, large hormathiid anemones, deep-water red crabs (Figure 3.8h) and cephalodods.

***Middle slope assemblages, 800-1500 m:*** The invertebrate assemblages at the two sites sampled between 800-900 m were distinguished from the remaining mid-slope sites by their high relative densities of a small galatheoid squat lobster (Anomura msp-1), which accounted for 88.3% (40352 ind. $ha^{-1}$) of the total observed invertebrate density at site 14C04, and 58.8% (3883 ind. $ha^{-1}$) at site 14D02. Burrowing ophiuroids observed at the shallower sites were also frequently seen (3491 and 1534 ind. $ha^{-1}$) along with intermediate numbers of epibenthic ophiuroids (Ophiuroidea msp-3, 164 and 171 ind. $ha^{-1}$).

Invertebrates typifying the remaining mid-slope sites included zoroasterid sea stars, small ophiuroids (Ophiuroidea msp-2), and a group of medium to large-sized asteroids (Asteroidea msp-7, possibly Goniasteridae and Porcellanasteridae) (Table S3.9), with the two latter morphospecies often seen partially buried. The distributions of the numerically dominant morphospecies and the densities of the significant indicator species suggest that the compositional difference among the different sampling areas at depths between about 1100-1500 m resulted largely from differences in relative abundance distributions as well

as records of rarer taxa. For example, densities and relative proportions of Asteroidea msp-7 were higher in Area D (75-115 ind. $ha^{-1}$, 2.5-5.6%) compared to those in Area B (10-20 ind. $ha^{-1}$, 0.2-1.5%). In addition, assemblages in Area D had larger proportions of medium to large-sized epibenthic shrimp species (Caridoid msp-3, 358-493 ind. $ha^{-1}$, 7.7-27.1%) compared to assemblages in both Area B (10-63 ind. $ha^{-1}$, 0.7-6%) and Area C (21-91 ind. $ha^{-1}$, 1.2-1.4%). By contrast, assemblages in Area C were distinct in having both larger numbers and higher proportions of Ophiuroidea msp-2 (609-1189 ind. $ha^{-1}$, 17-8-34.1%) compared to assemblages in Area B (9-46 ind. $ha^{-1}$, 0.8-3.5%) and Area D (25-166 ind. $ha^{-1}$, 0.9-4.1%). They also exhibited higher densities and slightly larger proportions of zoroasterid sea stars (53-457 ind. $ha^{-1}$, 3-6.8%) compared to records from Areas B and D (13-27 ind. $ha^{-1}$, 0.4-2.6%). Among the less common morphospecies, low numbers of small echinoids (Echinoidea msp-4) and the large synallactid *Paelopatides* msp-1 were recorded in Areas B and C (echinoids 10-75 ind. $ha^{-1}$, holothurians 7-83 ind. $ha^{-1}$), while these taxa were not observed at the mid-slope sites in Area D. Similarly, small cerianthid specimens (Ceriantharia msp-2) were seen in both Area C and D (15-215 ind. $ha^{-1}$) but not in Area B, and Area D consistently supported low numbers of janiroid isopods (Isopoda msp-1 and msp-2, 7-94 ind. $ha^{-1}$), while these morphotypes were only very rarely seen at the two other areas. Other rare taxa seen on the middle slope were the large holothurians *Benthothuria* at sites between about 1000-1100 m (15-45 ind. $ha^{-1}$), and *Mesothuria* (9-65 ind. $ha^{-1}$) and *Peniagone* msp-2 (9-13 ind. $ha^{-1}$) at sites below 1300 m. The regular echinoid *Phormosoma* msp-1 was also seen in small numbers (11-77 ind. $ha^{-1}$) at several sites, with the exception of site 14C05 (1047 m), where it reached densities of 314 ind. $ha^{-1}$.

***Lower slope assemblages, 1750-2300 m:*** Invertebrate assemblages on the lower slope were characterised by an overall decrease in the proportion and numerical density of arthropods and an increase in the relative abundance of mainly larger-bodied echinoderms compared to the upper and middle slope. Porifera were absent or extremely scarce (up to 1% of invertebrates and 12 ind. $ha^{-1}$), whereas cnidaria were present in variable proportions (6.6-38.8% reaching numerical densities (175-933 ind. $ha^{-1}$) similar to the range in cnidaria densities recorded on the middle slope.

In terms of compositional differences, the assemblages of the three shallowest sites sampled in Area A (1770-1870 m) were typified by the presence of the elasipodid *Psychropotes* msp-1, which was recorded at all three sites belonging to this group (19-76

ind. $ha^{-1}$), but was seen at only one station below 1900 m. By contrast, the assemblages of the five deepest sites were typified by the presence and dominance of the irregular urchin *Pourtalesia* msp-1, as well as the occurrence of a large red unidentified brittle star (Ophiuroidea msp-5, Figure 3.8m). Pourtalesiid numbers (575-4151 ind. $ha^{-1}$) tended to decrease with increasing depth, while the density of the ophiuroid (21-221 ind. $ha^{-1}$) was highest at the deeper sites.

The holothurian *Paelopatides* msp-1 and the brittle star Ophiuroidea msp-1 (likely an Ophiomusaidae) were among the taxa present at the majority of lower slope sites. However, while the abundance of *Paelopatides* was relative constant among sites (121-203 ind. $ha^{-1}$), the density of the brittlestars was one to two orders of magnitude lower at the three shallower sites (13-18 ind. $ha^{-1}$) compared to the deeper sub-group (285-1330 ind. $ha^{-1}$) and the lower slope site sampled in Area D (933 ind. $ha^{-1}$). Other taxa regularly recorded across the lower slope in low to intermediate numbers were cerianthids, *Peniagone* msp-1, several octocoral species, including *Umbellula*, and a small actinian, Actiniaria msp-10, whose densities (12-219 ind. $ha^{-1}$) peaked at the five deepest sites, where it occurred predominantly on dead urchin tests. Asteroids were represented by large astropectinids in low to intermediate numbers (9-66 ind. $ha^{-1}$) at most lower slope sites. Taxa recorded at only a few sites included the urchin *Hygrosoma*, the elasipodid *Benthodytes*, aristeid shrimps, and octopods.

**Figure 3.12** Relative densities of the most dominant invertebrate morphospecies recorded on the Angolan continental slope in 2014, expressed as percentage of maximum density of each morphotype and keyed to study area (A-D). Included are the top five most abundant morphospecies at each photographic site: (1) Pennatulacea msp-1 (2) Pennatulacea msp-2 (3) Gastropoda msp-1 (4) Gastropoda msp-2 (5) Onuphidae (6) *Nematocarcinus* msp-1 (7) Caridoid msp-3 (8) Caridea msp-3 (9) Caridoid indeterminate (10) Ophiuroidea msp-4 (11) Pennatulacea msp-6 (12) Polychaeta msp-5 (13) Ceriantharia msp-1 (14) Anomura msp-1 (15) Asteroidea msp-5 (16) Ophiuroidea msp-3 (17) *Phormosoma* msp-1 (18) Hexacorallia msp-4 (19) Porifera msp-1 (20) Indeterminate msp-2 (21) Ophiuroidea msp-2 (22) Asteroidea msp-7 (23) Zoroasteridae (24) Caridoid msp-1 (25) Cirripedia (26) Ceriantharia msp-2 (27) Echinoidea msp-4 (28) *Elpidia* msp-1 (29) Hexacorallia msp-1 (30) *Paelopatides* msp-1 (31) *Peniagone* msp-1 (32) *Psychropotes* msp-1 (33) Octocorallia msp-4 (34) Indeterminate msp-46 (35) Anomura msp-6 (36) Ophiuroidea msp-1 (37) *Pourtalesia* msp-1 (38) Pennatulacea msp-5 (39) Actiniaria msp-10 (40) Ophiuroidea msp-5. Morphospecies are ordered from left to right in increasing depth of maximum relative density.

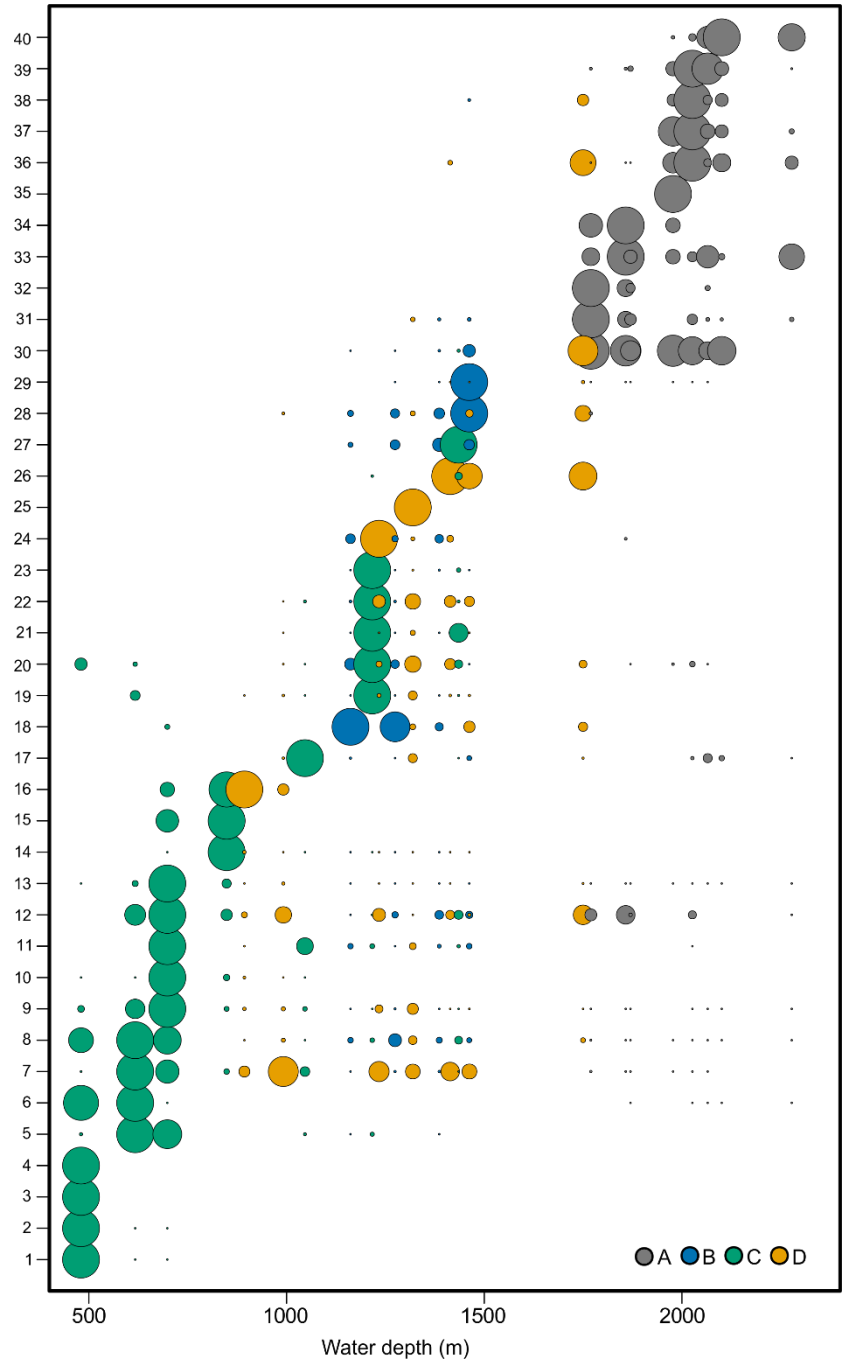

Analysis of the whole invertebrate data set (2005, 2008 and 2014 data) showed a higher multivariate dispersion for communities sampled in 2005 and 2008 compared to the 2014 data (Figure S3.10a). This was likely to be expected owing to the lower sampling effort and the subsequent absence or reduced density of less common morphospecies. Sites sampled in Area A grouped well within the respective mid-slope and lower-slope clusters, including a subset of morphospecies observed in 2014. In Area A, aggregations of the elasipodid *Scotoplanes* were present at two sites (05A01 and 05A02) in 2005, reaching densities of 895 and 909 ind. $ha^{-1}$. Pourtalesiids were seen in both years, again at depths below 1900 m. In 2005, echinoid densities (5089-5261 ind. $ha^{-1}$) were comparable to those recorded at nearby sites in 2014. In 2008, echinoid densities were more variable, reaching densities of 5737 ind. $ha^{-1}$ at site 08A04 and 16385 ind. $ha^{-1}$ at site 08A03, but being absent or rarely seen at the remaining lower slope sites deeper than 1900 m. Similarly, there was a noticeable absence of *Paelopatides* at all lower slope sites (< 1500 m) in 2008.

#### 3.3.2.2 Ichthyofauna

We restricted the assessment of demersal fishes to the 2014 dataset because of the very low number of fish observations made in 2005 and 2008 (790 specimens recorded in 2014 vs 16 specimens seen in the combined 2005 and 2008 data set). The bootstrapped mean numerical density of fish showed a strong and highly significant monotonic decrease with increasing water depth ($r_s$ = -0.89, $p < 0.01$, Table 3.1), with mean densities declining by about two orders of magnitude from 2305 ind. $ha^{-1}$ on the upper slope at site 14C01 to between 13-54 ind. $ha^{-1}$ at depths below 2000 m (Figure 3.13a). For approximated ichthyofaunal biomass, a weak, non-significant negative correlation between the bootstrapped median biomass and water depth was observed ($r_s$ = -0.52, $p > 0.05$, Table 3.1), with estimated values ranging from 83 kg fwwt $ha^{-1}$ at site 14A03 (1870 m) and 0.08 kg fwwt $ha^{-1}$ at site 14A05 at about 2000 m water depth (Figure 3.13b). Precision of the standing stock estimates based on the Coefficient of Variation significantly ($p < 0.01$) decreased with increasing water depth for both numerical density ($r_s$ = 0.83) and approximated biomass ($r_s$ = 0.78), reflecting the strong decline in the number of recorded fish specimens with increasing depth.

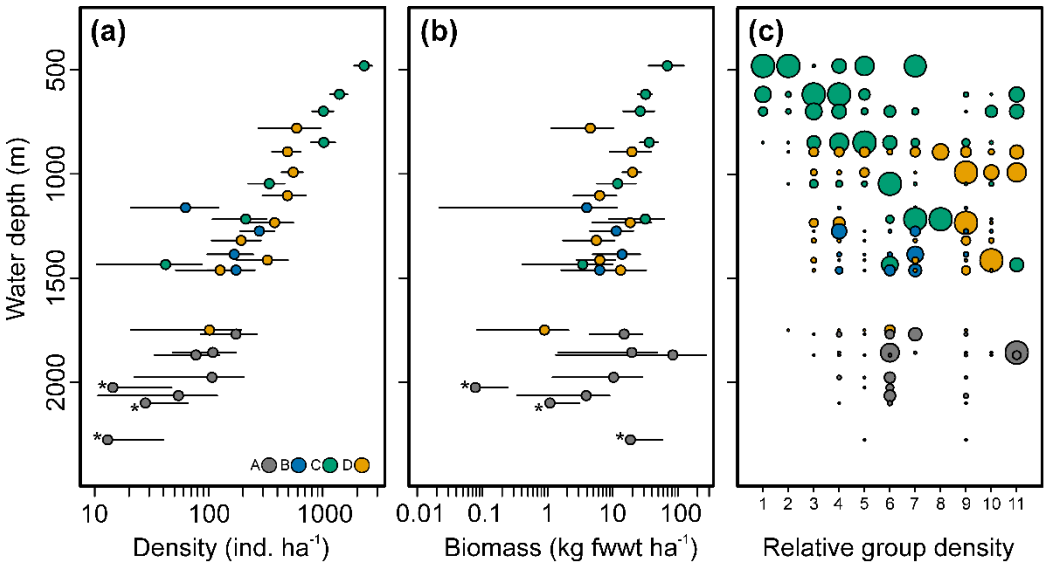


**Figure 3.13** Bathymetric variation in standing stock of benthic and benthopelagic fishes recorded along the Angolan continental slope in 2014, keyed to study area (A-D). Total fish standing stock estimates are shown as transect mean density **(a)** and median biomass **(b)** as calculated from bootstrapping (see Methods). Error bars represent 95% confidence intervals and asterisks denote a lower confidence interval of zero. **(c)** Relative percentage densities of higher taxonomic fish groups, expressed as percentage of maximum density of each group: (1) Pleuronectiformes, (2) Lophiiformes, (3) Ophidiiformes (4) Indeterminate Actinopterygii morphospecies (e.g. Actinopterygii msp-9) (5) Gadiformes (6) Aulopiformes (7) Anguilliformes (8) Scorpaeniformes (9) Notacanthiformes (10) Osmeriformes (11) Chondrichthyes. Groups are ordered from left to right in increasing depth of maximum relative density. Relative group densities are based on the observed standardised fish densities. Note that group densities are not shown for sites 14D01 and 14D04 because of lower certainty in morphospecies identificatitons owing to poorer image quality (see Methods).

To examine compositional differences, fish specimens were classified into 42 distinct morphospecies belonging to two classes, Chondrichthyes and Actinopterygii. As for the invertebrate megafauna, this is likely an underestimation of species diversity, possibly to a larger degree owing to the difficulty in identifying diagnostic characters, such as fin morphology and position, from the vertical images analysed in this study. For instance, for alepocephalid fish consistent identification among images of varying altitudes was only possible to family level. Furthermore, the number of unclassified specimens was relatively high, accounting for 8.9% of the total 2014 fish count. Among the classified morphospecies, most were rare, with 13 morphotypes (31%) recorded at only one site and 31 (74%) being found at five or less sites. In terms of abundance contributions, about 31% of the fish morphospecies were represented by one or two specimens. Ophidiiformes were the group with the most differentiated morphotypes (11 nominal taxa), followed by gadiform fishes and indeterminate Actinopterygii morphotypes, with 10 and 8 nominal taxa, respectively.

The bathymetric change in the relative density of higher taxonomic groups showed that pleuronectiform fishes were restricted to the upper slope at sites above 900 m (Figure 3.13c; Table S3.10), where they were represented by two morphotypes, (1) a medium-sized sole, which was recorded occasionally at the two shallowest sites at observed densities of 24 and 93 ind. $ha^{-1}$, and (2) a small tonguefish (likely belonging to the genus *Cynoglossus*), which numerically dominated the ichthyofauna assemblages at the three shallowest sites with densities between 279 and 697 ind. $ha^{-1}$ (26-30% of total fish density at these sites). Ogcocephalid anglerfish (Lophiiformes) also reached their maximum densities at the three shallowest sites with 212-649 ind. $ha^{-1}$, making up between 17-28% of the total observed numerical density. Other anglerfishes encountered were sea toads (Chaunacidae), which were restricted to the shallowest site 14C01 (337 ind. $ha^{-1}$, 14% of total fish density at the site), and rare sightings of large lophiid specimens.

Ophidiiform taxa were most abundant at upper slope depths between 600-700 m with observed densities of 187 ind. $ha^{-1}$ at site 14C02 and 134 ind. $ha^{-1}$ at site 14C03, which accounted for about 13% of the ichthyofaunal densities at each site. The numerically dominant ophidiiform at site 14C02 was a medium-sized morphotype (163 ind. $ha^{-1}$, Figure 3.8p), which was also occasionally recorded down to about 1500 m. Smaller ophidiiform specimens (msp-5) were common at site 14C03 (134 ind. $ha^{-1}$) and site 14C04 (94 ind. $ha^{-1}$). Ophidiiform cusk-eels of the genus *Dicrolene* were recorded at low numbers (11-47 ind. $ha^{-1}$) at the majority of sites at mid-slope depths between about 900 to 1800 m.

Gadiform fishes were represented by several grenadier morphotypes and the morid cods *Antimora* msp-1 and *Laemonema* msp-1, the latter being restricted to the shallowest site 14C01 with observed densities of 168 ind. $ha^{-1}$. Grenadiers were most abundant at the upper and middle slope at depth down to about 1000 m, where numerical densities ranged from 112 to 464 ind. $ha^{-1}$. The most frequently observed rattail was a medium-sized Macrourinae (msp-03), which possibly included several species, including individuals of the genus *Nezumia*. Specimens of this morphotype dominated the fish assemblages at depths between about 850 to 1050 m (30-40% of total fish density), reaching a maximum density of 464 ind. $ha^{-2}$ at site 14C04 (848 m). Other rattails seen on the upper slope included *Trachyrincus* msp-1, which was observed only at site 14C02 (152 ind. $ha^{-1}$). Below 1000 m, macrourids were either not observed or rare with densities being about one magnitude lower (15-43 ind. $ha^{-1}$) compared to those recorded at shallower depths.

Tripodfishes (genus *Bathypterois*, Aulopiformes) were recorded at the majority of sites from about 700 m in low densities of 7-45 ind. $ha^{-1}$. A similarly wide depth range was observed for the Halosauridae, which were recorded at 23 out of the 26 assessed sites, reaching maximum densities of up to 164 ind. $ha^{-1}$ at the mid sections of the slope between about 850 and 1500 m. They were likely represented by two genera, *Aldrovandia* and *Halosaurus*, with specimens of both groups seen feeding in the sediment, which might be partly responsible for the numerous ovoid seabed depressions that were observed across the middle-slope region. Among the cutthroat eels (Synaphobranchidae), large *Synaphobranchus* specimens were the most widely distributed with sightings at depths between about 850 to 1850 m and densities of up to 76 ind. $ha^{-1}$. Smaller specimens of the genus *Ilyophis* appeared to have a more restricted depth range, with records between about 1275-1460 m and densities up to 27 ind. $ha^{-1}$. Slickheads (Alepocephalidae) were found at most sites between about 620 to 1870 m water depth, while elasmobranchs and Psychrolutidae were only occasionally sighted.

#### 3.3.1.3 Foraminifera

A variety of tubular, spherical and arborescent structures were observed, some of which we believe to be epibenthic Foraminifera. However, diagnostic features were usually not visible to identify them with certainty as foraminiferans, with the exception of larger forms, which we classified into six morphospecies (Table S3.4). The latter showed considerable differences in numerical densities and distribution (Figure 3.14a). The most common morphotype was a thin tubular form with an agglutinated dichotomously branching test (Figure 3.14b), occasionally with accumulated sediment around its apertures. This morphotype most resembles species in the genus *Schizammina* (Heron-Allen and Earland, 1929) described from shallow waters (<100 m) off West Africa, including the Angolan shelf (Buchanan, 1960; Nørvang, 1961), but it may also belong to the genus *Rhabdammina* (Gooday, pers. comm.). Densities varied widely across the recorded depth range (~ 600-2000 m), peaking in the mid-slope region between about 1000-1750 m with observed densities of up to about 20100 ind. $ha^{-1}$. Differences along the slope were also evident, with the mid-slope sites sampled in Area B showing consistently lower densities compared to sites sampled at similar depths in Areas C and D. Likewise, while branching foraminerans were very common at the lower slope in Area D (site

14D09, 1750 m, ~17600 ind. ha$^{-1}$), they were absent or only rarely seen on the seabed along the lower slope in Area A.

A second tubular but unbranched type of agglutinated foraminiferan (Figure 3.14c) resembling specimens of the genus *Bathysiphon* and *Rhabdammina* numerically dominated the megafaunal assemblages at the two mid-slope sites sampled in Area C, with densities of about 29800 ind. ha$^{-1}$ at site 14C06 (1217 m) and 19600 ind. ha$^{-1}$ at site 14C07 (1435 m), which represented about 84 and 92% of the total observed megafaunal density at these sites, respectively. Locally, maximum densities of up to 29 ind. m$^{-2}$ were seen at site 14C06 based on single images. Specimens of this morphotype appeared to be laying horizontally on the seabed and were typically covered in part with sediment. The remaining observed foraminiferans were Xenophyophores, which were recorded in low numbers (combined standardised densities of 9-20 ind. ha$^{-1}$). They were represented by specimens with plate-like and reticulated (Figure 3.14d) morphologies.

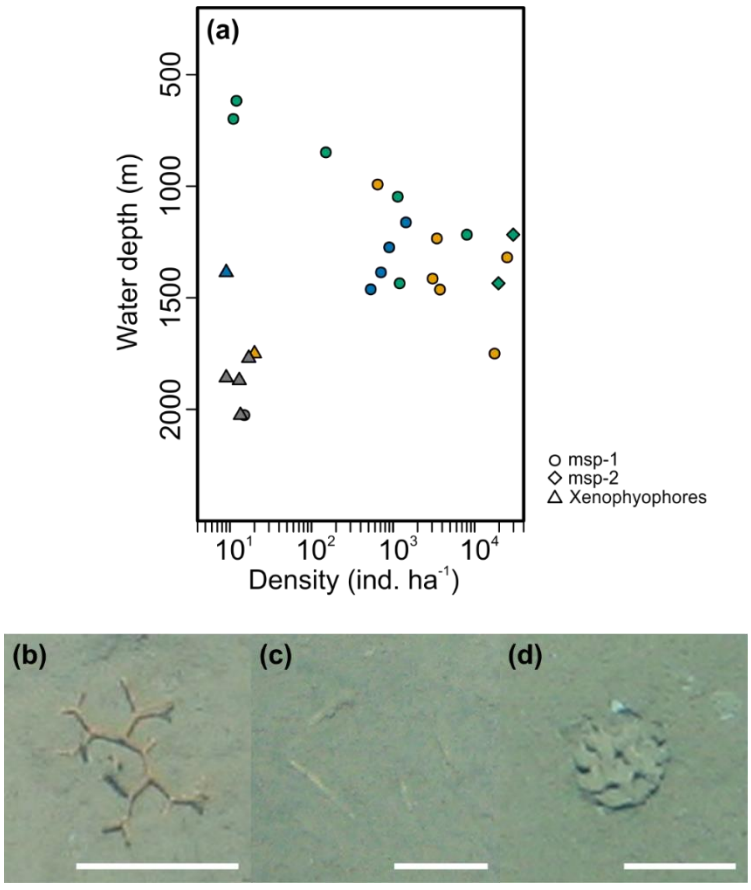


**Figure 3.14 (a)** Numerical densities of megabenthic Foraminifera observed along the Angolan continental slope in 2014, keyed to study areas A (grey), B (blue), C (green), and D (yellow). Densities are the standardised transect totals for Foraminifera msp-1 **(b)**, Foraminifera msp-2 **(c)**, and the sum of all classified Xenophyophores, including reticular-shaped specimens **(d)**. Scale bars represent 5 cm.

### 3.3.3 Associations between environmental and biological data

Scatterplots of the selected environmental variables (Figure 3.12) and their associated pairwise Spearman rank correlations (Table S3.6) showed that many of the environmental predictors were highly inter-correlated. A strong positive monotonic relationship was observed between water depth and bottom-water oxygen concentration ($r_s = 0.90$, $p < 0.01$, Table S3.6). Bottom-water temperature and estimated POC flux were both negatively correlated with water depth ($r_{s,\,T} = -0.98$, $r_{s,\,POC\ flux} = -0.95$, $p < 0.01$) and with dissolved oxygen concentration ($r_{s,\,T} = -0.89$, $r_{s,\,POC\ flux} = -0.87$, $p < 0.01$). Sediment percent clay showed a strong significant monotonic decline with increasing water depth ($r_s = -0.81$, $p < 0.01$), while the fraction of sediment material coarser than 63 μm was positively correlated with depth ($r_s = 0.59$, $p < 0.05$). Correlations also exists among the assessed hydrographic and sedimentary variables (Table S3.6).

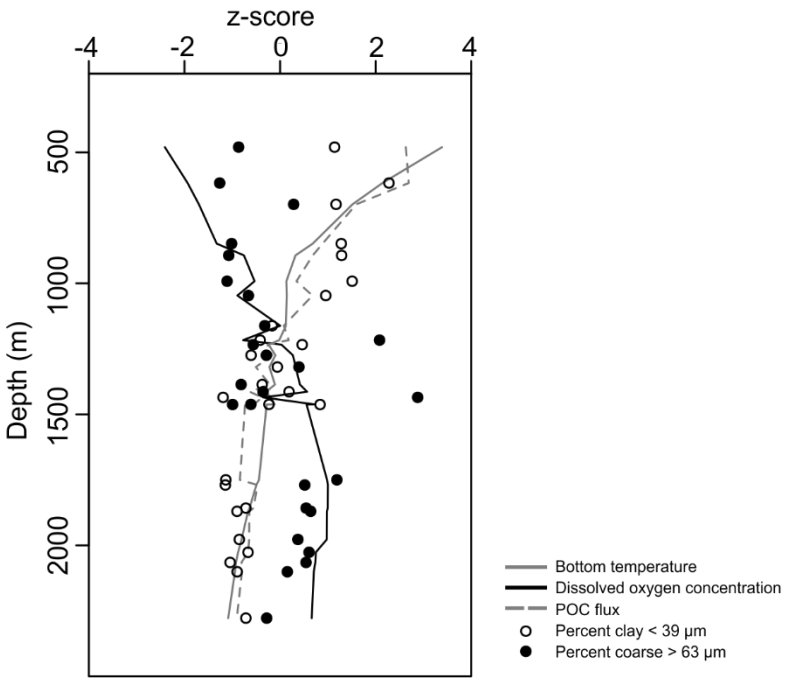


**Figure 3.15** Comparison of bathymetric changes in environmental parameters measured at or near the photographic sites sampled in 2014. To facilitate comparisons, environmental values were normalised to zero mean and unit variance (z-score).

Pairwise Spearman rank correlations among ecological and environmental parameters (Table 3.2) showed significant ($p < 0.01$) negative monotonic trends in ichthyofauna density with water depth ($r_s = -0.89$), dissolved oxygen ($r_s = -0.72$), and percent coarse material > 63 μm ($r_s = -0.64$), and significant ($p < 0.01$) positive correlations of fish density with bottom water temperature ($r_s = 0.84$), POC flux ($r_s = 0.83$), and clay content ($r_s =$

0.82). Approximated ichthyofaunal biomass was significantly positively correlated with estimated POC flux ($r_s$ = 0.59, $p < 0.05$). Invertebrate density was significantly ($p < 0.05$) correlated with depth ($r_s$ = -0.70), temperature ($r_s$ = 0.67), and dissolved oxygen concentrations ($r_s$ = -0.68) for photographic sites sampled above 1900 m water depth. In contrast, no significant monotonic associations were detected between invertebrate densities and environmental parameters when the whole sampled depth ranged was considered (Table 3.2).

**Table 3.2** Spearman rank correlations ($r_s$) between environmental parameters and ecological descriptors. White = not significant, light grey $p < 0.05$, dark grey $p < 0.01$ - after sequential Bonferroni adjustments.

| | Depth | T | DO | POC flux | % Clay | % Coarse |
|---|---|---|---|---|---|---|
| Density $_{2014\ Invertebrates}$ | -0.430 | 0.417 | -0.496 | 0.371 | 0.450 | -0.199 |
| Density $_{2014\ fish}$ | -0.887 | 0.838 | -0.716 | 0.834 | 0.820 | -0.642 |
| Biomass $_{2014\ fish}$ | -0.517 | 0.489 | -0.437 | 0.585 | 0.487 | -0.348 |
| $^{0}D_{180,\ 2014\ Invertebrates}$ | 0.416 | -0.414 | 0.476 | -0.419 | -0.512 | 0.359 |
| $^{0}D_{180,\ 2014\ Invertebrates < 1900\ m}$ | 0.700 | -0.645 | 0.687 | -0.669 | -0.690 | 0.492 |
| $MDS_{x,\ 2014\ Invertebrates}$ | 0.819 | -0.775 | 0.753 | -0.712 | -0.744 | 0.397 |
| Density $_{2014\ Invertebrates < 1900\ m}$ | -0.701 | 0.674 | -0.679 | 0.581 | 0.607 | -0.356 |
| Density $_{All\ years\ Invertebrates}$ | -0.194 | - | - | - | - | - |
| Density $_{All\ years\ Invertebrates < 1900\ m}$ | -0.621 | - | - | - | - | - |

Apparent non-monotonic associations between environmental parameters and ecological metrics were not tested. T- bottom water temperature (°C); DO - dissolved oxygen concentrations close to the seabed (ml $l^{-1}$ ); POC flux - approximated POC flux to the seabed using the Lutz algorithm (15 year mean, mg C $m^{-2}$ $day^{-1}$); % Clay - < 39 μm; % Coarse - all material > 63 μm; $^{0}D_{180}$ - expected morphospecies invertebrate richness for 180 individuals; $MDS_x$ - X-ordinate of 2D multidimensional scaling.

The lack of significance among the many moderate monotonic correlations between ecological and environmental parameters may to some extent reflect the conservative nature of the sequential Bonferroni method, which was applied to minimise the inflation of false positives when testing multiple hypotheses. Holm's (1979) method, like others that adjust p-values by controlling the family-wise error rate, is considered conservative in that it trades the reduction of false positives for some loss of power, leading to inflated Type II errors (false negatives), in particular when running multiple tests with several highly correlated variables (Garcia, 2004; Rice 1989), such is the case here. Less conservative multiplicity adjustment methods could be applied, for example those controlling for the false discovery rate (FDR, e.g. Benjamini and Hochberg, 1995). While

this will provide more power to detect significant associations, inferences about causal relationships remain constrained by the high degree of correlation that was detected among the environmental variables.

It must also be noted that the constraints of the survey design by oil and gas licence blocks meant that photographic sites cannot be considered independent of each other. Auto-correlation might also have resulted from the use of two different camera systems. This lack of independence needs to be considered carefully when interpreting broad-scale spatial trends in faunal assemblage composition and diversity.

## 3.4 Discussion

This study is one of the few that targets Angolan margin benthic megafauna from the most common habitat, soft sediments. It is by far the largest quantitative study of megafaunal community ecology conducted in the region. Several of the BIOZAIRE sites are on the Angolan margin and correspond in depth to those investigated here (Site ZA: 1300-1400 m depth; Tete: 277- 1594 m; Guiness: 750 m; Sibuet and Vangriesheim, 2009). Megafauna were assessed at some of these sites using ROV and beam trawl but the results of these investigations have focussed on the chemosynthetic fauna (Sibuet and Vangriesheim, 2009), and cannot be used to make comparisons with these data. The few megafaunal taxa associated with soft sediments near asphalt mounds (Jones et al., 2014) are found in this study, but comparison offers little ecological insight. The extensive sampling of the DIVA expeditions (e.g. Kröncke and Türkay, 2003), at the Angola Abyssal Plain, and the Congolobe sampling, at the terminal lobe of the Congo sea fan (Rabouille et al. 2017a, b), are both too deep to be meaningfully compared to results presented here. The fishes of the Angolan margin are slightly better reported than the invertebrate megafauna, with observations of fishes observed from the DELOS observatory (Milligan et al., 2020), at artificial baits (Jamieson et al. 2017), and at natural food falls (Higgs et al., 2014). In all cases, quantitative comparisons are not possible for megafaunal communities and only more qualitative direct comparisons can be made, for example assessing patterns in individual species. In addition, interpretations of faunal-environment relations are confounded by the high collinearity among the environmental variables that were analysed in this study. As such, only general inferences can be made here supported by patterns observed elsewhere in the Atlantic, often at sites at great distances from Angola.

### 3.4.1 Abundance and biomass

Invertebrate numerical density decreased monotonically by about two orders of magnitude with increasing depth up to about 1900 m water depth. Below 1900 m localised higher densities were observed, associated with a corresponding peak in approximated invertebrate wet biomass.

The faunal densities were generally similar in magnitude to those recorded from other margins of the eastern Atlantic Ocean (Figure 3.16). Megafaunal densities at mid-slope depths between about 900-1500 m compare favourably with values reported from similar depths on the Nigerian slope (Jones et al., 2013), and densities at lower slope depths < 1900 m are of similar magnitude to those found on the lower slope of the Northwest African margin (Rice et al., 1979). Megafaunal densities recorded from the upper slope off southern Mauritania at c. 750 m depth (Jones et al., 2012) fall at the lower limit of densities found at similar depths in this study (c. 780 m in Area D).

Off Cap Blanc on the northern Mauritanian margin (c. 19-21°N), invertebrate megafaunal densities on the lower slope (c. 1600-2100 m water depth; Galéron et al., 2000) were, for the most part, higher than the values recorded in this study from the mid and lower slope sites at depths between about 1000 to 1900 m. Sampling off Mauritania was carried out using demersal gear, which is known to give lower faunal densities compared to estimates based on seabed photographs (e.g. Haedrich et al. 1975; Thurston et al., 1994), suggesting that the differences in densities may be even more pronounced. The northern parts of the Mauritanian margin are, like the Angolan margin, characterised by strong seasonal coastal upwelling (Galéron et al., 2000). Morel et al. (1996) reported high chlorophyll concentrations year-round for nearshore waters off Cap Blanc; therefore, the higher megafaunal densities observed off Mauritania relative to the mid-slope sites sampled off Angola may be the result of less pronounced seasonal fluctuations in surface production and more continous fluxes of organic matter to the seafloor.

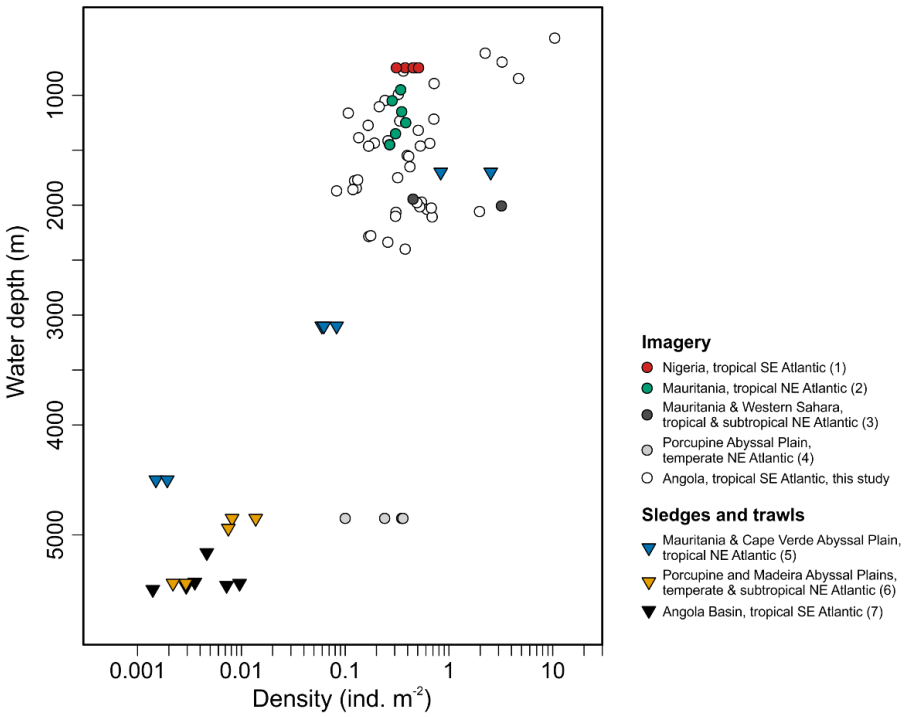


**Figure 3.16** Megafaunal densities (ind. $m^{-2}$) recorded in this study and from continental slopes and abyssal plains of the eastern Atlantic Ocean. Figure has been extended from Jones et al. (2012). Literature sources: (1) Jones et al., 2013, seabed slope < 3°; (2) Jones et al., 2012; (3) Rice et al., 1979; (4) Durden et al., 2015, flat terrain; (5) Galéron et al., 2000; (6) Thurston et al., 1994; (7) Kröncke and Türkay, 2003.

There has been a long-standing notion that food availability is a key driver of faunal distributions and community dynamics in deep waters (e.g. McClain et al., 2012; Rex et al., 2005; Sibuet et al., 1989), and changes in the standing stocks of deep-sea invertebrate communities with water depth have long been associated with gradients in detrital fluxes to the seabed (e.g. Billet et al., 2010; Johnson et al., 2007; Galéron et al., 2000; McClain et al., 2012; Rex et al., 2006; Sibuet, 1985). At broader scales, the flux of particulate organic carbon decreases rapidly with increasing water depth as organic matter is consumed and remineralized while sinking to the seafloor (Gooday, 2002; Lutz et al., 2007; Suess, 1980).

We found no correlation between approximated POC flux and invertebrate densities and biomass. However, this might not be surprising for several reasons. First, we did not account for the time needed for detrital material to reach the seafloor. Second, common algorithms to approximate POC fluxes, such as those used in this study, assume a strict downward flux of organic material from the euphotic zone to the ocean floor. However, on margins, organic matter distribution is far more complex and often influenced by

processes such as lateral displacements by subsurface currents, vertical mixing or riverine runoff (Johnson et al., 2007). In addition, topographic features can alter the distribution of organic material by controlling hydrodynamic conditions and accompanying particle transport direction and settlement rate (e.g. Genin et al., 1986; Morris et al., 2016). It has been suggested that detrital matter distribution on the Angolan margin is complex (Sibuet and Vangriesheim, 2009). Tidally-induced vertical mixing occurs, at least locally, along the upper slope (Hanz et al., 2019), and downslope transport has been predicted for the mid to lower slope sections (Rabouille et al., 2009).

The highest invertebrate density was recorded at the shallowest site (480 m, Area C), which reflected a high density of suspension feeding sea pens. The occurrence of dense suspension-feeding communities has been linked to enhanced bottom shear stress and turbulences, which increases the availability of food in the water column near the seabed by enhancing the resuspension of organic matter in surficial sediments and that of sinking phytodetritus (e.g. Mosch et al, 2012; Rice et al., 1990). The presence of visible ripples on the seabed were restricted to the shallowest site, providing a strong indication of comparatively strong currents at these depths. In addition, recent hydrographic work conducted c.60 km south of Area C (Hanz et al., 2019) has revealed a thick nephloid layer between 200-350 m water depth and strong tidally-induced vertical mixing of upper ocean layers, suggesting increased downward transport of organic matter at upper slope depths.

The supply of organic material to the upper slope sites may further be enhanced owing to their position below the permanent OMZ. Reduced dissolved oxygen concentrations of < 1 ml $l^{-1}$ occur between about 300 and 600 m within the permanent thermocline (Chapman and Shannon, 1987), with minimum oxygen concentrations of < 0.5 ml $l^{-1}$ reported from its core (Helly and Levin, 2004). In this study, minimum oxygen values of 0.29 and 0.37 ml $l^{-1}$ were, respectively recorded in Area C and D at depths between about 340-360 m. Other margins with mid-water oxygen minima (e.g. Peru, Oman, California, India) exhibit a sharp increase in densities of epibenthic megafauna near the lower boundaries of the OMZ, which is often accompanied by a decrease in assemblage evenness (e.g. Hunter et al., 2011; Levin, 2003; Mosch et al., 2012; Sellanes et al., 2010; Wishner et al., 1990). For example, Mosch et al. (2012) documented increased numbers of epibenthic gastropods, ophiuroids, and sea pens from the lower OMZ boundary along the Peruvian margin. Off Oman in the Arabian Sea, dense megafaunal assemblage near the lower OMZ boundary

were dominated by ophiuroids, spider crabs and galatheid decapods (Levin, 2003), while on the Pakistan margin ophiuroids, sea pens and tunicates were prevalent (Gooday et al., 2009; Murty et al., 2009). These sharp increases in megafaunal densities near the lower boundaries of OMZs have been related to an increased supply of relative undegraded organic matter to these areas resulting from slow degradation and consumption within the OMZ core (e.g. Levin, 2003; Wishner et al., 1999). A similar 'edge effect' (Mullins et al., 1985) might control megafaunal population densities on the upper Angolan slope; however further sampling at shallower depths would be required to test this hypothesis.

The increase in invertebrate densities at the lower slope below 1900 m was driven by large numbers of the irregular urchin *Pourtalesia* sp., which was present in all three sampling years. In addition, local aggregations of the holothurian *Scotoplanes* sp. were observed in 2005 at sites between c. 1780-1850 m water depths. Substantial spatial and temporal variability in invertebrate megafaunal densities, particularly of motile detritivore echinoderms, have been documented from soft-bottom habitats at both bathyal (e.g. Gutt and Piepenburg, 1991; Smith and Hamilton, 1983) and abyssal (e.g. Billett et al., 2001; Kuhnz et al., 2014) depths. Such changes have been associated with variations in organic matter supply, ranging from finer scale patchy depositions of phytodetrital material driven by local processes (e.g. Billett and Hansen, 1982) to larger-scale intra- and inter-annual fluctuations regulated by climate-driven changes in surface production or shifts in upper ocean dynamics (e.g. Billet et al., 2010; Kuhnz et al., 2020). For the elasipodid *Scotoplanes*, tracer studies suggest a preference for recently settled detritus (Miller et al., 2000), and specimens of this genus have previously been observed to aggregate, possibly in response to favourable feeding grounds (Smith and Hamilton, 1983). Small-scale spatial and temporal variations in the distribution and density of this morphospecies might therefore also be expected along the Angolan margin.

The widespread presence of *Pourtalesia* in all three sampling years in Area A at depths below 1900 m might indicate relative stable fluxes of organic matter that can facilitate locally high echinoid populations throughout the year. Area A is located below the highly productive waters associated with the Congo River outflow (Figure 3.5). Estimated NPP values suggest lower seasonal variation in production across most of Area A compared to Areas B to D, suggesting more steady fluxes in organic matter throughout the year. The conspicuous absence of echinoids above 1900 m, however, points to additional controls,

possibly related to broader scale variations in seafloor topography or sediment properties. For instance, the less regular terrain at lower slope depths in Area A (Figure 3.1) may enhance the lateral supply of phytodetritus by channelling bottom currents. Alternatively, variations in substratum characteristics such as the observed change from more irregular surfaces with ovoid depressions at mid slope depths to relative flat substratum below c. 1800-1900 could be favourable for the echinoids. A more balanced, spatially replicated sampling of deep-water assemblages across the Angolan slope would be needed to better understand whether or to what extend echinoid population densities relate to overhead production or local environmental conditions. In addition, spatially replicated measurements of carbon fluxes, organic matter, or sediment pigment concentrations would help to assess to what extent alongslope differences in primary production translate into differences in food availability along the slope.

The trend in approximated wet biomass mostly followed the pattern in faunal densities, except at the lower slope between c. 1750-1900 m water depths where low numerical densities were accompanied by high biomass, which were driven by the large synallactid *Paelopatides* sp. High megafaunal biomass at lower slope and abyssal depths has been observed on other eastern Atlantic margins, such as off Mauritania (Ramos and Ramil, 2017), in the Porcupine Seabight (Lampitt et al., 1986), and across the Goban Spur on the Celtic continental margin (Duineveld et al., 1997). Similar to this study, the comparatively high megafauna biomass at deeper sites across the Goban Spur (Duineveld et al., 1997) were driven by large motile holothurians. The authors concluded that the seasonally driven input of phytodetritus favours larger motile taxa owing to their lower relative metabolic demands and ability to move around to locate patches of fresh detritus. The high biomass values observed in the deep-waters off Mauritania (Ramos and Ramil, 2017) have been related to enhanced rates of organic matter supply by the Senegal River and nearby canyon systems. It is likely that the biomass patterns observed in this study reflect a combination of influences, including the enhanced organic matter supply from the highly productive waters surrounding the Congo River outflow and taxa-specific adaptations to resource availability, expressed via, for example body-size (Duineveld et al., 1997) or feeding activity (Durden et al., 2019).

For demersal fish, a monotonic decline in densities by about two orders of magnitude was found, from c. 2300 ind. $ha^{-1}$ at around 500 m to c. 370-500 ind. $ha^{-1}$ at 1000 m and < 50

ind. $ha^{-1}$ below 2000 m. These density estimates and their magnitude of change closely resembles those reported for demersal fish assemblages on the northwest African margins off Morocco (Merrett and Domanski, 1985) and Mauritania and Western Sahara (Merrett and Marshall, 1981). Merrett and Domanski (1985) documented a two-fold decline in relative abundance from c. 500 ind. $ha^{-1}$ at around 1000 m to < 5 ind. $ha^{-1}$ at 3000 m, while Merrett and Marshall (1981) reported an exponential decline from c. 1000 ind. $ha^{-1}$ at 500 m to c. 500 ind. $ha^{-1}$ at 500 m, < 20 ind. $ha^{-1}$ below 2000 m and < 5 ind. $ha^{-1}$ below 3000 m water depth. Both studies are based on demersal gear samples, and therefore direct comparisons with values from this photographic study are problematic (e.g. Haedrich et al., 1975). Nevertheless, the comparisons suggests similar rates of change in fish densities on the Angolan and NW African slopes.

### 3.4.3 Diversity

Comparisons of species diversities estimated in this study with those reported from neighbouring regions are difficult because of the limited number of studies in the SE Atlantic, differences in sampling methodologies, and varying levels of taxonomic resolution. Visually, many of the more common invertebrate morphospecies appear similar to those documented from other bathyal environments in the Gulf of Guinea (Lebrato and Jones, 2009; Jones et al., 2013), and off north-west Africa (Aldred et al., 1979; Jones et al., 2012; Ramil and Ramos, 2017; Rice et al., 1979). This included the common occurrence of several caridean shrimp species, including *Nematocarcinus*, on the upper slope (Ramil and Ramos, 2017), the presence of *Phormosoma* at upper to mid-slope depths (Jones et al., 2012, 2013; Ramil and Ramos, 2017), and the presence of *Benthothuria* and *Paelopatides* in deeper areas (Ramil and Ramos, 2017). The small galatheid squat lobsters that dominated at upper slope sites between 800-900 m resembles a species recorded on the central Mauritanian slope (Jones et al., 2012), and the large specimens of *Actinoscyphia* are similar to specimens photographed off central (Jones et al., 2012) and northern (Aldred et al., 1979) Mauritania.

Comparisons of invertebrate morphospecies richness estimated for each photographic site suggested a trend of increasing richness from the upper slope to deeper areas. An increase in species richness from shallower to intermediate depths has been documented for several macro- and megafaunal groups, often as part of a parabolic trend (e.g. Cordes et al., 2010;

Levin et al., 2001; Menot et al., 2010a; Pequegnat, 1990; Rex, 1981; Wei and Rowe, 2009). Pooling the photographic sites by depth bands (Figure 3.17) shows a unimodal trend in expected richness as well as in the expected number of common and dominant morphospecies. However, these patterns must be interpreted cautiously, as the higher number of morphospecies at mid-slope depths might be related to the greater number of Areas that were sampled along the middle slope. In particular, the extent to which the distinct decline in diversity below 1900 m reflects regional patterns is unknown since samples at lower slope depths were only taken in Area A. The low diversity below 1900 m is predominantly driven by the dominance of irregular echinoids, which may, as previously discussed, reflect favourable habitat conditions in terms of sediment topography or higher food availability. More locations along the lower slope will need to be sampled to get a more representative view of invertebrate morphospecies richness at lower slope depths.

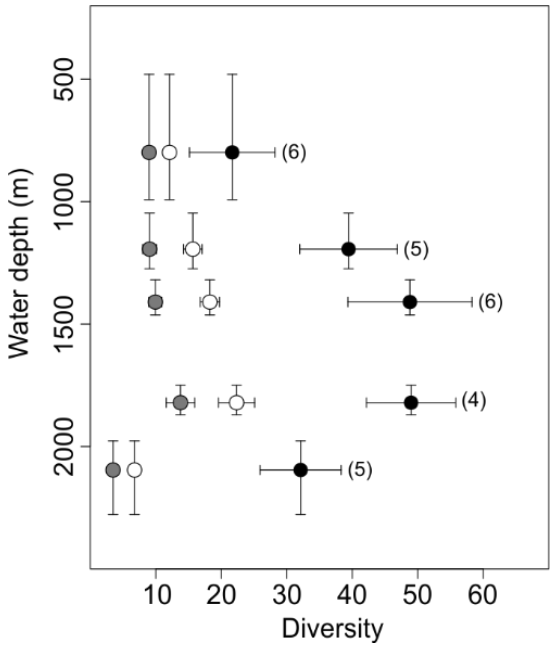


**Figure 3.17** Variation in invertebrate diversity with water depth, based on pooled photographic material collected in 2014. Data from the 26 transects were grouped into five depth strata: 400-1000 m, 1000-1300 m, 1300-1600 m, 1600-1900 m, and below 1900 m. Rarefied morphospecies richness (black circles), exponential Shannon entropy exp H' (white circles) and inverse Simpson concentration 1/D (grey circles) per 440 individuals of invertebrate megafauna. Horizontal error bars represent the 95% confidence intervals for the interpolated values. Vertical error bars show the depth range of each pooled sample. The numbers in parentheses are the number of transects pooled for each sample.

The drivers for the observed trends in invertebrate diversities cannot be resolved in this study, but are likely to involve both historical and contemporary processes. For instance, phenotypic and genotypic variation of several macro- and megafaunal species have been found to be higher at upper bathyal depths than at lower bathyal and abyssal depths, suggesting higher rates of diversification at intermediate depths (Carney, 2005). Contemporary forces proposed to control bathymetric diversity patterns include sediment heterogeneity, environmental stability, and energy availability (e.g. Levin et al., 2001; McClain and Schlacher, 2015). The latter has been given particular attention, and many of the mechanistic theories that have been proposed to explain depth-related diversity trends in the deep-sea involve the influence of productivity. For example, the high inputs of organic matter encountered at upper bathyal depths have been suggested to facilitate competitive exclusion by favouring population growth of opportunistic taxa, thereby leading to less diverse and more unevenly distributed communities (Levin et al., 2001). Other hypotheses put forward to explain lower diversity at shallower depths include increased stochasticity at shallower depths owing to more variable levels of surface production (Levin et al., 2001), and hypotheses based on productivity-driven environmental stability and predator-prey interactions (Rex et al., 2005a). It is also possible that the increase in invertebrate diversity observed in this study was driven by the change from hypoxic to oxic conditions. Positive relationships between alpha diversity of megafauna and dissolved oxygen concentrations have, for example, been found across the core and lower transition zone of the OMZ on the Chilean margin (Sellanes et al., 2010).

### 3.4.2 Faunal composition

Invertebrate community composition changed continuously along the depth gradient sampled as a result of morphospecies replacement. Depth-related changes in benthic community composition from shelf to abyssal depths are well documented from many basins for both megabenthic invertebrate (Carney, 2005; McClain and Rex, 2015; Menot et al., 2010a), and demersal fish (e.g. Bianchi, 1992; Haedrich et al., 1980; Koslow, 2013; Sobrino et al, 2012) communities. These changes are generally thought to reflect taxon-specific evolutionary adaptations to deep-water conditions, such as pressure, temperature, or organic matter supply, which will determine their vertical distribution limits (Carney,

2005). Overlapping species range distributions will lead to the gradual replacement of species that is often seen on contintental margins (Carney, 2005; Gage and Tyler, 2010).

For the invertebrate megafauna, cluster analysis indicated the presence of three main faunal groups within the sampled depth range (480-2400 m): (1) an upper slope group up to about 700 m water depth typified by sea pens, zoanthids, squat lobster, quill worms, burrowing ophiuroids and caridean shrimps, (2) a middle slope group characterised by squat lobsters, zoroasterid sea stars, small ophiuroids, and asteroids, and (3) a lower slope group below about 1700 m depth dominated by deposit-feeding echinoderms. Faunal turnover was mostly gradual, with larger turnover occurring at mid-slope depths between about 1400-1500 m, between the deepest site of Area D (1750 m) and the shallowest site in Area A (1770 m), and between the two sites sampled between 600-700 m water depth. These areas of larger change may reflect smaller-scale variations in environmental conditions or area-wide vertical distribution patterns. In a review of zonation patterns on continental margins, Carney (2005) found common zones of more rapid faunal turnover on the upper slope at around 1000 m and at the slope-abyss transition between about 2000-3000 m. Although the position and vertical extent of these transition zones vary among regions as well as taxonomic groups, their ubiquity suggests that they represent common barriers in the distribution of deep-water fauna (Carney, 2005). The mechanisms creating these barriers remain uncertain but it has been suggested that thermal effects and declining fluxes of organic matter may play an important role (Brown and Thatje, 2014; Carney, 2005).

Whether the enhanced rate of faunal turnover observed between about 1400-1500 m water depth represents a mid-bathyal transition zone is uncertain, given the lack of sampling between 1500-1750 m water depth. The position of faunal transition zones has been linked to changes in hydrographic properties, such as those occurring between water masses (e.g. Bett, 2001; Williams et al., 2010). For the South East Atlantic, Antarctic Intermediate Water is reported down to about 1200 m (Stramma and Schott, 1999), above the area of increased faunal rate. In addition, the CTD data collected as part this study showed relative stable conditions between 1200-1500 m depth, suggesting a weak influence of water mass structure on the observed increased rate of turnover at 1400-1500 m depth. The rate increase at about 1750 m depth reflected differences between communities sampled in

Area D and those sampled in Area A, and might be related to variations in local environmental conditions.

Community composition and faunal turnover at upper bathyal depths might be influenced by the OMZ. Previous studies across OMZs detected distinct zonation patterns in epibenthic invertebrates at lower OMZ boundaries, characterised by high faunal densities and high levels of turnover in dominant species (Gooday et al., 2010; Levin, 2003). The high turnover has been attributed to the combined influence of different physiological oxygen limits and a rich supply of high quality organic matter at lower OMZ boundaries that results from the slow degradation and consumption within the OMZ (Levin, 2003). In this study, relative high dominance of invertebrate communities by a few taxa prevailed to about 900 m depth, showing local variations with communities dominated by sea pens (480 m), caridean shrimp (620 m), burrowing ophiuroids (700 m), or small squat lobsters (800-900 m). However, whether this indicates an influence of the overlying OMZ is uncertain. The presence of sea pen dominated assemblages at the shallowest site is, as previously discussed, likely facilitated by higher bottom currents and enhanced organic matter supply via tidal mixing. Furthermore, the observed dominance of small squat lobsters at 800-900 m water depth might be indicative of fishing impacts. Disturbances caused by bottom trawling have been linked with shifts to smaller sized fauna, and may also reduce species richness (Jennings and Kaiser, 1998). Demersal fishing is taking place along the upper Angolan slope (Saetersdal et al., 1999) and has been observed in Area D prior to sampling site 14D01 (780 m; data from this site were only included in standing stock estimates). The marked 15-fold reduction in invertebrate densities at site 14D01 in Area D compared to densities found at comparable depth in Area C most likely reflected the direct effects of demersal trawling. Seabed images collected at the site revealed trawl marks and elevated levels of suspended sediments, indicating recent trawling activity. Invertebrate diversity at sites sampled between 800-900 m was lower compared to shallower sites, which, together with evidence of fishing and the high dominance of small squat lobsters might indicate a fishing impact.

The composition of the invertebrate communities at mid-slope depths showed geographic differences among sampling areas B, C and D, which were predominantly driven by the occurrence of rare morphospecies and variations in the densities and relative abundance distributions of common morphospecies. These differences in faunal composition may, at

least partly, reflect sampling biases owing to using two different imaging systems. Different lightning and image resolutions might have affected the detectactibility and taxonomic resolution of faunal identifications, in particular for smaller morphotypes. In addition, differences in local population densities may reflect the underlying heterogeneity of the physical habitat, in terms of local topography and sedimentary properties and related hydrodynamic conditions, which may influence megafaunal distributions by regulating food availability, dispersal and recruitment patterns (e.g. Billett and Hansen, 1982; Haedrich et al., 1975; Hecker et al., 1990). The sediment data showed clear differences in sediment grain size distributions and sediment organic matter content between Area C and Areas B and D. Further work is needed to better understand the variations in faunal composition at mid-slope depths, and an analysis of individual morphospecies distributions or feeding guilds in relation to sediment properties would seem potentially useful.

# 3.5 Supporting information

## 3.5.1 Transect metadata

**Table S3.1** Details of photographic data used to assess megafaunal assemblages across sedimentary habitats. Area labels are ordered from North to South, and transects are listed in increasing mean transect water depth for each sampling year. Transect represents the original transect name, and site code is the label used in this study. Central latitude and longitude are the approximate centre points of each photographic transect. Images represent the number of annotated photographs retained for faunal analysis, i.e. all annotated images taken between 0.8 to 3.5 m above the seabed. Taxa represents the number of metazoan morphospecies retained for analysis of diversity and faunal composition.

| Area | Transect | Site code | Date | Mean Depth (m) | Central Latitude (°) | Central Longitude (°) | Camera | Images | Seafloor area ($m^2$) | Taxa | Metazoan density (ind $m^{-2}$) | Metazoan biomass (g fwwt $m^{-2}$) |
|---|---|---|---|---|---|---|---|---|---|---|---|---|
| A | BW2 | 05A01 | 02/11/2005 | 1778 | -6.23274 | 10.81756 | OSIL Mk7 | 49 | 268 | 6 | 0.12 | 31.51 |
| A | BW1 | 05A02 | 02/11/2005 | 1846 | -6.23293 | 10.79321 | OSIL Mk7 | 72 | 297 | 8 | 0.13 | 41.1 |
| A | BW3 | 05A03 | 03/11/2005 | 1972 | -6.23149 | 10.7556 | OSIL Mk7 | 70 | 346 | 7 | 0.54 | 48.15 |
| A | SV11 | 05A04 | 04/11/2005 | 2039 | -6.24976 | 10.7214 | OSIL Mk7 | 15 | 67 | 4 | 0.62 | 66.44 |
| B | CE8 | 05B01 | 24/10/2005 | 1548 | -7.93325 | 11.96778 | OSIL Mk7 | 25 | 81 | 5 | 0.4 | 4.47 |
| B | PC8 | 05B02 | 20/10/2005 | 1556 | -7.85862 | 11.82719 | OSIL Mk7 | 53 | 154 | 9 | 0.41 | 10.29 |
| B | CE7 | 05B03 | 24/10/2005 | 1651 | -7.97842 | 11.93776 | OSIL Mk7 | 42 | 133 | 9 | 0.42 | 6.87 |
| A | R5 | 08A01 | 19/04/2008 | 1438 | -6.41205 | 10.97592 | Kongsberg | 73 | 75 | 9 | 0.65 | 5.36 |
| A | R3 | 08A02 | 04/04/2008 | 2015 | -6.78229 | 10.7798 | Kongsberg | 30 | 54 | 10 | 0.52 | 2.68 |
| A | R6 | 08A03 | 12/04/2008 | 2058 | -6.12897 | 10.62705 | Kongsberg | 57 | 85 | 12 | 1.97 | 56.3 |
| A | R4 | 08A04 | 05/04/2008 | 2107 | -6.80214 | 10.73552 | Kongsberg | 35 | 44 | 4 | 0.69 | 32.84 |
| A | R10 | 08A05 | 06/04/2008 | 2285 | -6.77708 | 10.6056 | Kongsberg | 41 | 53 | 6 | 0.15 | 0.59 |
| A | R8 | 08A06 | 11/04/2008 | 2337 | -6.18856 | 10.49549 | Kongsberg | 33 | 54 | 5 | 0.26 | 4.09 |
| A | R9 | 08A07 | 10/04/2008 | 2400 | -6.27693 | 10.47709 | Kongsberg | 27 | 37 | 6 | 0.38 | 7.58 |
| A | CAMR1 | 14A01 | 20/08/2014 | 1770 | -6.20764 | 10.82252 | Kongsberg | 310 | 1147 | 32 | 0.13 | 17.88 |
| A | CAMR2 | 14A02 | 20/08/2014 | 1858 | -6.19094 | 10.78864 | Kongsberg | 330 | 1105 | 28 | 0.12 | 16.55 |
| A | RD7 | 14A03 | 19/08/2014 | 1870 | -6.30884 | 10.81005 | Kongsberg | 447 | 1538 | 31 | 0.08 | 16.81 |
| A | CAMR3 | 14A04 | 25/08/2014 | 1977 | -6.15532 | 10.72355 | Kongsberg | 122 | 468 | 21 | 0.49 | 44.56 |
| A | MEW01 | 14A05 | 25/08/2014 | 2026 | -6.03167 | 10.66531 | Kongsberg | 193 | 668 | 27 | 0.67 | 41.02 |
| A | CAMR4 | 14A06 | 19/08/2014 | 2065 | -6.32818 | 10.74601 | Kongsberg | 290 | 909 | 31 | 0.31 | 29.85 |
| A | L1[1] | 14A07 | 16/08/2014 | 2101 | -6.18178 | 10.58841 | Kongsberg | 298 | 1079 | 27 | 0.31 | 33.02 |
| A | N4 | 14A08 | 16/08/2014 | 2278 | -6.21093 | 10.5187 | Kongsberg | 195 | 790 | 23 | 0.17 | 12.35 |

**Table S3.1** continued

| Area | Transect | Site code | Date | Mean Depth (m) | Central Latitude (°) | Central Longitude (°) | Camera | Images | Seafloor area ($m^2$) | Taxa | Metazoan density (ind $m^{-2}$) | Metazoan biomass (g fwwt $m^{-2}$) |
|---|---|---|---|---|---|---|---|---|---|---|---|---|
| B | rnd1C | 14B01 | 27/08/2014 | 1162 | -7.76105 | 12.10496 | Kongsberg | 245 | 964 | 23 | 0.11 | 2.2 |
| B | rnd4C | 14B02 | 26/08/2014 | 1274 | -7.83432 | 12.16382 | Kongsberg | 420 | 1516 | 43 | 0.17 | 1.76 |
| B | rnd7C | 14B03 | 30/08/2014 | 1386 | -7.90263 | 12.18498 | Kongsberg | 344 | 1076 | 29 | 0.14 | 3.02 |
| B | rnd10C | 14B04 | 27/08/2014 | 1462 | -7.92473 | 12.09972 | Kongsberg | 417 | 923 | 37 | 0.53 | 2.59 |
| C | 400-500 | 14C01 | 04/08/2014 | 480 | -9.23088 | 12.61234 | Kongsberg | 301 | 416 | 39 | 10.44 | 14.02 |
| C | 600-700 | 14C02 | 10/08/2014 | 617 | -8.97127 | 12.72901 | Kongsberg | 484 | 857 | 39 | 2.23 | 8.47 |
| C | B19-700 | 14C03 | 03/09/2014 | 698 | -9.19237 | 12.55888 | Kongsberg | 360 | 897 | 42 | 3.24 | 11.26 |
| C | 800-900 | 14C04 | 05/08/2014 | 848 | -9.17208 | 12.5196 | Kongsberg | 258 | 733 | 33 | 4.68 | 15.08 |
| C | 1000-1100 | 14C05 | 06/08/2014 | 1047 | -9.06943 | 12.50509 | Kongsberg | 272 | 887 | 27 | 0.244 | 6.6 |
| C | 1200-1300 | 14C06 | 12/08/2014 | 1217 | -8.75238 | 12.55092 | Kongsberg | 283 | 656 | 31 | 0.71 | 7.06 |
| C | 1400-1500 | 14C07 | 10/08/2014 | 1435 | -8.8483 | 12.38378 | Kongsberg | 484 | 938 | 31 | 0.19 | 2.67 |
| D | Z1[2] | 14D01 | 04/09/2014 | 780 | -12.13236 | 13.32783 | Kongsberg | 183 | 184 | 7 | 0.36 | 1.12 |
| D | Z2 | 14D02 | 04/09/2014 | 893 | -12.13721 | 13.27628 | Kongsberg | 700 | 932 | 28 | 0.71 | 3.21 |
| D | Z3 | 14D03 | 04/09/2014 | 992 | -12.12963 | 13.21654 | Kongsberg | 740 | 1344 | 33 | 0.33 | 5.55 |
| D | 1000-1100[2] | 14D04 | 21/07/2014 | 1104 | -12.1215 | 13.1568 | Imenco | 234 | 405 | 13 | 0.21 | 0.97 |
| D | 1200-1300 | 14D05 | 23/07/2014 | 1234 | -12.23479 | 13.0648 | Imenco | 205 | 422 | 19 | 0.34 | 2.24 |
| D | Z4 | 14D06 | 06/09/2014 | 1319 | -11.85789 | 13.06833 | Kongsberg | 514 | 783 | 39 | 0.51 | 1.03 |
| D | Proposed well | 14D07 | 24/07/2014 | 1414 | -12.09433 | 12.93791 | Imenco | 340 | 461 | 25 | 0.26 | 2.35 |
| D | 1400-1500 | 14D08 | 29/07/2014 | 1463 | -11.80288 | 12.97833 | Imenco | 367 | 788 | 24 | 0.17 | 1.67 |
| D | 1600-1700 | 14D09 | 25/07/2014 | 1750 | -12.23228 | 12.69269 | Imenco | 254 | 493 | 26 | 0.32 | 9.24 |
| | | | | | | | **TOTAL** | 10212 | 25127 | 200 | | |

[1] Several patches of asphalt extrusions and reduced sediments were present along this transect. Respective images were removed for analysis and are not listed.

[2] Owing to poor quality images from these transects were only used to quantify metazoan density and biomass. Images taken along transect 14D01 showed high loads of resuspended sediments likely due to demersal fishing observed prior to the camera deployment (IMAR Survey, 2015a). The majority of images taken along transect 14D04 were out of focus.

### 3.5.2 Environmental parameters

#### 3.5.2.1 Sediment properties

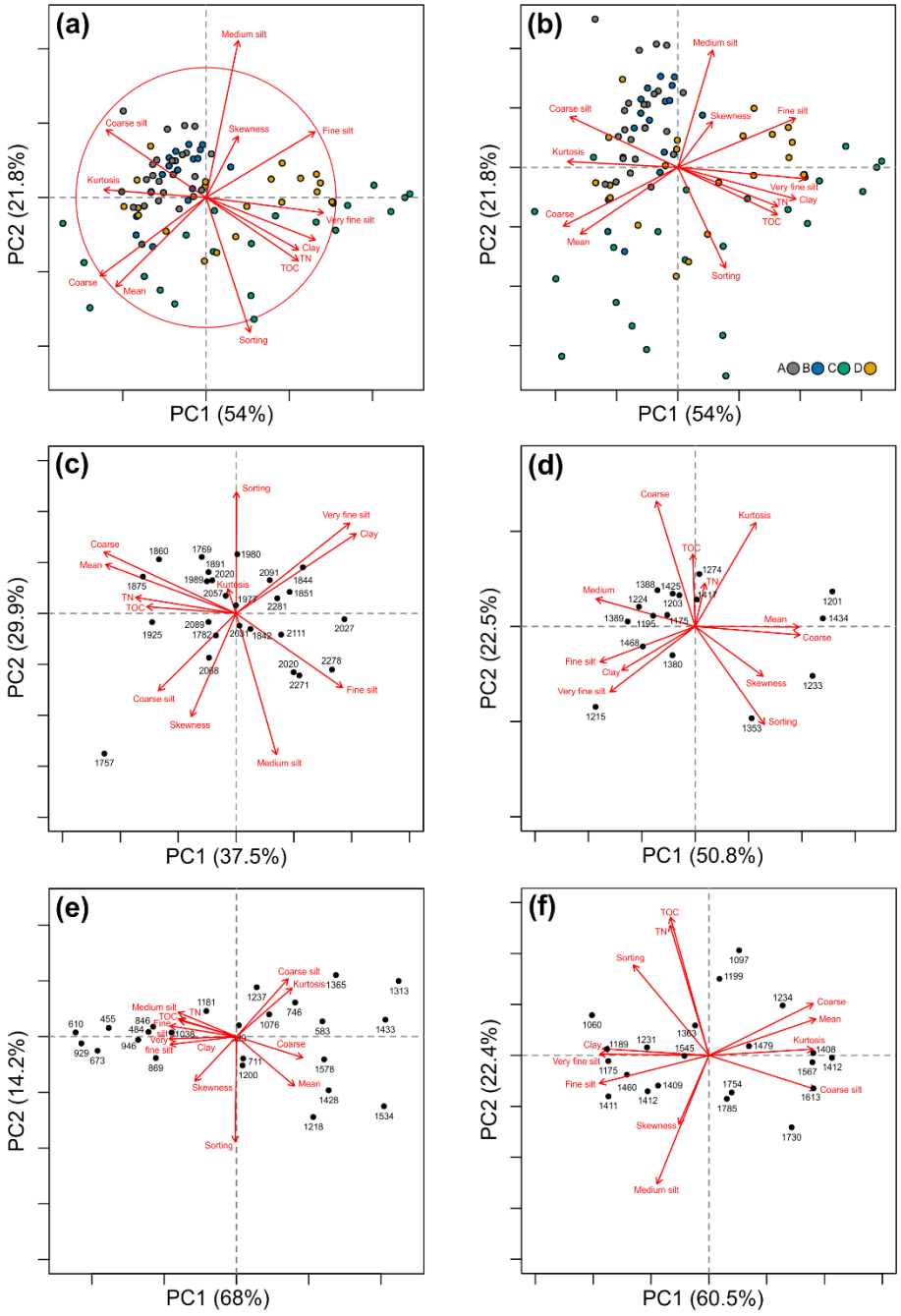


**Figure S3.1** Principal Components Analyses of Euclidean distances between normalised (zero mean and unit variance) sediment parameters of surficial sediment samples taken along the Angolan continental slope in 2014. **(a)** Distance biplot (scaling type 1) of all samples, keyed to study area (A-D). **(b)** Corresponding correlation biplot (scaling type 2). Distance biplots for samples taken in Area A **(c)**, B **(d)**, C **(e)**, and D **(f)**. The coarse sediment fraction combines all particles > 63 µm. Centred-log-ratio transformations were applied to the weight percentages of the grain size fractions prior to normalising the data to overcome the closed structure of compositional data (Aitchison, 1982). Numbers represent water depth at core station.

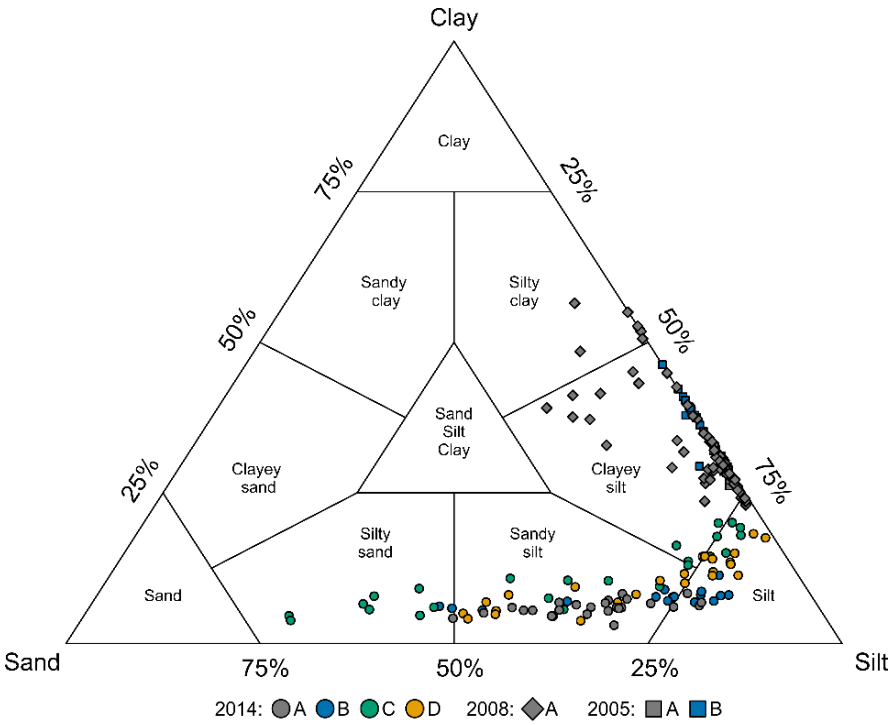


**Figure S3.2** Ternary diagram showing the proportions of sand-, silt- and clay-sized particles in surficial sediment samples taken along the Angolan continental slope, keyed to study area (A-D) and sampling year (2005, 2008 and 2014). Textural classes are based on the Shepard (1954) sediment classification. Each point represents one sediment sample. Coarse particles (> 2 mm) were absent from all samples taken in 2005 and 2008. In 2014, 7% of samples contained coarse material making up between 0.05 to 0.98% of the sediment sample. The sand-, silt- and clay-class proportions for these samples were re-calculated to sum up to 100%.

**Table S3.2** Spearman rank correlations between sedimentary parameters, assessed across all megacore stations sampled per year, and individually for each sampling area (A-D). white = not significant, light grey $p < 0.05$, dark grey $p < 0.01$ - after sequential Bonferroni adjustment based on 234 tests. Numbers in brackets represents the number of megacore sites sampled at each site and year.

| Variable 2 | Variable 2 | 2014 | | | | | 2005 | | | 2008 |
|---|---|---|---|---|---|---|---|---|---|---|
| | | All | A | B | C | D | A + B | A | B | A |
| | | (82) | (25) | (16) | (24) | (17) | (34) | (17) | (17) | (63) |
| Depth | Mud | -0.252 | 0.425 | 0.044 | -0.591 | -0.027 | -0.370 | 0.432 | -0.052 | -0.277 |
| Depth | Clay | -0.619 | 0.314 | -0.278 | -0.653 | -0.409 | -0.631 | 0.500 | -0.066 | 0.248 |
| Depth | Silt | -0.093 | 0.352 | 0.059 | -0.571 | 0.064 | 0.706 | -0.498 | 0.140 | -0.320 |
| Depth | Mean | 0.324 | -0.413 | -0.021 | 0.659 | 0.233 | 0.588 | -0.507 | 0.123 | -0.438 |
| Depth | Sorting | -0.427 | -0.289 | -0.200 | 0.084 | -0.603 | 0.542 | -0.456 | -0.132 | -0.023 |
| NPP | Depth | 0.003 | -0.582 | -0.022 | -0.828 | -0.885 | 0.629 | -0.353 | -0.778 | -0.073 |
| NPP | Dist. land | 0.117 | -0.627 | -0.750 | -0.918 | -0.961 | 0.729 | -0.282 | -0.027 | -0.214 |
| NPP | Lat | 0.545 | 0.822 | -0.293 | -0.047 | -0.630 | 0.980 | 0.890 | 0.947 | 0.860 |
| Lutz flux | Depth | -0.936 | -0.924 | -0.974 | -0.990 | -0.993 | -0.386 | -0.998 | -0.990 | -0.856 |
| Lutz flux | Dist. Land | -0.720 | -0.923 | -0.094 | -0.936 | -0.873 | -0.254 | -0.983 | -0.490 | -0.910 |
| Lutz flux | TN | 0.681 | 0.660 | 0.539 | 0.620 | 0.836 | 0.215 | 0.720 | -0.300 | 0.736 |
| Lutz flux | TOC | 0.726 | 0.644 | 0.541 | 0.706 | 0.868 | 0.315 | 0.596 | -0.006 | 0.833 |
| SVI | Lat | -0.643 | -0.458 | -0.689 | 0.569 | -0.676 | -0.838 | -0.384 | -0.289 | -0.438 |
| Depth | TN | -0.811 | -0.629 | -0.535 | -0.619 | -0.847 | 0.474 | -0.720 | 0.286 | -0.551 |
| Depth | TOC | -0.842 | -0.559 | -0.549 | -0.703 | -0.862 | 0.414 | -0.607 | -0.021 | -0.722 |
| TN | TOC | 0.957 | 0.796 | 0.634 | 0.922 | 0.967 | 0.680 | 0.706 | 0.447 | 0.726 |
| TOC | Mud | 0.380 | -0.394 | 0.265 | 0.728 | -0.052 | -0.397 | 0.037 | 0.057 | 0.043 |
| TOC | Silt | 0.221 | -0.315 | 0.309 | 0.661 | -0.112 | 0.627 | 0.241 | 0.026 | 0.469 |
| TOC | Clay | 0.660 | -0.481 | 0.161 | 0.824 | 0.260 | -0.610 | -0.160 | 0.039 | -0.490 |
| TOC | Mean | -0.458 | 0.437 | -0.174 | -0.784 | -0.124 | 0.581 | 0.053 | -0.104 | 0.396 |
| TOC | Sorting | 0.404 | 0.039 | -0.306 | 0.128 | 0.498 | 0.556 | 0.004 | -0.017 | -0.201 |
| TN | Mud | 0.379 | -0.501 | -0.040 | 0.746 | 0.018 | -0.391 | -0.311 | 0.074 | 0.048 |
| TN | Silt | 0.219 | -0.399 | 0.073 | 0.700 | -0.048 | 0.581 | 0.344 | -0.081 | 0.566 |
| TN | Clay | 0.644 | -0.464 | 0.066 | 0.817 | 0.280 | -0.550 | -0.305 | 0.141 | -0.620 |
| TN | Mean | -0.461 | 0.535 | 0.065 | -0.788 | -0.187 | 0.540 | 0.272 | -0.136 | 0.364 |
| TN | Sorting | 0.392 | 0.111 | -0.217 | 0.066 | 0.487 | 0.569 | 0.245 | 0.190 | -0.240 |

Percentage mud, clay, silt, total organic carbon (TOC) and total nitrogen (TN); mean grain size (Mean); standard deviation of grain size (Sorting); distance from land (Dist. land); latitude (Lat); estimated annual net primary production of overlying waters (NPP, gC $m^{-2}$ $year^{-1}$); approximated POC flux to the seabed using the Lutz algorithm (Lutz flux, mgC $m^{-2}$ $day^{-1}$); Seasonal variation index of NPP (SVI)

### 3.5.2.2 Primary productivity and export flux

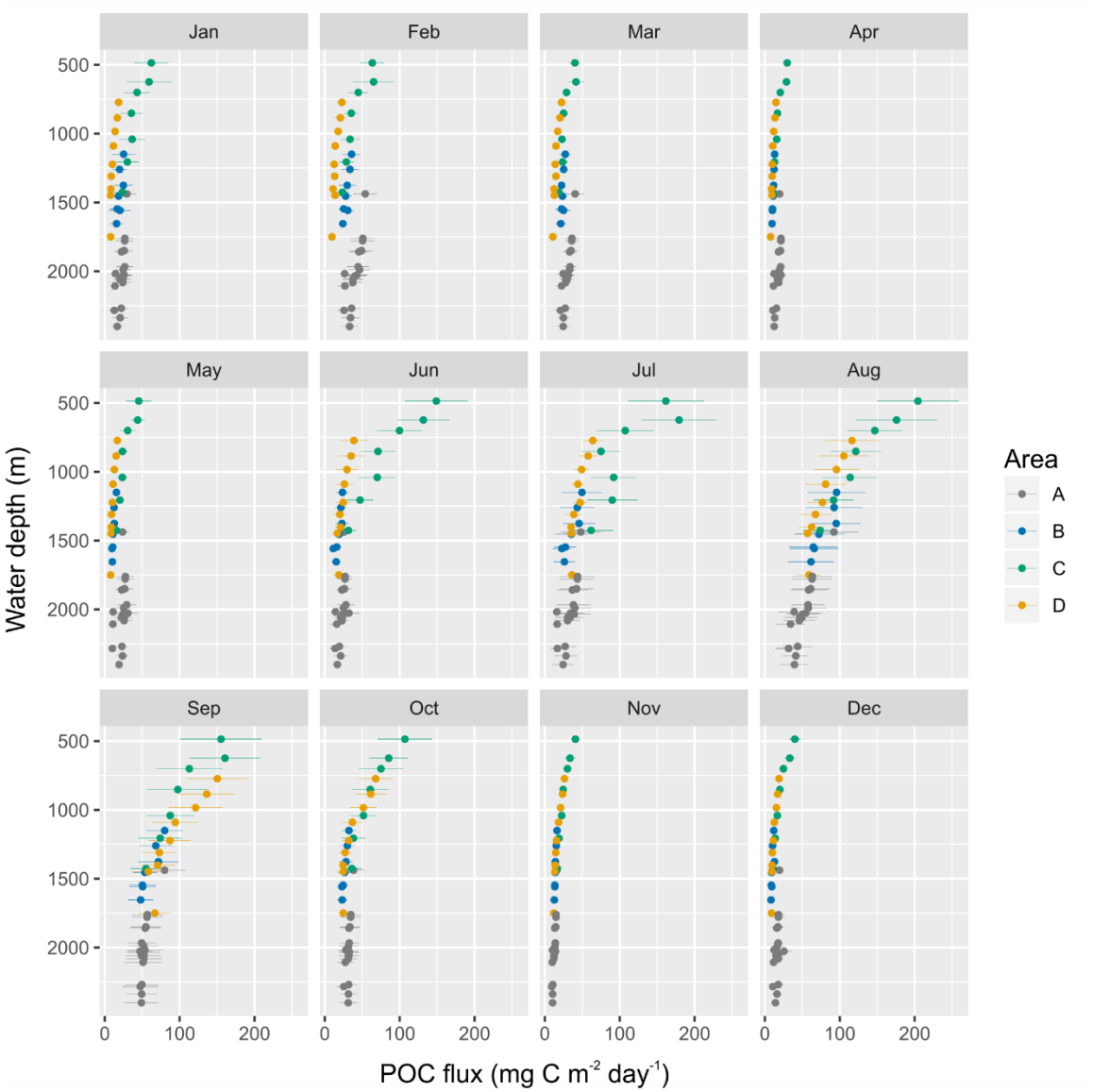


**Figure S3.3** Mean monthly estimated POC flux to the seabed for photographic sites sampled in 2005, 2008 and 2014, keyed to study area. POC flux was approximated using the Pace algorithm (Pace et al., 1987) and represents monthly flux rates (mean and 95% CIs) averaged for the period from 2003 to 2017. NPP estimates used in the flux calculations were derived from 15 years of monthly NPP values based on the Vertically Generalized Production Model of Behrenfeld and Falkowski (1997)

### 3.5.3 Standing stocks

#### 3.5.3.1 Estimation of metazoan biomass

To approximate metazoan biomass, we applied the generalised volumetric method of Benoist et al. (2019), which uses biovolume as predictor for body mass. Most morphotypes were classified as cylinders and individual body volume was calculated from equivalent cylindrical length and diameter measurements. The volume of regular echinoids was assumed to be equivalent to that of an oblate spheroid (Echinidae and Acroechinoidea) or half of an oblate spheroid (Echinothurioida). The volume of the irregular urchin *Pourtalesia* sp. was approximated as a prolate spheroid where the maximum width of the specimen represents the equatorial diameter of the spheroid and the total visible length represents its height. For asteroids, we applied a cylindrical shape for the central disc and a triangular prism for each of the arms. The surface area of each arm was approximated from the length of a normal-sized arm and the arm width adjacent to the central disc, while the surface area of the disc was derived from the disc diameter. For numerically abundant natant decapods, we established scaling relationships from a subset of 150-160 randomly selected specimens per morphotype to minimise the effort of volumetric measurements. All relationships were expressed as power equations in the form of $V = a \times L^b$ (Figure S3.6), where $V$ represents the biovolume ($cm^3$) estimated using the generalised volumetric method, $L$ is the measured dimension (cm) recorded during annotation, and $a$ and $b$ are the fitted model parameters, which were obtained from ordinary least squares linear regression (model I) on natural log-transformed data, using the base command 'lm' in R (R Core Team, 2020) (Table S3.2). Model assumptions were validated by visual assessment of standardised residuals, cook distance and QQ plots. Finally, for partially buried specimens for which linear dimensions could not be measured, biovolume was equated to the median from individually calcaluted biovolumes of the respective morphotype. Estimated specimen volume was converted to fresh body mass (g fresh wet weight) assuming a volumetric mass density of 1 g $cm^{-3}$.

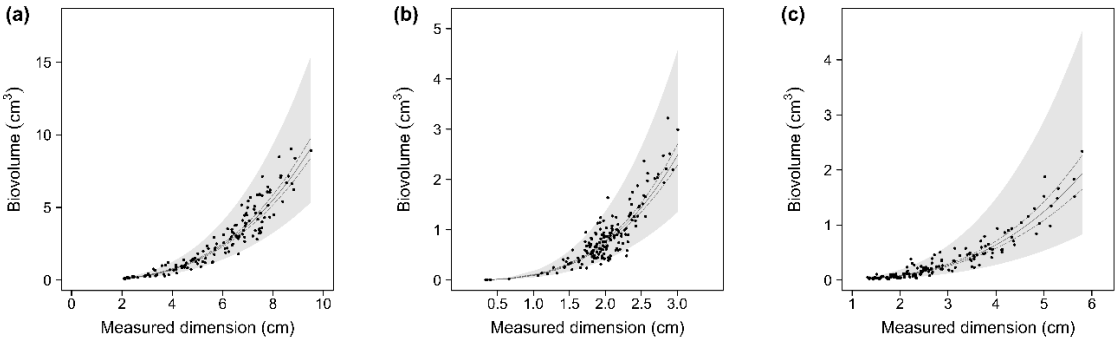


**Figure S3.4** Scaling relationships between measured dimension (L) and biovolume (V) used to approximate biomass of abundant decapod crustaceans from the Angolan continental slope. Predicted models are plotted in the form of $V = a \times L^b$ with superimposed fitted power models (solid lines), 95% confidence intervals of the fitted values (dashed lines), and 95% prediction intervals (shaded areas). **(a)** *Nematocarcinus* msp-1, $V = 0.0135\ x\ L^{2.89}$ **(b)** Anomura msp-1, $V = 0.096\ x\ L^{2.95}$ **(c)** Caridoid Indeterminate, $V = 0.0103\ x\ L^{2.98}$. For all three morphotypes, L has been measured as the distance between the anterior end of the eyes and the beginning of the telson.

**Table S3.3** Regression coefficients and statistics for fitted power models relating biovolume (V) estimated using the generalised volumetric method to the dimension (L) measured during annotation. 95% CI confidence intervals for regression coefficients were calculated from the Standard Error of estimation.

| Morphotype | Model | Slope (95% CI) | Intercept (95% CI) | F | $R^2$ (%) |
|---|---|---|---|---|---|
| Nematocarcinus msp-1 | log (V) ~ log (L) | 2.89 (2.79 - 3.00) | -4.31 (-4.49 - -4.12) | 2898 $^{****}_{[1,147]}$ | 95.1 |
| Anomura msp-1 | log (V) ~ log (L) | 2.95 (2.80 - 3.11) | -2.34 (-2.45 - -2.23) | 1398 $^{****}_{[1,160]}$ | 89.7 |
| Caridoid Indeterminate | log (V) ~ log (L) | 2.98 (2.80 - 3.17) | -4.58 (-4.77 - -4.39) | 1026 $^{****}_{[1,148]}$ | 87.3 |

$^{****}$ $p < 0.0001$

### 3.5.3.2 Invertebrate Abundance-Biomass comparisons

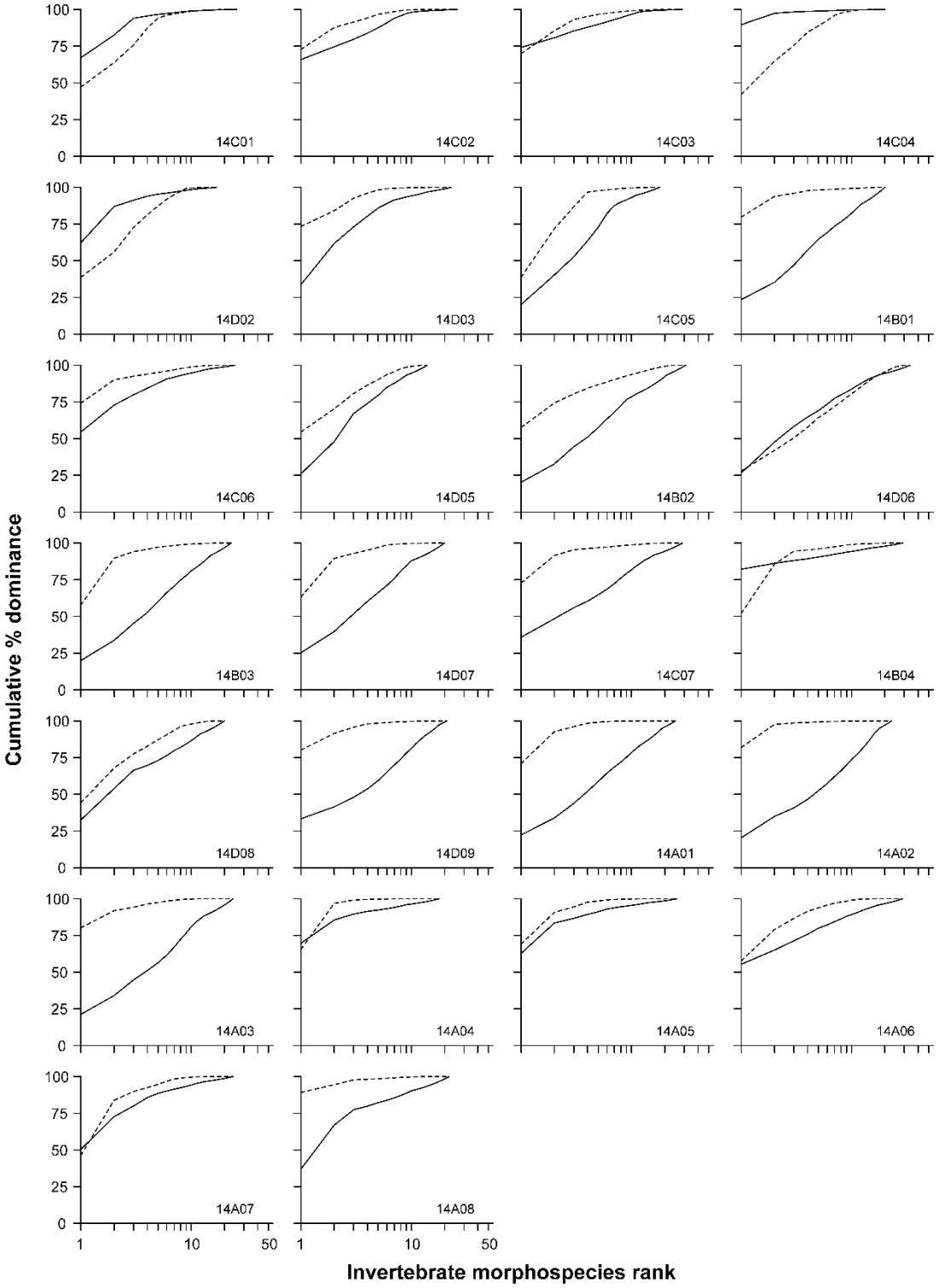


**Figure S3.5** ABC curves of invertebrate biomass (dashed lines) and numerical density (solid lines) for photographic transects sampled in 2014. Cumulative ranked morphospecies abundances and biomass are plotted against the relevant invertebrate morphospecies rank. Graphs are ordered in increasing transect depth by row from left to right. Transect names as in Table S.3.1.

## 3.5.4 Morphospecies

**Table S3.4** Taxonomic resolution for each of the metazoan megafaunal morphotypes (> 1 cm) identified in images taken between 0.8-3.5 m across sedimentary habitats along the Angolan continental slope in 2005, 2008 and 2014. Morphospecies are listed according to the taxonomic level to which they were identified along with the number of morphospecies recorded for each level. For example, Porifera msp with morphospecies n = 4 equates to four morphospecies identified to Phylum Porifera. Respective morphospecies are labelled Porifera msp-1, Porifera msp-2 etc. For morphospecies that could not consistently be identified to the same taxonomic rank across all processed images, the number of observed morphotypes is given in brackets behind the number of morphospecies retained for analyses. For example, two genera of halosaurs were recorded but consistent identification was only possible at family level Halosauridae. The taxonomic classification follows the hierarchical system of the World Register of Marine Species (WoRMS Editorial Board, 2020). * indicates pelagic and benthopelagic morphospecies excluded from all analyses ** indicates morphospecies excluded from the assessment of alpha diversity and faunal composition

| Phylum / Subphylum | Class / Subclass | Order | Family | Label | Morpho-species (n) |
|---|---|---|---|---|---|
| FORAMINIFERA | Monothalamea | | | Foraminifera msp | 6 |
| PORIFERA | | | | Porifera msp | 4 |
| CTENOPHORA | | | | Ctenophora msp* | 3 |
| | | | | Ctenophora spp. indet.* | na |
| | Tentaculata | Lobata | | Lobata msp* | 2 |
| CNIDARA | | | | Cnidaria msp-1 | 1 |
| | Anthozoa / Hexacorallia | | | Anthozoa msp-1 | 1 |
| | | | | Hexacorallia msp | 3 |
| | | Actiniaria | | Actiniaria msp | 13 |
| | | | Actinoscyphiidae | Actinoscyphia msp-1 | 1 |
| | | | Actinostolidae | Actinostolidae msp-1 | 1 |
| | | | Hormathiidae | Metridioidea msp | 4 |
| | | Zoantharia | | Zoantharia msp | 2 |
| | | | Epizoanthidae | Epizoanthidae | 1 |
| | | Scleractinia | | Scleractinia msp-1 | 1 |
| | Anthozoa / Ceriantharia | | | Ceriantharia msp | 4 |
| | | | | Ceriantharia indet.* | na |
| | Anthozoa / Octocorallia | | | Octocorallia msp | 4 |
| | | Alcyonacea | | Alcyonacea msp-1 | 1 |
| | | Pennatulacea | | Pennatulacea msp | 4 |
| | | | Anthoptilidae | Pennatulacea msp-3 | 1 |
| | | | Protoptilidae | Pennatulacea msp-5 | 1 |
| | | | Umbellulidae | Umbellula msp-1 | 1 |
| | | | | Cnidaria spp. indet.** | na |
| | Scyphozoa | | | Scyphozoa msp* | 4 |
| | | | | Scyphozoa spp. indet.* | na |
| CHAETOGNATHA | | | | Chaetognatha msp* | 2 |
| NEMERTEA | | | | Nemertea msp | 2 |
| ANNELIDA | | | | Annelida msp-1 | 1 |
| | Polychaeta | Eunicida | Onuphidae | Onuphidae | 1 |
| | | Phyllodocida | Polynoidae | Polychaeta msp-1 | 1 |
| | | | | Polychaeta msp | 4 |
| ARTHROPODA | Hexanauplia | | | Cirripedia | 1 |
| | Malacostraca | | | Malacostraca msp-1 | 1 |
| | | Decapoda | | Paguroidea | 1 |
| | | | | Anomura msp | 4 |
| | | | | Brachyura msp | 1 (2) |
| | | | | Caridea msp | 4 |
| | | | | Caridoid msp | 5 |
| | | | Polychelidae | *Polycheles* sp. 01 | 1 |
| | | | Munidopsidae | Munidopsidae msp | 2 |
| | | | Aristeidae | Aristeidae msp | 4 |

**Table S3.4** continued

| | | | | | |
|---|---|---|---|---|---|
| | | | Geryonidae | Geryonidae msp-1 | 1 |
| | | | Polybiidae | *Bathynectes* sp. 01 | 1 |
| | | | Nematocarcinidae | Nematocarcinus msp-1 | 1 |
| | | | Bythocarididae | Bythocaris msp-1 | 1 |
| | | Isopoda | | Isopoda msp | 4 |
| | | | Aegidae | Isopoda msp-4 | 1 |
| | | | | Decapoda spp. indet.** | na |
| | | | | Crustacea spp. indet. msp-01* | na |
| MOLLUSCA | Bivalvia | | | Bivalvia msp | 2 |
| | Cephalopoda | Octopoda | Megaleledonidae | Cephalopoda msp | 2 |
| | | | Enteroctopodidae | Cephalopoda msp | 1 |
| | Gastropoda | | | Gastropoda msp | 7 |
| | | | | Gastropoda spp. indet.** | na |
| ECHINODERMATA | Echinoidea | | | Echinoidea msp | 4 |
| | | | | Acroechinoidea msp-1 | 1 |
| | | Camarodonta | Echinidae | Echinidae msp | 2 |
| | | Echinothurioida | Phormosomatidae | *Phormosoma* sp. 01 | 1 |
| | | | Echinothuriidae | *Hygrosoma* sp. 01 | 1 |
| | | Holasteroida | Pourtalesiidae | *Pourtalesia* sp. 01 | 1 |
| | Asteroidea | | | Asteroidea msp | 5 |
| | | Forcipulatida | Zoroasteridae | Zoroasteridae msp-1 | 1 |
| | | Valvatida | | Asteroidea msp | 1 |
| | | Valvatida | Goniasteridae | Goniasteridae msp-1 | 1 |
| | | Paxillosida | Astropectinidae | Asteroidea msp | 2 |
| | | | | Asteroidea spp. indet.** | na |
| | Holothuroidea | | | Holothuroidea msp | 4 |
| | | Elasipodida | Psychropotidae | *Benthodytes* sp. 01 | 1 |
| | | | Psychropotidae | *Psychropotes* sp. 01 | 1 |
| | | | Elpidiidae | Elpidia msp-1 | 1 |
| | | | | Elpidiidae msp-2 | 1 |
| | | | | Peniagone msp-1 | 1 |
| | | | | Peniagone msp-2* | 1 |
| | | | | *Scotoplanes* sp. 01 | 1 |
| | | Synallactida | Synallactidae | Paelopatides msp-1 | 1 |
| | | Persiculida | | *Benthothuria* sp. 01 | 1 |
| | | Holothuriida | Mesothuriidae | Mesothuria msp-1 | 1 |
| | Ophiuroidea | | | Ophiuroidea msp | 8 |
| | | | | Ophiuroidea spp. indet.** | na |
| TUNICATA | Ascidiacea | | | Ascidiacea | 1 |
| VERTEBRATA | Actinopterygii | | | Actinopterygii msp | 8 |
| | | | | Actinopterygii spp. indet.** | na |
| | | Osmeriformes | Alepocephalidae | Alepocephalidae spp. | 1 (3) |
| | | Lophiiformes | Chaunacidae | Chaunacidae msp | 2 |
| | | | Lophiidae | Lophiidae msp-1 | 1 |
| | | | Ogcocephalidae | Ogcocephalidae msp | 2 |
| | | Aulopiformes | Ipnopidae | *Bathypterois* spp. | 1 (2) |
| | | Ophidiiformes | | Ophidiiformes msp | 5 |
| | | | Bythitidae | *Cataetyx* sp. 01 | 1 |
| | | | Ophidiidae | *Dicrolene* spp. | 1 (2) |
| | | Gadiformes | Moridae | *Antimora* sp. 01 | 1 |
| | | | | *Laemonema* sp. 01 | 1 |
| | | | Macrouridae | *Trachyrincus* sp. 01 | 1 |
| | | | | Macrouridae msp | 7 |
| | | Pleuronectiformes | Cynoglossidae | Cynoglossidae msp-1 | 1 |
| | | | Soleidae | Soleidae msp-1 | 1 |
| | | Notacanthiformes | Halosauridae | Halosauridae spp. | 1 (2) |
| | | Anguilliformes | Synaphobranchidae | *Ilyophis* sp. 01 | 1 |
| | | | | *Simenchelys* sp. 01 | 1 |

**Table S3.4** continued

| | | | | | |
|---|---|---|---|---|---|
| | | | | Synaphobranchus msp-1 | 1 |
| | | | | Synaphobranchidae msp-1 | 1 |
| | | Scorpaeniformes | Psychrolutidae | *Psychrolutes* sp. 01 | 1 |
| | Elasmobranchii | Rajiformes | | Rajiformes | 1 (2) |
| | | Squaliformes | Somniosidae | *Centroscymnus* sp. 01 | 1 |
| INDETERMINATE | | | | Vermiform msp | 4 |
| | | | | Animalia indet. msp | 14 |
| | | | | Animalia spp. indet.** | na |
| | | | | **TOTAL**[1] | 208 (217) |

[1] Distinct morphospecies excluding broad groups (e.g. Animalia spp. indet.) and invertebrate morphospecies recorded only off-bottom

Several records had to be excluded from the analysis as it could not be determined whether they represented benthic specimens, life traces or planktonic material deposited on the seabed. Among these omitted records, two occurred in noticeable larger numbers:

(1) In 2005, large numbers of elongated, transparent to semi-transparent specimens were recorded at all three sites sampled in Area B with densities ranging from 0.86 to 1.24 ind. $m^{-2}$. Specimens were often seen in or near small seabed depressions and some appeared deflated. No appendages or other distinct features were visible to determine whether these specimens may be part of the local megafaunal assemblage (e.g. elpidiid holothurians or ascidians) or of planktonic origin, potentially pyrosome carcasses. A small number of transparent specimens resembling those observed in 2005 were recorded in Area D in 2014, again with no visible features to conclude whether they belonged to the benthic community.

(2) In 2014, small oval sediment-coloured structures between about 1-3 cm long were observed across all depths and sampling areas, most obviously at sites 14C02 and 14D02. Some of these records may have been smaller megabenthic specimens such as gastropods, sponges or elpidiid holothurians; however, as these labels could not be distinguished from traces or sediment clumps with certainty they were excluded from the 2014 dataset.

### 3.5.5 Supplementary Figures - Diversity

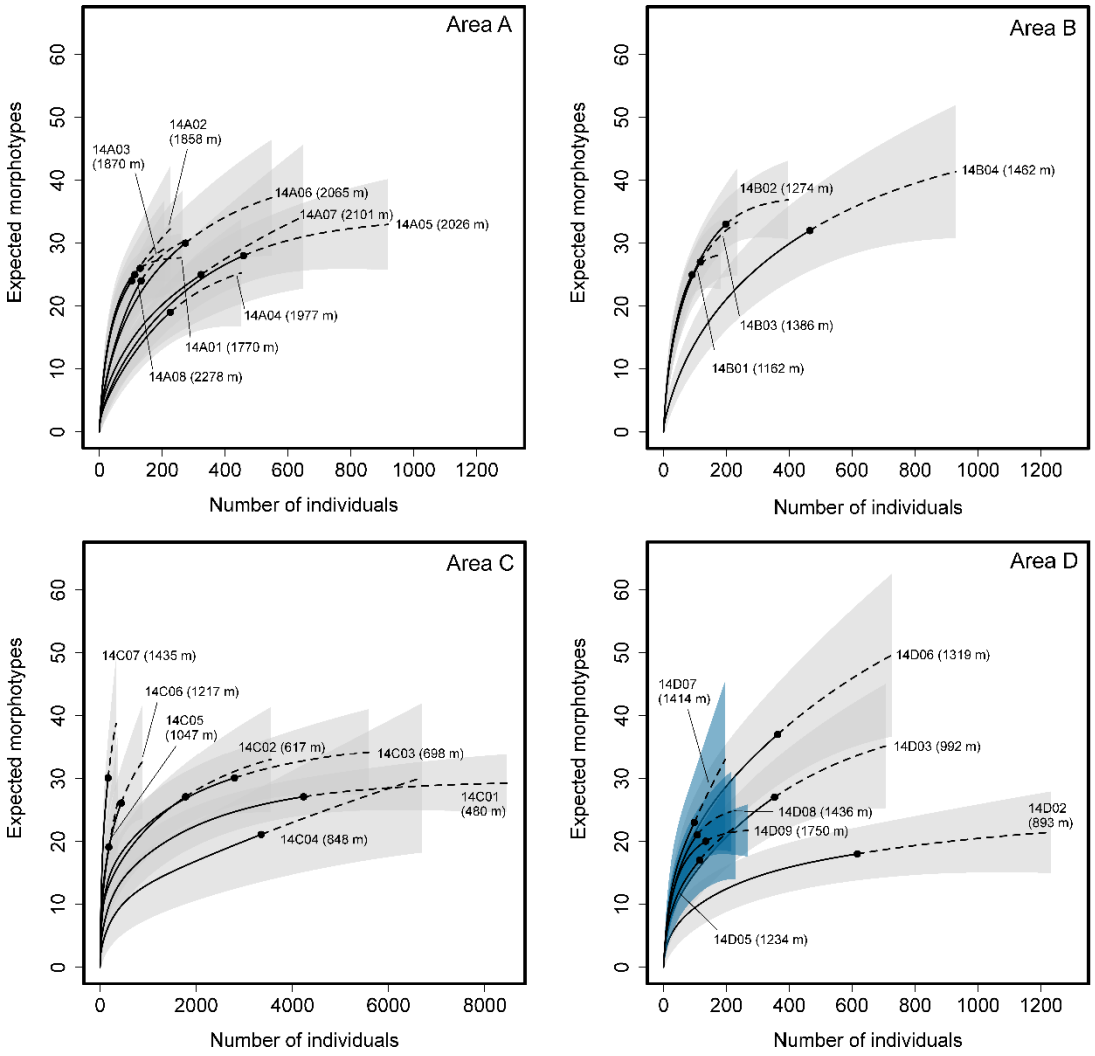


**Figure S.3.6** Sample-based rarefaction (solid curves) and extrapolation (dashed curves) of invertebrate morphotype richness at photographic transects sampled along the Angolan continental slope in 2014, presented by study area (A-D). Observed numbers of invertebrate morphotypes for each transect are denoted by solid dots. Curves were extrapolated up to double the observed number of individuals. Shaded areas represent 95% unconditional confidence intervals. Grey confidence intervals denote transects photographed with the Kongsberg OE14-208 still camera; blue confidence intervals show transects sampled with the Imenco TigerShark SDS1210 camera.

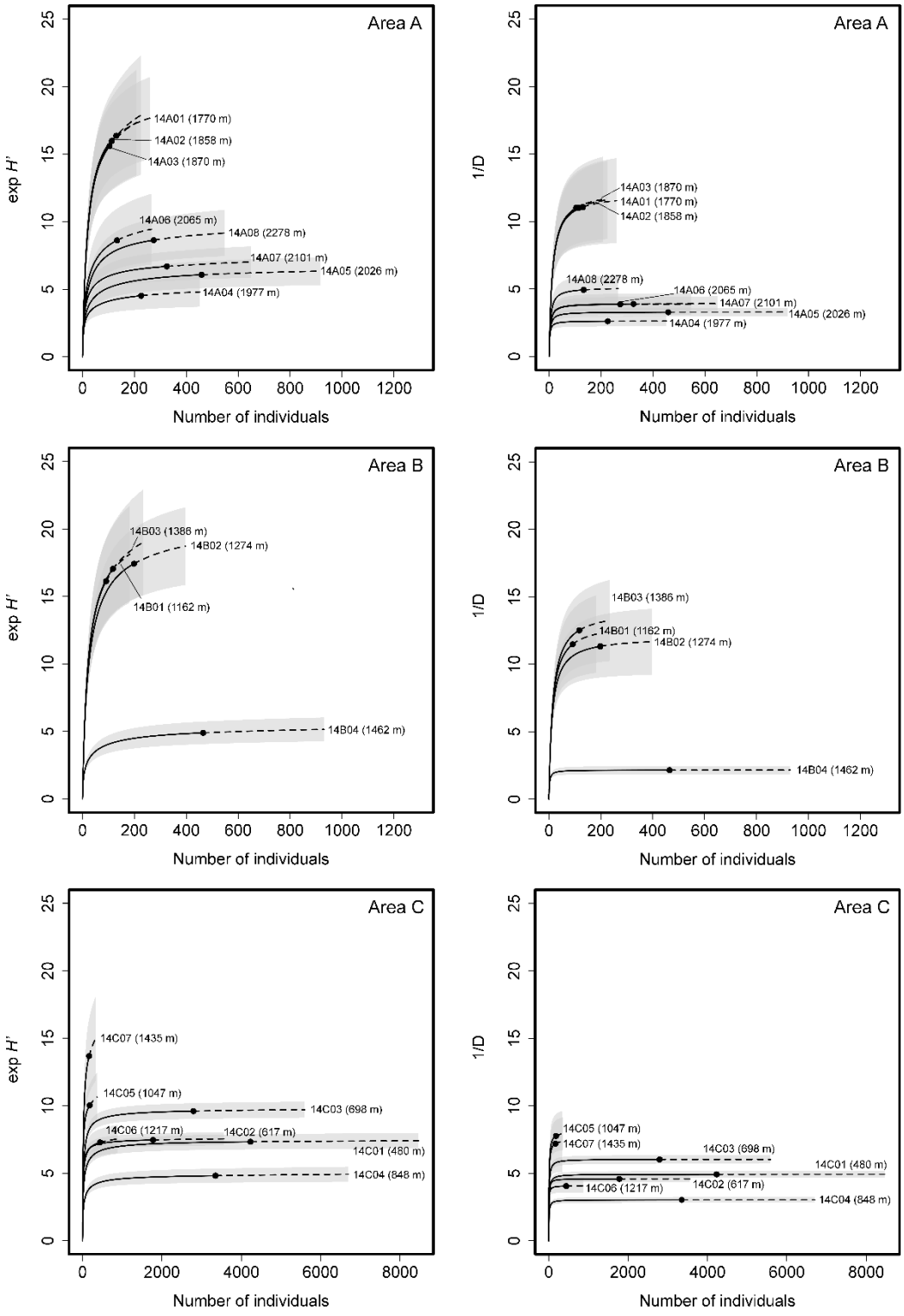


**Figure S3.7** Sample-based rarefaction (solid curves) and extrapolation (dashed curves) with 95% confidence intervals (shaded areas) of invertebrate exponential Shannon entropy exp *H'* (left panels) and inverse Simpson diversity 1/D (right panels) for photographic transects sampled along the Angolan continental slope in 2014, presented by study area (A-D). The observed number of invertebrate morphotypes for each transect is denoted by a solid dot. Curves were extrapolated up to double the observed number of individuals of each transect. Grey confidence intervals denote transects photographed with the Kongsberg OE14-208 still camera; blue confidence intervals show transects sampled with the Imenco TigerShark SDS1210 camera.

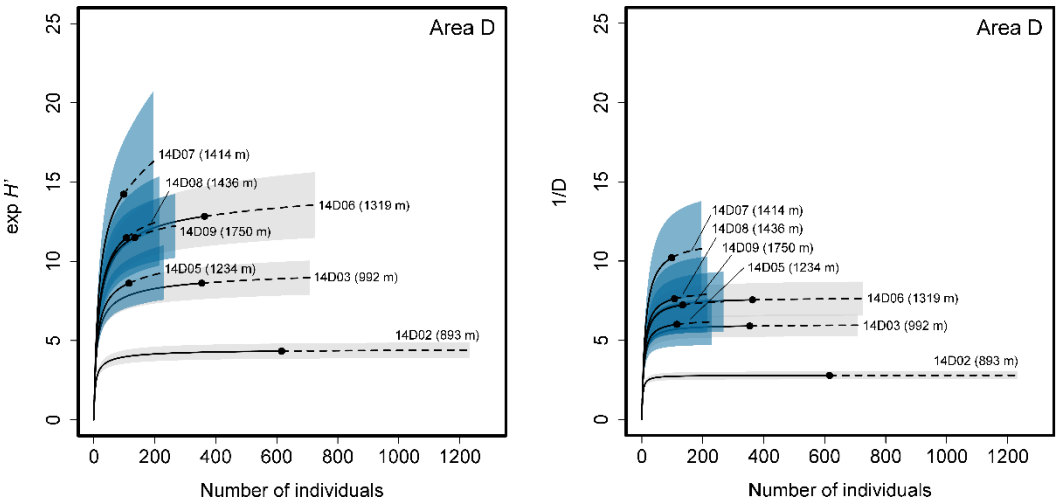


**Figure S3.7** cont.

**Table S3.5** Spearman rank correlations between expected invertebrate diversities for the 26 photographic sites sampled in 2014. White = not significant, grey $p < 0.01$ - after sequential Bonferroni adjustments.

| Var 1 | Var 2 | rho | Var 1 | Var 2 | rho | Var 1 | Var 2 | rho |
|---|---|---|---|---|---|---|---|---|
| $^0D_{90}$ | $^0D_{180}$ | 0.953 | $^0D_{90}$ | $^1D_{90}$ | 0.929 | $^1D_{90}$ | $^2D_{90}$ | 0.966 |
| $^1D_{90}$ | $^1D_{180}$ | 0.995 | $^0D_{90}$ | $^2D_{90}$ | 0.839 | $^1D_{180}$ | $^2D_{180}$ | 0.961 |
| $^2D_{90}$ | $^2D_{180}$ | 1 | $^0D_{180}$ | $^1D_{180}$ | 0.873 | $^1D_{0.833}$ | $^2D_{0.833}$ | 0.967 |
| $^0D_{400}$ | $^0D_{800}$ | 0.910 | $^0D_{180}$ | $^2D_{180}$ | 0.757 | $^1D_{0.904}$ | $^2D_{0.904}$ | 0.963 |
| $^1D_{400}$ | $^1D_{800}$ | 0.990 | $^0D_{0.833}$ | $^1D_{0.833}$ | 0.874 | $^1D_{400}$ | $^2D_{400}$ | 0.962 |
| $^2D_{400}$ | $^2D_{800}$ | 0.992 | $^0D_{0.833}$ | $^2D_{0.833}$ | 0.762 | $^1D_{800}$ | $^2D_{800}$ | 0.966 |
| $^0D_{0.833}$ | $^0D_{0.904}$ | 0.973 | $^0D_{0.904}$ | $^1D_{0.904}$ | 0.820 | $^0D_{90}$ | **W** | 0.840 |
| $^1D_{0.833}$ | $^1D_{0.904}$ | 0.987 | $^0D_{0.904}$ | $^2D_{0.904}$ | 0.681 | $^1D_{90}$ | **W** | 0.872 |
| $^2D_{0.833}$ | $^2D_{0.904}$ | 0.998 | $^0D_{400}$ | $^1D_{400}$ | 0.102 | $^2D_{90}$ | **W** | 0.803 |
| $^0D_{90}$ | $^0D_{0.833}$ | 0.934 | $^0D_{400}$ | $^2D_{400}$ | -0.025 | $^0D_{180}$ | **W** | 0.776 |
| $^0D_{90}$ | $^0D_{0.904}$ | 0.885 | $^0D_{800}$ | $^1D_{800}$ | 0.017 | $^1D_{180}$ | **W** | 0.846 |
| $^0D_{180}$ | $^0D_{0.833}$ | 0.944 | $^0D_{800}$ | $^2D_{800}$ | -0.133 | $^2D_{180}$ | **W** | 0.803 |
| $^0D_{180}$ | $^0D_{0.904}$ | 0.940 | $^2D_{90}$ | **J** | 0.975 | | | |

Observed Pielou evenness (J); W-statistic (W); expected morphospecies richness $^0D$ to $^2D$ for 90 ($D_{90}$) and 180 ($D_{180}$) individuals and for sample coverages of 83.3% ($D_{0.833}$) and 90.4% ($D_{0.904}$); expected morphospecies densities $^0D$ for 400 $m^2$ ($D_{400}$) and 800 $m^2$ ($D_{800}$).

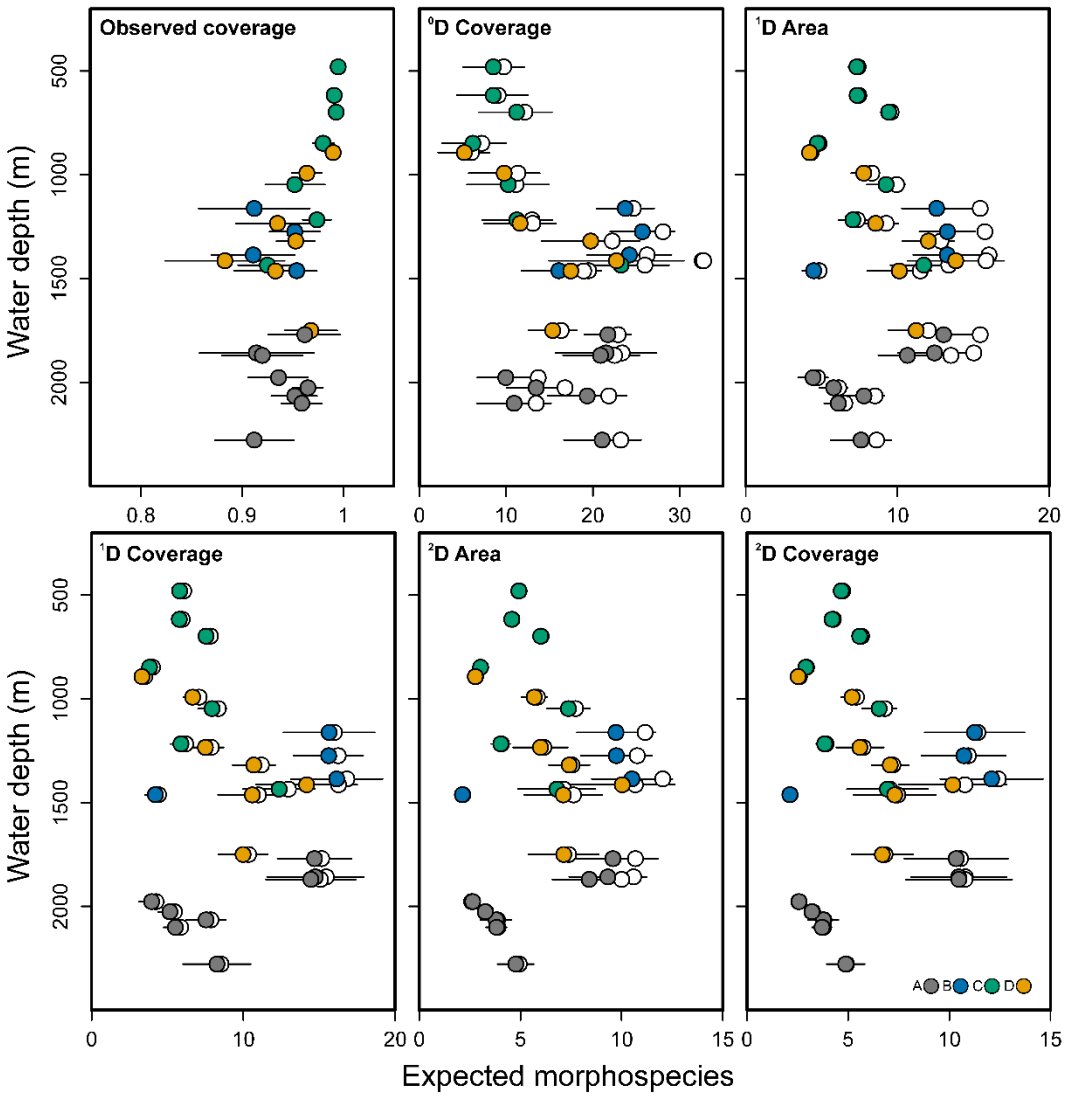


**Figure S3.8** Bathymetric variation in invertebrate diversity measures, keyed to study area. Top left: Observed sample coverage. Remaining plots: Variation in $^{0}D$, $^{1}D$ and $^{2}D$ diversity when standardised on sample area and sample coverage. Filled symbols show the expected number of morphospecies rarefied to either 400 $m^2$ of seabed sampled or a sample coverage of 88.3%, the latter being the highest common sample coverage among all photographic sites included in the analysis. Error bars represent the corresponding 95% confidence intervals for the rarefied diversity values. Open symbols show diversities for a standardised area of 800 $m^2$ and a sample coverage of 90.4%, respectively. Confidence intervals of the extrapolated values were omitted for better readability.

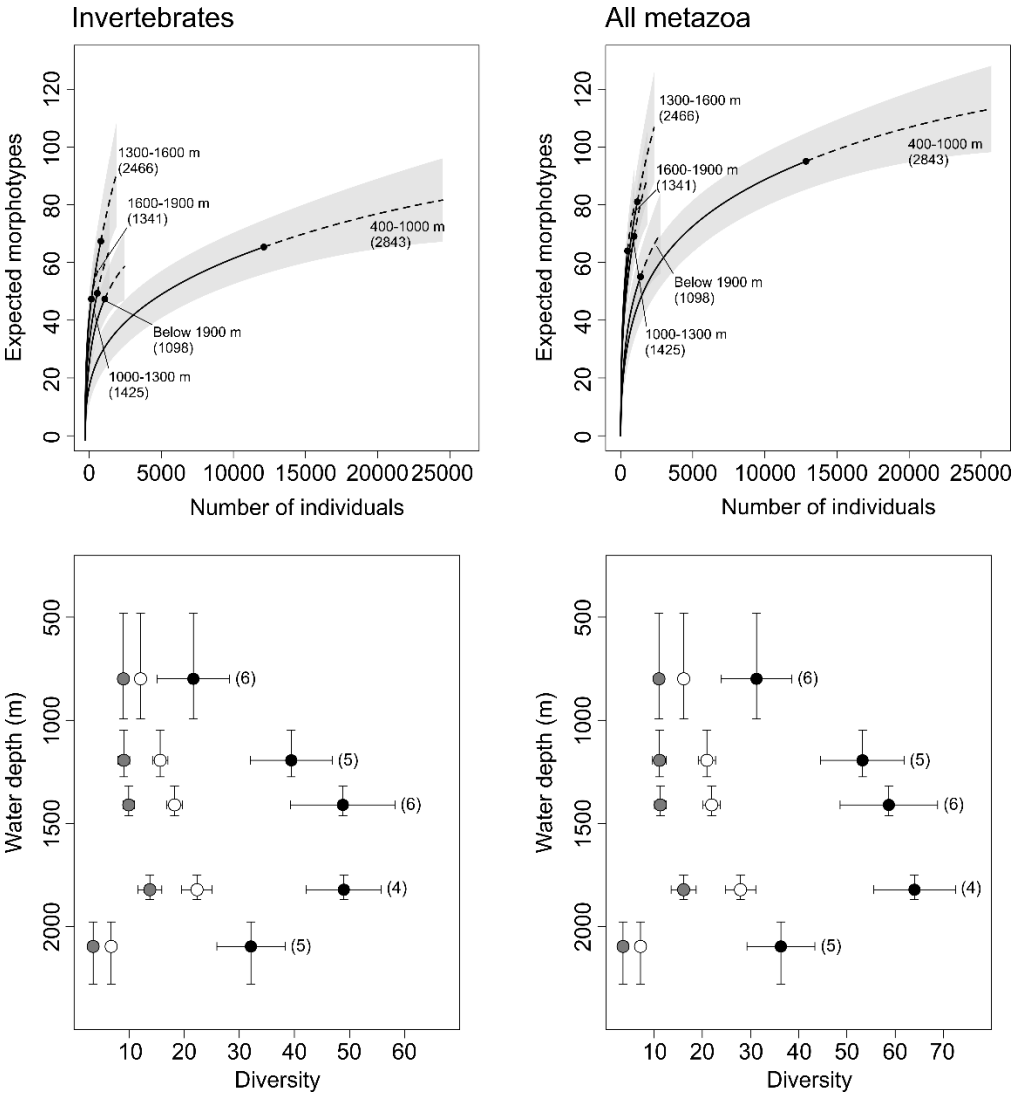


**Figure S3.9** Variation in invertebrate (left panels) and total metazoa (invertebrates and demersal fish, right panels) diversity based on pooled photographic material collected in 2014. Data from the 26 transects were grouped into five depth strata: 400-1000 m, 1000-1300 m, 1300-1600 m, 1600-1900 m, and below 1900 m. Top panels: Sample-based rarefaction (solid curves) and extrapolation (dashed curves) for morphospecies richness as a function of the number of sampled individuals with 95% confidence intervals (shaded areas). Observed numbers of morphotypes are denoted by solid dots. Curves were extrapolated up to double the observed number of individuals of each pooled sample. The numbers in parentheses are the number of images of each pooled sample. Bottom panels: Bathymetric variation in rarefied morphospecies richness (black circles), exponential Shannon entropy exp *H'* (white circles) and inverse Simpson concentration 1/D (grey circles) per 440 individuals of invertebrate megafauna, and per 480 individuals of the total metazoan megafauna. Horizontal error bars represent the 95% confidence intervals for the interpolated values. Vertical error bars show the depth range of each pooled sample. The numbers in parentheses are the number of transects pooled for each sample.

**Table S3.6** Spearman rank correlations between environmental parameters for the photographic sites sampled in 2014; n = 28, except for correlations involving TOC and TN with n = 24. White = not significant, light grey $p < 0.05$, dark grey $p < 0.01$ - after sequential Bonferroni adjustments.

| | Depth | T | DO | POC flux | Mean (φ) | Sorting (φ) | % Silt | % Clay | % Coarse | TOC |
|---|---|---|---|---|---|---|---|---|---|---|
| T | -0.980 | | | | | | | | | |
| DO | 0.898 | -0.892 | | | | | | | | |
| POC flux | -0.952 | 0.955 | -0.870 | | | | | | | |
| Mean (φ) | -0.662 | 0.627 | -0.634 | 0.571 | | | | | | |
| Sorting (φ) | -0.552 | 0.464 | -0.531 | 0.482 | 0.349 | | | | | |
| % Silt | -0.326 | 0.355 | -0.301 | 0.287 | 0.798 | -0.124 | | | | |
| % Clay | -0.813 | 0.770 | -0.764 | 0.717 | 0.926 | 0.581 | 0.603 | | | |
| % Coarse | 0.585 | -0.580 | 0.549 | -0.521 | -0.958 | -0.149 | -0.918 | -0.830 | | |
| TOC | -0.790 | 0.728 | -0.626 | 0.636 | 0.816 | 0.474 | 0.448 | 0.849 | -0.724 | |
| TN | -0.775 | 0.721 | -0.602 | 0.633 | 0.813 | 0.421 | 0.461 | 0.834 | -0.723 | 0.970 |

T- bottom water temperature (°C), DO - dissolved oxygen concentrations close to the seabed (ml $l^{-1}$), POC flux - approximated POC flux to the seabed using the Lutz algorithm (15 year mean, mg C $m^{-2}$ $day^{-1}$), % Coarse - all material > 63 μm.

### 3.5.6 Faunal composition

***Invertebrates***

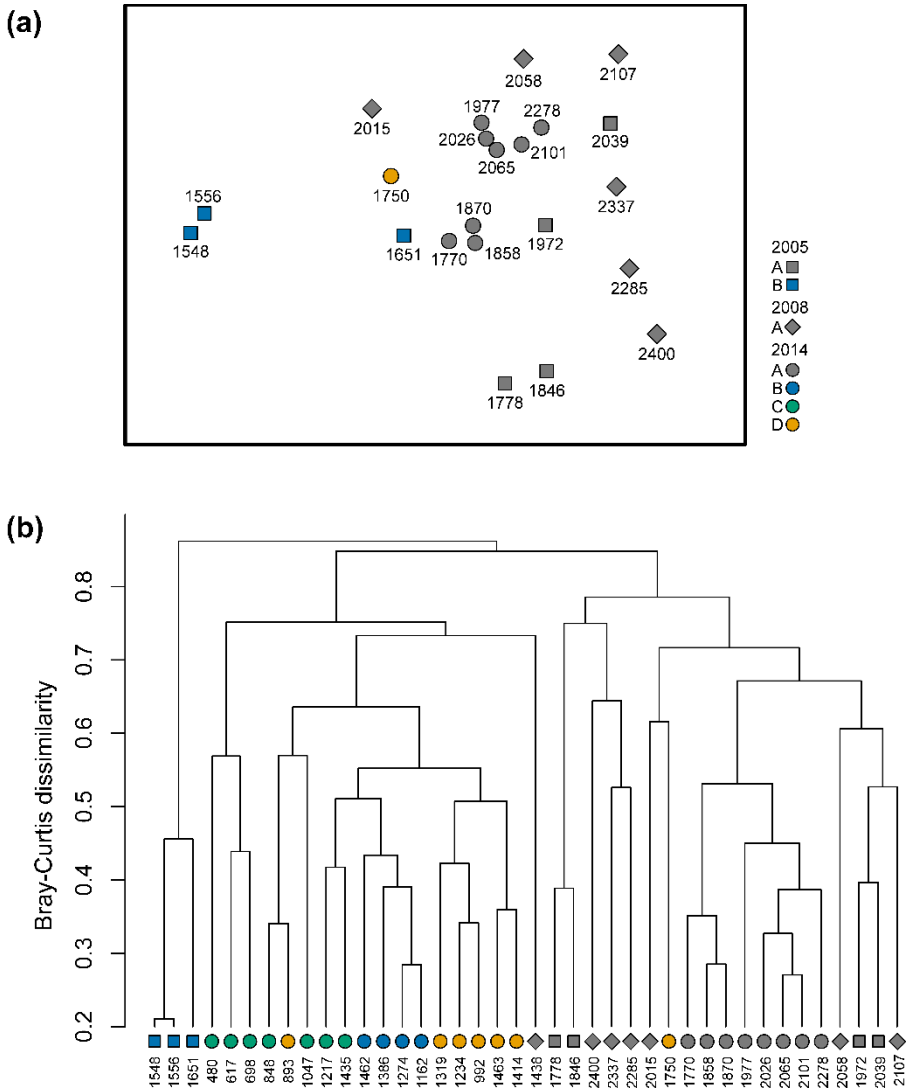


**Figure S3.10** Compositional differences in invertebrate assemblages along the Angolan continental slope, based on the combined photographic data set collected between 2005 and 2014. **(a)** Two-dimensional NMDS ordination of sites sampled below 1500 m (MDS stress: 0.155). **(b)** Between-group average linkage cluster analysis of all sites. Sites are keyed to study area (A-D) and sampling year. Analyses were based on the fourth-root transformed standardised numerical densities. Numbers below site symbols represent mean transect depths.

**Table S3.7** Relative contribution (%) of major invertebrate taxonomic groups to the total invertebrate density (ind. $ha^{-1}$) along the Angolan continental slope for sites surveyed in 2014. Proportions are based on the standardised densities retained in the analysis of faunal composition (i.e. excluding unclassified specimens). Groups: (1) Porifera, (2) Cnidaria, (3) Nemertea, (4) Annelida, (5) Mollusca, (6) Arthropoda, (6a) Anomura, (6b) Brachyura, (6c) Caridean shrimp, (6d) Isopoda, (6e) Other arthropods, (7) Echinodermata, (7a) Echinoidea, (7b) Holothuroidea, (7c) Ophiuroidea, (7d) Asteroidea, (8) Ascidiacea, (9) Undetermined morphospecies, e.g. Animalia indet. msp-2

| Site | Depth | Density | 1 | 2 | 3 | 4 | 5 | 6 | 6a | 6b | 6c | 6d | 6e | 7 | 7a | 7b | 7c | 7d | 8 | 9 |
|---|---|---|---|---|---|---|---|---|---|---|---|---|---|---|---|---|---|---|---|---|
| 14C01 | 480 | 101736 | - | 82.9 | - | 0.1 | 3.2 | 13.5 | 0.2 | <0.1 | 12.6 | - | 0.6 | 0.1 | - | - | 0.1 | - | - | 0.1 |
| 14C02 | 617 | 20760 | 4.6 | 5.8 | 0.2 | 8.5 | 0.1 | 76.9 | 0.5 | - | 76.3 | <0.1 | <0.1 | 3.3 | - | - | 3.3 | - | - | 0.6 |
| 14C03 | 698 | 31147 | - | 10.0 | 1.4 | 4.9 | 0.2 | 18.3 | 2.0 | 0.2 | 16.1 | - | - | 65.1 | - | - | 64.7 | 0.4 | - | 0.2 |
| 14C04 | 848 | 45697 | - | 1.2 | 0.2 | 0.2 | <0.1 | 89.9 | 88.4 | <0.1 | 1.5 | <0.1 | - | 8.4 | <0.1 | - | 8.0 | 0.4 | - | 0.1 |
| 14D02 | 893 | 6607 | 0.3 | 0.8 | - | 0.6 | 0.2 | 71.6 | 58.9 | 1.3 | 10.2 | 1.1 | - | 25.8 | - | - | 25.8 | - | - | 0.6 |
| 14D03 | 992 | 2626 | 9.3 | 7.8 | - | 4.5 | 0.3 | 72.8 | 23.2 | - | 47.9 | 1.7 | - | 5.1 | 0.8 | 1.1 | 2.8 | 0.3 | - | 0.8 |
| 14C05 | 1047 | 2038 | 7.1 | 9.9 | - | 7.1 | - | 52.0 | 14.8 | - | 36.3 | - | - | 19.8 | 15.4 | 2.2 | 1.1 | 1.1 | - | 4.9 |
| 14B01 | 1162 | 928 | 1.1 | 19.8 | - | 4.4 | 2.2 | 47.3 | 20.9 | - | 26.4 | - | - | 15.4 | 3.3 | 5.5 | 2.2 | 4.4 | - | 9.9 |
| 14C06 | 1217 | 6690 | 52.8 | 2.5 | - | 3.0 | 0.2 | 5.9 | 1.4 | 0.5 | 4.1 | - | - | 31.0 | 1.1 | - | 18.0 | 11.8 | 0.5 | 4.6 |
| 14D05 | 1234 | 2697 | 13.9 | 1.7 | - | 3.5 | 0.9 | 72.2 | 12.2 | - | 53.9 | 6.1 | - | 5.2 | - | - | 1.7 | 3.5 | - | 2.7 |
| 14B02 | 1274 | 1306 | 9.6 | 11.1 | - | 3.5 | - | 51.5 | 10.7 | - | 40.4 | 0.6 | - | 17.7 | 4.0 | 4.4 | 5.0 | 4.5 | - | 6.6 |
| 14D06 | 1319 | 4636 | 18.7 | 3.6 | - | 1.1 | 0.6 | 59.2 | 15.7 | 0.3 | 36.4 | 2.5 | 4.4 | 12.4 | 1.9 | 0.8 | 5.8 | 3.9 | - | 4.4 |
| 14B03 | 1386 | 1053 | 12.8 | 23.9 | - | 6.8 | - | 38.5 | 0.9 | - | 31.6 | 6.0 | - | 17.9 | 2.6 | 10.3 | 0.9 | 4.3 | - | - |
| 14D07 | 1414 | 2110 | 12.2 | 15.3 | 1.2 | 4.1 | 1.0 | 34.7 | 2.0 | - | 30.6 | 2.0 | - | 20.4 | 1.0 | 3.1 | 12.2 | 4.1 | - | 11.2 |
| 14C07 | 1435 | 1784 | 12.0 | 9.0 | - | 3.6 | 0.6 | 11.4 | 0.6 | - | 10.2 | 0.6 | - | 54.5 | 6.6 | 6.6 | 35.9 | 5.4 | 0.6 | 8.4 |
| 14B04 | 1462 | 4847 | 0.6 | 81.6 | - | 1.1 | 0.2 | 6.2 | 0.4 | - | 5.6 | 0.2 | - | 9.5 | 1.3 | 6.7 | 0.9 | 0.6 | - | 0.9 |
| 14D08 | 1463 | 1333 | 17.8 | 20.6 | - | 3.7 | 0.9 | 43.0 | 4.7 | - | 34.6 | 3.7 | - | 12.1 | 1.9 | 2.8 | 1.9 | 5.6 | - | 1.9 |
| 14D09 | 1750 | 2717 | 0.7 | 34.3 | - | 6.7 | - | 6.7 | - | - | 6.0 | 0.7 | - | 47.0 | 0.7 | 11.9 | 34.3 | - | - | 4.5 |
| 14A01 | 1770 | 1121 | - | 23.8 | - | 7.7 | 0.8 | 14.6 | - | 1.5 | 11.5 | 1.5 | - | 44.6 | - | 40.0 | 1.5 | 3.1 | - | 8.5 |
| 14A02 | 1858 | 1016 | - | 27.4 | - | 13.3 | 0.9 | 19.5 | - | - | 19.5 | - | - | 31.0 | - | 28.3 | 1.8 | 0.9 | - | 8.0 |
| 14A03 | 1870 | 665 | 1.0 | 38.8 | - | 3.9 | 1.0 | 17.5 | - | - | 17.5 | - | - | 36.9 | 1.0 | 28.2 | 1.9 | 5.8 | - | 1.0 |
| 14A04 | 1977 | 4782 | - | 6.6 | - | - | - | 2.7 | 0.9 | - | 1.8 | - | - | 89.8 | 69.0 | 4.4 | 15.9 | 0.4 | - | 0.9 |
| 14A05 | 2026 | 6709 | - | 7.8 | - | 0.9 | 1.5 | 2.4 | - | - | 2.4 | - | - | 86.5 | 62.3 | 3.5 | 20.5 | 0.2 | - | 0.9 |
| 14A06 | 2065 | 3006 | - | 15.0 | - | - | 0.7 | 2.2 | - | - | 2.2 | - | - | 81.4 | 59.4 | 5.1 | 13.9 | 2.9 | - | 0.7 |
| 14A07 | 2101 | 2977 | - | 7.7 | - | - | 0.6 | 3.4 | 0.6 | - | 2.8 | - | - | 88.0 | 51.5 | 7.1 | 29.3 | - | - | 0.3 |
| 14A08 | 2278 | 1662 | 0.8 | 10.5 | - | 0.8 | 3.0 | 8.3 | - | - | 8.3 | - | - | 75.2 | 35.3 | 0.8 | 38.3 | 0.8 | - | 1.5 |

**Table S3.8** Silhouette scores (Si) of each photographic site for the three and eleven cluster solution computed on the fourth-root transformed invertebrate densities recorded in 2014. The best clustering solution based on the overall average silhouette coefficient ($Si_{Total}$) was achieved by partitioning the dataset into three clusters ($Si_{Total}$ = 0.279), followed by two ($Si_{Total}$ = 0.268) and eleven clusters ($Si_{Total}$ = 0.214). $Si_{avg}$ represents the average silhouette width of the respective cluster, and Neighbour is the neighbouring cluster for each site.

| | 3 cluster solution | | | | 11 cluster solution | | | |
|---|---|---|---|---|---|---|---|---|
| Site | Cluster | Neighbour | Si | $Si_{Avg}$ | Cluster | Neighbour | Si | $Si_{Avg}$ |
| 14A01 | 3 | 1 | 0.260 | | 11 | 10 | 0.163 | |
| 14A02 | 3 | 1 | 0.332 | | 11 | 10 | 0.205 | |
| 14A04 | 3 | 1 | 0.407 | | 11 | 10 | 0.300 | 0.269 |
| 14A06 | 3 | 1 | 0.452 | | 11 | 10 | 0.307 | |
| 14A07 | 3 | 1 | 0.427 | 0.347 | 11 | 10 | 0.370 | |
| 14A05 | 3 | 1 | 0.416 | | 10 | 11 | 0.295 | |
| 14A08 | 3 | 1 | 0.392 | | 10 | 11 | 0.433 | 0.371 |
| 14A03 | 3 | 1 | 0.379 | | 10 | 9 | 0.391 | |
| 14D09 | 3 | 1 | 0.062 | | 9 | 8 | - | - |
| 14C07 | 1 | 3 | 0.272 | | 8 | 7 | 0.266 | 0.290 |
| 14D08 | 1 | 3 | 0.267 | | 8 | 7 | 0.315 | |
| 14D07 | 1 | 3 | 0.243 | | 7 | 8 | 0.133 | |
| 14B04 | 1 | 3 | 0.164 | | 7 | 3 | 0.134 | 0.109 |
| 14B01 | 1 | 3 | 0.308 | | 7 | 2 | 0.061 | |
| 14B02 | 1 | 3 | 0.353 | | 2 | 7 | - | - |
| 14B03 | 1 | 3 | 0.230 | 0.232 | 3 | 7 | 0.207 | 0.154 |
| 14C05 | 1 | 2 | 0.181 | | 3 | 1 | 0.101 | |
| 14C06 | 1 | 2 | 0.237 | | 1 | 2 | 0.182 | |
| 14D05 | 1 | 2 | 0.308 | | 1 | 3 | 0.200 | 0.211 |
| 14D03 | 1 | 2 | 0.283 | | 1 | 3 | 0.281 | |
| 14D06 | 1 | 2 | 0.308 | | 1 | 7 | 0.182 | |
| 14D02 | 1 | 2 | 0.120 | | 6 | 7 | 0.309 | 0.366 |
| 14C04 | 1 | 2 | -0.024 | | 6 | 5 | 0.423 | |
| 14C01 | 2 | 1 | 0.322 | | 5 | 6 | 0.164 | 0.155 |
| 14C02 | 2 | 1 | 0.317 | 0.296 | 5 | 4 | 0.146 | |
| 14C03 | 2 | 1 | 0.250 | | 4 | 5 | - | - |

**Table S3.9** Results of the indicator species analysis for invertebrate communities sampled in 2014, based on the 3 (left hand side) and 11 (right hand side) cluster solution. Shown are significant morphospecies associations ($p < 0.05$) with their respective site specificity (A), site fidelity B), and overall indicator value (C). Morphospecies with wide depth ranges identified as typifying the majority of groups were omitted. The groups for the 11 cluster solution correspond to the following sites: Upper slope 1 - 14C01; 2 - 14C02 & 14C03; Middle slope 3 - 14C04 & 14D02; 4 - 14C05; 5 -14C06 & 14C07; 6 - 14B01, 14B02, 14B03 & 14B04; 7 - 14D03, 14D05 & 14D06, 8 - 14D07 &14D08; Lower slope 9 - 14D09, 10 - 14A01, 14A02 & 14A03; 11 - 14A04, 14A05, 14A06, 14A07, 14A08.

| Group | Morphospecies | A | B | C | Cluster group | Morphospecies | A | B | C |
|---|---|---|---|---|---|---|---|---|---|
| Upper slope (480-700 m) | Anomura msp-2 | 1 | 1 | 1 | 2 | Nemertea msp- 4 | 1 | 1 | 1 |
| | Pennatulacea msp-1 | 1 | 1 | 1 | 1+2 | Anomura msp- 2 | 1 | 1 | 1 |
| | Pennatulacea msp-2 | 1 | 1 | 1 | | Pennatulacea msp- 1 | 1 | 1 | 1 |
| | Zoantharia msp-1 | 1 | 1 | 1 | | Pennatulacea msp- 2 | 1 | 1 | 1 |
| | *Nematocarcinus* msp-1 | 0.88 | 1 | 0.93 | | Zoantharia msp- 1 | 1 | 1 | 1 |
| | Onuphidae | 0.87 | 1 | 0.93 | | *Nematocarcinus* msp- 1 | 0.89 | 1 | 0.94 |
| | Ophiuroidea msp-4 | 0.84 | 1 | 0.92 | 1+2+4 | Onuphidae | 0.83 | 1 | 0.91 |
| | Malacostraca msp-1 | 1 | 0.67 | 0.82 | 1+2+3+4 | Ophiuroidea msp- 4 | 0.97 | 1 | 0.99 |
| | Metridioidea msp-1 | 1 | 0.67 | 0.82 | 3+4+5+6+7+8 | Anomura msp- 1 | 0.95 | 0.86 | 0.9 |
| | Nemertea msp-4 | 1 | 0.67 | 0.82 | 6 | Ascidiacea msp-1 | 1 | 1 | 1 |
| | Brachyura msp-4 | 0.79 | 0.67 | 0.73 | | Asteroidea msp-9 | 1 | 1 | 1 |
| | Nemertea msp-1 | 0.78 | 0.67 | 0.72 | 8 | Anomura msp-4 | 1 | 1 | 1 |
| Middle slope (700-1500 m) | Asteroidea msp-7 | 1 | 0.79 | 0.89 | 5+6 | Zoroasteridae | 0.89 | 1 | 0.94 |
| | Ophiuroidea msp-2 | 1 | 0.79 | 0.89 | | Echinoidea msp- 4 | 1 | 0.83 | 0.91 |
| | Isopoda msp-4 | 1 | 0.5 | 0.71 | 3+7 | Isopoda msp- 1 | 0.89 | 1 | 0.94 |
| | Zoroasteridae | 1 | 0.5 | 0.71 | 7+8 | Isopoda msp- 2 | 1 | 1 | 1 |
| Lower slope (below 1700 m) | Ophiuroidea msp-1 | 0.94 | 1 | 0.97 | 8+9 | Polychaeta msp- 1 | 1 | 1 | 1 |
| | Actiniaria msp-10 | 1 | 0.89 | 0.94 | 5+8+9 | Cerianthid msp- 2 | 1 | 1 | 1 |
| | Octocorallia msp-4 | 1 | 0.89 | 0.94 | 6+9+10+11 | Hexacorallia msp- 1 | 0.92 | 0.9 | 0.91 |
| | Ceriantharia msp-3 | 1 | 0.78 | 0.88 | 4+5+6+9+10+11 | *Paelopatides* msp-1 | 1 | 0.88 | 0.94 |
| | *Umbellula* msp-1 | 1 | 0.78 | 0.88 | 4+5+6+7+8 | Asteroidea msp- 7 | 1 | 0.92 | 0.96 |
| | *Paelopatides* msp-1 | 0.7 | 0.89 | 0.84 | 8+9+10+11 | Ophiuroidea msp- 1 | 1 | 0.91 | 0.95 |
| | *Peniagone* msp-1 | 0.82 | 0.78 | 0.8 | 10 | Actiniaria msp-5 | 1 | 1 | 1 |
| | Asteroidea msp-2 | 0.92 | 0.67 | 0.78 | | *Psychropotes* msp-1 | 0.87 | 1 | 0.93 |
| | Animalia indet. msp-5 | 1 | 0.56 | 0.75 | 11 | Ophiuroidea msp-5 | 1 | 1 | 1 |
| | Ophiuroidea msp-5 | 1 | 0.56 | 0.75 | | *Pourtalesia* msp-1 | 1 | 1 | 1 |
| | *Pourtalesia* msp-1 | 1 | 0.56 | 0.75 | 10+11 | Actiniaria msp-10 | 1 | 1 | 1 |
| | Pennatulacea msp-5 | 0.92 | 0.56 | 0.72 | | Octocorallia msp-4 | 1 | 1 | 1 |
| Upper and middle slope | Porifera msp-1 | 1 | 0.82 | 0.91 | | Ceriantharia msp-3 | 1 | 0.88 | 0.94 |
| | Anomura msp-1 | 1 | 0.76 | 0.87 | | *Umbellula* msp-1 | 1 | 0.88 | 0.94 |
| | Paguroidea | 0.94 | 0.71 | 0.82 | 9+11 | Pennatulacea msp-5 | 0.91 | 0.83 | 0.87 |

## 3.5.7 Ichthyofauna

**Table S3.10** List of fish morphospecies recorded along the Angolan continental slope during the 2014 photographic survey with their observed depth ranges, and maximum observed density (ind. $ha^{-1}$) and associated depth. Ind. is the number of recorded specimens for each morphotype. Depth represents the mean transect depth.

| Morphospecies | Ind. | Depth range (m) | Max. density | Depth max. density (m) | Remarks |
|---|---|---|---|---|---|
| **Pleuronectiformes** | | | | | |
| Cynoglossidae msp-1 | 94 | 480-848 | 697 | 480 | Most likely *Cynoglossus* |
| Soleidae | 9 | 480-617 | 93 | 617 | |
| **Lophiiformes** | | | | | |
| Chaunacidae msp-1 | 7 | 480 | 168 | 480 | cf. *Chaunax* |
| Chaunacidae msp-2 | 7 | 480 | 168 | 480 | Potential colour morph of Chaunacidae msp-1 |
| Lophiidae msp-01 | 2 | 480-698 | 24 | 480 | cf. *Lophius* |
| Ogcocephalidae_01 | 19 | 480-1047 | 264 | 480 | |
| Ogcocephalidae_02 | 56 | 480-1750 | 385 | 480 | cf. *Dibranchus* |
| **Ophidiiformes** | | | | | |
| Ophidiiformes msp-1 | 28 | 617-1463 | 163 | 617 | Possibly Bythitidae |
| Ophidiiformes msp-2 | 2 | 480-1047 | 24 | 480 | Potentially pearlfish Carapidae |
| Ophidiiformes msp-3 | 3 | 617-848 | 23 | 617 | |
| Ophidiiformes msp-4 | 1 | 848 | 14 | 848 | |
| Ophidiiformes msp-5 | 19 | 698-848 | 134 | 698 | |
| *Dicrolene* spp. | 19 | 893-1770 | 47 | 1234 | Likely several species; some cf. *D. intronigra and D. kanazawai* |
| *Cataetyx* msp-1 | 1 | 1870 | 6 | 1870 | cf. *C. laticeps* |
| **Gadiformes** | | | | | |
| *Trachyrincus* msp-1 | 13 | 617 | 152 | 617 | |
| Macrouridae_msp-1 | 1 | 1770 | 9 | 1770 | cf. *Coryphaenoides* |
| Macrouridae_msp-2 | 1 | 1977 | 21 | 1977 | cf. *Coryphaenoides* |
| Macrouridae_msp-3 | 109 | 480-1414 | 464 | 848 | Medium sized specimens; possibly several species including *Nezumia* |
| Macrouridae_msp-4 | 1 | 1274 | 7 | 1274 | cf. *Coryphaenoides* |
| Macrouridae_msp-5 | 4 | 1274-2026 | 15 | 2026 | |
| Macrouridae_msp-6 | 6 | 480-1750 | 72 | 480 | Small specimens; possibly several species |
| Macrouridae_msp-7 | 10 | 480-1750 | 72 | 480 | Large specimens; possibly several species |
| *Antimora* msp-1 | 1 | 2278 | 12 | 2278 | cf. *A. rostrata* |
| *Laemonema* msp-1 | 7 | 480 | 168 | 480 | cf. *L. laureysi* |
| **Aulopiformes** | | | | | |
| Bathypterois | 30 | 698-2101 | 45 | 1047 | Likely to include several species; some cf. *B. atricolor* or *B. phenax* |
| **Anguilliformes** | | | | | |
| Synaphobranchus msp-1 | 27 | 848-1858 | 76 | 1217 | |
| Synaphobranchidae msp-4 | 3 | 480 | 72 | 480 | |
| Simenchelys mps-1 | 5 | 698-992 | 22 | 698 | |
| Ilyophis msp-1 | 7 | 1274-1462 | 27 | 1386 | |
| **Scorpaeniformes** | | | | | |
| Psychrolutes msp-1 | 2 | 893-1217 | 15 | 1217 | |
| **Notacanthiformes** | | | | | |
| Halosauridae | 89 | 617-2278 | 164 | 992 / 1234 | Likely two genera: *Aldrovandia* and *Halosaurus* with cf. *H. ovenii* |
| **Osmeriformes** | | | | | |
| Alepocephalidae | 58 | 617-1870 | 172 | 1414 | Several species, including genus *Conocara* and *Alepocephalus* |
| **Chondrichthyes** | | | | | |
| Rajiformes | 8 | 617-1870 | 18 | 1858 | Several species, including *Bathyraja* |
| *Centroscymnus* msp-1 | 1 | 1435 | 11 | 1435 | Probably *C. ceololepis* |
| **Indeterminate** | | | | | |
| Actinopterygii msp-9 | 1 | 1274 | 7 | 1274 | |
| Actinopterygii msp-10 | 3 | 1217-1274 | 23 | 1234 | Medium sized specimens; resembles ophidiiform |
| Actinopterygii msp-12 | 32 | 480-1462 | 105 | 617 | Potentially Zoarcidae; often seen resting in pits, probably created by fish |
| Actinopterygii msp-13 | 14 | 617-1234 | 67 | 698 | Group of very small black elongated specimens |
| Actinopterygii msp-14 | 2 | 1870-2101 | 9 | 2101 | Ophidiid or Halosaur |
| Actinopterygii msp-15 | 2 | 992-1750 | 20 | 1750 | |
| Actinopterygii msp-16 | 13 | 992-1858 | 46 | 1274 | |
| Actinopterygii msp-21 | 3 | 1870-1977 | 21 | 1977 | Habitus resembles Actinopterygii msp-14 but considerably smaller |

# Chapter 4

# Cold-water coral reef complexes on the upper Angolan continental slope


## Abstract

Cold-water corals form reef structures in many areas of the deep sea. The distribution of cold-water coral reefs is well known in the North Atlantic, but few reefs have been documented in the South Atlantic. Here we report the discovery of numerous reef features off Angola (09°13'S 12°40'E) between c. 325-470 m water depth identified from acoustic signatures. An ecological assessment of five of these target locations based on seafloor imagery confirms the occurrence of dense living cold-water corals systems located on the levees of a downslope gulley system. The coral frameworks appeared to be readily detected as discrete areas of low amplitude in the first return of seabed seismic data. The main reef building coral was *Desmophyllum pertusum*, which occurred as discrete, isolated colonies or in dense thickets on dead coral framework. There was a high diversity of associated megafauna, including abundant sponges, cnidarians, decapod crustaceans, echinoderms, and fish. By comparison with metazoan communities on adjacent fine-grained substratum, increased invertebrate richness was found within open and dense coral thicket. Both fish and invertebrate community composition differed between soft substratum and coral habitats. Furthermore, total fish densities were enhanced across areas containing live coral colonies and dead coral framework. Aggregations of sea pens and actinian corals were present on soft substratum surrounding the reefs, highlighting the importance of the study area in supporting suspension-feeding communities.

## 4.1 Introduction

Scleractinian cold-water corals (CWC) form reef-like structures in many areas of the ocean (Roberts et al., 2006), such as inshore fjords (e.g. Jonsson et al., 2004), continental shelves (e.g. Jensen and Frederiksen, 1992; Roberts et al., 2005), and deep offshore settings, including continental slopes (e.g. Buhl-Mortensen et al., 2017; Dorschel et al., 2009; Muñoz et al., 2012; Wienberg et al., 2008), canyons (e.g. De Mol et al., 2011; Huvenne et al., 2011), and seamounts (e.g. Davies et al., 2015; Duineveld et al., 2004). Reef-like formations can occur as dense dead coral skeleton colonised by live coral stands (Arnaud-Haond et al., 2017; Mortensen et al., 2001), or as smaller isolated coral colonies (Duineveld et al., 2004). Six scleractinian species are known to create dense deep-water (< 200 m) reefs, of which *Desmophyllum pertusum* (synonym: *Lophelia pertusa* (Addamo et al., 2016)) is the most widespread (Roberts et al., 2009). Over longer time periods, alternating cycles of coral growth and bioerosion of dead coral skeleton coupled with sediment infill can create coral carbonate mounds of varying size and shape (Roberts et al., 2009). Examples of large deep-water (< 200 m) coral carbonate mound features in the Atlantic include the Belgica mound complex in the Porcupine Basin off Ireland (De Mol et al., 2002) and the mound province along the Mauritania margin (Wienberg et al., 2018).

Deep-water Scleractinian reefs form an important component of deep-sea benthic systems (Roberts et al., 2006). The complex three-dimensional structure of the coral skeleton offers a variety of different ecological niches for microbial to megafaunal species (Buhl-Mortensen et al., 2010), including substratum of sessile suspension feeders (e.g. Jonnson et al., 2004; Roberts et al., 2008), and refuge, foraging and nursery sites for many fish species (Mortensen et al., 1995; Ross and Quattrini, 2007). By comparison with adjacent non-reef habitats, some reefs habitats support higher richness of macrofaunal (Henry and Roberts, 2007) and megafaunal (e.g. Jonnson et al., 2004, Mortensen et al., 1995) invertebrates as well as fishes (e.g. Costello et al., 2005).

The fragility of the coral skeleton combined with slow growth rates make CWC reefs highly sensitive to physical disturbances from human activities, such as bottom trawling (e.g. Buhl-Mortensen et al., 2017; Stone, 2006) and seabed infrastructure developments (Cordes et al., 2017). In light of this, several national and international nature conservation legislations and commitments have been introduced that require the protection of

Scleractinian reefs (Cordes et al., 2017). At the same time, scientific efforts to map and predict the extent of cold-water coral occurrences, and quantify their morphological and ecological characteristics have grown (Roberts et al., 2006). Nevertheless, only few reefs have been documented in the eastern South Atlantic (Buhl-Mortensen et al., 2017; Hebbeln et al., 2020; Le Guilloux et al., 2009).

First insights into the structure and ecology of Angolan CWC reefs were given by Le Guilloux et al. (2009), who studied a small cluster of mostly elongated coral mounds at c. 400 m water depth on the northern margin (c. 7°18'S). The mounds are about 30 m high, and up to 300 m wide and 1.5 km long. Their orientation appear to follow the direction of underlying faults originating from salt tectonic processes. Common megafaunal species associated with the reefs included macrourids and scorpaenid fish, gorgonians, echinoids, and the glass sponge *Aphrocallistes* sp. Reduced sediments with bacterial mats and Lucinid bivalves were recorded at sites surrounding the reefs, suggesting active fluid escape across the study area. More recent acoustic mapping and ROV investigations along the central Angolan slope (c. 9°40'S - 9°50'S; Hebbeln et al., 2016) found dense living reefs on up to 100 m high mounds, which occurred either isolated or as long ridges (Hanz et al., 2019). Coral aggregations were, like those located further north, formed predominantly by *D. pertusum* interspersed with some colonies of *Madrepora oculata* (Hebbeln et al., 2016). The largest aggregations were recorded at depths between 330-470 m (Hebbeln et al., 2020), coinciding with the core of the OMZ where dissolved oxygen concentrations were as low as 0.5 ml l-1 (Hanz et al., 2019).

Here we extend the characterisation of coral mounds from the tropical SE Atlantic by documenting the presence and general structure of mound formations along the central part of the upper Angolan continental slope (study Area C). These were identified from BP 3D seismic data and suggest the presence of coral reef complexes associated with a downslope gully system. We use photographic material, collected by BP, to describe the structure of metazoan megafaunal assemblages associated with living reefs and their surrounding soft substratum. We then examine the ecological importance of the reefs and predict that the habitat provided by live and dead coral facies support locally unique communities of megafaunal invertebrates and fish. We further investigate whether the reefs increase diversity of associated invertebrates, test whether megafaunal community

structure differs among coral facies, and compare community turnover (beta diversity) within reef and non-reef areas.

## 4.2 Materials and methods

The seafloor topography in the wider study region is highly variable (Figure 4.1a). In the northern part, a large sinous submarine canyon and several associated channel complexes dissect the slope in a predominantly southeast to northwest direction In addition, bathymetric data indicate the presence of numerous parallel, downslope trending gullies along the upper and middle slope in the southern portion of the study area, which includes the area of expected cold-water coral habitat investigated in this study (Figure 4.1b). Across the deeper slope sections, deeper than 1000 m, seafloor ridges formed by salt uplift (BP, 2013) are prominent.

### 4.2.1 Collection of photographic data

A total of five photographic transects were surveyed on board the RSS *Ocean Discovery* in September 2014 (Figure 4.1b) using a towed camera platform (Seatronics DTS 6000) fitted with a vertically mounted, downward facing wide angle high-definition video camera (SubCControl 1Cam), a downward facing 5 megapixel Kongsberg OE14-208 digital stills camera (2592 x 1944 pixels), and two sets of parallel scaling lasers spaced 7 and 10 cm apart. Video footage was continuously recorded while digital stills were automatically captured every 15 seconds. The position of the camera frame was logged every 3 seconds with an ultra-short base line (USBL) beacon linked to the ship's Sonardyne acoustic tracking system.

All transect locations were selected non-randomly in areas where coral reef complexes were suspected based on low intensity returns of acoustic backscatter data. Transects were completed in a SW to NE direction covering both crests and flanks of suspected coral reefs as well as areas of adjoining soft substratum free of coral remnants. One coral reef complex was surveyed along each transect, except at Site 3 where two coral fields located approximately 1.1 km apart were imaged together with the interjacent coral free soft substratum (Figure 4.1b). Photographic sites were located in water depths between about 300 and 470 m, and spanned a seabed distance of about 255 to 1600 m (Table 4.1).

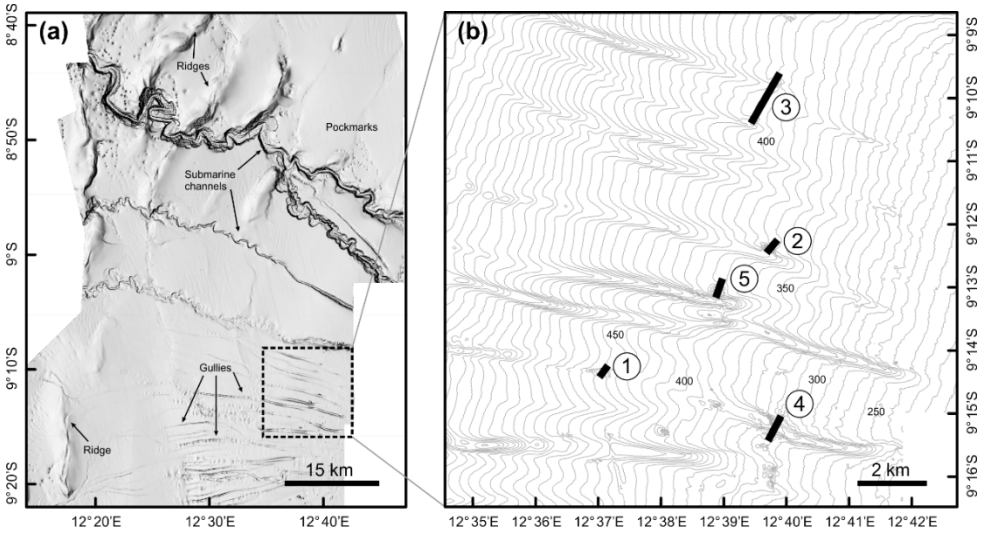


**Figure 4.1** Shaded relief map of the wider study area along the Angolan continental slope marked with the main topographical features **(a)**, and the locations of the five sites photographed in 2014 to study cold-water coral reef systems **(b)**. Bathymetric data are based on depth-converted first-return signals of large scale seismic data and were supplied by BP processed to 25 x 25 m. Depth conversions were based on Advocate and Hood's (1993) depth velocity model. Shaded reliefs were derived from multidirectional hillshading as implemented in ArcGIS v10.5 and are vertically exaggerated by a factor of two.

### 4.2.2 Analysis of photographic data

The diversity and composition of megafaunal assemblages were quantified based on analysis of still photographs taken below 4 m from the seabed, using the image annotation software BIIGLE 2.0 (Langenkämper et al., 2017). The video footage was used to delineate boundaries between substratum types and to facilitate taxa identifications. Photographs that were overexposed, out of focus, or where suspended matter obscured view of most of the seabed were excluded. To maximise the number of suitable images, image edges affected by backscatter or vignetting were cropped. The seabed area covered by an image was calculated using the scale provided by the point laser markers following

the trigonometric approach outlined in Durden et al. (2016) with scaling measurements made using the ImageJ software (Schneider et al., 2012). To identify sets of non-overlapping images, image footprints were mapped based on image size, image position, and approximated camera heading, using functions from the 'sp' (Pebesma and Bivand, 2005) and 'rgdal' (Bivand et al., 2019) packages in R (R Core Team, 2020). Image positions were extracted from the raw USBL senor files and smoothened prior to mapping using a 9-point, centred weighted moving average to correct recording errors. Camera heading was not recorded during the survey and was therefore estimated visually from the orientation of the camera in relation to the transect line by viewing representative sections of the video footage.

**Table 4.1** Photographic sites surveyed in 2014 to study cold-water coral habitats on the upper continental slope off Angola. Transect length represent the planar distance surveyed. Area is the seabed area covered for images obtained in faunal analyses.

| | **Site 1** | **Site 2** | **Site 3** | **Site 4** | **Site 5** |
|---|---|---|---|---|---|
| Date | 02/09/2014 | 02/09/2014 | 02/09/2014 | 03/09/2014 | 02/09/2014 |
| Start position | 9°14′18.25″S<br>12°36′58.86″E | 9°12′23.95″S<br>12°39′47.2″E | 9°10′21.24″S<br>12°39′29.42″E | 9°15′22.75″S<br>12°39′46.14″E | 9°13′2.65″S<br>12°38′57.06″E |
| End position | 9°14′9.2″S<br>12°37′3.06″E | 9°12′17.25″S<br>12°39′51.91″E | 9°9′39.78″S<br>12°40′0.9″E | 9°15′3.98″S<br>12°39′54.2″E | 9°12′51.91″S<br>12°39′1.77″E |
| Transect length | 305 m | 255 m | 1600 m | 635 m | 360 m |
| Depth range | 443-466 m | 352-388 m | 396-430 m | 325-369 m | 370-406 m |
| Suitable images | 86 | 93 | 426 | 190 | 115 |
| Area ($m^2$) | 281 | 222 | 1046 | 407 | 399 |

To describe the spatial change in coral facies, each image was visually assigned to one of four categories, defined by the relative coverage of different substratum types (Table 4.2). In addition, the proportion of seabed covered with live coral stands and large unbroken dead framework was estimated at intervals of < 10%, 10-25%, 25-50%, and > 50% coverage. The occurrence of noticeable seabed features such as ripples, hard substratum, and shell hash was recorded for qualitative descriptions. Water depth for each image was extracted from a 25 x 25 m resolution digital elevation model covering the study area (as shown in Figure 4.1), which was supplied by BP.

**Table 4.2** Substratum categories used to classify seafloor types (adapted from Dorschel et al., 2009, and Wienberg et al., 2008).

| Category | Characteristics |
|---|---|
| Soft substratum | Fine-grained sediment with or without ripples, shell hash and/or signs of bioturbation; occasionally with isolated outcrops of hard substratum. |
| Soft substratum with sparse coral rubble | Fine-grained sediment with low amounts of coral rubble and occassional medium-sized coral debris covering < 5% of the underlying substratum; no live coral colonies. |
| Mixed substratum | A mixture of fine-grained sediment and coral rubble interspersed with isolated pieces of dead coral framework covering < 10% of the underlying substratum; dead framework occasionally colonised by small live colonies of *Desmophyllum pertusum* or *Madrepora oculata*. |
| Open coral thicket | Medium-sized to large live coral colonies on top of dead coral framework amongst sediment and scattered coral rubble. Live colonies and dead coral framework covering between 10-75% of the underlying substratum. |
| Dense coral thicket | Dense live coral colonies on top of dead framework, covering more than 75% of the underlying substratum. |

In each photograph, all fauna was recorded, including partially buried or hidden megafaunal specimens with visible body parts, such as ophiuroids amongst coral framework. In line with the annotation protocol adopted in Chapter 3, surface dwelling specimens, epibenthic gastropods, and mobile tubicolous polychaetes (quill worms) were recorded when trails behind the specimen indicated recent movement or when parts of the organism's soft tissue were visible. Sediment tubes extruding from the seabed were not counted as it was impossible to determine whether they were inhabited. Colonial organisms as well as zoanthids colonising the glass sponge *Aphrocallistes* were counted as single specimens. Likewise, densely grouped sponge individuals, such as aggregations of *Sympagella* sp. were counted as one entity. The recorded specimens were classified to the lowest possible taxonomic level based on visible morphological features, facilitated through a reference morphospecies image catalogue, which was developed by reference to deep-water taxonomic literature and image-based morphospecies lists from the region (Buhl-Mortensen et al., 2017; Le Guilloux et al., 2009; Jamieson et al., 2017; Jones et al., 2014; Vardaro et al., 2013).

### 4.2.3 Data analysis

Only low numbers of photographs classed as 'Soft substratum with sparse coral rubble' were available. These images were therefore excluded from the quantitative comparisons of ecological parameters. Faunal records from the remaining images were grouped into different sets to allow comparisons of ecological parameters (1) among substratum classes

across all photographic sites combined, and (2) among sites for individual substratum classes.

Differences in alpha diversity were assessed for invertebrates by comparing sample-based rarefaction and extrapolation curves for the effective number of species (i.e. Hill numbers, *sensu* Hill, 1973), expressed as (1) morphotype richness $^{0}D$, (2) the effective number of common morphotypes (exponential form of Shannon entropy exp $H'$ or $^{1}D$), and (3) the effective number of dominant morphotypes (reciprocal of Simpson's concentration index 1/D or $^{2}D$). For morphospecies richness, sample-based rarefaction and extrapolation curves and associated unconditional variance estimates were computed based on the analytical method of Colwell et al. (2012) using the EstimateS v9.1 software (Colwell, 2013), with individual photographs as sampling units and based on 100 random permutations without replacement. Morphospecies richness was extrapolated to double the number of sampling units (images) annotated for each group, following the recommendation of Colwell et al. (2012). For $^{1}D$ and $^{2}D$, sample-based rarefaction curves with associated 95% confidence intervals were computed based on 100 random permutations with replacement, again using individual photographs as sampling units. Non-overlapping 95% confidence intervals were taken as indicative of significant differences at a level < 5%. In addition to Hill numbers $^{0}D$ to $^{2}D$, we estimated invertebrate beta diversity (morphospecies turnover) for two substratum classes (soft substratum vs coral thicket) using Whittaker's diversity index $\beta_W$ (1960, 1972), expressed as $\beta_W = \gamma / \overline{\alpha}$, where $\overline{\alpha}$ is the average value of local (within substratum class) diversity and $\gamma$ represents the total diversity of each substratum class (Magurran, 2004). To account for sample size dependencies on the number of taxa encountered (e.g. Gotelli and Colwell, 2001), beta diversity was calculated using rarefied diversity estimates, set to 350 individuals to estimate local (alpha) diversities and to 1750 individuals for total (gamma) diversity.

For the purpose of analysing differences in numerical densities and faunal composition between sites and substratum classes, the data were portioned into three groups: (1) soft substratum, (2) mixed substratum and open coral thicket with up to 25% coverage of live coral stands and dead framework, and (3) open and dense coral thicket with coverage > 25%. Numerical densities were calculated for both invertebrates and the ichthyofauna, using a modified form of non-parametric bootstrapping to obtain variance estimates (Davison and Hinkley, 1997; Puth et al., 2015). To account for differences in sampling

effort and image altitudes between areas with soft substratum and cold-water coral reef habitat, calculations were conducted on a down-sampled image data set comprising approximately 55 $m^2$ of seabed for each assessed site and substratum class. To calculate the bootstrapped mean densities, each image data set was first randomly resampled with replacement to cover 55 $m^2$ of seabed. Resampling was repeated 100 times, and invertebrate and fish numerical density were then computed for each of the 100 bootstrapped samples, from which mean densities were subsequently derived. Corresponding 95% confidence intervals for the parameter estimates were approximated using the simple percentile method, with the upper and lower confidence bounds expressed as the 2.5% and 97.5% percentile of the bootstrapped replicates (Davison and Hinkley, 1997). Resampling, bootstrapping, and density calculations were performed in R (R Core Team, 2020) using a series of custom scripts.

Differences in community composition were examined for both invertebrates and the ichthyofauna, based on Bray-Curtis dissimilarities (Bray and Curtis, 1957), which were calculated from square-root transformed morphospecies densities standardised to unit area ($m^{-2}$). Non-metric multi-dimensional scaling (NMDS) was applied to visualise assemblage dissimilarities, and Analysis of Similarities (ANOSIM) was used to test for significant differences in morphospecies composition among the three selected substratum classes (soft, 5-25% coral coverage, >25% coral coverage). ANOSIM generates a test statistic (R), which can range from -1 to 1. R will be close to 1 when communities have a very dissimilar structure, whereas R values close to zero indicate little or no difference in community composition among the compared groups (Clarke and Warwick, 2001). All multivariate calculations were carried out in R (R Core Team, 2020) using functions from the 'vegan' and 'stats' packages.

## 4.3 Results

### 4.3.1 Cold-water coral habitat

Live cold-water scleractinian coral colonies were present at all five surveyed sites, dominated by white colour varieties of *D. pertusum* with some occurrences of *Madrepora oculata* colonies and rarer sightings of red *D. pertusum* colonies. Seabed areas with low acoustic amplitude (Figure 4.2a) showed good correspondence with observed occurrences

of live scleractinian coral colonies and dead coral skeleton. Based on the distribution of low amplitude signatures (Figure 4.2a), this suggests, that in the wider study area cold-water coral reef habitats are restricted to water depths above 600 m, with an upper limit to least 350 m water depth. Bathymetric data and seismic profiles across the study area (Figure 4.2b) revealed that coral complexes are located predominantly at the levees of the downslope trending gullies, which are about 30-50 m deep across the surveyed depth range. Individual coral complexes appear to form distinct topographical highs up to at least 30 m high.

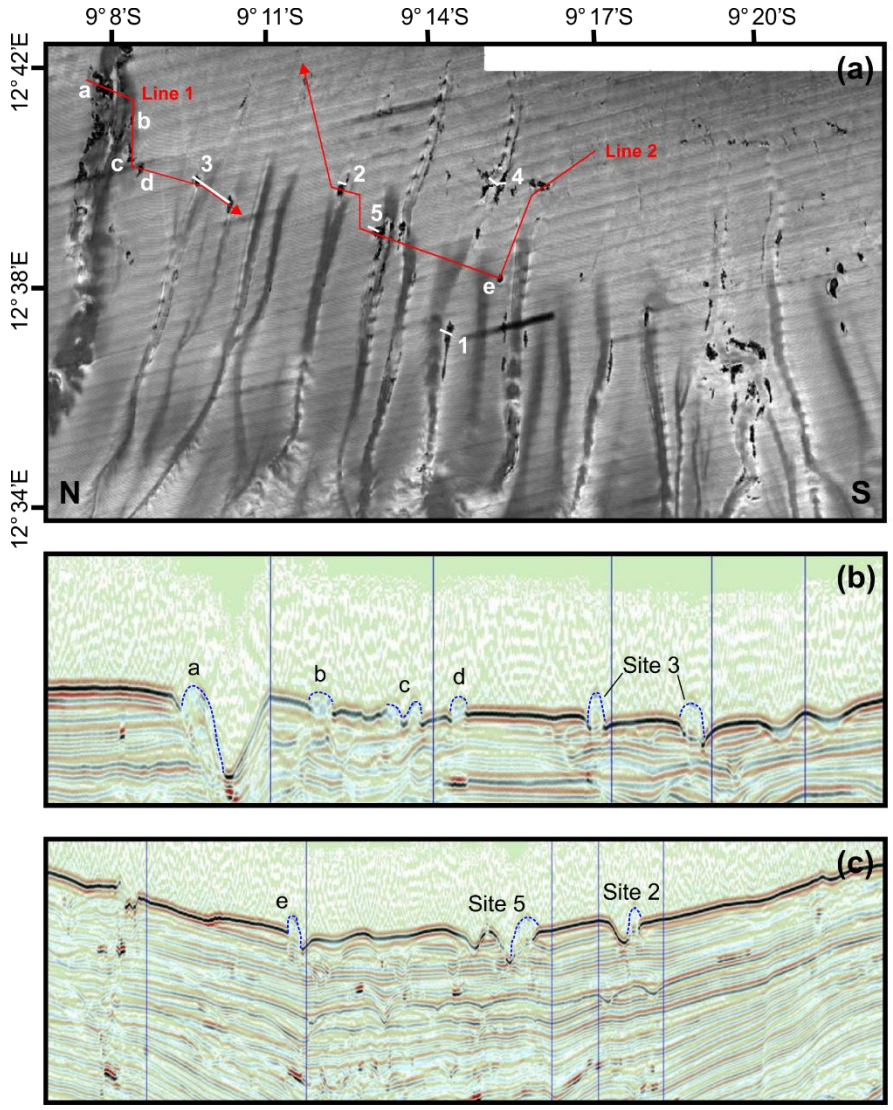


**Figure 4.2 (a)** Seabed amplitude of the wider study region, marked with the location of the five sites investigated (1-5) and other potential cold-water coral reef habitats (a-e) identified from interpretations of 3D seismic data. Areas with lower amplitude correspond to darker colours. **(b** and **c)** Seismic lines (Line 1 and 2) through the downslope gully system crossing areas with expected cold-water coral reef. Blue broken lines indicate confirmed and potential coral complexes. Seafloor amplitude data and seismic profiles with interpretations of potential reef locations were provided by BP. Note the two seismic profile lines run in opposite directions.

The distribution of substratum types across cold-water coral habitats followed a general succession from soft substratum, soft substratum with sparse coral rubble, mixed substratum to open coral thicket, with dense coral thickets recorded at the summits of coral mounds at Sites 2 and 5, and the flank of the first coral complex imaged at Site 3 (Figure 4.3). Outcrops of hard substratum were present adjacent to and at the floor of the gully traversed at Site 4. Small patches of dark grey to black sediment about 1 to 30 cm in diameter occurred locally along the flanks of the coral mounds surveyed at Sites 1 and 4. In addition, one yellow bacterial mat was observed at Site 1. Aggregations of empty bivalve shells, possibly Lucinidae (Cosel, 2006), were seen on and partially buried in sediments at the base of several mounds. On the surrounding soft substratum, seafloor ripples were visible at Sites 1 and 4, being more prominent at Site 4. Oblique faunal burrows were commonly observed across soft substratum with a noticeable larger degree of bioturbation occurring at Site 2. Small about 1-3 cm wide more or less circular patches of light sediment were present at all sites, ranging in densities from 0.09 $m^{-2}$ at Site 4 to 5.0 $m^{-2}$ at Site 3.

Vertical profiles of temperature, salinity and dissolved oxygen concentrations taken on 5$^{th}$ August 2014 about 9 to 15 km downslope from the surveyed coral reef sites recorded bottom water temperatures of 7.4-12.4°C, salinities of 34.7-35.2 PSU, and dissolved oxygen concentrations of 0.36-0.75 ml $l^{-1}$ at water depths between 300-470 m (Chapter 3, Figure 3.4).

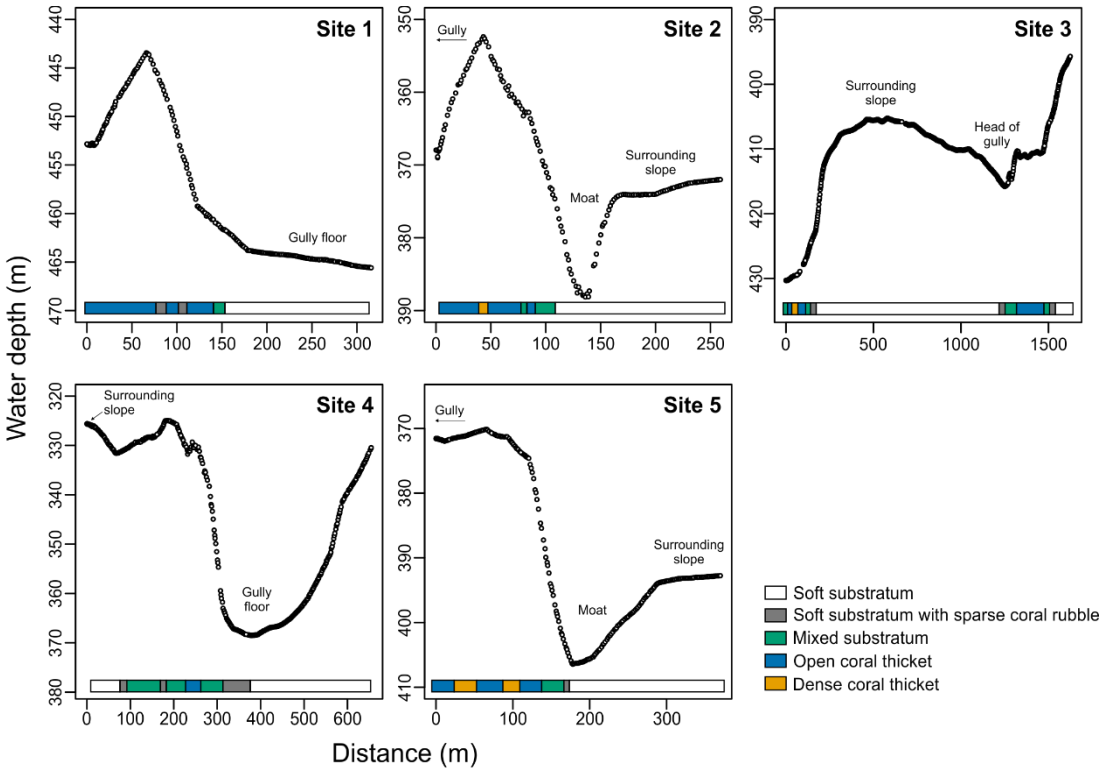


**Figure 4.3** Bathymetric profile and distribution of main substratum classes along each photographic transect. Points represent the water depth for each image taken, including images excluded from faunal analyses. All transects were run SW to NE, but covered different parts of reef complexes. Transect 1 crossed a reef summit and its flanks, and finished at what appeared to be the head of a gully. Transects 2 and 5 crossed the summit of reef complexes located at the northern flanks of downslope gullies, ending at surrounding slope habitat. In both cases, the coral mound was surrounded by a small moat. Transect 3 imaged two reef complexes located at the northern flanks of gullies and adjoining open slope habitat. The second reef complex was imaged near the base along its eastern boundary. Transect 4 imaged a reef complex at the southern flank of a gully, the associated gully floor and parts of its northern side.

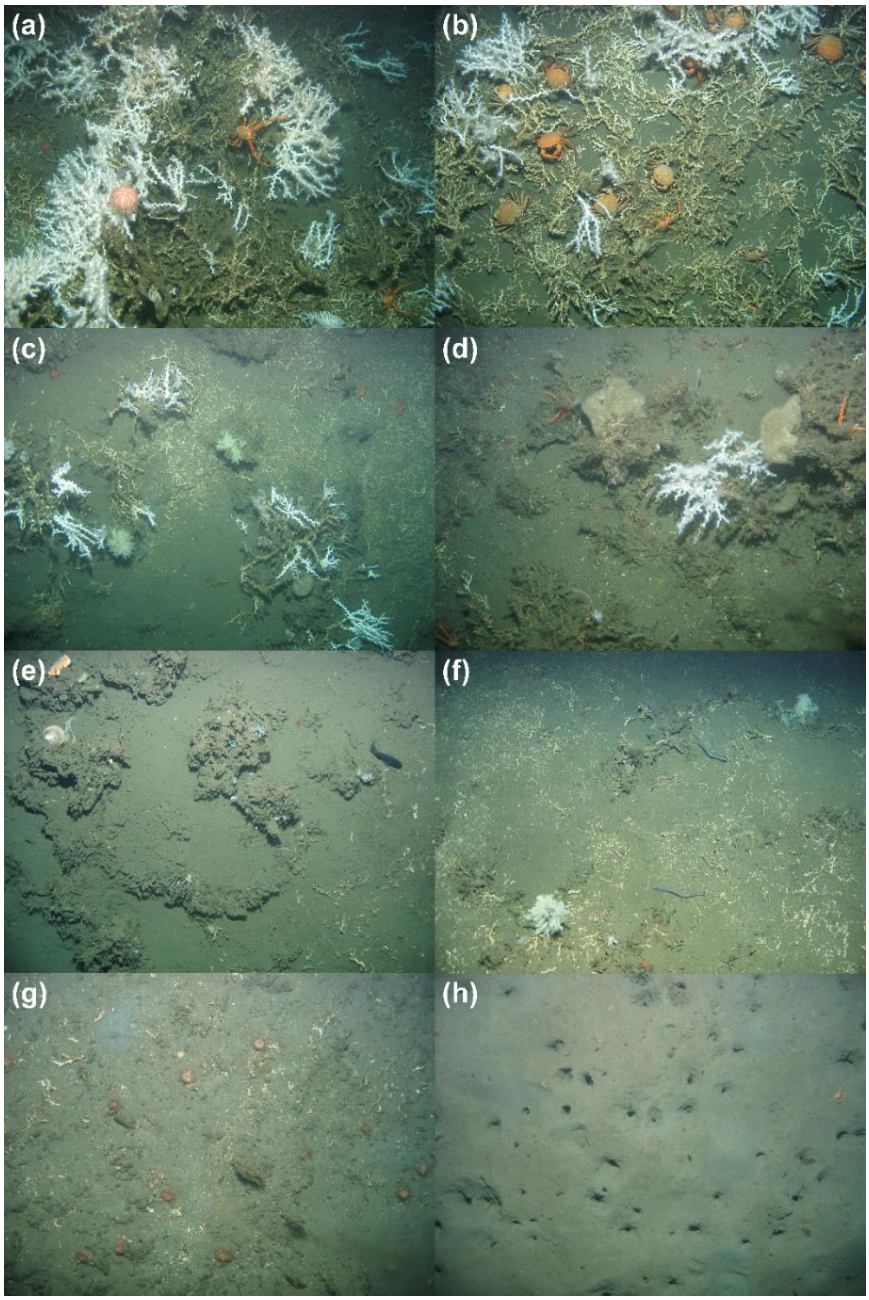


**Figure 4.4** Example images showing the different seabed types observed along the five studied sites. **(a)** Dense live *D. pertusum* colonies growing on extensive dead framework on the summit of Site 5, associated with large squat lobsters, echinoids and sea stars on top of coral colonies and framework, and ophiuroids and nettastomatid eels among the framework; note the small *M. oculata* colony at the bottom of the image. **(b**) Live colonies o *D. pertusum* among dense dead framework with abundant red crabs at the summit of Site 5. Small red actinians were common on the sediment between coral blocks. **(c)** Isolated patches of live coral colonies and dead coral frame among sediment and scattered coral rubble on the summit of Site 5, colonised by sponges, cnidarians and bryozoans, including the glass sponge *Aphrocallistes* with associated yellow Zoanthids. **(d)** Overgrown dead coral frame with isolated colony of live *D. pertusum* and large plate-like sponges at Site 4. **(e)** Low-lying dead coral framework overgrown with sheets of dead glass sponges at the base of a coral reef complex at Site 3, with large *Acesta*, Goniasterid, and aggregations of the glass sponge *Sympagella*. **(f)** Mixed substratum of fine-grained sediment, scattered coral rubble, and small coral frame at the base of Site 3 with synaphobranchid eels. **(g)** Mixed substratum of fine-grained sediments, coral rubble, and bivalve shells at the bottom of the gully surveyed at Site 4 with abundant Hormathiidae. **(h)** Heavily bioturbated fine-grained sediment adjacent to the gully surveyed at Site 2.

### 4.3.2 Associated metazoan megafauna

A total of 154 metazoan morphospecies were differentiated from the 910 images analysed (Table S4.1). Among them, two invertebrate morphospecies were subsequently excluded from all analyses owing to the majority of recorded specimens being smaller than 1 cm. The first comprised globular, white specimens, possibly sponges, with diameters of about 0.3-1.5 cm, which were recorded on soft substratum at four out of the five sites sampled. The second excluded morphospecies was a small actinian (*Clavularia* sp.) populating dead coral framework and larger coral rubble, which was however only visible in lower altitude images.

#### *Invertebrate diversity*

The retained specimens were differentiated into 32 morphologically distinct fishes, 2 ascidians, and 118 invertebrate morphospecies (Table. S4.1). Higher level taxonomic units omitted from the analysis of diversity and composition (e.g. Actinopterygii spp. indet) included seven invertebrate groups and one fish group, which comprised about 5.6% and 12% of the total invertebrate and fish count, respectively. Among the invertebrates (incl. Ascidiacea), 15 morphospecies were restricted to soft substratum, while 62 morphospecies were only recorded amongst mixed substratum with coral rubble and in areas with open and dense coral thicket. About 23% of invertebrate morphospecies were represented by one or two individuals, and two thirds by more than five specimens. Among the Actinopterygii, three morphospecies were only seen on soft substratum, and thirteen were restricted to mixed substratum with coral rubble and in areas with open and dense coral thicket. Cnidaria were the most morphospecies-rich invertebrate phylum (50 morphospecies), followed by Arthropoda (20), and Porifera (16).

When assessed across all sites, expected invertebrate morphospecies richness ($^0$D, Figure 4.5a), heterogeneity diversity ($^1$D) and Simpson diversity ($^2$D; Figure S4.1a) were significantly lower on soft substratum than on both open and dense coral thicket, and mixed substratum and coral thicket for all rarefied and extrapolated sample sizes. Comparisons of morphospecies richness accumulation curves based on the percentage cover of coral colonies and dead framework (Figure 4.5b) indicate significant lower invertebrate richness on soft substratum compared to areas with < 10%, 10-25%, and 25-50% coverage. For $^1$D and $^2$D larger differences were observed among the four coral

substratum types, with substrates with < 10% and > 50% coral coverage both supporting a significantly lower number of common invertebrate morphospecies and exhibiting greater morphospecies dominance compared to substrates with 10-25% and 25-50% coral coverage (Figure S4.1b).

Significant differences in invertebrate richness were also found among photographic sites. On soft substratum, the invertebrate community at site 4 contained significantly more morphospecies than those at sites 1 and 3 up to sample sizes of at least 450 individuals (Figure 4.5c). A reverse pattern was found on mixed substratum and coral thicket, where expected invertebrate richness at site 4 was significantly lower compared to that at sites 1 and 3 (Figure 4.5d). This pattern was also observed for areas with 5-25% coral coverage, which showed significantly lower rarefied richness at site 4 compared to site 1 for sample sizes of at least 329 individuals, and site 3 up to at least 1200 sampled individuals (Figure 4.5e). Soft substratum at site 4 also exhibited the highest number of common morphospecies and the most even morphospecies abundances (Figure S4.1c). On mixed substratum and coral thicket, $^{1}D$ and $^{2}D$ were lowest at site 4, as for expected richness, and highest at sites 3 and 5 with sites 1 and 2 reaching intermediate values and significant differences being present between all five sites (Figure S4.1d). However both dominance and heterogeneity diversity patterns varied with the degree of coral coverage. On areas with 5-25% coverage, invertebrate communities at site 3 showed the highest heterogeneity diversity and lowest dominance followed by those at site 5, 2 and 1 (Figure S4.1e). In contrast, for areas with > 25% coral coverage, $^{1}D$ and $^{2}D$ were highest at sites 1 and 5 (Figure S4.1f).

Total expected morphospecies richness on soft substratum was about 2.2 times the average for that of the five individual transects (Table 4.3). Beta diversity of the five coral reef complexes was slightly lower, suggesting that relative to the total number of expected morphospecies for each substratum class, individual reef complexes shared more species. The reverse pattern was found for $^{1}D$ and $^{2}D$, which showed higher turnover in the expected number of common and dominant invertebrate morphospecies between individual coral reef complexes than between sampled areas in the surrounding soft substratum.

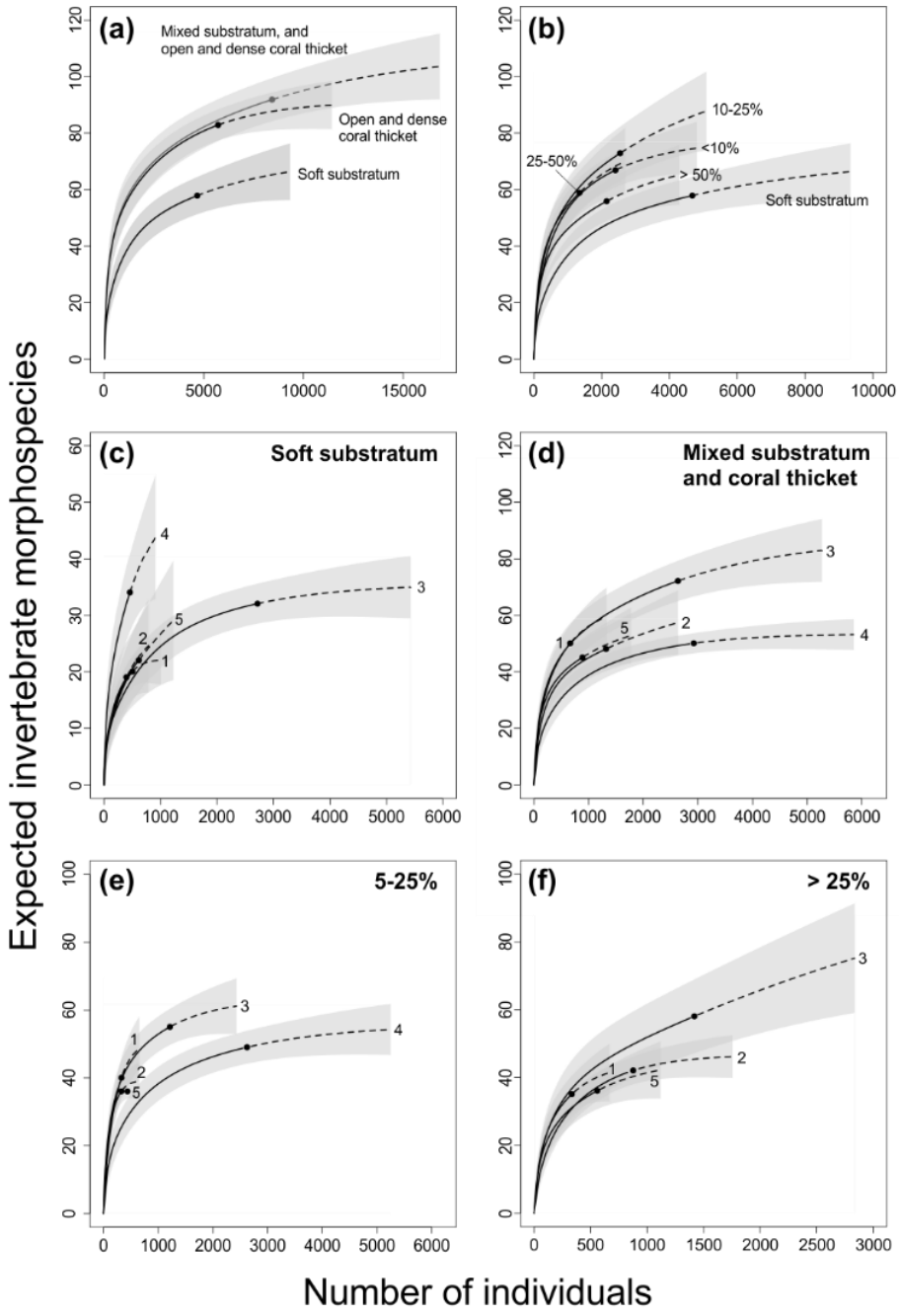


**Figure 4.5** Sample-based rarefaction (solid curves) and extrapolation (dashed curves) of invertebrate morphospecies richness among different substratum classes observed along each photographic site. **(a)** Comparison of main substrate classes for all sites combined. **(b)** Comparison of secondary substrate classes for all sites combined. Percentage is the percentage cover of dead coral framework and live coral stands. Site-level (1- 5) comparisons for: **(c)** Soft substratum. **(d)** Mixed substratum and coral thicket. **(e)** Mixed substratum and open coral thicket up to 25% coverage. **(f)** Areas with coral thicket coverage > 25%. Site 4 was excluded owing to the low number of images for this category. Observed numbers of invertebrate morphotypes for each class are denoted by solid dots. Curves were extrapolated up to double the observed number of individuals. Shaded areas represent 95% unconditional confidence intervals.

**Table 4.3** Invertebrate morphospecies alpha, beta, and gamma diversities for Hill numbers $^0D$ (richness), $^1D$ (exponential Shannon), and $^2D$ (inverse Simpson). Average substratum diversity $\overline{\alpha}$ is based on expected site diversities (Site 1 to 5) rarefied to 350 individuals, and total substratum diversity γ is based on 1750 individuals. Mixed and coral thicket = substratum with > 10% coral coverage. Combined = both substratum classes combined. $\overline{\alpha}_{CV}$ - Coefficient of Variation for average substratum diversity.

| Substratum class | $^0D$ | | | | $^1D$ | | | | $^2D$ | | | |
|---|---|---|---|---|---|---|---|---|---|---|---|---|
| | $\overline{\alpha}$ | $\overline{\alpha}_{CV}$ | γ | $\beta_W$ | $\overline{\alpha}$ | $\overline{\alpha}_{CV}$ | γ | $\beta_W$ | $\overline{\alpha}$ | $\overline{\alpha}_{CV}$ | γ | $\beta_W$ |
| Soft substratum | 20.1 | 0.29 | 44.9 | 2.2 | 5.7 | 0.66 | 6.2 | 1.1 | 3.8 | 0.79 | 3.0 | 0.8 |
| Mixed and coral thicket | 35.1 | 0.16 | 64.3 | 1.8 | 11.8 | 0.36 | 14.9 | 1.3 | 6.3 | 0.46 | 6.1 | 1.0 |
| Combined | 38.1 | 0.08 | 75.6 | 2.0 | 13.1 | 0.18 | 18.9 | 1.4 | 6.9 | 0.22 | 8.6 | 1.2 |

### *Metazoan density*

Both invertebrate and fish numerical densities were highly variable among photographic sites and substratum types (Figure 4.6). Mean invertebrate density was highest across areas with 5-25% coral coverage at site 4 and in open and dense thicket at site 2. In both cases, the high densities resulted from enhanced numbers of a small actinian (Actiniaria msp-11), which, respectively, accounted for 59% and 50% of the invertebrate density at these two sites. By comparison of 95% confidence intervals, there was no trend in mean invertebrate densities among substratum types (Figure 4.6a). For instance, invertebrate density was significantly lower on soft substratum at sites 2 to 4, but significantly higher at sites 1 and 5 compared to substratum with coral remnants. In contrast, fish numerical densities were always significantly higher across open and dense coral thicket (> 25%) than on soft substratum and substratum with < 25% coral coverage (Figure 4.6b). Fish densities across areas with < 25% coral coverage were significantly greater than densities observed on soft substratum at four out of five sites. Fish density peaked in open and coral thicket areas (> 25%) at Site 3, driven by high densities of nettastomatid eel.

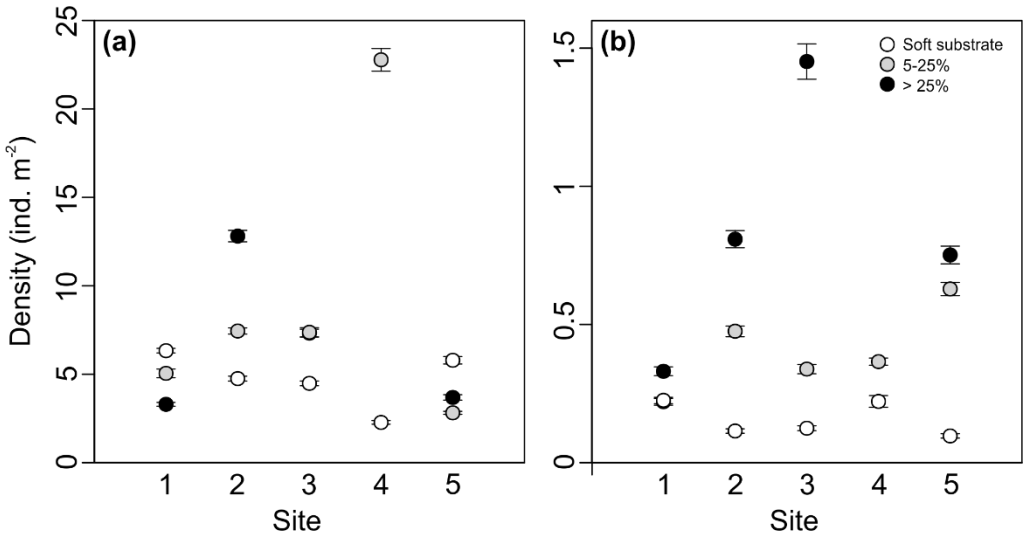


**Figure 4.6** Variation in invertebrate **(a)** and ichthyofauna **(b)** numerical densities with substratum type for each surveyed photographic site (1-5), as calculated from bootstrapping (see Methods). Category 5-25% includes mixed substratum and open coral thicket up to 25% coverage. Coverage > 25% represents substratum with open and dense coral thicket coverage > 25%. Note that no densities were calculated for > 25% at Site 4 owing to the limited number of images scored for this category.

### *Assemblage composition*

ANOSIM pairwise comparisons based on square-root faunal densities revealed significant differences in fish and invertebrate assemblage composition between soft substratum and (1) substratum with 10-25% coral and framework coverage and (2) substratum with >25% coral and framework coverage (Table S4.3). Ordination suggests further differences in invertebrate soft substratum assemblages between sites, with sites 4 and 1 being dissimilar from sites 2, 3 and 5 (Figure 4.7a) A similar grouping of sites was observed for substratum containing coral colonies and framework though differences were less pronounced. For fish assemblages recorded on soft substratum, site 2 was well separated from the remaining sites (Figure 4.7b). For assemblages on substratum with coral coverage, the ordination suggest a separation of Site 1 from the other sites.

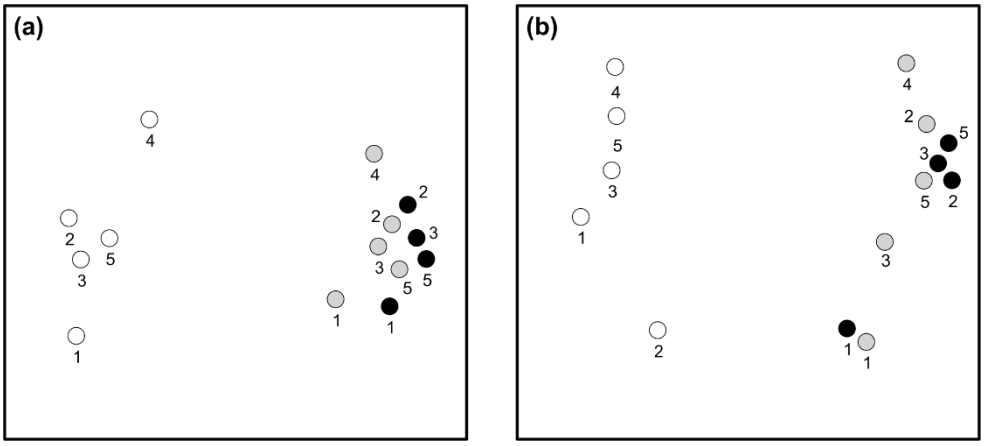


**Figure 4.7** Two-dimensional NMDS ordination plots showing spatial variation in metazoan morphospecies composition among substratum classes and sites (1-5), based on Bray-Curtis dissimilarities computed on square-root transformed standardised numerical densities. **(a)** Invertebrates, MDS stress: 0.042. **(b)** Ichtyofauna, MDS stress: 0.075. Open symbols = soft substratum; light grey symbols = substratum with 5-25% coral coverage; black symbols = substratum with > 25% coral coverage.

The invertebrate communities on soft substratum at sites 1, 2, 3 and 5 were dominated by Virgularid sea pens (52.3-67.9%, 2.8-3.8 ind. $m^{-2}$; Table S4.4). The caridean shrimp *Nematocarcinus* was frequently seen at these four sites (3.8-20.8%, 0.2-1.3 ind. $m^{-2}$) together with other several natant decapods species and small actinians. By contrast, at site 4 the relative abundance distributions of invertebrates was more even, with large Metridioidea being the most abundant morphospecies (19.4%, 0.4 ind. $m^{-2}$), followed by a small caridean shrimp (15.6%) and three actinians with a combined relative density of 29.2%. Virgularid sea pen densities were markedly reduced compared to the other sites (0.2 ind. $m^{-1}$). Across all sites, large crabs (*Bathynectes* and *Geryon)* were occasionally seen with densities between 0.006 and 0.03 ind. $m^{-2}$.

On mixed substratum and open coral thicket up to 25% coral coverage, small actinians populating the sediment, and bryozoans and colonial anthozoans growing on coral skeleton were consistently among the most abundant invertebrate morphospecies (Table S4.4). Serpulids and several sponge morphospecies were also frequently seen at most sites. The large glass sponge *Aphrocallistes* was recorded at sites 2, 3, and 5, often in association with dead sponge framework covering dead coral framework. Large crabs (*Bathynectes* and *Geryon*) together with the squat lobster *Eumunida* were occasionally seen. The faunal make up of invertebrate assemblages of open and dense coral thicket (> 25%) was similar

to that of the < 25% substratum class, with small actinians populating the sediment between live and dead coral being the most abundant invertebrate at most sites (24.8-49.5% relative density). In addition, large ophiuroids (Ophiuroidea msp-10) were present among live coral colonies and dead framework, likely in much larger numbers than recorded here. Red crabs, *Bathynectes*, and *Eumunida* were seen at most sites along with large asteroids and echinoids, the latter predominantly on live coral colonies.

Fish morphospecies seen at most sites associated with soft substratum included a medium-sized grenadier (Macrouridae msp-6), the morid cod *Laemonema*, the rattail *Coelorinchus*, and a tongue fish (*Cynoglossidae*). Macrouridae msp-6 dominated the fish assemblage at sites 3, 4 and 5 (36.4-72.8% relative densities), while tongue fishes were the most abundant fish observed at site 1 (50%). Areas with 5-25% and > 25% coral coverage were characterised by large proportions of nettastomatid eels and small rockfishes (Scorpaeniformes msp-2, possibly *Helicolenus*). At site 1, Nettastomatidae dominated the fish community at areas with coral coverage (65.6 and 71.4%), while Scorpaeniformes msp-2 was not seen, which has likely contributed to the separation of this site from the remaining sites in the ordination space. Other, less abundant taxa seen at several sites across the two coral substratum classes included the short-tail eel *Coloconger*, beryciform fish (possibly *Gephyroberyx*), small eels (Anguilliformes msp-1), and a medium-sized unidentified morphospecies (Actinopterygii msp-19).

## 4.4 Discussion

### 4.4.1 Reef characteristics

The presence of cold-water coral reefs within the downslope gully system was first inferred from low intensity returns of acoustic backscatter data and interpretations of seismic profiles. The analysis of the photographic material confirmed the presence of five life cold-water coral reef complexes located at the gully levees on top of small mounds of up to 30 m in height. Like the previously described CWC reefs on the northern (Le Guilloux et al., 2009) and central (e.g. Hebbeln et al., 2016) Angolan slope and a reef on the upper slope off Ghana (Buhl-Mortensen et al., 2017), the main reef building coral is *D. pertusum* interspersed with colonies of *M. oculata*.

The structural elements of the reef complexes described here are similar to those of small cold-water coral mounds described from the northern part of the Angolan slope (c. 400 m depth and 7°18´S; Le Guilloux et al., 2009), containing coral rubble, larger coral debris, and few live coral colonies along the flanks of the mounds and denser coral thicket on the summits.

The presence of bacterial mats and patches of black sediment indicate active fluid flow in the underlying sediments on and near the coral mounds. The occurrence of coral reefs among hydrocarbon-rich sediments has also been reported for areas off Norway (Hovland and Thomson, 1997; Hovland et al., 1998). Based on these observations, the authors suggested that the distribution of reefs might be directly controlled by the seepage of light hydrocarbons, which was thought to support an abundant microbial community that provide the food source for the corals. However, more recent isotopic analyses of coral polyps from the NE Atlantic (Duineveld et al., 2004) and the West African margin (Le Guilloux et al., 2009) do not indicate a chemosynthesis-based nutrition.

A more widely held view is that the formation of cold-water coral reefs is largely controlled by local hydrographic conditions and the supply of suspended organic matter (e.g. Davies et al., 2009, Henry and Roberts, 2017). Many reefs are closely aligned with topographical features such as troughs, outcrops and bathymetric highs, and it is suggested that these either enhance current activity thereby increasing the rate of food supply, or change flow patterns thereby concentrating food supply (Mortensen et al., 2001 and references therein; Thiem et al., 2006).

In the case of the reefs described here, reef development may be promoted by an increased supply of suspended matter by tidal mixing (Hanz et al., 2019). Near-bottom sediment trap and current meter data collected from the recently mapped coral mound province at c. 9°45’S (Hebbeln et al., 2016) revealed a thick bottom nepheloid layer above the coral mound zone between 200-350 m water depth, which contains high concentrations of suspended particulate organic matter of both marine and terrestrial origin (Hanz et al., 2019). These data also indicate tidally induced vertical mixing of up to 130 m above and below the coral mounds. The coral reefs studied here are located at comparable depths than those reported by Hebbeln et al. (2016), about 60 km to the north, and may be influenced by similar hydrodynamic processes.

Many of the known deep-water coral mounds off Angola, including those described in this study, are located in oxygen-depleted waters, which contradicts with the physiological limits of *D. pertusum* and *M. oculata* predicted from earlier studies (Hebbeln et al., 2020). It has been hypothesised that this may be possible due to two mechanisms, both facilitated by vertical mixing (Hanz et al., 2019). First, periodically mixing of water masses may transport more oxic waters from shallower and deeper layers to the corals thereby improving ambient environmental conditions. Second, high particle loads originating from the overlying nephloid layer may offset any potential physiological stress responses induced by low oxygen concentrations (Hanz et al., 2019; Hebbeln et al., 2020). More insights into how resource availability and oxygen limitations may interact to promote reef formation and stability may be gained from relict cold-water coral mounds off Namibia. There, severe anoxic conditions (0-0.15 ml $l^{-1}$) caused by intense coastal upwelling are thought to prevent present-day coral growth at upper slope depths (Hanz et al., 2019). Contrary to the Angolan reefs, no live corals are present on the Namibian mounds and dead coral framework is predominalty populated with sponges and encrusting bryozoans, which is likely a reflection of their higher tolerance for hypoxic and anoxic conditions (Hanz et al., 2019). As for the Angolan reefs, periodically vertical tidal movements are suggested to facilitate the development of epibenthic communities by enhancing organic matter supply and bottom water oxygen concentrations (Hanz et al., 2019).

### 4.4.2 Associated metazoan communities

The cold-water coral reef complexes supported a diverse set of metazoan megafauna that represent a variety of living and feeding types, ranging from sessile epibiotic suspension feeding sponges, actinians, and bryozoans colonising the coral framework or live coral, to actinians populating the sediment between coral structures, motile echinoids and decapods associated with the upper layers of the reef structures, as well as ophiuroids and fishes hiding among the coral framework. Quantitative comparisons of megafaunal community attributes between those reported here and those found in reefs in other regions is challenging for various reasons, such as differences in sampling effort, or, as in the case of photographic studies, differences in the resolution of taxonomic identifications. The suite of conspicuous megafauna observed in this study showed many similarities with that observed at other known reefs off Angola (Hebbeln et al., 2016; Le Guilloux et al., 2009) and at a reef off Ghana in the Gulf of Guinea to the north (Buhl-Mortensen et al., 2017).

Shared taxonomic groups included the glass sponge *Aphrocallistes* sp. with symbiotic yellow Zoanthidae, large squat lobsters, crabs and echinoids, red coloured ophiuroids, bryozoans, and a diverse fish fauna including Sebastinae, macrourids and nettastomatid eels. However, unlike the coral reef sections imaged off Ghana, the reefs studied here also supported a diverse sponge fauna and several taxa of colonial corals including gorgonians. As such, they also supported many sessile taxonomic groups commonly reported from NE Atlantic (e.g. van Soest et al., 2007; Wienberg et al., 2008) and NW African (Westphal et al., 2012) coral mounds. Other observed conspicuous taxa such as large decapods, grazing echinoids, sea stars and the file clam *Acesta* are also commonly reported from North Atlantic reefs (e.g. Buhl-Mortensen et al., 2017; Purser et al., 2013; Stevenson and Rocha, 2013; Westphal et al., 2012). Overall, these comparisons suggest that the Angolan reefs offer habitats for broadly similar invertebrate megafaunal taxa than their counterparts in the north eastern Atlantic with the addition of the glass sponge *Aphrocallistes*. A comparison of the taxonomic composition of the fish fauna between the Angolan and NW African reefs (Westphal et al., 2012) also showed many similarities, including the common occurrence of nettastomatid eels, rockfish *Helicolenus,* and colocongrid eels as well as sightings of *Trachyscorpia*, red fish *Gephyroberyx,* batfishes, macrourids and of the ateleopodid *Guentherus* (listed as Actinopterygii msp-20).

A contribution of the skeleton of *Aphrocallistes* sp. to the reef framework structure has been reported for the Ghanaian reef (Buhl-Mortensen et al., 2017). We also observed large erect specimens of *Aphrocallistes* and locally dense covers of dead sponge skeleton over coral framework. However, more information on the sponge's distribution across the different coral facies and its associated fauna is needed to evaluate its effect on reef complexity and biodiversity.

There were significant differences in both the diversity and composition of invertebrate assemblages between soft substratum and areas of mixed substratum and open and dense coral thickets. Enhanced species richness within reefs compared to surrounding non-reef areas have been reported from other reefs and are believed to reflect the increased habitat heterogeneity provided by the coral structures, which provides abundant surfaces for attachment of sessile species, abundant food sources for predators, and suitable complexity for refuge (e.g. Buhl-Mortenson et al., 2017; Henry and Roberts, 2007; Jonnson et al., 2004; Mortensen et al., 1995). In this study, 82% of the invertebrate taxa exclusively found

in areas of mixed substratum and coral thicket were sessile. A small actinian observed on the sediments underlying coral framework constituted large proportions of the invertebrate fauna at several reef complexes, which might reflect suitable feeding conditions.

Our observations of significantly different fish communities between reef areas and non-reef areas and significantly higher fish densities on reefs conform to records from other deep-water Scleractinian reefs (e.g. Husebo et al., 2002; Milligan et al., 2016; Ross and Quattrini, 2007). For example, in the northern Ionian Sea D'Onghia et al. (2010) found greater fish densities in cold-water coral reefs than outside the reefs, while in the NE Atlantic greater fish species richness and abundances were documented on-reef than off-reef (Costello et al., 2005). Although not standardised to sample size, we also observed a larger number (13) of fish morphospecies exclusively recorded on mixed substratum and in areas with coral thicket compared to areas of soft substratum (3). Overall, existing studies of deep-water fish communities have demonstrated that cold-water coral reefs form an important habitat for fish spawning, predatory refuge, feeding, and breeding (Costello et al., 2005).

Comparison of Whittaker's beta diversities suggested that, relative to their total richness, soft substratum areas supported a more heterogenous invertebrate megafauna than adjacent coral reef habitats. This could be the result of a more pronounced bathymetric zonation of soft substratum communities relative to communities associated with coral facies. The ordination plot (Figure 4.7a) shows samples from both coral and non-coral facies to be generally arranged by water depth, with the shallowest sites (Site 4) and the deepest sites (Site 1) placed at opposite ends in the ordination space. Samples taken from soft substratum showed wider multivariate dispersion, which might indicate that invertebrate distribution patterns on soft substratum are more constrained by depth-related changes in ambient conditions than the distribution of invertebrates associated with coral facies.

Alternatively, the higher compositional turnover of invertebrates among soft substratum could reflect a more heterogenous physical environment across the sampled gully and open slope sections. Three of the five transects (Sites 2, 3 and 5) covered open slope soft substratum and the small moats surrounding the coral mounds. The seabed at these sites showed changing coverage with shell hash and varying degrees of bioturbation. At the two

remaining sites, the gully adjoining the reefs was sampled; at Site 1 the gully floor, and at Site 4 the gully floor and its adjoining flank. Small patches of hard substratum were present within the gully sampled at Site 4. In addition, the seabed at Site 4 had pronounced seafloor ripples, indicating active sediment transport within the gully. These differences in substratum and hydrodynamic conditions are likely to give rise to greater environmental heterogeneity among the soft substratum sites, which in turn may promote higher beta diversity.

Similar patterns of higher turnover in benthic fauna within non-reef habitats were encountered on coral mounds in the North East Atlantic. On Hatton Bank, the turnover of megafaunal invertebrates was considerable lower among patches of well-developed coral reef framework than among samples from mud, sand and coral rubble habitats (Roberts et al., 2008). Similarly, in a study of macrofaunal communities associated with coral mounds in the Porcupine Seabight, Henry and Roberts (2007) found greater similarity in faunal composition among samples taken from reef framework than in samples taken from off-mound habitats. In both cases, it has been argued that while coral framework exhibits high vertical structural complexity its horizontal heterogeneity might be more predictable, and therefore it might support a more homogenous fauna than off-reef habitats where less-predictable fine-scale substratum heterogeneity is believed to increase faunal turnover. Further analysis of invertebrate community variation in relation to fine-scale changes in seafloor characteristics (e.g. slope, degree of bioturbation) and broader scale depth-related gradients in environmental conditions is planned to elucidate factors driving the faunal patterns observed in this study.

## 4.5 Conclusion

The study established the presence of cold-water coral reef complexes along the upper slope of the Angolan margin. Compared with adjacent soft substratum, the reefs harboured more diverse invertebrate assemblages and higher fish densities. There was also a clear distinction between the composition of metazoan communities found on coral habitat and those on the surrounding soft substratum, with reefs supporting a diverse epifaunal community. Moreover, several species were restricted to either soft substratum or coral habitats, leading to enhanced gamma diversity. These findings show the positive effect of environmental heterogeneity on megafaunal biodiversity. They also suggest that cold-

water coral reefs may be an important contributor to regional megafaunal diversity off Angola. To further assess the relative contribution of these reefs in maintaining regional diversity, more comprehensive mapping and sampling of the wider region will be needed, which would need to include similarly complex habitats. Considering their role in increasing biodiversity and high sensitivity to abrasive bottom activities, together with their occurrence in trawlable depth and areas of active hydrocarbon exploration, cold-water coral reefs off Angola should be considered in environmental management and conservation plans for this region.

# 4.6 Supplementary information

**Table S4.1** Taxonomic resolution of metazoan morphospecies included in faunal analyses. Morphospecies are listed according to the taxonomic level to which they were identified along with the number of morphospecies recorded for each level. For example, Porifera msp with morphospecies n = 15 equates to 15 morphospecies identified to Phylum Porifera. Respective morphospecies are labelled Porifera msp-1, Porifera msp-2 etc. The taxonomic classification follows the hierarchical system of the World Register of Marine Species (WoRMS Editorial Board, 2020). * indicates morphospecies excluded from the assessment of alpha diversity and faunal composition

| Phylum / Subphylum | Class / Subclass | Order | Family | Label | Morpho-species (n) |
|---|---|---|---|---|---|
| PORIFERA | | | | Porifera msp | 15 |
| | | | | Porifera spp. indet* | na |
| | Hexactinellida | Lyssacinosida | Rossellidae | *Sympagella* msp-1 | 1 |
| | | Sceptrulophora | Aphrocallistidae | *Aphrocallistes* msp-1 | 1 |
| CNIDARA | | | | Cnidaria msp | 8 |
| | | | | Anthozoa msp | 16 |
| | Hexacorallia | Actiniaria | | Actiniaria msp | 12 |
| | | | Actinoscyphiidae | Actinoscyphia msp-2 | 1 |
| | | | Hormathiidae | Metridioidea msp-5 | 1 |
| | | Zoantharia | | Zoantharia msp-3 | 1 |
| | | Scleractinia | | Scleractinia msp | 3 |
| | | Antipatharia | | Antipatharia msp-1 | 1 |
| | Ceriantharia | | | Ceriantharia msp | 4 |
| | Octocorallia | Alcyonacea | | Alcyonacea msp | 2 |
| | | Pennatulacea | | Pennatulacea msp | 3 |
| | | | | Cnidaria spp. indet.* | na |
| ANNELIDA | Polychaeta | Eunicida | Onuphidae | Onuphidae | 1 |
| | | Sabellida | Serpulidae | Serpulidae | 1 |
| | | | Sabellidae | Sabellidae | 1 |
| | | | | Polychaeta msp-9 | 1 |
| ARTHROPODA | Malacostraca | | | Malacostraca msp-1 | 1 |
| | | Decapoda | | Paguroidea | 1 |
| | | | | Anomura msp | 3 |
| | | | | Brachyura msp | 2 |
| | | | | Caridea msp | 2 |
| | | | | Caridoid msp | 5 |
| | | | Chirostyloidea | *Euminida* msp-1 | 1 |
| | | | Aristeidae | Aristeidae msp-1 | 1 |
| | | | Geryonidae | Geryonidae msp-1 | 1 |
| | | | Polybiidae | *Bathynectes* msp-1 | 1 |
| | | | Nematocarcinidae | Nematocarcinus msp-1 | 1 |
| | | | | Decapoda msp | 2 |
| | | | | Decapoda spp. indet.* | na |
| MOLLUSCA | Bivalvia | Limida | Limidae | *Acesta* msp-1 | 1 |
| | Cephalopoda | | | Cephalopoda msp-4 | 1 |
| | Gastropoda | | | Gastropoda msp | 6 |
| ECHINODERMATA | Echinoidea | Camarodonta | Echinidae | Echinidae msp-4 | 1 |
| | | | | *Gracilechinus* mps-1 | 1 |
| | Asteroidea | | | Asteroidea msp | 2 |
| | | Valvatida | Goniasteridae | Goniasteridae msp-2 | 1 |
| | | | | Asteroidea spp. indet.* | na |
| | Holothuroidea | Dendrochirotida | Psolidae | Psolidae msp-1 | 1 |
| | Ophiuroidea | | | Ophiuroidea msp | 2 |
| BRYOZOA | | | | Bryozoa msp | 2 |
| CHORDATA | Ascidiacea | | | Ascidiacea msp | 2 |
| | Actinopterygii | | | Actinopterygii msp | 7 |
| | | | | Actinopterygii spp. indet.* | na |

**Table S4.1** continued

| | | | | |
|---|---|---|---|---|
| | Lophiiformes | Chaunacidae | Chaunacidae msp | 2 |
| | | Lophiidae | Lophiidae msp-1 | 2 |
| | | Ogcocephalidae | Ogcocephalidae msp | 2 |
| | Beryciformes | | Beryciformes msp-1 | 1 |
| | Scorpaeniformes | | Scorpaeniformes msp | 3 |
| | Aulopiformes | Chlorophthalmidae | Chlorophthalmidae msp-1 | 1 |
| | Gadiformes | Moridae | *Laemonema* sp. 01 | 1 |
| | | Macrouridae | Macrouridae msp | 3 |
| | | | *Coelorinchus* msp-2 | 1 |
| | Pleuronectiformes | Cynoglossidae | Cynoglossidae msp-1 | 1 |
| | | Soleidae | Soleidae msp-1 | 1 |
| | Notacanthiformes | Halosauridae | Halosauridae | 1 |
| | Anguilliformes | Synaphobranchidae | *Ilyophis* msp-1 | 1 |
| | | | Synaphobranchidae msp-4 | 1 |
| | | Nettostomatidae | Nettostomatidae msp-1 | 1 |
| | | Ophichthidae | Ophichthidae msp-1 | 1 |
| | | Colocongridae | *Coloconger* msp-1 | 1 |
| | | | Anguilliformes msp-1 | 1 |
| INDETERMINATE | | | Animalia indet. msp | 9 |
| | | | Animalia spp. indet.* | na |
| | | | **TOTAL**[1] | 152 |

[1] Distinct morphospecies included in the analyses of diversity and community composition.

**Table S4.2** Number of metazoan specimens and morphospecies recorded across each substratum category, combined for all five photographic sites (top), and separately for each site (bottom). Area represents the seabed area analysed for each substratum class. np = class was not recorded

| | | Soft substratum | Soft substratum with sparse coral rubble | Mixed substratum | Open coral thicket | Dense coral thicket |
|---|---|---|---|---|---|---|
| Specimens | Actinopterygii | 167 | 15 | 100 | 625 | 119 |
| | Invertebrates | 4927 | 1098 | 4799 | 5881 | 463 |
| Morphospecies | Actinopterygii | 19 | 6 | 23 | 23 | 9 |
| | Invertebrates | 58 | 47 | 78 | 83 | 27 |
| Area ($m^2$) | | 1084 | 85 | 327 | 750 | 108 |
| Site 1 | | 26 | 10 | 13 | 59 | np |
| Site 2 | | 27 | np | 38 | 56 | np |
| Site 3 | | 45 | 14 | 71 | 84 | 18 |
| Site 4 | | 40 | 44 | 60 | 37 | np |
| Site 5 | | 28 | np | 36 | 55 | 30 |
| Total | | 77 | 53 | 101 | 106 | 36 |

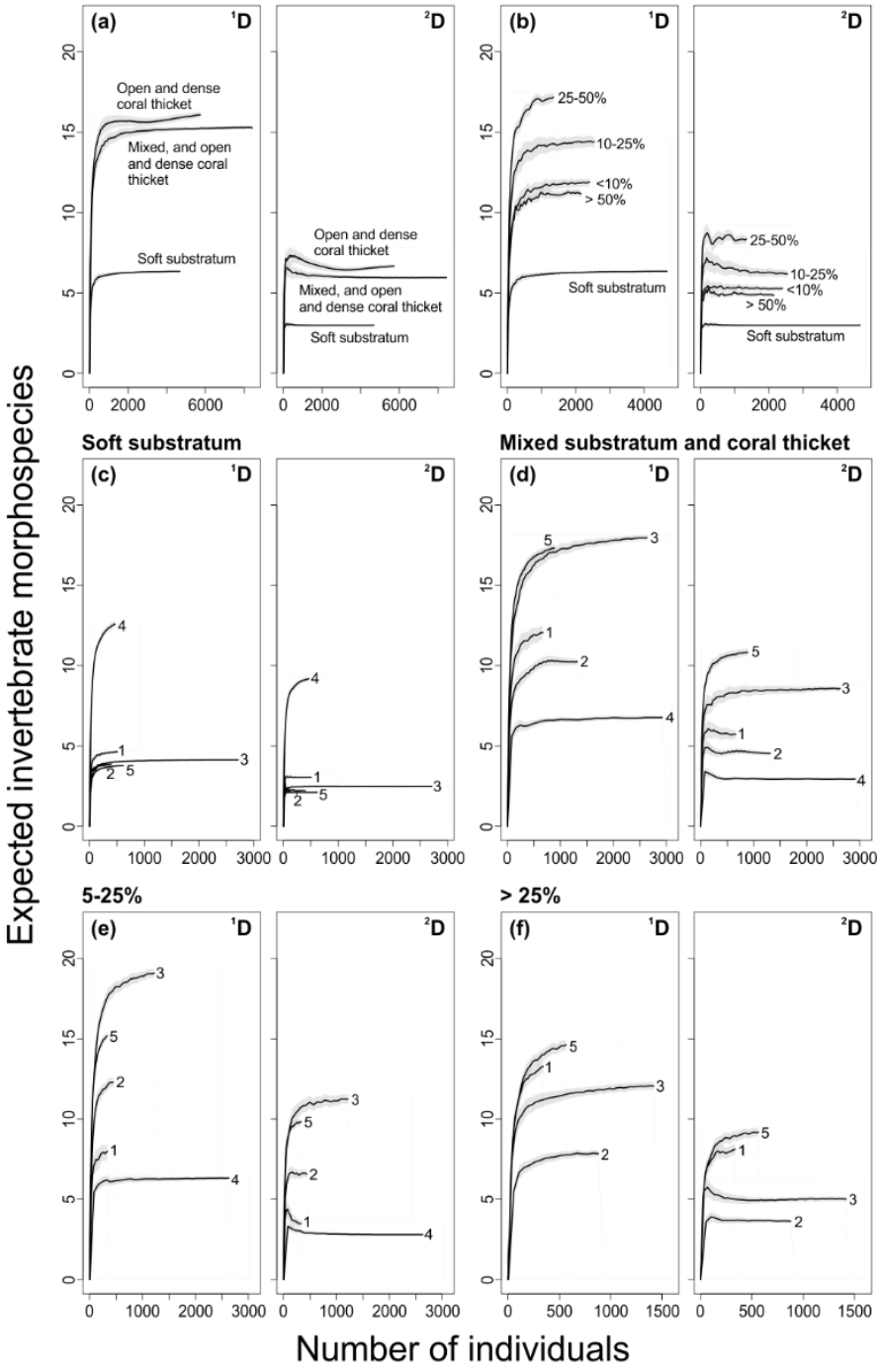


**Figure S4.1** Sample-based rarefaction curves with 95% confidence intervals (shaded areas) of invertebrate exponential Shannon entropy $^1D$ and inverse Simpson diversity $^2D$ for different substratum classes. **(a)** Comparison of main substrate classes for all sites combined. **(b)** Comparison of secondary substrate classes for all sites combined. Percentage is the percentage cover of dead coral framework and live coral stands. Site-level (1- 5) comparisons for: **(c)** Soft substratum. **(d)** Mixed substratum and coral thicket. **(e)** Mixed substratum and open coral thicket up to 25% coverage. **(f)** Areas with coral thicket coverage > 25%. Site 4 was excluded owing to the low number of images for this category. Observed numbers of invertebrate morphotypes for each class are denoted by solid dots. Curves were extrapolated up to double the observed number of individuals. Shaded areas represent 95% unconditional confidence intervals.

**Table S4.3** Results of Analysis of Similarities (ANOSIM) for invertebrate and ichthyofaunal assemblages, based on standardised square-root transformed densities. ns = not significant

| Compared substratum types | Invertebrates | | Fish | |
|---|---|---|---|---|
| | **R** | ***p*** | **R** | ***p*** |
| Global test | 0.64 | < 0.01 | 0.60 | < 0.01 |
| Soft, 5-25% | 0.98 | < 0.01 | 0.89 | < 0.01 |
| Soft, > 25% | 0.99 | < 0.01 | 0.97 | < 0.01 |
| 5-25%, > 25% | -0.06 | ns | -0.08 | ns |

**Table S4.4** Top 10 ranked invertebrate and tunicate morphospecies by numerical density with their relative densities (%) for soft substratum, 5-25% coral and framework coverage, and > 25 % coral and framework coverage. Number on top of relative densities represents the standardised density (ind. $m^{-2}$) for each substratum class.

| **Site 1** | | | | | | |
|---|---|---|---|---|---|---|
| **Rank** | **Soft substratum** | **6.3** | **5 to 25 %** | **5.0** | **> 25 %** | **3.2** |
| 1 | Pennatulacea msp-1 | 52.3 | Actiniaria msp-15 | 54.1 | Bryozoa msp-1 | 22.7 |
| 2 | *Nematocarcinus* msp-1 | 20.8 | Bryozoa msp-1 | 12.2 | Actiniaria msp-15 | 21.5 |
| 3 | Pennatulacea msp-2 | 8.8 | Antipatharia msp-1 | 3.6 | *Aphrocallistes* msp-1 | 9.9 |
| 4 | Caridoid msp-9 | 7.8 | Pennatulacea msp-1 | 3.0 | Porifera msp-27 | 6.0 |
| 5 | Caridoid msp-3 | 3.4 | Actiniaria msp-11 | 1.8 | Zoantharia msp-3 | 5.4 |
| 6 | Gastropoda msp-1 | 1.6 | Porifera msp-27 | 1.8 | Porifera msp-16 | 3.9 |
| 7 | Actiniaria msp-15 | 0.8 | Scleractinia msp-3 | 1.8 | Antipatharia msp-1 | 3.0 |
| 8 | Gastropoda msp-2 | 0.8 | Cnidaria msp-10 | 1.5 | Serpulidae | 3.0 |
| 9 | Animalia indet. msp-2 | 0.4 | Porifera msp-16 | 1.5 | Ophiuroidea msp-10 | 2.7 |
| 10 | Caridoid msp-1 | 0.4 | *Aphrocallistes* msp-1 | 1.2 | Cnidaria msp-10 | 2.4 |
| **Site 2** | | | | | | |
| **Rank** | **Soft substratum** | **4.7** | **5 to 25 %** | **7.4** | **> 25 %** | **12.7** |
| 1 | Pennatulacea msp-1 | 66.3 | Actiniaria msp-11 | 34.3 | Actiniaria msp-11 | 49.5 |
| 2 | Caridoid msp-7 | 9.2 | Bryozoa msp-1 | 11.8 | Ophiuroidea msp-10 | 12.6 |
| 3 | Brachyura msp-4 | 7.9 | Colonial Anthozoa msp-8 | 10.0 | Bryozoa msp-1 | 8.2 |
| 4 | *Nematocarcinus* msp-1 | 3.8 | Serpulidae | 6.1 | Serpulidae | 4.8 |
| 5 | Alcyonacea msp-3 | 3.1 | Colonial Anthozoa msp-6 | 4.8 | *Eumunida* msp-1 | 4.6 |
| 6 | Actiniaria msp-8 | 2.3 | Porifera msp-14 | 3.9 | Colonial Anthozoa msp-8 | 1.8 |
| 7 | Caridoid msp-3 | 2.0 | *Aphrocallistes* msp-1 | 3.6 | Cnidaria msp-6 | 1.1 |
| 8 | Actiniaria msp-38 | 1.5 | *Eumunida* msp-1 | 2.5 | Cnidaria msp-10 | 1.1 |
| 9 | Pennatulacea msp-2 | 0.8 | Zoantharia msp-3 | 2.5 | Pennatulacea msp-1 | 1.1 |
| 10 | Actiniaria msp-34 | 0.5 | Caridoid msp-7 | 1.6 | Porifera msp-14 | 1.1 |

**Table S4.4** continued

| | | | | | | |
|---|---|---|---|---|---|---|
| **Site 3** | | | | | | |
| **Rank** | **Soft substratum** | **4.6** | **5 to 25 %** | **7.2** | **> 25 %** | **7.0** |
| 1 | Pennatulacea msp-1 | 60.6 | Actiniaria msp-15 | 19.7 | Actiniaria msp-11 | 42.5 |
| 2 | Pennatulacea msp-10 | 18.8 | Actiniaria msp-11 | 14.4 | Ophiuroidea msp-10 | 7.5 |
| 3 | *Nematocarcinus* msp-1 | 6.3 | Bryozoa msp-1 | 10.2 | *Aphrocallistes* msp-1 | 5.4 |
| 4 | Pennatulacea msp-2 | 3.2 | Serpulidae | 7.6 | Bryozoa msp-1 | 5.1 |
| 5 | Caridoid msp-7 | 3.1 | Porifera msp-27 | 5.2 | Serpulidae | 4.5 |
| 6 | Actiniaria msp-8 | 2.2 | *Aphrocallistes* msp-1 | 4.6 | *Eumunida* msp-1 | 4.4 |
| 7 | Caridoid msp-3 | 1.4 | Colonial Anthozoa msp-8 | 3.5 | Cnidaria msp-10 | 4.1 |
| 8 | Brachyura msp-4 | 1.3 | *Sympagella* msp-1 | 3.4 | Zoantharia msp-3 | 3.1 |
| 9 | Actiniaria msp-32 | 0.3 | Caridoid msp-7 | 2.5 | Colonial Anthozoa msp-8 | 2.4 |
| 10 | Paguroidea | 0.3 | Porifera msp-24 | 2.2 | Alcyonacea msp-2 | 1.8 |
| **Site 4** | | | | | | |
| **Rank** | **Soft substratum** | **2.3** | **5 to 25 %** | **22.8** | | |
| 1 | Metridioidea msp-5 | 19.4 | Actiniaria msp-11 | 58.7 | | |
| 2 | Caridoid msp-7 | 15.6 | Caridoid msp-7 | 5.8 | | |
| 3 | Actiniaria msp-38 | 12.3 | Colonial Anthozoa msp-8 | 5.2 | | |
| 4 | Actiniaria msp-8 | 8.8 | Bryozoa msp-1 | 5.0 | | |
| 5 | Actiniaria msp-15 | 8.1 | Serpulidae | 4.0 | | |
| 6 | Pennatulacea msp-1 | 7.7 | Animalia indet. msp-59 | 3.9 | | |
| 7 | Alcyonacea msp-3 | 5.9 | Colonial Anthozoa msp-6 | 3.7 | | |
| 8 | Brachyura msp-4 | 4.4 | Porifera msp-27 | 2.1 | | |
| 9 | Paguroidea | 2.9 | Porifera msp-14 | 1.8 | | |
| 10 | Ophiuroidea msp-11 | 2.6 | Scleractinia msp-3 | 1.1 | | |
| **Site 5** | | | | | | |
| **Rank** | **Soft substratum** | **5.6** | **5 to 25 %** | **2.7** | **> 25 %** | **3.6** |
| 1 | Pennatulacea_01 | 67.9 | Bryozoa msp-1 | 19.9 | Actiniaria msp-11 | 24.8 |
| 2 | Actiniaria msp-15 | 8.5 | Actiniaria msp-11 | 14.4 | *Geryon* msp-1 | 12.3 |
| 3 | *Nematocarcinus* msp-1 | 6.9 | *Aphrocallistes* msp-1 | 14.1 | Bryozoa msp-1 | 10.4 |
| 4 | Actiniaria msp-8 | 4.1 | Porifera msp-13 | 7.3 | Ophiuroidea msp-10 | 7.9 |
| 5 | Caridoid msp-7 | 3.8 | Zoantharia msp-3 | 6.4 | *Eumunida* msp-1 | 4.8 |
| 6 | Actiniaria msp-38 | 1.5 | Colonial Anthozoa msp-8 | 5.8 | *Aphrocallistes* msp-1 | 4.6 |
| 7 | Caridoid msp-3 | 1.1 | Alcyonacea msp-2 | 3.1 | Serpulidae | 4.6 |
| 8 | Pennatulacea msp-2 | 1.1 | Cnidaria msp-10 | 2.8 | Scleractinia msp-3 | 4.5 |
| 9 | Brachyura msp-4 | 1.0 | *Bathynectes* msp-1 | 2.4 | Cnidaria msp-10 | 3.4 |
| 10 | *Geryon* msp-1 | 0.7 | Scleractinia msp-3 | 2.4 | Porifera msp-13 | 2.7 |

**Table S4.5** Top 10 ranked fish morphospecies by numerical density with their relative densities (%) for soft substratum, 5-25% coral and framework coverage, and > 25 % coral and framework coverage. Number on top of relative densities represents the standardised density (ind. $m^{-2}$) for each substratum class.

| **Site 1** | | | | | | |
|---|---|---|---|---|---|---|
| **Rank** | **Soft substratum** | **0.23** | **5 to 25 %** | **0.21** | **> 25 %** | **0.1** |
| 1 | Cynoglossidae | 50 | Nettastomatidae | 71.4 | Nettastomatidae | 65.6 |
| 2 | Macrouridae msp-6 | 27.8 | Actinopterygii msp-22 | 7.1 | *Chaunax* msp-1 | 6.3 |
| 3 | *Chaunax* msp-1 | 5.6 | *Coloconger* msp-1 | 7.1 | *Coloconger* msp-1 | 6.3 |
| 4 | *Laemonema* msp-1 | 5.6 | Macrouridae msp-6 | 7.1 | Macrouridae msp-6 | 6.3 |
| 5 | Macrouridae msp-8 | 5.6 | Synaphobranchidae msp-4 | 7.1 | Actinopterygii msp-22 | 3.1 |
| 6 | Ogcocephalidae msp-1 | 5.6 | | | Actinopterygii msp-25 | 3.1 |
| 7 | | | | | Chlorophthalmidae | 3.1 |
| 8 | | | | | *Ilyophis* msp-1 | 3.1 |
| 9 | | | | | Synaphobranchidae msp-4 | 3.1 |
| **Site 2** | | | | | | |
| **Rank** | **Soft substratum** | **0.12** | **5 to 25 %** | **0.49** | **> 25 %** | **0.81** |
| 1 | *Chaunax* msp-1 | 30 | Nettastomatidae | 27.6 | Nettastomatidae | 50 |
| 2 | Actinopterygii msp-24 | 10.0 | Beryciformes msp-1 | 24.1 | Scorpaeniformes msp-2 | 19.6 |
| 3 | Chaunacidae msp-2 | 10.0 | Scorpaeniformes msp-2 | 17.2 | Beryciformes msp-1 | 12.5 |
| 4 | *Coelorinchus* msp-2 | 10.0 | Actinopterygii msp-19 | 10.3 | Actinopterygii msp-19 | 5.4 |
| 5 | Lophiidae msp-1 | 10.0 | Lophiidae msp-1 | 10.3 | Actinopterygii msp-25 | 3.6 |
| 6 | Macrouridae msp-6 | 10.0 | Anguilliformes msp-1 | 6.9 | *Coloconger* msp-1 | 3.6 |
| 7 | Macrouridae msp-8 | 10.0 | *Laemonema* msp-1 | 3.4 | Anguilliformes msp-1 | 1.8 |
| 8 | Nettastomatidae | 10.0 | | | Lophiidae msp-1 | 1.8 |
| 9 | | | | | Soleidae | 1.8 |
| **Site 3** | | | | | | |
| **Rank** | **Soft substratum** | **0.13** | **5 to 25 %** | **0.32** | **> 25 %** | **1.42** |
| 1 | Macrouridae msp-6 | 43.8 | Nettastomatidae | 41.8 | Nettastomatidae | 82.9 |
| 2 | Ogcocephalidae msp-2 | 12.5 | Scorpaeniformes msp-2 | 10.9 | Scorpaeniformes msp-2 | 10.5 |
| 3 | *Coelorinchus* msp-2 | 10.0 | Anguilliformes msp-1 | 9.1 | Actinopterygii msp-19 | 1.4 |
| 4 | *Laemonema* msp-1 | 10.0 | *Coloconger* msp-1 | 5.5 | Anguilliformes msp-1 | 1.0 |
| 5 | Actinopterygii msp-13 | 3.8 | *Laemonema* msp-1 | 5.5 | Actinopterygii msp-23 | 0.7 |
| 6 | *Chaunax* msp-1 | 3.8 | Actinopterygii msp-22 | 3.6 | *Coloconger* msp-1 | 0.7 |
| 7 | Cynoglossidae | 3.8 | Macrouridae msp-3 | 3.6 | Scorpaeniformes msp-1 | 0.7 |
| 8 | Halosauridae | 3.8 | Soleidae | 3.6 | Soleidae | 0.7 |
| 9 | Chaunacidae msp-2 | 2.5 | Synaphobranchidae msp-4 | 3.6 | Actinopterygii msp-25 | 0.3 |
| 10 | Ophichthidae | 2.5 | Actinopterygii msp-23 | 1.8 | Coelorinchus msp-2 | 0.3 |
| **Site 4** | | | | | | |
| **Rank** | **Soft substratum** | **0.21** | **5 to 25 %** | **0.36** | | |
| 1 | Macrouridae msp-6 | 72.7 | Scorpaeniformes msp-2 | 48.8 | | |
| 2 | *Laemonema* msp-1 | 15.9 | Actinopterygii_19 | 31.7 | | |
| 3 | Scorpaeniformes msp-3 | 4.5 | *Laemonema* msp-1 | 4.9 | | |
| 4 | Chlorophthalmidae | 2.3 | Scorpaeniformes msp-1 | 4.9 | | |
| 5 | *Coelorinchus* msp-2 | 2.3 | Actinopterygii msp-23 | 2.4 | | |
| 6 | Ophichthidae | 2.3 | Nettastomatidae | 2.4 | | |
| 7 | | | Ogcocephalidae msp-2 | 2.4 | | |
| 8 | | | Soleidae | 2.4 | | |

**Table S4.5** continued

| **Site 5** | | | | | | |
|---|---|---|---|---|---|---|
| **Rank** | **Soft substratum** | **0.1** | **5 to 25 %** | **0.63** | **> 25 %** | **0.7** |
| 1 | Macrouridae msp-6 | 36.4 | Scorpaeniformes msp-2 | 53.9 | Nettastomatidae | 38 |
| 2 | *Laemonema* msp-1 | 27.3 | Nettastomatidae | 27.6 | Scorpaeniformes msp-2 | 32.4 |
| 3 | Coelorinchus msp-2 | 9.1 | Anguilliformes msp-1 | 7.9 | Anguilliformes msp-1 | 10.2 |
| 4 | Cynoglossidae | 9.1 | Actinopterygii msp-19 | 1.3 | Beryciformes msp-1 | 8.3 |
| 5 | *Ilyophis* msp-1 | 9.1 | Actinopterygii msp-20 | 1.3 | Actinopterygii msp-19 | 3.7 |
| 6 | Soleidae | 9.1 | Actinopterygii msp-22 | 1.3 | Actinopterygii msp-25 | 2.8 |
| 7 | | | Actinopterygii msp-23 | 1.3 | Actinopterygii msp-20 | 1.9 |
| 8 | | | Actinopterygii msp-25 | 1.3 | Actinopterygii msp-23 | 0.9 |
| 9 | | | Macrouridae msp-6 | 1.3 | Ogcocephalidae msp-2 | 0.9 |
| 10 | | | Scorpaeniformes msp-1 | 1.3 | Scorpaeniformes msp-1 | 0.9 |

# Chapter 5

# Megafaunal assemblages in a highly complex topographic setting from the lower continental slope off Angola, SE Atlantic


## Abstract

The Angolan continental margin contains a variety of geomorphological and geochemical features, created through a long history of salt tectonics and hydrocarbon formation and migration. The subsurface processes responsible for their development are relatively well understood owing to extensive seismic and geotechnical studies conducted in search for deep-water hydrocarbon reserves. On the contrary, the diversity of seafloor habitats found across these features and their associated fauna remain less known. Here we report preliminary findings on the spatial heterogeneity of seabed morphologies and their associated megabenthic communities along the middle and lower Angolan continental slope between c. 1400-2400 m water depths. Visual interpretation of seabed slope angles derived from multibeam bathymetry data suggests considerable topographic variation with a diverse range of morphological features of varying size and extent, including shallow linear furrows, pockmarks and broader scale ridges and isolated seafloor mounds presumably formed through updoming of underlying salt structures. Analysis of seafloor images taken along line transects at 32 sites revealed the presence of predominantly fine grained sediments dominated by echinoderms. Hard substratum is present locally in the form of clay outcrops and black gravel along sloping terrain, supporting mainly small sessile species such as globular sponges, solitary cup corals, and possibly brachiopods. Asphalt concretions were recorded at several sites, confirming previous predictions of widespread escape of heavy hydrocarbons throughout the study area.

The presence of active seepage of light hydrocarbons has been found in pockmarks, evidenced by black reduced sediments, authigenic carbonates and patches of living bathymodiolin mussels. Further work is planned to assess the relationships of topographic and sedimentological heterogeneity to observed megabenthic species distributions and beta diversity. In addition, classification methods to quantify and map the spatial complexity of the seabed terrain across the study area are currently being explored.

## 5.1 Introduction

Seafloor morphology is among several aspects known to influence the occurrence and distribution of benthic species in deep-water systems from regional to local scales (Levin, 2001; Levin and Dayton, 2009). Its effect on communities may be direct by offering habitat that supports distinct fauna (Levin, 2001; McClain and Barry, 2010), or indirect through its influence on surrounding environmental processes such as local flow and sedimentation patterns (Genin et al., 1986; Kunze and Llewellyn-Smith, 2004) and associated dispersal dynamics (Palardy and Witman, 2011) and rates in food supply (Clark et al., 2010; Durden et al., 2015; Morris et al., 2016). Gradients in seafloor slope, for instance, have been linked to varying densities of suspension- and deposit-feeding metazoan megafauna on the upper Nigerian slope, where densities of deposit-feeders decreased with increasing slope, possibly as a result of higher current flows and associated lower food availability on the seafloor across steeper terrain (Jones et al., 2013). Similarly in the deep North Atlantic, higher megaepifaunal biomass and larger proportions of suspension-feeding taxa on abyssal hills relative to adjacent abyssal plain sediments were interpreted to reflect increased rates of laterally organic matter supply mediated by topographically enhanced near-bottom currents (Morris et al., 2016). The availability of hard substratum directly regulates the occurrence of many suspension-feeding species that rely on solid ground for attachment (e.g. Baker et al., 2012; Edinger et al., 2011; Jones et al., 2014; Lacharité and Metaxas, 2017), and as such acts as a strong determinant of species diversity. Secondary attributes of hard structures, such as size, stability, and density may further regulate species distributional patterns, abundances, and biodiversity (e.g. Amon et al., 2016; Baker et al., 2012; Robert et al., 2014; Simon-Lledó et al., 2019b). In regions affected by subsurface hydrocarbon migration, fluid escape features such as pockmarks,

authigenic carbonates, and cold seeps amplify the degree of surface complexity. In addition, the unique physicochemicl conditions associated with active fluid flow (Levin et al., 2016) support highly specialised chemosynthetic communities characterised by high standing stocks, patchiness, and beta diversity (Cordes et al., 2010; Levin et al., 2016; Olu et al., 2010). Overall, the structural heterogeneity provided by different seafloor morphologies increases habitat heterogeneity in deep-water environments, thereby increasing diversity (McClain and Barry, 2010; Tews et al., 2004) and potentially enhancing ecosystem functioning and stability (Ives and Carpenter, 2007).

The seabed of the Angolan Continental Margin is a place of remarkable heterogeneity. A long history of salt tectonics and hydrocarbon formation and migration has created a variety of geomorphological and geochemical features on a wide range of scales from broader scale diapiric ridges to localised fluid flow features less than a meter across (Chapter 2). The processes related to margin evolution and hydrocarbon migration are relatively well understood, owing to extensive seismic mapping and geotechnical investigations that have been taken place in response to the region's geologic complexity and enormous petroleum potential (Brownfield and Charpentier, 2006; Burwood, 1999). Biological studies, on the other hand are scarce, and with the exception of the deepest studies in the Angolan Basin (e.g. Arbizu and Schminke, 2005; Kröncke and Türkay, 2003) have focussed mainly on chemosynthetic habitats or those associated with the Congo River outflow (e.g. Olu-Le Roy et al., 2007; Rabouille et al., 2017a, 2017b; Sen et al., 2017; Sibuet and Vangriesheim, 2009; Wenau et al., 2015a).

Over the last two decades, a series of geophysical, geotechnical and ecological surveys were undertaken by BP Exploration Ltd off Angola to plan deep-water oil and gas developments and obtain baseline data for impact assessments and future environmental monitoring. These surveys included areas in Licence Block 31 (Area A) located to the south of the Congo submarine canyon. In this study, we use photographic material collected as part of the ecological survey programme to document the structure of epibenthic megafaunal communities associated with different seafloor morphologies, and compare these to the structure of communities found on neighbouring open slope sedimentary habitats.

## 5.2 Environmental characteristics of the study area

The study area covers the middle and lower continental slope in water depths ranging from 1400 to 2400 m between about 6°1'S and 6°53'S (Figure 5.1). Geologically, it is a part of the Lower Congo Basin (LCB), one of several Mesozoic rift basins found along the West African passive margin (Torsvik et al., 2009) that have been subject to the deposition of large volumes of evaporites during mid to late Aptian time (Karner and Gambôa, 2007; Moulin et al., 2005). Intensive deformations of the salt and their overlying sequences by raft (e.g. Anderson et al., 2000; Valle et al., 2001) and salt (e.g. Brun and Fort, 2004; Cramez and Jackson, 2000) tectonics followed non-periodically from the Albian through to present times (Marton et al., 2000), which has created distinct tectonic provinces characterised by a basinward transition from mostly extensional to compressional sub-surface structures (Marton et al., 2000; Spathopoulos, 1996). The shelf and upper slope sections throughout the study area are dominated by alternating rafts and grabens filled with syndeformational sequences (Rouby et al., 2002; Spathopoulos, 1996). Here, Aptian salt is thin or absent owing to its gravitational displacement downslope (Marton et al., 2000). The compressional domain on the mid to lower slope is characterised by diapiric salt structures that show intermitted growth (Gay et al., 2007).

Active doming of salt structures has formed a highly irregular and uneven seabed topography (Savoye et al., 2009) with elevated terrain in the form of broad bathymetric highs (Serié et al., 2017), elongated diapiric ridges (van Weering and van Iperen, 1984; Wenau et al., 2015a), and isolated seafloor mounds (Hill et al., 2011). Salt tectonism has also had a marked effect on the location of subsurface hydrocarbon accumulation and migration. Interpretations of high-resolution seismic data have revealed a widespread and active hydrocarbon migration system in the LCB (Jatiault et al., 2019a), which is most pronounced in the compressional domain at mid to lower slope depths (e.g. Andresen, 2012; Gay et al., 2007; Ho et al., 2012; Jatiault et al., 2019b). Fluid flow involves both thermogenic hydrocarbons formed under elevated pressures and temperatures as well as biogenic methane produced during the anaerobic decomposition of organic matter in organic rich sediments (e.g. Andresen and Huuse, 2011; Gay et al., 2006a, 2006b, 2007; Jatiault et al., 2019a; Wenau et al., 2015a). On the seafloor, fluid release has formed a wide range of hydrocarbon escape features, including pockmarks (e.g. Andresen and

Huuse, 2011; Gay et al., 2007), precipitates of authigenic carbonate (e.g. Ondréas et al., 2005; Ho et al., 2012), methane plumes (e.g. Charlou et al., 2004; Sahling et al., 2008; Wenau et al., 2015a), and asphalt mounds (e.g. Jones et al., 2014).

Pockmarks, circular or elliptic seafloor depressions, are particularly prominent in the deep sections of the LCB, reaching up to several tens of meters deep (Andresen and Huuse, 2011; Gay et al., 2007) and up to 1000 m wide (e.g. Ondréas et al., 2005; Wenau et al., 2017). The occurrence of chemosynthetic communities has been reported from pockmarks in the northern Congo deep-sea fan (Kouilou pockmark at c. 3100 m; Sahling et al., 2008; Astrid pockmark, c. 2820 m; Cosel and Olu, 2009) and near the Congo submarine channel (Regab pockmark, c. 3160 m, e.g. Olu-Le Roy et al., 2007; Sibuet et al., 2002), from the salt front to the west of the study area (Wenau et al., 2015a), and from the organic-rich sediments found across the distal lobe complex of the Congo deep-sea fan (4750-5070 m; e.g. Khripounoff et al., 2005; Sen et al., 2017). The large symbiont-bearing foundation taxa encompassed vesicomyid clams (Cosel and Olu, 2008, 2009; Krylova and Cosel, 2011), the siboglinid tubeworm *Escarpia southwardae* (Anderson et al., 2004), and mytilid mussels belonging to the *Bathymodiolus* aff. *boomerang* complex (Olu-Le Roy et al., 2007). Common associated heterotrophic megafauna included alvinocarid shrimps, galatheid crabs (Munidopsis sp.), and holothurians of the genus *Chiridota* (e.g. Olu-Le Roy et al., 2007; Marcon et al., 2004). In the southern part of the study area (Figure 5.1), patches of chemosynthetic mussels, clams and tubeworms were observed nearby asphalt mounds, which appear to be widespread in Licence Block 31 (Jones et al., 2014). The mounds represent solidified thermogenic hydrocarbons, and seem to by colonised by non-chemosynthetic epifauna, including megafaunal poriferans, anthipatharians, actinians and alcyonaceans, and smaller-sized polychaetes and ophiuroids (Jones et al., 2014). In many cases, methane-derived authigenic carbonates formed through the anaerobic oxidation of methane and associated sulphate reduction (Feng et al., 2010; Pierre et al., 2012) have locally been observed in association with hydrocarbon seepage. They are present both on the seafloor where they can form massive crusts up to several metres long (e.g. Jones et al., 2014; Ondréas et al., 2005; Sahling et al., 2008; Wenau et al., 2015a) and in the shallow subsurface where they occur in the form of small nodules or thin discontinues layers of semi-cemented sediment (e.g. Anka et al., 2013; Pierre and Fouquet, 2007; Wenau et al., 2015b). Throughout Licence Block 31, sediment cores and interpretations of sub-bottom

profiler data have revealed discontinuous beds of carbonate claystones between 0.1-0.7 m thick in the top 30-40 m of sediment (Hill et al., 2011a, 2011b).

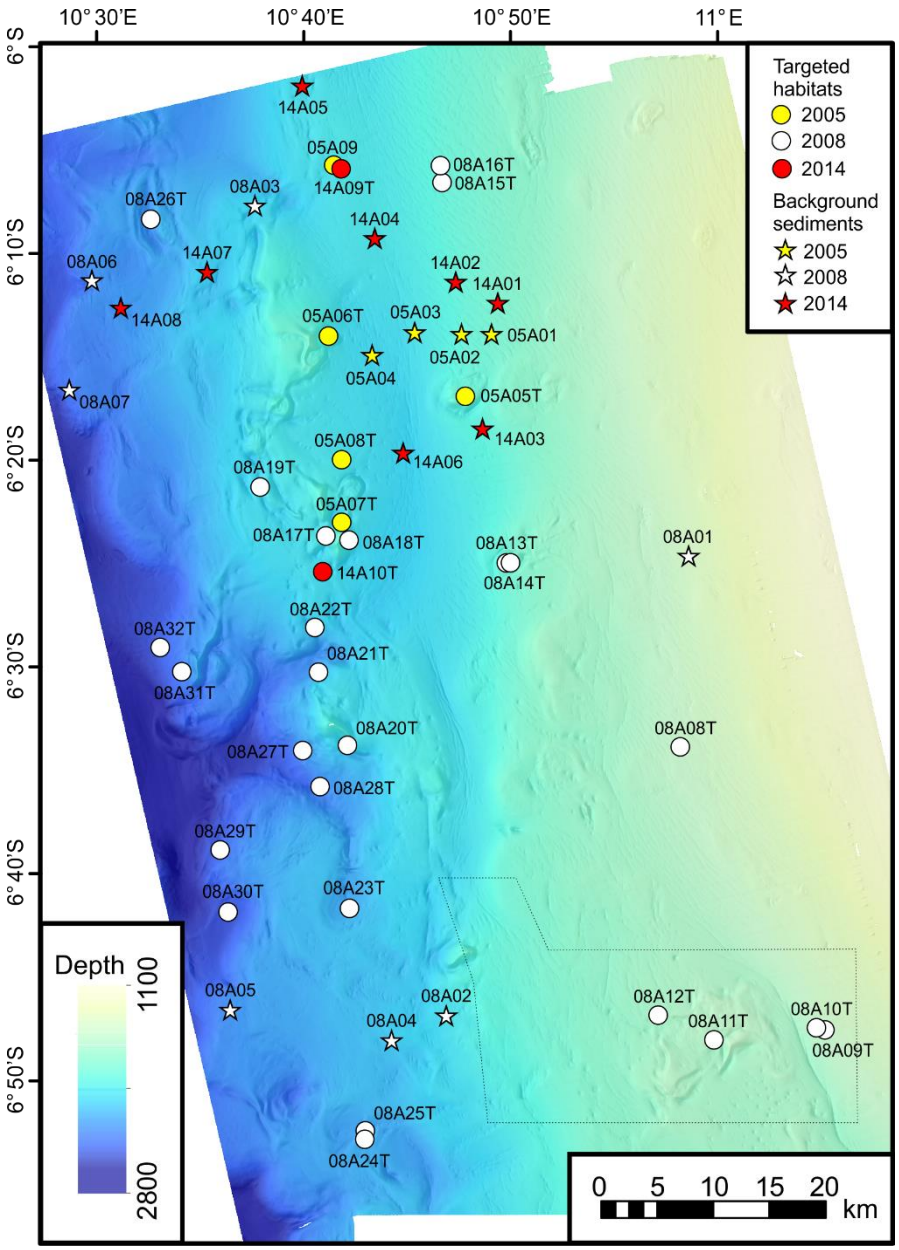


**Figure 5.1** Shaded relief bathymetry map of the study area, showing the centre locations of camera deployments, keyed to sampling year and survey design. Bathymetric data are based on the first return of large scale seismic data and were supplied by BP processed to 25 x 25 m resolution. Shaded reliefs were derived from multidirectional hillshading, as implemented in ArcGIS v10.5, and are vertically exaggerated by a factor of two. The rectangle indicates the survey area covered by Jones et al. (2014) to study asphalt mounds. Site codes as listed in Table S5.1. Map projection Camacupa TM 12SE.

## 5.3 Materials and methods

### 5.3.1 Collection of photographic data

The faunal analyses were based on photographic material collected during three cruises conducted on behalf of BP plc in 2005 (Bett, 2007), 2008 (Hughes and Hund, 2008) and 2014 (IMAR Survey, 2015a). Interpretations of existing acoustic data were used prior to each survey to non-randomly select a wide range of different seafloor features, which were subsequently surveyed using towed deep-water camera systems with more or less constant speeds along pre-defined line transects. A total of 32 sites were targeted in this ways across all years (Table S5.1), sampling five broad types of seafloor settings: (1) areas covered with small furrows, (2) areas with potential for asphalt mounds, (3) pockmarks, (4) diapirs and ridges in the central parts of the study area, and (5) areas with steeper terrain predominantly located at the western edge of the central diapiric area (Figure 5.1).

**2005 survey**: In 2005, the National Oceanography Centre's (NOC) Wide-Angle Seabed Photography (WASP) system was deployed at five locations in the north of the study area to survey one pockmark (05A09T), three diapirs (05A05T to 05A07T), and one site at the foot of a diapir (05A08T), achieving transect lengths of between 340 and 1750 m (Table S5.1). Still images were taken automatically every 12 seconds with a vertically mounted, downward facing OSIL Mk7 film camera (Bett, 2007) and recorded onto 35 mm Kodak Vision 250D film along with frame identification number and camera altitude. Camera height above the seabed was recorded with a Simrad Mesotech 200 kHz altimeter fitted to the camera frame. Vehicle navigation was achieved using an acoustic telemetry system, which consisted of an active transmitter (10 kHz) on the camera frame, a submerged downward-looking tow fish as transducer and a "Waterfall" system on the survey vessel to provide continuous monitoring of acoustic signals.

**2008 survey**: During the 2008 survey, 25 deployments were carried out at depths of about 1500-2500 m using the Seatronics DTS 6000 Mini Multiplexer camera platform. All five feature types were imaged with a downward-facing Kongsberg OE14-2008 still camera (2592 x 1944 pixels), which was triggered manually, typically every 10 seconds, to account for varying flash recharge times and movements of the camera frame caused by swell of the towing vessel (Hughes and Hunt, 2008). Camera positions were logged with

an USBL transponder beacon, and a pair of parallel point lasers spaced 38 cm apart was used to estimate image size.

**2014 survey:** In 2014, two photographic transects were sampled, targeting diapiric areas and potential pockmarks in the northern and central parts of the study area. Video was continuously recorded using a wide angle high-definition video camera (SubCControl 1Cam), while still images were taken automatically every 15 s with a 5 megapixel Kongsberg OE14-208 camera (2592 x 1944 pixels). Two sets of parallel lasers spaced 7 and 10 cm apart provided capabilities for scaling. Positional information of the imaging platform was recorded at 3 second interval with an USBL beacon linked to the ship's Sonardyne USBL acoustic tracking system.

**Table 5.1** Photographic sites sampled non-randomly in 2005, 2008 and 2014 along the lower Angolan continental slope (Area D) and targeted seabed features.

| Feature | No | Coverage and sampling sites |
|---|---|---|
| MV *Ocean Endeavour* 13/10-06/11 2005 | | |
| Diapirs and surrounding seabed | 4 | Top of diapir - 05A05T, 05A06T, flank of diapir - 05A07T, foot of diapir - 05A08T |
| Pockmark | 1 | 05A09T |
| MV *Sea Trident* 28/03-23/04 2008 | | |
| Diapirs and ridges | 7 | 08A13T, 08A14T, 08A17T-08A19T, 08A24T, 08A25T |
| Steep terrain | 10 | Steeper terrain at the edge of diapiric areas - 08A20T-08A22T, 08A26T-08A32 |
| Pockmark | 1 | 08A23T |
| Blister areas | 4 | Potential asphalt mounds - 08A09T-08A12T |
| Seabed furrows | 3 | Shallow furrows - 08A08T, 08A15T, 08A16T |
| MV *Ocean Discovery* 04/07-11/09 2014 | | |
| Diapiric area and pockmark | 1 | Across diapiric area and potential pockmark 14A10T |
| Pockmark | 1 | 14A09T |

In addition to the targeted sampling, systematic random sampling of relative featureless fine-grained substratum stratified by water depth was completed in all years to investigate broad-scale patterns in epibenthic megafauna across the Angolan continental slope, as detailed in Chapter 3. The faunal records from these sites were used to compare the epibenthic megafauna of the open slope sedimentary habitats with those of the targeted

morphological features. Previously excluded images from site 14A07 that showed asphalt mounds and oil-stained sediments were included in the current analysis.

### 5.3.2 Analysis of photographic data

Faunal patterns were quantified based on analysis of the still images. Photographs that were overexposed, out of focus, or where suspended matter obscured view of most of the seabed were excluded. To maximise the number of suitable images, photographs whose edges were affected by backscatter or vignetting were cropped, either to pre-defined sizes using the batch processing tool in Adobe Photoshop CS6 or, in the case of the films, by identifying unsuitable areas as part of the annotation process. The seabed area covered by an image was calculated based on camera acceptance angles and image altitude (2005 data) as described by Jones et al. (2009) or, when camera height was unknown (2008 and 2014 data), by using the scale provided by the laser markers following the trigonometric approach outlined in Durden et al. (2016). Scaling measurements were made using the ImageJ software (Schneider et al., 2012). To ensure only non-overlapping images were retained, image footprints were mapped based on image position, image size, and if known, camera heading, using multiple functions from the 'stringi' (Gagolewski, 2019), 'sp' (Pebesma and Bivand, 2005) and 'rgdal' (Bivand et al., 2019) packages in R (R Core Team, 2020). In the case of the films, where positioning information could not reliably be matched to individual frames, potential overlaps were first estimated from calculated vessel speeds, and then verified during the annotation process.

The digital still images collected in 2008 and 2014 were annotated with the image analysis software Image-Pro Plus v7.0 (MediaCybernetics) in random order to minimise potential detection biases towards specimens recorded in previously seen images (Durden et al. 2016). Image magnification was held constant to log the presence of specimens, while taxonomic identification and measurements of physical dimensions were made, if required, at higher magnification. The photographic films collected in 2005 were annotated with a Carl Zeiss Jena DLZ Dokumator microfilm viewer, set to a constant 9x zoom for specimen detection.

In each photograph, all fauna was recorded and measured using a standard dimension pre-defined for each expected faunal class. In line with the annotation protocol applied in Chapters 3 and 4, partially buried megafaunal specimens with body parts extruding above

the sediment, such as ophiuroids and asteroids, were included, as were surface dwelling specimens and epibenthic gastropods when trails behind the specimen indicated recent movement or when parts of the organism's soft tissue were visible. Sediment tubes extruding from the seabed were noted but not counted as it was impossible to determine whether they were inhabited. Aggregations of zoanthids were counted as single specimen. The recorded specimens were classified to the lowest possible taxonomic level based on visible morphological features, facilitated through a reference morphospecies image catalogue, which was developed by reference to deep-water taxonomic literature and image-based morphospecies lists from the region (Jamieson et al., 2017; Jones et al., 2014; Vardaro et al., 2013).

### 5.3.3 Environmental data

Two bathymetry data sets, both supplied by BP, were used to visualise seabed features. The first set, covering the whole study area, is based on the first return signal of large-scale 3D/2D exploration seismic data acquired across the wider region (BP, pers. comm.), processed to 25 x 25 m (Figure 5.1). A second, higher resolution (3 x 3 m) set of multibeam bathymetry data was collected across the central and south-western parts during a series of surveys between 2005 and 2008, using C&C Technologies' Autonomous Underwater Vehicle C-Surveyor II™ equipped with an Ultra High-Resolution (UHR) multi-channel 2D seismic system.

## 5.4 Preliminary observations

### 5.4.1 Seafloor morphology

Bathymetry data of the study area reveal a variety of geomorphologies at different spatial scales (Figure 5.2). The mid-slope sections on the eastern side down to about 1500-1600 m exhibit a relative low relief with slope angles generally between 1-2°. The most common morphological features are linear, closely spaced furrows up to 200 m wide, approximately 1-3 m deep, and trending predominantly NW to SE. The mid and eastern parts of the study are dissected by isolated seafloor mounds (e.g. Figure 5.2c, 5.2d) and several ridges (Figure 5.1) with slope angles of up to 18° (Figure 5.2a). Several mounds show a moat at their base (Figure 5.2b). Seafloor furrows are present in the central part but appear to be absent from the western side of the study area. Their orientation changes locally and seems

to align with the main isobaths. Small circular depressions (presumed to be pockmarks) are present throughout the central and western sections, but appear to absent from the most western parts. Pockmarks occur isolated or in clusters on the open slope (e.g. Figure 5.2a) and on top of mounds (e.g. Figure 5.2b).

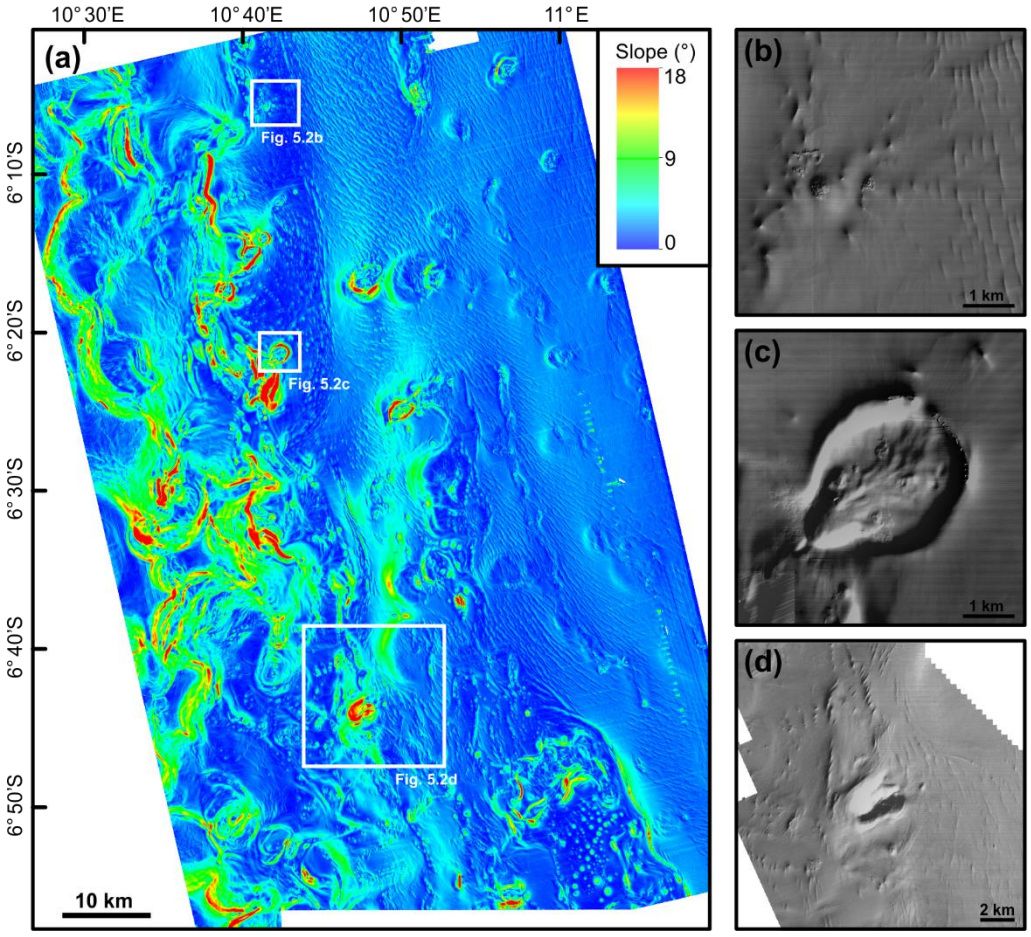


**Figure 5.2** Seabed slope across the study area **(a)**, and shaded topography of selected features: **(b)** Shallow furrows and small pockmarks with potential seepage; **(c)** Diapiric mound with small depressions on top; **(d)** Small seafloor mound surrounded by shallow furrows to the east, and elongated and circular depressions to the north and west. Shaded reliefs were derived from multidirectional hillshading as implemented in ArcGIS v10.5 and are vertically exaggerated by a factor of two. Slope angles were calculated using the Benthic Terrain Modeler extension (Walbridge et al., 2018) for ArcGIS. Maps were produced using bathymetry data supplied by BP at 25 x 25 m resolution (a), and 3 x 3 m resolution (b-d).

### 5.4.2 Habitat types and megafaunal assemblages

The imagery showed three broad substratum types: (1) reduced environments characterised by patches of black sediments or chemosynthetic communities, (2) hard ground characterised by hard substrate of varying size, and (3) and fine grained substratum, which dominated across the surveyed area. A total of 183 morphospecies were identified, comprising 19 fishes, 155 invertebrates, and 9 Foraminifera. Among the invertebrates, 30 were only recorded on hard substratum, 8 were associated with reducing environments, and 110 were only observed on soft substratum.

#### *Fine-grained substratum*

Areas of fine grained sediments contained a similar suite of invertebrate megafauna than those observed on relative featureless terrain (Chapter 3) being dominated by echinoderms. A change to a *Pourtalesia* sp. dominated assemblage occurred at about 1900 m, mirroring the depth trend observed for the background sediments (Chapter 3). Above 1900 m, invertebrate communities were locally dominated by the elasipodid *Scotoplanes* sp. Invertebrate densities followed the depth trend seen for the background assemblages, showing increased densities at depths below 1900 m (Figure 5.3a). Additional data from this study suggests a monotonic decline in densities below 1900 m. Foraminifera exhibited a larger number of morphologies compared to those recorded on background sediments. Consistently high densities occurred at the deepest sampling sites (Figure 5.3b).

#### *Hardgrounds*

At site 08A22T, potential clay outcrops and hard substrate (Figure 5.4g) were observed along a distance of about 230 m along sloping terrain (c. 8-18°) near the base of a topographic high. These sections supported a very sparse fauna comprising mainly small globular sponges, possibly brachiopods, and larger tubular structures, tentatively identified as Foraminifera. Larger cnidarians, encrusting specimens, and larger ophiuroids (Ophiuroidea msp-1) were occasionally seen. Xenophyophores with a plate-like morphology occurred adjacent to this section, but were absent from the remaining transect. At site 08A20T, mixed substratum of mainly finer grained sediment interspersed with black gravel was present at a steep (15-17°) flank in the central diapiric domain. Small solitary cup corals and large Ophiuroidea were frequently seen (Figure 5.4h).

The remaining hard substrate observed comprised asphalt mounds (Figure 5.4j). All four areas targeted in the south-eastern part of the study area (08A09T-08A12T) contained visible asphalt concretions. A comprehensive characterisation of the asphalt mounds in this area was previously undertaken by Jones et al. (2014) showing their widespread occurrence. As reported by Jones et al. (2014) epifaunal coverage of individual asphalt concretions varied considerably. Unidentified encrusting specimens, small ophiuroids, and globular sponges resembling those documented on hard grounds at site 08A22T were the most frequently observed morphospecies in this study. Ophiuroids were seen aggregating near the base of asphalt extrusions. Asphalt mounds very also observed in the central (08A13T and 08A28T) and northern (14A07) parts of the study area, confirming previous predictions of widespread hydrocarbon escape throughout the study area (Jatiault et al., 2019a).

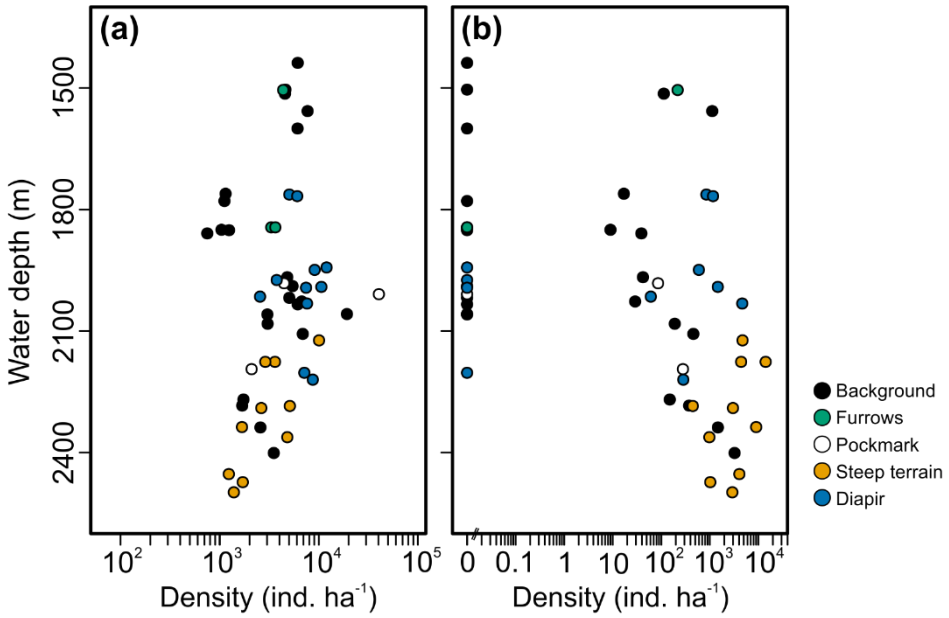


**Figure 5.3** Numerical densities of **(a)** megabenthic invertebrates, and **(b)** Foraminifera associated with fine grained substratum, keyed to targeted morphological feature. Images with discrete hard substratum and reducing environments were excluded from density calculations. Diapir = diapirs and surrounding areas sampled in the central part of the study area; Steep terrain = sloping terrain sampled along the western part of the study area.

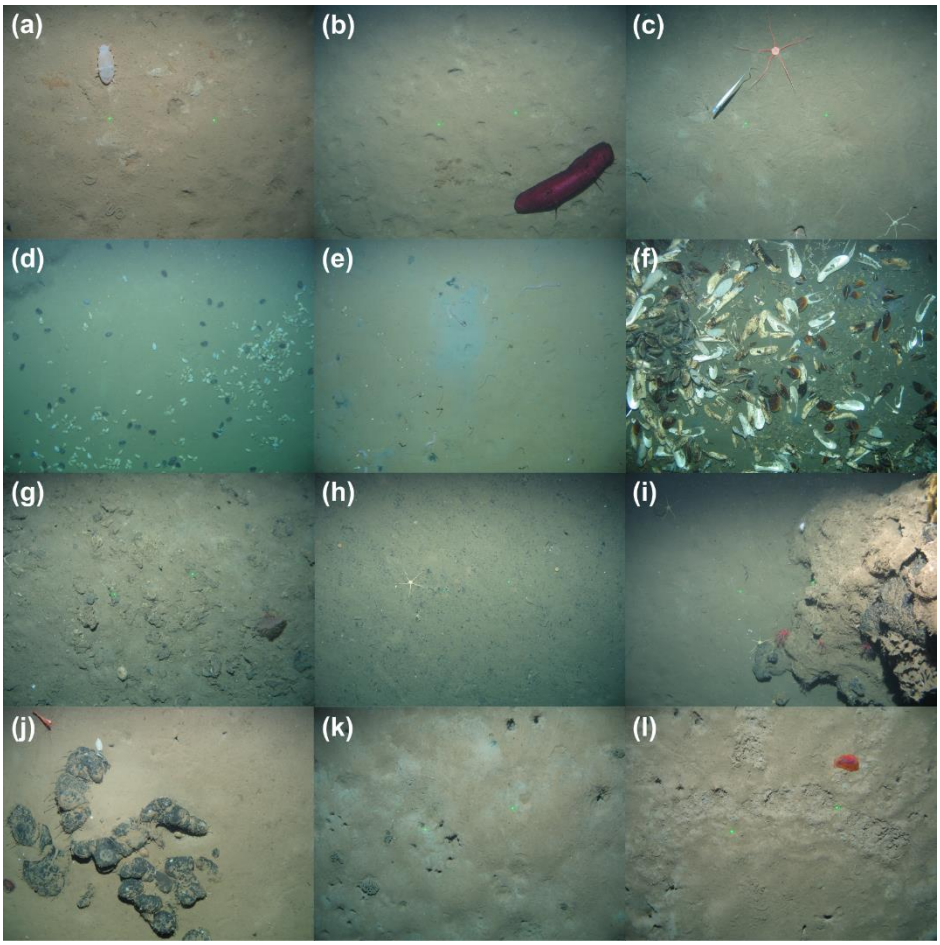


**Figure 5.4** Photographs showing different substratum types observed across the study area on the lower Angolan continental slope. **(a)** Soft substratum with *Scotoplanes* sp. and conspicuous phytodetritus and spiral faecal casts, possibly from *Scotoplanes* sp. (site 08A13T, 1763 m). **(b)** Soft substratum with *Benthodytes* sp. and shallow ovoid depressions (08A16T, 1844 m). **(c)** Flat soft substratum with ophiuroids and Halosauridae (08A24T, 2203 m). **(d)** Aggregation of the echinoid *Pourtalesia* sp. among echinoid tests within small depression (14A09T, 1982 m). **(e)** Soft substratum with the holothurian *Chiridota* sp., unidentified faunal tubes, and patches of reduced sediment within the pockmark at site 14A09T. **(f)** Patch of living *Bathymodiolus* sp. among mussel shells and carbonate nodules within pockmark at site 14A09T. **(g)** Patch of hard ground at site 08A22T (2176 m). **(h)** Mixed substratum with ophiuroids and solitary cup corals (site 08A20T, 2123m). **(i)** Authigenic carbonate mound interspersed with solidified asphalt. Conspicuous epifauna include sponges, *Anthomastus* sp., and brachiopods. Ophiuroids aggregate at the edge of the structure (1600 m, 08A12T). **(j)** Asphalt mound at site 14A07 (2082 m). **(k)** Brown and grey sediment with xenophyophores and oblique burrows often arranged in a circle (site 08A21T, 2176 m). **(l)** Soft substratum with *Peniagone* msp-1 and "plough" trace of unknown origin, the latter being frequently seen at the deepest sites (08A32T, 2473 m). Depth represents depth at transect centre point.

## *Reducing environments*

A small patch of bathymodiolin mussels (Figure 5.4f) and black reduced sediment showed evidence of active seepage of light hydrocarbons within the pockmark sampled at site 14A09T. The mussels were located amongst abundant shells and irregular nodules, possibly authigenic carbonates. Associated megafauna amongst the mussels included the holothurian *Chiridota heheva* (Thomas et al., 2020), galatheoid crabs (possibly

*Munidopsis* sp.), sponges, and small actinians growing on dead mussel shells. *C. heheva* was also seen near black sediments and at the fringes of the mussel patch. Here, a marked increase in seabed tracks was noted. The fauna was dominated by slender tubes, tentatively identified as *Bathysiphon* msp-2. A small area with authigenic carbonates associated with dead bivalve tests and galatheoids were observed within the pockmark sampled at site 05A09T. Aggregations of Bathysiphon msp-2 were also observed near oil-stained sediments at site 14A07, near asphalt extrusions at site 08A28T, and at site 08A25T.

The descriptions presented here will be extended with a quantitative assessment of assemblage distributions. As shown from the bathymetric data, the study area exhibits considerable topographical and geomorphological heterogeneity at various spatial scales. Areas subject to past or present hydrocarbon seepage contain habitats for communities distinct from the surrounding soft bottom environment. Seabed slope is being hypothesized to contribute to habitat heterogeneity by determining flow conditions, substratum conditions, and organic matter supply. Its effect on the observed species distributions will be tested in future work.

## 5.5 Supplementary information

**Table S5.1** Locations and depth ranges of photographic sites sampled non-randomly in 2005, 2008 and 2014 along the lower Angolan continental slope (Area A) and targeted seabed features. Lat and Lon represent the latitude and longitude (°) at the approximate centre point of each photographic transect. Image is the number of annotated photographs retained for faunal analysis, and area is the estimated seabed area of all annotated images.

| Site | Date | Lat | Lon | Depth range (m) | Length | Image | Area ($m^2$) | Target |
|---|---|---|---|---|---|---|---|---|
| 05A05T | 04/11/2005 | -6.2829 | 10.7959 | 1809-1827 | 701 | 22 | 80 | Diapir |
| 05A06T | 04/11/2005 | -6.2339 | 10.6861 | 1922-1944 | 343 | 27 | 87 | Diapir |
| 05A07T | 02/11/2005 | -6.3839 | 10.6965 | 1876-2037 | 636 | 58 | 285 | Diapir |
| 05A08T | 03/11/2005 | -6.3333 | 10.6965 | 1987-1991 | 1748 | 190 | 774 | Diapir |
| 05A09T | 03/11/2005 | -6.0960 | 10.6908 | 2001-2008 | 367 | 33 | 110 | Pockmark |
| 08A09T | 21/04/2008 | -6.7942 | 11.0854 | 1505-1507 | 593 | 38 | 42 | Blister areas |
| 08A10T | 21/04/2008 | -6.7922 | 11.0786 | 1492-1577 | 2592 | 287 | 278 | Blister areas |
| 08A11T | 20/04/2008 | -6.8020 | 10.9955 | 1545-1595 | 1316 | 97 | 132 | Blister areas |
| 08A12T | 20/04/2008 | -6.7819 | 10.9507 | 1597-1611 | 1714 | 94 | 116 | Blister areas |
| 08A13T | 18/04/2008 | -6.4168 | 10.8318 | 1759-1880 | 2605 | 125 | 163 | Diapir |
| 08A14T | 18/04/2008 | -6.4178 | 10.8303 | 1742-1832 | 2535 | 146 | 180 | Diapir |
| 08A17T | 14/04/2008 | -6.3949 | 10.6835 | 1914-2027 | 1246 | 133 | 225 | Diapiric area |
| 08A18T | 15/04/2008 | -6.3984 | 10.7021 | 1801-2027 | 2389 | 212 | 285 | Diapiric area |
| 08A19T | 14/04/2008 | -6.3552 | 10.6307 | 1981-2048 | 1167 | 70 | 139 | Diapiric area |
| 08A24T | 07/04/2008 | -6.8814 | 10.7137 | 2165-2206 | 1977 | 43 | 48 | Diapiric area |
| 08A25T | 07/04/2008 | -6.8747 | 10.7140 | 2182-2225 | 1092 | 62 | 77 | Diapiric area |
| 08A23T | 17/04/2008 | -6.6952 | 10.7017 | 2175-2203 | 1646 | 97 | 143 | Pockmark |
| 08A08T | 19/04/2008 | -6.5656 | 10.9689 | 1499-1507 | 578 | 43 | 46 | Furrows |
| 08A15T | 13/04/2008 | -6.1100 | 10.7781 | 1832-1860 | 1236 | 82 | 103 | Furrows |
| 08A16T | 13/04/2008 | -6.0967 | 10.7768 | 1827-1858 | 1527 | 104 | 129 | Furrows |
| 08A20T | 16/04/2008 | -6.5637 | 10.7004 | 2088-2131 | 467 | 66 | 93 | Steep terrain |
| 08A21T | 15/04/2008 | -6.5047 | 10.6772 | 2080-2277 | 2865 | 147 | 244 | Steep terrain |
| 08A22T | 15/04/2008 | -6.4686 | 10.6747 | 2082-2175 | 1721 | 154 | 245 | Steep terrain |
| 08A26T | 11/04/2008 | -6.1393 | 10.5431 | 2160-2304 | 2163 | 115 | 157 | Steep terrain |
| 08A27T | 18/04/2008 | -6.5677 | 10.6644 | 2230-2356 | 2573 | 90 | 133 | Steep terrain |
| 08A28T | 17/04/2008 | -6.5972 | 10.6784 | 2253-2402 | 1149 | 227 | 313 | Steep terrain |
| 08A29T | 09/04/2008 | -6.6479 | 10.5977 | 2340-2526 | 2763 | 132 | 194 | Steep terrain |
| 08A30T | 09/04/2008 | -6.6981 | 10.6039 | 2495-2502 | 1265 | 95 | 144 | Steep terrain |
| 08A31T | 09/04/2008 | -6.5039 | 10.5673 | 2285-2411 | 1604 | 51 | 102 | Steep terrain |
| 08A32T | 09/04/2008 | -6.4845 | 10.5496 | 2450-2499 | 772 | 58 | 117 | Steep terrain |
| 14A09T | 24/08/2014 | -6.0991 | 10.6968 | 1971-1987 | 1525 | 126 | 543 | Pockmark |
| 14A10T | 17/08/2014 | -6.4240 | 10.6810 | 2014-2026 | 2138 | 293 | 1174 | Diapiric area |

# Chapter 6
# Synthesis and future directions

## 6.1 Synthesis of findings

This study sought to improve understanding of megabenthic ecology along the Angolan deep continental margin. Literature about the margin's evolution, oceanography and biology was reviewed and synthesised to highlight knowledge gaps and guide future research (Chapter 2). In addition, three quantitative studies (Chapters 3 to 5) characterised the diversity and structure of epibenthic megafaunal communities associated with different seabed habitats. Assemblage patterns were quantified using photographic material collected on behalf of BP from four locations along the northern and central parts of the Angolan slope spanning a depth range of 300-2500 m. In addition, sedimentological and oceanographic data were examined to improve understanding of the environmental conditions and examine their influence on the faunal patterns observed.

### Chapter 2

The literature review presented in Chapter 2 highlights the Angolan margin as an area of high environmental heterogeneity. Important sources of variability affecting the distribution of deep-water benthic habitats and species assemblages include subsurface salt tectonics and hydrocarbon migration, which have created a complex seafloor topography and a suite of fluid escape features that form the basis of different benthic habitats and faunal communities. At the surface, the Congo River outflow together with seasonal coastal upwelling creates horizontal and temporal gradients in surface production, while an oxygen minimum zone at upper slope depths causes strong vertical gradients in oxygen conditions. Biological studies investigating megafaunal communities are scarce, and with the exception of studies in the Angolan Basin, have concentrated mainly on discrete habitats provided by cold-water coral reefs, cold seeps, asphalt mounds, large food falls, and organic rich sediments found across the terminal lobes of the Congo deep-sea fan.

## Chapter 3

In Chapter 3, I used seabed imagery to quantify bathymetric and geographic variations in the standing stocks (abundance and biomass), diversity, and composition of epibenthic megafaunal communities associated with soft sedimentary habitats at broader spatial scales (c. 480-2500 m water depth; four sampling areas located between 6° and 12°S). Strong structural changes in metazoan communities with water depth were identified, which were accompanied by variations at local scales. Invertebrate densities showed a monotonic decline with increasing water depth to about 1900 m, followed by an increase at deeper sites driven predominantly by the presence of the irregular echinoid *Pourtalesia*. Pronounced along-slope differences in invertebrate densities were observed on the upper slope between c. 700-900 m, possibly reflecting the impacts of demersal fishing activities. Approximated wet biomass for megafaunal invertebrates peaked at the lower slope (< 1700 m) owing to large deposit-feeding holothurians and *Pourtalesia*. Fish densities declined monotonically by about two orders of magnitude. Invertebrate morphospecies richness was low on the upper slope, then increased peaking at depths between about 1150 and 1900 m. Sites sampled below 1900 m exhibited lower overall diversity, resulting from the high dominance of the irregular echinoids. Invertebrate community composition changed gradually with depth as a result of morphospecies replacement. Multivariate analyses identified three main faunal groups; an upper slope group up to about 700 m depth, characterised by sea pens, zoanthids, squat lobster, quill worms, burrowing ophiuroids and nematocarcinid shrimp, a middle slope group typified by squat lobsters, zoroasterid sea stars, small ophiuroids, and asteroids, and a lower slope group below about 1700 m water depth dominated by detritivorous echinoderms. The composition of fish assemblages changed from a dominance of smaller, benthic taxa on the upper slope to larger benthopelagic morphospecies in deeper waters. Branching protists, possibly belonging to the genus *Schizammina*, were abundant at intermediate depths.

## Chapter 4

In chapter 4, I characterised the structure and biodiversity of five previously unexplored Scleractinian cold-water coral reefs on the upper Angolan continental slope (c. 325-470 m water depth) and highlighted their potential as an important contributor to regional megafaunal diversity off Angola. The reefs are located within a downward trending gully

system on small mounds of at least 30 m in height. A variety of substratum classes were observed, comprising live framework building corals (mainly *Desmophyllum pertusum*), dead coral framework, coral rubble, and mixed substratum of soft sediments scattered with coral debris. An analysis of the associated megafaunal biodiversity confirmed the ecological importance of the Scleractinian corals as habitat engineers. The reefs supported a unique community of fish and invertebrates as well as higher invertebrate diversity and larger fish densities relative to surrounding soft substratum habitats. Epibenthic megafauna associated with open slope soft substratum surrounding the reefs were dominated by aggregations of sea pens. Ambient hydrographic conditions were characterised by low dissolved oxygen concentrations (locally < 0.5 ml $l^{-1}$), reflecting the location of the study area within an oxygen minimum zone. Enhanced downward fluxes of organic matter by tidally-induced vertical mixing of an upper ocean nephloid layer were suggested to be the driving forces for maintaining the suspension-feeding dominated communities under these extreme conditions.

## Chapter 5

In Chapter 5, I analysed bathymetry data and seafloor images to characterise the spatial heterogeneity of seabed morphologies and their associated megabenthic communities along the middle and lower Angolan continental slope between c. 1400-2400 m water depths. A large variety of topographic features and sedimentological conditions were observed that supported a range of megafaunal communities including aggregations of chemosynthetic bathymodiolin mussels. Hard substratum, found locally in the form of clay outcrops, black gravel and asphalt deposits, harboured megafaunal invertebrate communities distinct from the surrounding soft bottom environment. Differences in megafaunal species-occurrences, particularly in the densities of xenophyophores, were noted between sedimentary habitats sampled across steeper terrain and those found on adjacent flat terrain, probably reflecting differences in hydrodynamic activity and resource availability. The findings suggest that the large terrain variability at lower slope depths increases habitat diversity and megafaunal beta diversity, and as such may be an important contributor to regional diversity off Angola.

The present study shows that the Angolan continental margin is a place of high environmental heterogeneity that contains a variety of geomorphologic (e.g. canyons, diapiric ridges, pockmarks), geochemical (e.g. cold seeps, asphalt deposits) and hydrographic (e.g. OMZ) features. This complexity offers habitats for a wide variety of chemosynthetic and heterotrophic megafaunal communities. Observed megafaunal distributions, standing stocks and diversity were shown to vary at multiple spatial scales from broad-scale vertical changes with water depth (c. 480-2500 m), to along-slope variations between sampling areas (c. 100-600 km), within sampling areas (~ 10 km), and local-scale variations along photographic transects (~ m).

At the broadest scale, diversity, composition, and standing stocks of epibenthic megafauna showed strong depth-related trends, like in other deep-water ecosystems. It is suggested that these changes were likely governed by a combination of macro-evolutionary influences and contemporary processes, such as gradients in organic matter supply and dissolved oxygen concentrations. However, relating faunal patterns to particular environmental parameters was impeded by high collinearity among many of the analysed environmental variables, which remains a common problem in deep-water studies (Gage and Tyler, 2010).

The spatial patterns observed in this study have generally been documented on other continental margins. The observation of declining ichthyofaunal densities with increasing water depth is consistent with trends observed in other regions, such as the eastern Pacific (Pearcy et al., 1982) and the tropical Atlantic off northwest Africa (Merrett and Domanski, 1985; Merrett and Marshall, 1981). Likewise, the rapid decline in invertebrate densities from upper to mid-slope depths mirrors other regional patterns (e.g. Galéron et al., 2000) as well as global trends (Rex et al., 2006; Wei et al., 2010). The finding of locally high invertebrate biomass at lower slope depths, driven by large holothurians, agrees with patterns documented on the Celtic (Duineveld et al., 1997) and northwest African (Ramil and Ramos, 2017) margins.

The observed change in invertebrate community composition with water depth follows the global pattern of non-repeating vertical zonation on continental margins (Carney, 2005). The high invertebrate community dominance and the large turnover of highly abundant morphospecies at upper slope depths resemble community changes observed across other

lower OMZ boundaries (e.g. Levin, 2003; Gooday et al., 2009). Detailed comparisons between the megafaunal communities found off Angola with those documented in other regions are outstanding, but an initial assessment shows similarities with communities documented in the Gulf of Guinea (Jones et al., 2013) and on the north-west African continental slope (e.g. Aldred et al., 1979; Jones et al., 2012; Ramil and Ramos, 2017).

The diverse megafaunal invertebrate and fish fauna associated with cold-water coral reefs on the upper slope corroborate that coral reefs are 'biodiversity hotspots' (Henry and Roberts, 2017). Of potential ecological importance might also be the agglutinating Foraminifera that occurred in high densities at mid-slope depths. Megabenthic Astrorhizina are known to provide an important source of habitat heterogeneity by offering substratum, food, and refuge for invertebrate and protozoan species (Levin, 1991).

## 6.2 Limitations and targets for future work

Chapter 3: Though the quantification of megabenthic assemblage descriptors represents a first step towards understanding the broad-scale spatial structure of megabenthic communities associated with sedimentary habitats along the Angolan continental margin, more sampling will be needed to improve interpretations of spatial trends and their underlying causes. Specifically, the lack of samples from the lower slope outside the main influence of the Congo River outflow prevents generalisations about regional faunal patterns at lower slope depths. Variations in standing stocks and faunal distributions might be predicted based on the decline in total annual production and the increase in seasonal variation in waters overlaying the lower slope outside the influence of the Congo River plume (Chapter 2). Additional samples from the upper boundary of the oxygen minimum zone and above would provide a better understanding of faunal turnover at upper slope depths in relation to gradients in bottom water oxygen concentrations. In addition, further sampling at depths between 1450-1750 m would be desirable to clarify if the rate change in faunal turnover observed between 1400-1500 m represents an artefact of undersampling or a true phenomenon. Further data on spatial and temporal dynamics of sediment transport processes, and organic matter fluxes are needed at both broader and finer scales to better understand variations in faunal distributions and standing stocks. Such data would particularly be useful for lower slope depths where high variations in seafloor topography

due to underlying salt tectonics have likely lead to complex patterns in bottom currents and organic matter supply.

It would also be of great interest to extend sampling to areas on the southern slope, south of Area D, to gain an improved understanding of regional megafaunal diversity and to examine how variations in shelf width and seabed slope affect megafaunal communities. Sampling within the Angola-Benguela Frontal Zone and beyond would be valuable to test for large-scale latitudinal trends in megafaunal diversity and composition between the tropical waters off Angola and the subtropical region of the Benguela Upwelling System off Namibia and South Africa.

Chapter 4: The present study focussed on quantifying differences in megafaunal community structure between coral reefs and the surrounding soft substratum habitats. The results also suggested spatial trends in invertebrate community composition with water depth as well as differences among soft substratum habitats driven by fine-scale changes in substratum characteristics. Further work is planned to quantify the contributions of these factors to provide a better understanding of the drivers of faunal distributions. Large numbers of arborescent and tubular structures, possibly foraminiferans and tubicolous polychaetes, were noted across the sedimentary transect sections as well as on sediments between live coral colonies and dead framework. Quantitative or semi-quantitative analysis of these forms and their spatial distribution would provide a more comprehensive characterisation of epifaunal assemblages, and may also be used to extend existing regional comparisons of faunal patterns within and below OMZs (Gooday et al., 2009). In a broader context, better understanding about the distribution and extent of cold-water coral reefs as well as hard substrate that can support sessile suspension-feeding taxa would be useful to assess the relative contribution of reef systems to regional diversity. Acoustic backscatter data, as used in this study, could prove to be a valuable tool to predict coral reef occurrences across larger spatial scales.

Chapter 5: Due to time constraints, the analysis presented in Chapter 5 focussed on documenting the main structural differences between megabenthic assemblages associated with different seafloor morphologies. Further work, using PSA, bathymetric and acoustic backscatter data, is underway to provide a more systematic interpretation of seafloor morphologies and to quantify and map the spatial complexity of the seabed terrain across

the study area. Geotechnical information supplied by BP is also being reviewed to characterise underlying soil conditions. Moreover, data of organic carbon and nitrogen content and concentrations of sediment hydrocarbon are examined as a means of identifying organic carbon sources (i.e. biogenic vs petrogenic sources). A more detailed exploration of the relationships between faunal distributions and seafloor topography and substratum characteristics is also planned, which together with the environmental interpretations could facilitate predictive habitat mapping.

## 6.3 Theoretical and policy implications

Deep-water ecosystems are under increasing threats from expanding human impact footprints and the emerging effects of climate change, calling for improved efforts to develop and implement adequate conservation and management strategies (e.g. Danovaro et al., 2020; Mengerink et al., 2014; Ramirez-Llodra et al., 2011). Angola has committed to preserve its biodiversity and the sustainable use of its natural resources under both national legislation (e.g. Governo de Angola, 2019) and international commitments (e.g. United Nations Country Team Angola, 2019). Marine Spatial Planning is being developed to balance conservation goals with resource demands (Finke et al., 2020). In addition, Ecologically or Biologically Significant Marine Areas (EBSAs), covering both coastal and offshore settings (Figure 6.1), have been identified in support of MSP and to achieve global Aichi Biodiversity Targets (Institute for Coastal and Marine Research, 2021). However, baseline information on Angola's marine biodiversity and ecosystem services remain scarce (MARISMA EBSA Workstream, 2020b), particularly for the deep sea (Chapter 2), which raises questions about the sufficiency of the selected EBSAs and the suitability of current protection and management proposals. New data on the distribution and structure of deep-water benthic habitats and faunal communities, such as those provided in this study, will therefore be of great value to a number of stakeholders, including environmental managers and conservationists.

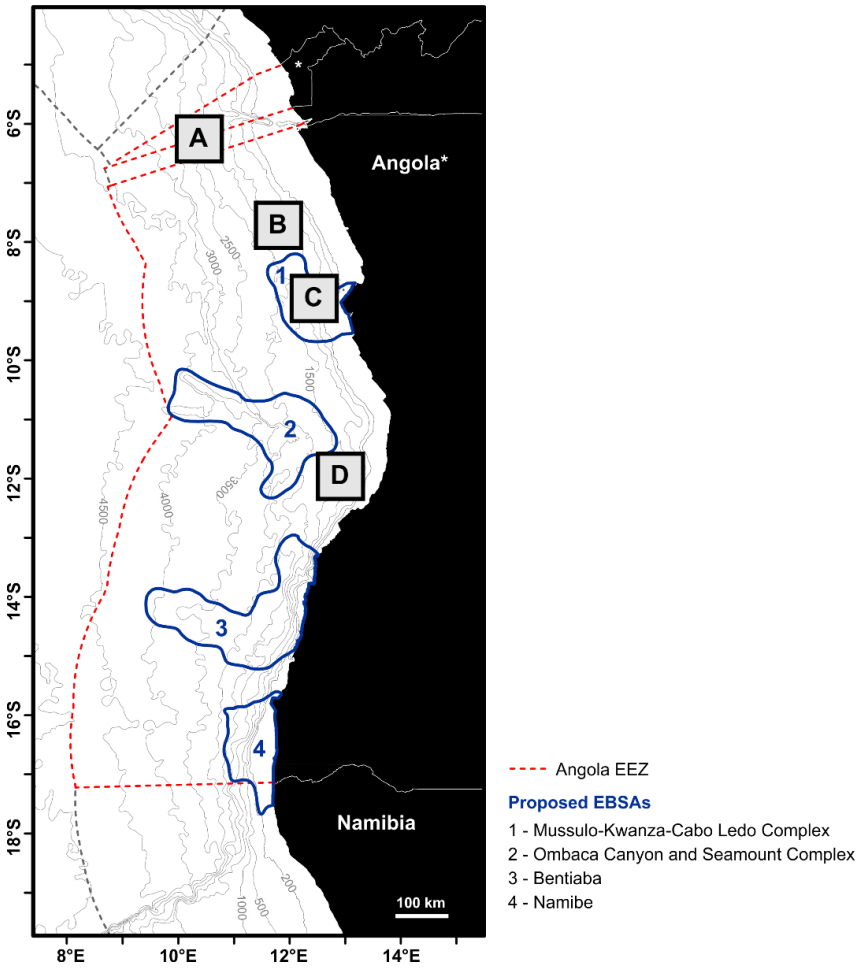


**Figure 6.1** Proposed offshore EBSAs comprising areas on the Angolan continental margin and positions of the four oil and gas provinces (A-D) sampled in this study. EBSA boundaries as per the South African Institute for Coastal and Marine Research (2021), and boundaries of Exclusive Economic Zones (EEZs) as per Flanders Marine Institute (2019). Bathymetry is shown as simplified contours based on GEBCO (General Bathymetric Chart of the Oceans) data (GEBCO Compilation Group, 2019).

### 6.3.1 Conservation

Data on ecological and environmental patterns across sampling Area C (Chapters 3 and 4) can be used to improve current descriptions (MARISMA EBSA Workstream, 2020a) and condition assessments (MARISMA EBSA Workstream, 2020a) for the proposed Mussulo-Kwanza-Cabo Ledo Complex EBSA, which stretches from the coast to the lower continental slope to about 2000 m water depth (Figure 6.1). Particularly relevant for both conservation and management are the data on the spatial extent, distribution and ecological structure of the Scleractinian coral reefs on the upper slope (Figure 6.2), considering their importance in increasing local habitat complexity and biodiversity (Chapter 4) and their

considerable contribution to ecosystem processes such as carbon cycling (e.g. Chatalot et al., 2015; Maier et al., 2021; van Oevelen et al., 2009). Profound long-lasting effects of bottom-tending fishing gear on deep-water Scleractian reefs are well documented (e.g. Althaus et al., 2009; du Preez et al., 2020; Fosså et al., 2002) and the basis for many protected areas and fisheries exclusion zones worldwide (Cordes et al., 2017). Commercial and artisanal fisheries, including benthic longlining, is widespread along the shelf and upper slope of the Mussulo-Kwanza-Cabo Ledo Complex (MARISMA EBSA Workstream, 2020b). The ecological condition of these areas is currently assessed as being mostly fair with some local areas possibly being in poor condition (MARISMA EBSA Workstream, 2020b). However, it appears that the potential presence of cold-water coral reefs has not been considered in these assessments. The mapped locations of known coral reefs (Chapter 4; Hebbeln et al., 2020) could provide the basis for further evaluations on the risk of reefs to be damaged or disturbed by current bottom fishing activities and the need for more stringent spatial protection measures than currently proposed. The uncommon occurrence of the Angolan cold-water coral reefs under hypoxic conditions (Chapter 4; Hebbeln et al., 2020; Orejas et al., 2021) shows their ecological importance on a global scale and further strengthens the call for their recognition in Angola's marine spatial planning and conservation strategy.

Besides Scleractinian coral reefs, the upper slope in Area C also supports aggregations of sea pens (Chapters 3 and 4). Similar to reef-building Scleractinian cold-water corals, sea pens are considered important foundation species as they increase environmental complexity and provide a suite of microhabitats to a variety of sessile and mobile taxa (e.g. Baillon et al., 2012, 2014; Buhl-Mortensen et al., 2010; De Clippele et al., 2015). Recent studies further indicate a role in facilitating organic matter deposition (Miatta and Snelgrove, 2021b) and in promoting macrofaunal community diversity in surrounding sediments (Miatta and Snelgrove, 2021a). Dense aggregations of sea pens are considered vulnerable marine ecosystems (VMEs) owing to their functional significance, fragility, and slow recovery from physical disturbances, such as those resulting from demersal fishing and oil and gas exploration and infrastructure installations activities (FAO, 2021). Therefore, sea pen communities are afforded increased protection through the implementation of MPAs (e.g. Muntoni et al., 2019) and fishing closures (e.g. NAFO, 2021) in national and international waters. The photographic data obtained in this study

could provide a starting point for assessing sea pen assemblage characteristics against conservation selection criteria. Data of current fisheries activities together with further targeted research exploring sea pen distribution, functional ecology, and population dynamics would be required to assess the risk of sea pen assemblages off Angola to be adversely affected by demersal fishing activities. The close proximity of Scleractinian coral reefs and sea pen fields observed in this study (Chapter 4) would deem the need for further impact assessments high priority.

Information on habitat and faunal distributions collected outside currently proposed EBSAs (Chapters 3 and 5) will be useful for evaluating the representativity of the candidate network. For example, the analysis of photographic material collected in Area A (Chapter 5) identified a range of habitat types (e.g. seeps, asphalt deposits, clay outcrops), expanding on the known locations of chemosynthetic and asphalt mound communities previously described from the Lower Congo Basin (reviewed in Chapter 2). These habitats enhance environmental heterogeneity, support a diverse, and in the case of cold seeps, unique fauna, and add to the regional species pool, which may warrant their consideration as potential areas of biological or ecological significance. Their distribution and extent in Angolan waters however is unknown, and as such it is unclear how adequately they would be represented in the current EBSA network.

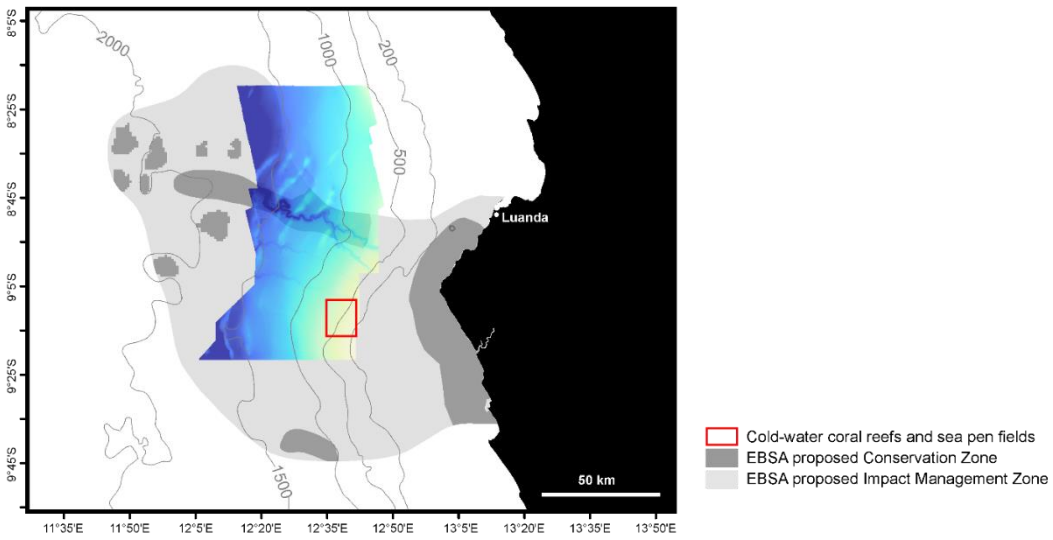


**Figure 6.2** Location of the Mussulo-Kwanza-Cabo Ledo Complex EBSA with proposed Conservation and Management Impact Zones (Institute for Coastal and Marine Research, 2021), superimposed with seafloor bathymetry across Area C and the location of the cold-water coral reef systems and sea pen fields studied in Chapter 4.

### 6.3.2 Resource management

The ongoing expansion of oil and gas operations into deeper and previously unexplored areas on the Angolan margin calls for improved baseline characterisations and monitoring to effectively identify and minimise potential impacts. The new data on megafaunal habitat and species distributions presented in this study may contribute to more comprehensive environmental assessments and more efficient monitoring. Observed broad-scale patterns in community composition (Chapter 3) may inform the spatial design of future site surveys to ensure representative sampling is achieved. Species accumulation rates and variance estimates (Chapter 3) could be considered to design statistically robust surveys capable of quantifying different community metrics with high precision. The morphospecies image catalogue (Appendix B) could guide identification of fauna in new image data sets, and may provide a reference that allows for standardisation across studies (Howell et al., 2020).

The lack of wider regional considerations in project-based EIAs can be a major risk to the environment, for example if connectivity pathways between ecological systems remain unknown or potential cumulative effects from multiple activities are disregarded. The benefits of adopting more coherent, regional environmental assessments are now widely recognised, including for the management of offshore hydrocarbon developments (e.g. Cordes et al., 2016; Fidler and Noble, 2012). The ongoing development of MSP by the Angolan government may provide opportunities to develop such an approach for the Angolan offshore oil and gas sector. Data sharing between regulatory bodies, operators, consultants and scientists should be encouraged in this context to enhance the evidence base of future EIAs (Gage et al., 2004). Collaborative research efforts between industry and academia may be beneficial to enhance data value or share resources (Levin et al., 2019). An example of such collaboration is this study, which provided new analyses of data initially collected by industry for impact assessment purposes.

# References

Addamo, A.M., Vertino, A., Stolarski, J., García-Jiménez, R., Taviani, M., Machordom, A., 2016. Merging scleractinian genera: the overwhelming genetic similarity between solitary *Desmophyllum* and colonial *Lophelia*. *BMC Evolutionary Biology*, 16(1), 108.

Advocate, D.M., Hood, K.C., 1993. An empirical time-depth model for calculating water depth, northwest Gulf of Mexico. *Geo-Marine Letters*, 13(4), 207-211.

Agard, J.B.R., Gobin, J., Warwick, R.M., 1993. Analysis of marine macrobenthic community structure in relation to pollution, natural oil seepage and seasonal disturbance in a tropical environment (Trinidad, West Indies). *Marine Ecology Progress Series*, 92(3), 233-243.

Aitchison, J., 1982. The Statistical Analysis of Compositional Data. *Journal of the Royal Statistical Society: Series B (Methodological)*, 44(2), 139-160.

Ala, M.A., Selley, R.C., 1997. Chapter 8 The West African Coastal Basins. In R.C. Selley (Ed.), *Sedimentary Basins of the World*, Vol. 3 (pp. 173-186): Elsevier.

Aldred, R.G., Riemann-Zurneck, K., Thiel, H., Rice, A.L., 1979. Ecological observations on the deep sea anemone *Actinoscyphia aurelia*. *Oceanologica Acta*, 2, 389-395.

Alt, C.H.S., Kremenetskaia, A., Gebruk, A.V., Gooday, A.J., Jones, D.O.B., 2019. Bathyal benthic megafauna from the Mid-Atlantic Ridge in the region of the Charlie-Gibbs fracture zone based on remotely operated vehicle observations. *Deep Sea Research Part I*, 145, 1-12.

Althaus, F., Williams, A., Schlacher, T.A., Kloser, R.J., Green, M.A., Barker, B., Bax, N.J., Brodie, P., Schlacher-Hoenlinger, M.A., 2009. Impacts of bottom trawling on deep-coral ecosystems of seamounts are long-lasting. *Marine Ecology Progress Series*, 397, 279-294.

Amon, D.J., Ziegler, A.F., Dahlgren, T.G., Glover, A.G., Goineau, A., Gooday, A.J., Wiklund, H., Smith, C.R., 2016. Insights into the abundance and diversity of abyssal megafauna in a polymetallic-nodule region in the eastern Clarion-Clipperton Zone. *Scientific Reports*, 6(1), 30492.

Andersen, A.C., Hourdez, S., Marie, B., Jollivet, D., Lallier, F.H., Sibuet, M., 2004. *Escarpia southwardae* sp. nov., a new species of vestimentiferan tubeworm (Annelida, Siboglinidae) from West African cold seeps. *Canadian Journal of Zoology*, 82(6), 980-999.

Anderson, J.E., Cartwright, J., Drysdall, S.J., Vivian, N., 2000. Controls on turbidite sand deposition during gravity-driven extension of a passive margin: examples from

Miocene sediments in Block 4, Angola. *Marine and Petroleum Geology*, 17(10), 1165-1203.

Anderson, M.J., Crist, T.O., Chase, J.M., Vellend, M., Inouye, B.D., Freestone, A.L., Sanders, N.J., Cornell, H.V., Comita, L.S., Davies, K.F., Harrison, S.P., Kraft, N.J.B., Stegen, J.C., Swenson, N.G., 2011. Navigating the multiple meanings of beta diversity: a roadmap for the practicing ecologist. *Ecology Letters*, 14(1), 19-28.

Andresen, K.J., 2012. Fluid flow features in hydrocarbon plumbing systems: What do they tell us about the basin evolution? *Marine Geology*, 332-334, 89-108.

Andresen, K.J., Huuse, M., 2011. 'Bulls-eye' pockmarks and polygonal faulting in the Lower Congo Basin: Relative timing and implications for fluid expulsion during shallow burial. *Marine Geology*, 279(1), 111-127.

Andrieux, O., Cooper, C.K., Wood, J., 2013. Turbidity current measurements in the Congo canyon. Paper presented at the Offshore Technology Conference, Houston, Texas. USA, May 2013. Paper Number: OTC-23992-MS.

Anka, Z., Ondrak, R., Kowitz, A., Schødt, N., 2013. Identification and numerical modelling of hydrocarbon leakage in the Lower Congo Basin: Implications on the genesis of km-wide seafloor mounded structures. *Tectonophysics*, 604, 153-171.

Anka, Z., Séranne, M., 2004. Reconnaissance study of the ancient Zaire (Congo) deep-sea fan. (ZaiAngo Project). *Marine Geology*, 209, 223-244.

Anka, Z., Séranne, M., Lopez, M., Scheck-Wenderoth, M., Savoye, B., 2009. The long-term evolution of the Congo deep-sea fan: A basin-wide view of the interaction between a giant submarine fan and a mature passive margin (ZaiAngo project). *Tectonophysics*, 470, 42-56.

ANPG, 2021. English version https://anpg.co.ao/sobre-nos/ (accessed September 2021).

Arango, C.P., 2009. New species and new records of sea spiders (Arthropoda: Pycnogonida) from deep waters in Western Australia. *Zootaxa*, 1977(1), 1-20.

Arbizu, P.M., Schminke, H.K., 2005. DIVA-1 expedition to the deep sea of the Angola Basin in 2000 and DIVA-1 workshop in 2003. *Organisms Diversity & Evolution*, 5, Supplement 1(0), 1-2.

Arnaud-Haond, S., Van den Beld, I.M.J., Becheler, R., Orejas, C., Menot, L., Frank, N., Grehan, A., Bourillet, J.F., 2017. Two "pillars" of cold-water coral reefs along Atlantic European margins: Prevalent association of Madrepora oculata with Lophelia pertusa, from reef to colony scale. *Deep Sea Research Part II*, 145, 110-119.

Axelsen, B.E., Zaera, D., Ostrowski, M., Lutuba-Nsilulu, H., Vaz-Velho, F., Basika, B., 2004. Surveys of the fish resources of Angola - Survey of the pelagic resources 28 July - 27 August 2004. *NORAD/FAO Project GCP/INT/730/NOR - Cruise reports Dr. Fridtjof Nansen*. Bergen: Institute of Marine Research.

Babonneau, N., Savoye, B., Cremer, M., Bez, M., 2004. Multiple terraces within the deep incised Zaire Valley (ZaiAngo Project): are they confined levees? In S.A. Lomas, P. Joseph (Eds.), *Confined Turbidite Systems*. Geological Society, London, Special Publications, 222, 91-114.

Babonneau, N., Savoye, B., Cremer, M., Bez, M., 2010. Sedimentary Architecture in Meanders of a Submarine Channel: Detailed Study of the Present Congo Turbidite Channel (Zaiango Project). *Journal of Sedimentary Research*, 80(10), 852-866.

Babonneau, N., Savoye, B., Cremer, M., Klein, B., 2002. Morphology and architecture of the present canyon and channel system of the Zaire deep-sea fan. *Marine and Petroleum Geology*, 19, 445-467.

Bachèlery, M.-L., Illig, S., Rouault, M., 2020. Interannual Coastal Trapped Waves in the Angola-Benguela Upwelling System and Benguela Niño and Niña events. *Journal of Marine Systems*, 203, 103262.

Bachèlery, M.L., Illig, S., Dadou, I., 2016. Forcings of nutrient, oxygen, and primary production interannual variability in the southeast Atlantic Ocean. *Geophysical Research Letters*, 43(16), 8617-8625.

Bailey, D.M., Collins, M.A., Gordon, J.D.M., Zuur, A.F., Priede, I.G., 2009. Long-Term Changes in Deep-Water Fish Populations in the Northeast Atlantic: A Deeper Reaching Effect of Fisheries? *Proceedings of the Royal Society of London B: Biological Sciences*, 276(1664), 1965-1969.

Bailey, D.M., King, N.J., Priede, I.G., 2007. Cameras and carcasses: historical and current methods for using artificial food falls to study deep-water animals. *Marine Ecology Progress Series*, 350, 179-192.

Baillon, S., Hamel, J.-F., Wareham, V.E., Mercier, A., 2012. Deep cold-water corals as nurseries for fish larvae. *Frontiers in Ecology and the Environment*, 10(7), 351-356.

Baillon, S., Hamel, J.F., Mercier, A., 2014. Diversity, Distribution and Nature of Faunal Associations with Deep-Sea Pennatulacean Corals in the Northwest Atlantic. *PLoS ONE*, 9(11), e111519. doi:111510.111371/journal.pone.0111519.

Baker, K.D., Wareham, V.E., Snelgrove, P.V.R., Haedrich, R.L., Fifield, D.A., Edinger, E.N., Gilkinson, K.D., 2012. Distributional patterns of deep-sea coral assemblages in three submarine canyons off Newfoundland, Canada. *Marine Ecology Progress Series*, 445, 235-249.

Barnes, A., T., Quetin, L.B., Childress, J.J., Pawson, D.L., 1976. Deep-Sea Macroplanktonic Sea Cucumbers: Suspended Sediment Feeders Captured from Deep Submergence Vehicle. *Science*, 194(4269), 1083-1085.

Bartek, L.R., Vail, P.R., Anderson, J.B., Emmet, P.A., Wu, S., 1991. Effect of Cenozoic ice sheet fluctuations in Antarctica on the stratigraphic signature of the Neogene. *Journal of Geophysical Research: Solid Earth*, 96(B4), 6753-6778.

Baselga, A., 2010. Partitioning the turnover and nestedness components of beta diversity. *Global Ecology and Biogeography*, 19, 134-143.

Baselga, A., Orme, D., Villeger, S., De Bortoli, J., Leprieur, F., 2018. betapart: Partitioning Beta Diversity into Turnover and Nestedness Components. R package version 1.5.1. https://CRAN.R-project.org/package=betapart.

Baudin, F., Disnar, J.-R., Martinez, P., Dennielou, B., 2010. Distribution of the organic matter in the channel-levees systems of the Congo mud-rich deep-sea fan (West Africa). Implication for deep offshore petroleum source rocks and global carbon cycle. *Marine and Petroleum Geology*, 27, 995-1010.

Baudin, F., Rabouille, C., Dennielou, B., 2020. Routing of terrestrial organic matter from the Congo River to the ultimate sink in the abyss: a mass balance approach. *Geologica Belgica*, 23(1-2), 41-52.

Baudin, F., Stetten, E., Schnyder, J., Charlier, K., Martinez, P., Dennielou, B., Droz, L., 2017b. Origin and distribution of the organic matter in the distal lobe of the Congo deep-sea fan - A Rock-Eval survey. *Deep Sea Research Part II*, 75-90.

Beaulieu, S.E., 2001. Life on glass houses: sponge stalk communities in the deep sea. *Marine Biology*, 138(4), 803-817.

Behrenfeld, M.J., Falkowski, P.G., 1997. Photosynthetic rates derived from satellite-based chlorophyll concentration. *Limnology and Oceanography*, 42(1), 1-20.

Benguela Current Convention, 2013. The Secretariat, Benguela Current Commission, Swakopmund, Namibia. Available at http://www.benguelacc.org/index.php/en/publications (accessed July 2021).

Benjamini, Y., Hochberg, Y., 1995. Controlling the False Discovery Rate: A Practical and Powerful Approach to Multiple Testing. *Journal of the Royal Statistical Society*: Series B (Methodological), 57(1), 289-300.

Benoist, N.M.A., Bett, B.J., Morris, K.J., Ruhl, H.A., 2019. A generalised volumetric method to estimate the biomass of photographically surveyed benthic megafauna. *Progress in Oceanography*, 178, 102188.

Benoist, N.M.A., Morris, K.J., Bett, B.J., Durden, J.M., Huvenne, V.A.I., Le Bas, T.P., Wynn, R.B., Ware, S.J., Ruhl, H.A., 2019. Monitoring mosaic biotopes in a marine conservation zone by autonomous underwater vehicle. *Conservation Biology*, 33(5), 1174-1186.

Berrit, G.R., 1976. Les eaux froides côtières du Gabon à l'Angola sontelles dues a un upwelling d'Ekman? *Cah. ORSTOM, Serie océanographie*, 14, 273-278.

Berrit, G.R., Dias, C.A., 1977. Hydroclimatologie des régions côtières de l'Angola : description des variations saisonnières à Lobito et Lucira. *Cahiers ORSTOM. Série Océanographie*, 2, 181-196.

Bessette, S., Moalic, Y., Gautey, S., Lesongeur, F., Godfroy, A., Toffin, L., 2017. Relative Abundance and Diversity of Bacterial Methanotrophs at the Oxic–Anoxic Interface of the Congo Deep-Sea Fan. *Frontiers in Microbiology*, 8(715).

Bett, B.J., 2001. UK Atlantic Margin Environmental Survey: Introduction and overview of bathyal benthic ecology. *Continental Shelf Research*, 21, 917-956.

Bett, B.J., 2003. Time-lapse Photography in the Deep Sea. *Underwater Technology*, 25(3), 121-128.

Bett, B.J., 2007. MV *Ocean Endeavour* Cruise 13 OCT - 06 NOV 2005. Seabed environmental study of Angola Blocks 18 and 31., *National Oceanography Centre: Research & Consultancy Report No. 27*: Southampton UK: National Oceanography Centre, Southampton, 56pp. (Unpublished report) *Commercial in Confidence*.

Bett, B.J., 2019. Megafauna. In J.K. Cochran, H.J. Bokuniewicz, P.L. Yager (Eds.), *Encyclopedia of Ocean Sciences (Third Edition)* (pp. 735-741). Oxford: Academic Press.

Bianchi, G., 1992. Demersal assemblages of the continental-shelf and upper slope of Angola. *Marine Ecology-Progress Series*, 81(2), 101-120.

Bianchi, G., Bjordal, Å., Koranteng, K.A., Tandstad, M., Sambe, B., Stromme, T., 2016. Collaboration between the Nansen Programme and the Large Marine Ecosystem Programmes. *Environmental Development*, 17, 340-348.

Billett, D.S.M., Bett, B.J., Reid, W.D.K., Boorman, B., Priede, I.G., 2010. Long-term change in the abyssal NE Atlantic: The ‘Amperima Event’ revisited. *Deep Sea Research Part II*, 57(15), 1406-1417.

Bivand, R., Keitt, T., Rowlingson, B., 2019. rgdal: Bindings for the 'Geospatial' Data Abstraction Library. R package version 1.4-4. https://CRAN.R-project.org/package=rgdal.

Blackburn, T.M., Gaston, K.J., 2003. Introduction: why macroecology? In T.M. Blackburn, K.J. Gaston (Eds.), *Macroecology: Concepts and Consequences: The 43rd Annual Symposium of the British Ecological Society held at the University of Birmingham, 17-19 April 2002*: Blackwell Science Ltd.

Blott, S.J., Pye, K., 2001. GRADISTAT: a grain size distribution and statistics package for the analysis of unconsolidated sediments. *Earth Surface Processes and Landforms*, 26(11), 1237-1248.

Bohn, J.M., 2006. Crinoidea and Holothuroidea (Echinodermata) of the abyssal Angola Basin - Results of the DIVA-1 expedition of FS "Meteor" (Cruise M48/1). *Zootaxa*, 1276, 1-31.

Bolli, H.M., Ryan, W.B.F., Foresman, J.B., Hottman, W.E., Kagami, H., Longoria, J.F., McKnight, B.K., Melguen, M., Natland, J., Proto-Decima, F., Siesser, W.G., 1978.

Angola Continental Margin Sites - 364 and 365. *Initial Reports of the Deep Sea Drilling Project Leg 40*, U.S. Government Printing Office, Washington.

Bond, G., 1978. Evidence for Late Tertiary Uplift of Africa Relative to North America, South America, Australia and Europe. *The Journal of Geology*, 86(1), 47-65.

Bornhold, B.D., 1973. Late quaternary sedimentation in the Eastern Angola Basin. *Technical report*.

Bouloubassi, I., Nabais, E., Pancost, R.D., Lorre, A., Taphanel, M.-H., 2009. First biomarker evidence for methane oxidation at cold seeps in the Southeast Atlantic (REGAB pockmark). *Deep Sea Research Part II*, 56(23), 2239-2247.

Bowden, D.A., Jones, D.O.B., 2016. Towed Cameras. In M.R. Clark, M. Consalvey, A.A. Rowden (Eds.), *Biological Sampling in the Deep Sea*: Wiley Blackwell.

BP, 2013. Geohazard Baseline Report. Kwanza Basin Block 19 and Northern Block 20, Angola Exploration Drilling Campaign. RDT Report No.: H/RDT/001/13. *Commercial in Confidence*.

BP Exploration, 2007. BP Angola Block 18 Western Area Development: Geotechnical Engineering and Geohazard Mitigation (Select: For pre-FEED). Report S/ABU/07/02 prepared by the BP Geohazard Assessment Team, Sunbury UK, for BP Exploration (Angola) Ltd. *Commercial in Confidence*.

Brault, S., Stuart, C.T., Wagstaff, M.C., McClain, C.R., Allen, J.A., Rex, M.A., 2013a. Contrasting patterns of alpha- and beta-diversity in deep-sea bivalves of the eastern and western North Atlantic. *Deep Sea Research Part II*, 92, 157-164.

Brault, S., Stuart, C.T., Wagstaff, M.C., Rex, M.A., 2013b. Geographic evidence for source-sink dynamics in deep-sea neogastropods of the eastern North Atlantic: An approach using nested analysis. *Global Ecology and Biogeography*, 22(4), 433-439.

Bray, J.R., Curtis, J.T., 1957. An Ordination of the Upland Forest Communities of Southern Wisconsin. *Ecological Monographs*, 27(4), 325-349.

Brice, S.E., Cochran, M.D., Pardo, G., Edwards, A.D., 1982. Tectonics and sedimentation of the South Atlantic Rift Sequence: Cabinda, Angola. *American Association Petroleum Geologists Memoir*, 34, 5-18.

Brind'Amour, A., Menot, L., Galéron, J., Crassous, P., 2009. Spatial organization of a sedimentary macrobenthic community located on the West African Equatorial margin. *Deep Sea Research Part II*, 56(23), 2292-2298.

Brix, S., 2007. Four new species of Desmosomatidae Sars, 1897 (Crustacea : Isopoda) from the deep sea of the Angola Basin. *Marine Biology Research*, 3(4), 205-230.

Brix, S., Leese, F., Riehl, T., Kihara, T.C., 2015. A new genus and new species of Desmosomatidae Sars, 1897 (Isopoda) from the eastern South Atlantic abyss described by means of integrative taxonomy. *Marine Biodiversity*, 45(1), 7-61.

Broucke, O., Temple, F., Rouby, D., Robin, C., Calassou, S., Nalpas, T., Guillocheau, F., 2004. The role of deformation processes on the geometry of mud-dominated turbiditic systems, Oligocene and Lower–Middle Miocene of the Lower Congo basin (West African Margin). *Marine and Petroleum Geology*, 21(3), 327-348.

Brown, A., Thatje, S., 2014. Explaining bathymetric diversity patterns in marine benthic invertebrates and demersal fishes: physiological contributions to adaptation of life at depth. *Biological Reviews*, 89(2), 406-426.

Brownfield, M.E., Charpentier, R.R., 2006. Geology and total petroleum systems of the West-Central Coastal Province (7203), West Africa. *U.S. Geological Survey Bulletin*, 2207-B, 52 p.

Brun, J.P., Fort, X., 2004. Compressional salt tectonics (Angolan margin). *Tectonophysics*, 382, 129-150.

Bruun, A.F., 1957. General introduction to the Galathea reports and list of deep-sea stations. In A.F. Bruun (Ed.), *Galathea Report Volume 1* (pp. 7-48). Copenhagen: University of Copenhagen.

Bruun, A.F., Greve, S.V., Mielche, H., Sparck, R., 1956. *The Galathea Deep Sea Expedition*. London: George Allen and Unwin Ltd.

Buchanan, J.B., 1960. On *Jullienella* and *Schizammina*, two genera of arenaceous Foraminifera from the tropical Atlantic, with a description of a new species. *Journal of the Linnean Society of London - Zoology*, 44(297), 270-277.

Buhl-Mortensen, L., Serigstad, B., Buhl-Mortensen, P., Olsen, M.N., Ostrowski, M., Błażewicz-Paszkowycz, M., Appoh, E., 2017. First observations of the structure and megafaunal community of a large Lophelia reef on the Ghanaian shelf (the Gulf of Guinea). *Deep Sea Research Part II*, 137, 148-156.

Buhl-Mortensen, L., Vanreusel, A., Gooday, A.J., Levin, L.A., Priede, I.G., Buhl-Mortensen, P., Gheerardyn, H., King, N.J., Raes, M., 2010. Biological structures as a source of habitat heterogeneity and biodiversity on the deep ocean margins. *Marine Ecology*, 31(1), 21-50.

Buhl-Mortensen, P., Gordon, J.D.C., Buhl-Mortensen, L., Kulka, D.W., 2017. First description of a Lophelia pertusa reef complex in Atlantic Canada. *Deep Sea Research Part I*, 126, 21-30.

Burwood, R., 1999. Angola: source rock control for Lower Congo Coastal and Kwanza Basin petroleum systems. *Geological Society, London, Special Publications*, 153(1), 181.

Cambon-Bonavita, M.A., Nadalig, T., Roussel, E., Delage, E., Duperron, S., Caprais, J.C., Boetius, A., Sibuet, M., 2009. Diversity and distribution of methane-oxidizing microbial communities associated with different faunal assemblages in a giant pockmark of the Gabon continental margin. *Deep Sea Research Part II*, 56(23), 2248-2258.

Carney, R.S., 2005. Zonation of deep biota on continental margins. In R.N. Gibson, R.J.A. Atkinson, J.D.M. Gordon (Eds.), *Oceanography and Marine Biology: An Annual Review, Vol. 43*, Vol. 43 (pp. 211-278): CRC Press.

Cathalot, C., Van Oevelen, D., Cox, T.J.S., Kutti, T., Lavaleye, M., Duineveld, G., Meysman, F.J.R., 2015. Cold-water coral reefs and adjacent sponge grounds: hotspots of benthic respiration and organic carbon cycling in the deep sea. *Frontiers in Marine Science*, 2(37).

CBD, 2008. Decision Adopted by the Conference of the Parties to the Convention on Biological Diversity at its Ninth Meeting. CBD CoP Decision IX/20. Marine and coastal biodiversity. Available at http://www.cbd.int/doc/decisions/cop-09/cop-09-dec20-en.pdf (accessed July 2021).

Chao, A., Hsieh, T.C., Ma, K.H., Gotelli, N.J., Sander, E.L., Colwell, R.K., Ellison, A.M., 2014. Rarefaction and extrapolation with Hill numbers: A framework for sampling and estimation in species diversity studies. *Ecological Monographs*, 84(1), 45-67.

Chao, A., Jost, L., 2012. Coverage-based rarefaction and extrapolation: standardizing samples by completeness rather than size. Ecology, 93(12), 2533-2547.

Chapman, P., Shannon, L.V., 1987. Seasonality in the oxygen minimum layers at the extremities of the Benguela system. *South African Journal of Marine Science*, 5(1), 85-94.

Charlou, J.L., Donval, J.P., Fouquet, Y., Ondreas, H., Knoery, J., Cochonat, P., Levaché, D., Poirier, Y., Jean-Baptiste, P., Fourré, E., Chazallon, B., 2004. Physical and chemical characterization of gas hydrates and associated methane plumes in the Congo–Angola Basin. *Chemical Geology*, 205(3-4), 405-425.

Chase, J.M., McGill, B.J., McGlinn, D.J., May, F., Blowes, S.A., Xiao, X., Knight, T.M., Purschke, O., Gotelli, N.J., 2018. Embracing scale-dependence to achieve a deeper understanding of biodiversity and its change across communities. *Ecology Letters*, 21(11), 1737-1751.

Chimienti, G., Angeletti, L., Mastrototaro, F., 2018. Withdrawal behaviour of the red sea pen Pennatula rubra (Cnidaria: Pennatulacea). *The European Zoological Journal*, 85(1), 64-70.

Clark, M.R., Bagley, N.W., Harley, B., 2016. Trawls. In M.R. Clark, M. Consalvey, A.A. Rowden (Eds.), *Biological Sampling in the Deep Sea*: Wiley Blackwell.

Clark, M.R., Rowden, A.A., Schlacher, T., Williams, A., Consalvey, M., Stocks, K.I., Rogers, A.D., O'Hara, T.D., White, M., Shank, T.M., Hall-Spencer, J.M., 2009. The Ecology of Seamounts: Structure, Function, and Human Impacts. *Annual Review of Marine Science*, 2(1), 253-278.

Clarke, K.R., 1990. Comparisons of dominance curves. *Journal of Experimental Marine Biology and Ecology*, 138(1), 143-157.

Clarke, K.R., Warwick, R.M., 2001. Change in Marine Communities: An Approach to Statistical Analysis and Interpretation. 2nd Edition, PRIMER-E, Ltd., Plymouth Marine Laboratory, Plymouth.

Cody, M.L., 1975. Towards a theory of continental species diversity: bird distribution on Mediterranean habitat gradients. In M.L. Cody, J.M. Diamond (Eds.), *Ecology and Evolution of Communities*. Cambridge, MA: Harvard University Press.

Colwell, R.K., 2013. EstimateS: Statistical estimation of species richness and shared species from samples. Version 9. User's Guide and application published at: http://purl.oclc.org/estimates.

Colwell, R.K., Chao, A., Gotelli, N.J., Lin, S.-Y., Mao, C.X., Chazdon, R.L., Longino, J.T., 2012. Models and estimators linking individual-based and sample-based rarefaction, extrapolation and comparison of assemblages. *Journal of Plant Ecology*, 5(1), 3-21.

Connallon, T., Sgrò, C.M., 2018. In search of a general theory of species' range evolution. *PLOS Biology*, 16(6), e2006735.

Constança, L.J., 1995. Evaluation of trawl surveys in Angolan waters. *ICES. C.M. 1995/G:34*.

Cordeiro, R.T.S., Castro, C.B., Pérez, C.D., 2015. Deep-water octocorals (Cnidaria: Octocorallia) from Brazil: Family Chrysogorgiidae Verrill, 1883. *Zootaxa*, 4058(1), 81-100.

Cordes, E.E., Jones, D.O.B., Schlacher, T.A., Amon, D.J., Bernardino, A.F., Brooke, S., Carney, R., DeLeo, D.M., Dunlop, K.M., Escobar-Briones, E.G., Gates, A.R., Génio, L., Gobin, J., Henry, L.A., Herrera, S., Hoyt, S., Joye, S., Kark, S., Mestre, N.C., Metaxas, A., Pfeifer, S., Sink, K., Sweetman, A.K., Witte, U.F.M., 2016. Environmental impacts of the deep-water oil and gas industry: a review to guide management strategies. *Frontiers in Environmental Science*, 4, doi.org/10.3389/fenvs.2016.00058.

Cordes, E., Arnaud-Haond, S., Bergstad, O.A., Bernal, P., da Costa Falcão, A.P., Freiwald, A., Roberts, J.M., 2017. Cold-Water Corals. In N. United (Ed.), *The First Global Integrated Marine Assessment: World Ocean Assessment I* (pp. 803-816). Cambridge: Cambridge University Press.

Cordes, E.E., Becker, E.L., Hourdez, S., Fisher, C.R., 2010. Influence of foundation species, depth, and location on diversity and community composition at Gulf of Mexico lower-slope cold seeps. *Deep Sea Research Part II*, 57, 1870-1881.

Cordes, E.E., Carney, S.L., Hourdez, S., Carney, R.S., Brooks, J.M., Fisher, C.R., 2007. Cold seeps of the deep Gulf of Mexico: Community structure and biogeographic comparisons to Atlantic equatorial belt seep communities. *Deep Sea Research Part I*, 54, 637-653.

Cosel, R.v., 2006. Taxonomy of tropical West African bivalves. VI. Remarks on Lucinidae (Mollusca, Bivalvia), with description of six new genera and eight new species. *Zoosystema*, 28(4), 805-851.

Cosel, R.v., Olu, K., 2008. A new genus and new species of Vesicomyidae (Mollusca, Bivalvia) from cold seeps on the Barbados accretionary prism, with comments on other species. *Zoosystema*, 30(4), 929-944.

Cosel, R.v., Olu, K., 2009. Large Vesicomyidae (Mollusca: Bivalvia) from cold seeps in the Gulf of Guinea off the coasts of Gabon, Congo and northern Angola. *Deep Sea Research Part II*, 56(23), 2350-2379.

Costello, M.J., McCrea, M., Freiwald, A., Lundälv, T., Jonsson, L., Bett, B.J., van Weering, T.C.E., de Haas, H., Roberts, J.M., Allen, D., 2005. Role of cold-water Lophelia pertusa coral reefs as fish habitat in the NE Atlantic. In A. Freiwald, J.M. Roberts (Eds.), *Cold-Water Corals and Ecosystems* (pp. 771-805). Berlin, Heidelberg: Springer Berlin Heidelberg.

Coynel, A., Seyler, P., Etcheber, H., Meybeck, M., Orange, D., 2005. Spatial and seasonal dynamics of total suspended sediment and organic carbon species in the Congo River. *Global Biogeochemical Cycles*, 19(4).

Cramez, C., Jackson, M.P.A., 2000. Superposed deformation straddling the continental-oceanic transition in deep-water Angola. *Marine and Petroleum Geology*, 17, 1095-1109.

Cristobo, F.J., Urgorri, V., Rios, P., 2005. Three new species of carnivorous deep-sea sponges from the DIVA-1 expedition in the Angola Basin (South Atlantic). *Organisms Diversity & Evolution*, 5, 203-213.

D'Onghia, G., Indennidate, A., Giove, A., Savini, A., Capezzuto, F., Sion, L., Vertino, A., Maiorano, P., 2011. Distribution and behaviour of deep-sea benthopelagic fauna observed using towed cameras in the Santa Maria di Leuca cold-water coral province. *Marine Ecology Progress Series*, 443, 95-110.

Da Costa, J.L., Schirmer, T.W., Laws, B.R., 2001. Lower Congo Basin, deep-water exploration province, offshore West Africa. In M.W. Downey, J.C. Threet, W.A. Morgan (Eds.), *Petroleum provinces of the twenty-first century.* AAPG Memoir 74, 517-530.

da Cunha, L.C., and Buitenhuis, E.T., 2013. Riverine influence on the tropical Atlantic Ocean biogeochemistry. *Biogeosciences*, 10(10), 6357-6373.

Daly, M., 2006. Boloceroides daphneae, a new species of giant sea anemone (Cnidaria: Actiniaria: Boloceroididae) from the deep Pacific. *Marine Biology*, 148(6), 1241-1247.

Danovaro, R., Snelgrove, P.V.R., Tyler, P., 2014. Challenging the paradigms of deep-sea ecology. *Trends in Ecology & Evolution*, 29(8), 465-475.

Danovaro, R., Fanelli, E., Aguzzi, J., Billett, D., Carugati, L., Corinaldesi, C., Dell'Anno, A., Gjerde, K., Jamieson, A.J., Kark, S., McClain, C., Levin, L., Levin, N., Ramirez-Llodra, E., Ruhl, H., Smith, C.R., Snelgrove, P.V.R., Thomsen, L., Van Dover, C.L., Yasuhara, M., 2020. Ecological variables for developing a global deep-ocean monitoring and conservation strategy. *Nature Ecology & Evolution*, 4(2), 181-192.

Davies, A.J., Duineveld, G.C.A., Lavaleye, M.S.S., Bergman, M.J.N., van Haren, H., Roberts, J.M., 2009. Downwelling and deep-water bottom currents as food supply mechanisms to the cold-water coral Lophelia pertusa (Scleractinia) at the Mingulay Reef Complex. *Limnology and Oceanography*, 54(2), 620-629.

Davies, J.S., Stewart, H.A., Narayanaswamy, B.E., Jacobs, C., Spicer, J., Golding, N., Howell, K.L., 2015. Benthic Assemblages of the Anton Dohrn Seamount (NE Atlantic): Defining Deep-Sea Biotopes to Support Habitat Mapping and Management Efforts with a Focus on Vulnerable Marine Ecosystems. *PLoS ONE*, 10(5), e0124815.

Davison, A.C., Hinkley, D.V., 1997. *Bootstrap Methods and their Application*. Cambridge: Cambridge University Press.

Davison, I., 2007. Geology and tectonics of the South Atlantic Brazilian salt basins. *Geological Society, London, Special Publications*, 272(1), 345.

De Barros Neto, V., de Fátima Jardim, M., de Vasconcelos, J.M.B., da Silva Tomás, A., Naruseb, A., Esau, B., Kandjoze, O., Shifeta, P., Peters, D., Molewa, E., Joseph Zwane, M., Zokwana, S., Hamukuaya, H., 2016. Two decades of inter-governmental collaboration: Three developing countries on the move towards ecosystem-based governance in the Benguela Current Large Marine Ecosystem. *Environmental Development*, 17, 353-356.

De Cáceres, M., Legendre, P., 2009. Associations between species and groups of sites: indices and statistical inference. *Ecology*, 90(12), 3566-3574.

De Clippele, L.H., Buhl-Mortensen, P., Buhl-Mortensen, L., 2015. Fauna associated with cold water gorgonians and sea pens. *Continental Shelf Research*, 105, 67-78.

De Leo, F.C., Smith, C.R., Rowden, A.A., Bowden, D.A., Clark, M.R., 2010. Submarine canyons: hotspots of benthic biomass and productivity in the deep sea. *Proceedings of the Royal Society B: Biological Sciences*, 277, 2738-2792.

De Matos-Pita, S.S., Ramil, F., 2014. Squat lobsters (Crustacea: Anomura) from Mauritanian waters (West Africa), with the description of a new species of Munidopsis. *Zootaxa*, 3765(5), 418-434.

De Mol, B., Van Rensbergen, P., Pillen, S., Van Herreweghe, K., Van Rooij, D., McDonnell, A., Huvenne, V., Ivanov, M., Swennen, R., Henriet, J.P., 2002. Large deep-water coral banks in the Porcupine Basin, southwest of Ireland. *Marine Geology*, 188, 193-231.

De Mol, L., Van Rooij, D., Pirlet, H., Greinert, J., Frank, N., Quemmerais, F., Henriet, J.-P., 2011. Cold-water coral habitats in the Penmarc'h and Guilvinec Canyons (Bay of Biscay): Deep-water versus shallow-water settings. *Marine Geology*, 282(1), 40-52.

Decker, C., Zorn, N., Le Bruchec, J., Caprais, J.C., Potier, N., Leize-Wagner, E., Lallier, F.H., Olu, K., Andersen, A.C., 2017. Can the hemoglobin characteristics of vesicomyid clam species influence their distribution in deep-sea sulfide-rich sediments? A case study in the Angola Basin. *Deep Sea Research Part II*, 142, 219-232.

Decker, C., Zorn, N., Potier, N., Leize-Wagner, E., Lallier, F.H., Olu, K., Andersen, A.C., 2014. Globin's Structure and Function in Vesicomyid Bivalves from the Gulf of Guinea Cold Seeps as an Adaptation to Life in Reduced Sediments. *Physiological and Biochemical Zoology: Ecological and Evolutionary Approaches*, 87(6), 855-869.

Dennielou, B., Droz, L., Babonneau, N., Jacq, C., Bonnel, C., Picot, M., Le Saout, M., Saout, Y., Bez, M., Savoye, B., Olu, K., Rabouille, C., 2017. Morphology, structure, composition and build-up processes of the active channel-mouth lobe complex of the Congo deep-sea fan with inputs from remotely operated underwater vehicle (ROV) multibeam and video surveys. *Deep Sea Research Part II*, 142, 25-49.

Dias, C.A., 1983. Note on the evidence of a permanent southward flow of the upper oceanic tropospheric waters off Angola at 128S. *Collection of Scientific Papers International Commission Southeast Atlantic Fisheries*, 10, 99-100.

Dolan, P., 1999. Western Africa: an unfinished story of oil and gas exploration. In: Cameron, N.R., Bate, R.H., and Clure, V.S. (Eds). *The Oil and Gas Habitats of the South Atlantic*. Geological Society, London, Special Publication, 153(1), 97-99.

Dorschel, B., Wheeler, A.J., Huvenne, V.A.I., de Haas, H., 2009. Cold-water coral mounds in an erosive environmental setting: TOBI side-scan sonar data and ROV video footage from the northwest Porcupine Bank, NE Atlantic. *Marine Geology*, 264(3), 218-229.

Douvere, F., 2008. The importance of marine spatial planning in advancing ecosystem-based sea use management. *Marine Policy*, 32, 762-771.

Droz, L., Marsset, T., Ondréas, H., Lopez, M., Savoye, B., Spy-Anderson, F.-L., 2003. Architecture of an active mud-rich turbidite system: The Zaire Fan (Congo-Angola margin southeast Atlantic). *AAPG Bulletin*, 87(7), 1145-1168.

Droz, L., Rigaut, F., Cochonat, P., Tofani, R., 1996. Morphology and recent evolution of the Zaire turbidite system (Gulf of Guinea). *GSA Bulletin*, 108(3), 253-269.

Dufrêne, M., Legendre, P., 1997. Species Assemblages and Indicator Species: The Need for a Flexible Asymmetrical Approach. *Ecological Monographs*, 67(3), 345-366.

Duineveld, G.C.A., Lavaleye, M.S.S., Berghuis, E.M., De Wilde, P.A.W.J., Van Der Weele, J., Kok, A., Batten, S.D., De Leeuw, J.W., 1997. Patterns of benthic fauna and benthic respiration on the celtic continental margin in relation to the distribution of phytodetritus. *Int. Revue ges. Hydrobiol.*, 82(3), 395-424.

Duineveld, G.C.A., Lavaleye, M.S.S., Berghuis, E.M., 2004. Particle flux and food supply to a seamount cold-water coral community (Galicia Bank, NW Spain). *Marine Ecology Progress Series*, 277, 13-23.

Duperron, S., Nadalig, T., Caprais, J.-C., Sibuet, M., Fiala-Médioni, A., Amann, R., Dubilier, N., 2005. Dual symbiosis in a Bathymodiolus mussel from a methane seep on the Gabon continental margin (South East Atlantic): 16S rRNA phylogeny and distribution of the symbionts in the gills. *Applied and Environmental Microbiology*, 71(4), 1694.

Duperron, S., Rodrigues, C.F., Léger, N., Szafranski, K., Decker, C., Olu, K., Gaudron, S.M., 2012. Diversity of symbioses between chemosynthetic bacteria and metazoans at the Guiness cold seep site (Gulf of Guinea, West Africa). *MicrobiologyOpen*, 1(4), 467-480.

Du Preez, C., Swan, K.D., Curtis, J.M.R., 2020. Cold-Water Corals and Other Vulnerable Biological Structures on a North Pacific Seamount After Half a Century of Fishing. *Frontiers in Marine Science*, 7(17).

Durden, J.M., Bett, B.J., Horton, T., Serpell-Stevens, A., Morris, K.J., Billett, D.S.M., Ruhl, H.A., 2016a. Improving the estimation of deep-sea megabenthos biomass: Dimension to wet weight conversions for abyssal invertebrates. *Marine Ecology Progress Series*, 552, 71-79.

Durden, J.M., Bett, B.J., Jones, D.O.B., Huvenne, V.A.I., Ruhl, H.A., 2015. Abyssal hills – hidden source of increased habitat heterogeneity, benthic megafaunal biomass and diversity in the deep sea. *Progress in Oceanography*, 137, 209-218.

Durden, J.M., Bett, B.J., Huffard, C.L., Pebody, C., Ruhl, H.A., Smith, K.L., 2019. Response of deep-sea deposit-feeders to detrital inputs: A comparison of two abyssal time-series sites. *Deep-Sea Research Part*, 104677.

Durden, J.M., Bett, B.J., Ruhl, H.A., 2020. Subtle variation in abyssal terrain induces significant change in benthic megafaunal abundance, diversity, and community structure. *Progress in Oceanography*, 186, 102395.

Durden, J.M., Schoening, T., Althaus, F., Friedman, A., Garcia, R., Glover, A.G., Greinert, J., Jacobsen Stout, N., Jones, D.O.B., Jordt, A., Kaeli, J., Köser, K., Kuhnz, L.A., Lindsay, D., Morris, K.J., Nattkemper, T.W., Osterloff, J., Ruhl, H.A., Singh, H., Tran, M., Bett, B.J., 2016b. Perspectives in visual imaging for marine biology and ecology: from acquisition to understanding. In R.N. Hughes, D.J. Hughes, I.P. Smith, A.C. Dale (Eds.), *Oceanography and Marine Biology: An Annual Review, Vol. 54* (pp. 1-72): CRC Press.

Duval, B., Cramez, C., Jackson, M.P.A., 1992. Raft tectonics in the Kwanza Basin, Angola. *Marine and Petroleum Geology*, 9(4), 389-404.

ECOLEX, 2021. The gateway to environmental law. Online resource https://www.ecolex.org/details/legislation/decree-no-3900-on-environmental-protection-measures-to-be-used-in-oil-activities-lex-faoc063760/ (accessed September 2021).

Edinger, E.N., Sherwood, O.A., Piper, D.J.W., Wareham, V.E., Baker, K.D., Gilkinson, K.D., Scott, D.B., 2011. Geological features supporting deep-sea coral habitat in Atlantic Canada. *Continental Shelf Research*, 31(2, Supplement), S69-S84.

Eerkes-Medrano, D., Drewery, J., Burns, F., Cárdenas, P., Taite, M., Mkay, D.W., Stirling, D., Neat, F., 2019. A community assessment of the demersal fish and benthic invertebrates of the Rosemary Bank Seamount marine protected area (NE Atlantic). *Deep Sea Research Part I*, 103180.

Eisma, D., Kalf, J., 1984. Dispersal of Zaire river suspended matter in the estuary and the Angola Basin. *Netherlands Journal of Sea Research*, 17(2), 385-411.

Eisma, D., van Bennekom, A.J., 1978. The Zaire river and estuary and the Zaire outflow in the Atlantic Ocean. *Netherlands Journal of Sea Research*, 12(3), 255-272.

Embley, R.W., Morley, J.J., 1980. Quaternary sedimentation and paleoenvironmental studies off Namibia (South-West Africa). *Marine Geology*, 36(3), 183-204.

ERT, 2006. BP Angola Environmental Survey, October/November 2005 - Physical/Chemical Analysis, Data report, ERT 1315/Rev1. ERT (Scotland) Ltd, Research Park South, Heriot-Watt University, Edinburgh EH14 4AP, UK. *Commercial in Confidence*.

ERT, 2008. BP Angola Environmental Survey, March/April 2008 - Physical/Chemical Analysis, Data report, ERT 1793/R001. ERT (Scotland) Ltd, Research Park South, Heriot-Watt University, Edinburgh EH14 4AP, UK. *Commercial in Confidence*.

Etter, R.J., Grassle, J.F., 1992. Patterns of species diversity in the deep sea as a function of sediment particle size diversity. *Nature*, 360, 576-578.

Evans, S.L., Jackson, C.A.-L., 2020. Base-salt relief controls salt-related deformation in the Outer Kwanza Basin, offshore Angola. *Basin Research*, 32(4), 668-687.

Fanelli, E., Bianchelli, S., Danovaro, R., 2018. Deep-sea mobile megafauna of Mediterranean submarine canyons and open slopes: Analysis of spatial and bathymetric gradients. *Progress in Oceanography*, 168, 23-34.

FAO, 2021. http://www.fao.org/in-action/vulnerable-marine-ecosystems/vme-indicators/en/ (accessed January 2021).

Federal Ministry for the Environment, Nature Conservation and Nuclear Safety, 2021. Conservation and Sustainable Use of the Benguela Current Large Marine

Ecosystem. Available at https://www.international-climate-initiative.com/en/details/project/conservation-and-sustainable-use-of-the-benguela-current-large-marine-ecosystem-13_IV+_041-402 (accessed September 2021).

Feng, D., Chen, D., Peckmann, J., Bohrmann, G., 2010. Authigenic carbonates from methane seeps of the northern Congo fan: Microbial formation mechanism. *Marine and Petroleum Geology*, 27(4), 748-756.

Ferry, J.N., Babonneau, N., Mulder, T., Parize, O., Raillard, S., 2004. Morphogenesis of Congo submarine canyon and valley: implications about the theories of the canyons formation. *Geodinamica Acta*, 17, 241-251.

Fidler, C., Noble, B., 2012. Advancing strategic environmental assessment in the offshore oil and gas sector: Lessons from Norway, Canada, and the United Kingdom. *Environmental Impact Assessment Review*, 34, 12-21.

Fiege, D., Ramey, P.A., Ebbe, B., 2010. Diversity and distributional patterns of Polychaeta in the deep South Atlantic. *Deep Sea Research Part I*, 57(10), 1329-1344.

Finke, G., Gee, K., Gxaba, T., Sorgenfrei, R., Russo, V., Pinto, D., Nsiangango, S.E., Sousa, L.N., Braby, R., Alves, F.L., Heinrichs, B., Kreiner, A., Amunyela, M., Popose, G., Ramakulukusha, M., Naidoo, A., Mausolf, E., Nsingi, K.K., 2020. Marine Spatial Planning in the Benguela Current Large Marine Ecosystem. *Environmental Development*, 36, 100569.

Fischer, W.G., Bianchi, G., Scott, W.B., 1981. FAO Species Identification Sheets for Fishery Purposes, Eastern Central Atlantic Fishing Areas, vol. 6. Canada, Ottawa: FAO & Department of Fisheries and Oceans.

Flanders Marine Institute, 2019. Maritime Boundaries Geodatabase: Maritime Boundaries and Exclusive Economic Zones (200NM), version 11. Available online at https://www.marineregions.org/. https://doi.org/10.14284/386 (accessed September 2021).

Florenchie, P., Lutjeharms, J.R.E., Reason, C.J.C., Masson, S., Rouault, M., 2003. The source of Benguela Niños in the South Atlantic Ocean. *Geophysical Research Letters*, 30(10).

Fofonoff, P., Millard, R.C., 1983. Algorithms for computation of fundamental properties of seawater. *UNESCO Technical Papers in Marine Science*, Vol. 44 (p. 55). Paris.

Folk, R.L., Ward, W.C., 1957. Brazos River bar: a study in the significance of grain size parameters. *Journal of Sedimentary Petrology*, 27, 3-26.

Fosså, J.H., Mortensen, P.B., Furevik, D.M., 2002. The deep-water coral Lophelia pertusa in Norwegian waters: distribution and fishery impacts. *Hydrobiologia*, 471, 1-12.

Fort, X., Brun, J.P., Chauvel, F., 2004. Salt tectonics on the Angolan margin, synsedimentary deformation processes. *AAPG Bulletin*, 88(11), 1523-1544.

Fraser, A.J., Hilkewich, D., Syms, R., Penge, J., Raposo, A., Simon, G., 2005. Angola Block 18: a deep-water exploration success story. In A.G. Doré, B.A. Vining (Eds.), *Petroleum Geology: North-West Europe and Global Perspectives - Proceedings of the 6th Petroleum Geology Conference, 1199–1216.* London: Geological Society.

Gage, J.D., 1986. The benthic fauna of the Rockall Trough: regional distribution and bathymetric zonation. *Proceedings of the Royal Society of Edinburgh. Section B. Biological Sciences*, 88, 159-174.

Gage, J.D., 2003. Benthic Biodiversity Across and Along the Continental Margin: Patterns, Ecological and Historical Determinants, and Anthropogenic Threats. In G. Wefer, D. Billett, D. Hebbeln, B.B. Jorgensen, M. Schliiter, T. van Weering (Eds.), *Ocean Margin Systems*. Berlin Heidelberg: Springer-Verlag

Gage, J.D., 2004. Diversity in deep-sea benthic macrofauna: the importance of local ecology, the larger scale, history and the Antarctic. *Deep Sea Research Part II*, 51(14-16), 1689-1708.

Gage, J.D., Lamont, P.A., Kroeger, K., Paterson, G.L.J., Vecino, J.L.G., 2000. Patterns in deep-sea macrobenthos at the continental margin: standing crop, diversity and faunal change on the continental slope off Scotland. *Hydrobiologia*, 440(1-3), 261-271.

Gage, J.D., Tyler, P.A., 2010. *Deep-Sea Biology: A Natural History of Organisms at the Deep-Sea*: Cambridge University Press, Cambridge.

Gagolewski, M., and others, 2019. R package stringi: Character string processing facilities. http://www.gagolewski.com/software/stringi/.

Galéron, J., Sibuet, M., Mahaut, M.-L., Dinet, A., 2000. Variation in structure and biomass of the benthic communities at three contrasting sites in the tropical Northeast Atlantic. *Marine Ecology Progress Series*, 197, 121-137.

Galéron, J., Menot, L., Renaud, N., Crassous, P., Khripounoff, A., Treignier, C., Sibuet, M., 2009. Spatial and temporal patterns of benthic macrofaunal communities on the deep continental margin in the Gulf of Guinea. *Deep Sea Research Part II*, 56, 2299-2312.

Gates, A.R., Morris, K.J., Jones, D.O.B., Sulak, K.J., 2017. An association between a cusk eel (*Bassozetus* sp.) and a black coral (*Schizopathes* sp.) in the deep western Indian Ocean. *Marine Biodiversity*, 47(3), 971-977.

Gauch, H.G., 1973. A Quantitative Evaluation of the Bray-Curtis Ordination. *Ecology*, 54(4), 829-836.

Gaudron, S.M., Hourdez, S., Olu, K., 2017. Aspects on gametogenesis, fertilization and embryogenesis of two deep-sea polychaetes from Eastern Atlantic cold seeps. *Deep Sea Research Part I*, 129, 59-68.

Gay, A., Lopez, M., Berndt, C., Séranne, M., 2007. Geological controls on focused fluid flow associated with seafloor seeps in the Lower Congo Basin. *Marine Geology*, 244, 68-92.

Gay, A., Lopez, M., Cochonat, P., Séranne, M., Levaché, D., Sermondadaz, G., 2006a. Isolated seafloor pockmarks linked to BSRs, fluid chimneys, polygonal faults and stacked Oligocene–Miocene turbiditic palaeochannels in the Lower Congo Basin. *Marine Geology*, 226(1-2), 25-40.

Gay, A., Lopez, M., Cochonat, P., Sermondadaz, G., 2004. Polygonal faults-furrows system related to early stages of compaction - upper Miocene to recent sediments of the Lower Congo Basin. *Basin Research*, 16(1), 101-116.

Gay, A., Lopez, M., Cochonat, P., Sultan, N., Cauquil, E., Brigaud, F., 2003. Sinuous pockmark belt as indicator of a shallow buried turbiditic channel on the lower slope of the Congo basin, West African margin. In P. van Rensbergen, R.R. Hillis, A.J. Maltman, C.K. Morley (Eds.). *Subsurface Sediment Mobilization*. London: Geological Society London, Special Publications, 216, 173-189.

Gay, A., Lopez, M., Ondreas, H., Charlou, J.L., Sermondadaz, G., Cochonat, P., 2006b. Seafloor facies related to upward methane flux within a Giant Pockmark of the Lower Congo Basin. *Marine Geology*, 226(1), 81-95.

GEBCO Compilation Group, 2019. GEBCO 2019 Grid (doi:10.5285/836f016a-33be-6ddc-e053-6c86abc0788e).

Gee, M.J.R., Gawthorpe, R.L., 2006. Submarine channels controlled by salt tectonics: Examples from 3D seismic data offshore Angola. *Marine and Petroleum Geology*, 23(4), 443-458.

Gee, M.J.R., Gawthorpe, R.L., Bakke, K., Friedmann, S.J., 2007. Seismic Geomorphology and Evolution of Submarine Channels from the Angolan Continental Margin. *Journal of Sedimentary Research*, 77(5), 433-446.

Genin, A., Dayton, P.K., Lonsdale, P.F., Spiess, F.N., 1986. Corals on seamount peaks provide evidence of current acceleration over deep-sea topography. *Nature*, 322(6074), 59-61.

George, K.H., Veit-Köhler, G., Arbizu, P.M., Seifried, S., Rose, A., Willen, E., Bröhldick, K., Corgosinho, P.H., Drewes, J., Menzel, L., Moura, G., Schminke, H.K., 2014. Community structure and species diversity of Harpacticoida (Crustacea: Copepoda) at two sites in the deep sea of the Angola Basin (Southeast Atlantic). *Organisms Diversity & Evolution*, 14(1), 57-73.

Gervais, A., Mulder, T., Savoye, B., Migeon, S., Cremer, M., 2001. Recent processes of levee formation on the Zaire deep-sea fan. *Comptes Rendus de l'Académie des Sciences - Series IIA - Earth and Planetary Science*, 332(6), 371-378.

Gilliland, P.M., Laffoley, D., 2008. Key elements and steps in the process of developing ecosystem-based marine spatial planning. *Marine Policy*, 32, 787-796.

Gil-Mansilla, E., GarcÍA-ÁLvarez, Ó., Urgorri, V., 2008. New Acanthomeniidae (Solenogastres, Cavibelonia) from the abyssal Angola Basin. *Zootaxa*, 1866(1), 175-186.

Glover, A.G., Wiklund, H., Chen, C., Dahlgren, T.G., 2018. Managing a sustainable deep-sea 'blue economy' requires knowledge of what actually lives there. *eLife*, 7, e41319.

Gooday, A.J., 2002. Biological Responses to Seasonally Varying Fluxes of Organic Matter to the Ocean Floor: A Review. *Journal of Oceanography*, 58(2), 305-332.

Gooday, A.J., Bett, B.J., Escobar, E., Ingole, B., Levin, L.A., Neira, C., Raman, A.V., Sellanes, J., 2010. Habitat heterogeneity and its influence on benthic biodiversity in oxygen minimum zones. *Marine Ecology*, 31(1), 125-147.

Gooday, A.J., Levin, L.A., Aranda da Silva, A., Bett, B.J., Cowie, G.L., Dissard, D., Gage, J.D., Hughes, D.J., Jeffreys, R., Lamont, P.A., Larkin, K.E., Murty, S.J., Schumacher, S., Whitcraft, C., Woulds, C., 2009. Faunal responses to oxygen gradients on the Pakistan margin: A comparison of foraminiferans, macrofauna and megafauna. *Deep Sea Research Part II*, 56(6), 488-502.

Gordon, A.L., Bosley, K.T., 1991. Cyclonic gyre in the tropical South Atlantic. *Deep Sea Research*, 38, Suppl. 1, S323-S343.

Gotelli, N.J., Colwell, R.K., 2001. Quantifying biodiversity: procedures and pitfalls in the measurement and comparison of species richness. *Ecology Letters*, 4(4), 379-391.

Gotelli, N.J., Colwell, R.K., 2011. Estimating species richness. In A.E. Magurran, B.J. McGill (Eds.), *Biological Diversity: Frontiers in Measurement and Assessment* (pp. 39-54): Oxford University Press.

Governo de Angola, 2014. Decreto Executivo n.° 97/14 de 8 de Abrill - Aprova o Regulamento sobre Gestão de Descargas Operacionais. Governo de Angola, Ministério dos Petróleos, Luanda. An English translation of an earlier version (Decree 224/12) was provided by BP.

Governo de Angola, 2000. Decreto n.° 39/00 de 10 de Outubro - Directrizes para a protecção ambiental na indústria petrolífera. Governo de Angola, Luanda. English version available at https://webgis.anpg.co.ao/wp-content/leis_en/Decree%2039-00.pdf (accessed September 2021).

Governo de Angola, 2019. Presidential Decree no. 26/20 of 06 February, National Biodiversity Strategy and Action Plan 2019-2025. English version available at https://www.cbd.int/doc/world/ao/ao-nbsap-v2-en.pdf (accessed September 2021).

Governo de Angola, 2020. Decreto Presidencial n. ° 117/20 de 20 de Abrill - Aprova o Regulamento Geral de Avaliação de Impacte Ambiental e do Procedimento de Licenciamento Ambiental. Governo de Angola, Luanda.

Governo de Angola, 2021. Voluntary National Review on the Implementation of the 2030 Agenda for Sustainable Development. Available at https://sustainabledevelopment.un.org/content/documents/286012021_VNR_Report_Angola.pdf (accessed September 2021).

Grassle, J.F., Maciolek, N.J., 1992. Deep-Sea Species Richness: Regional and Local Diversity Estimates from Quantitative Bottom Samples. *The American Naturalist*, 139(2), 313-341.

Grassle, J.F., Sanders, H.L., Rowe, G.T., McLellan, T., Hessler, R.R., 1975. Pattern and zonation: a study of the bathyal megafauna using the research submersible Alvin. *Deep Sea Research and Oceanographic Abstracts*, 22(7), 457-462,IN451-IN456,463-481.

Guiavarc'h, C., Treguier, A.M., Vangriesheim, A., 2008. Remotely forced biweekly deep oscillations on the continental slope of the Gulf of Guinea. *Journal of Geophysical Research: Oceans*, 113(C6).

Guillon, E., Menot, L., Decker, C., Krylova, E., Olu, K., 2017. The vesicomyid bivalve habitat at cold seeps supports heterogeneous and dynamic macrofaunal assemblages. *Deep Sea Research Part I*, 120, 1-13.

Guiraud, M., Buta-Neto, A., Quesne, D., 2010. Segmentation and differential post-rift uplift at the Angola margin as recorded by the transform-rifted Benguela and oblique-to-orthogonal-rifted Kwanza basins. *Marine and Petroleum Geology*, 27(5), 1040-1068.

Gunton, L., Gooday, A., Glover, A., Bett, B., 2015. Macrofaunal abundance and community composition at lower bathyal depths in different branches of the Whittard Canyon and on the adjacent slope (3500 m; NE Atlantic). *Marine Ecology Progress Series*, 240, 157-170.

Haas, A., Peckmann, J., Elvert, M., Sahling, H., Bohrmann, G., 2010. Patterns of carbonate authigenesis at the Kouilou pockmarks on the Congo deep-sea fan. *Marine Geology*, 268(1), 129-136.

Haedrich, R.L., Rowe, G.T., Polloni, P.T., 1975. Zonation and faunal composition of epibenthic populations on the continental slope south of New England. *Journal of Marine Research*, 33, 191-212.

Haedrich, R.L., Rowe, G.T., 1977. Megafaunal biomass in the deep sea. *Nature*, 269(5624), 141-142.

Hamukuaya, H., 2020. Benguela Current Convention supports ecosystem assessment and management practice. *Environmental Development*, 36, 100574.

Hansen, B., 1975. Systematics and Biology of the Deep-Sea Holothurians, Part 1. Elasipoda. In T. Wolff (Ed.), *Scientific Results of the Danish Deep-Sea Expedition Round the World 1950-52*, Vol. 13. Copenhagen: Scandinavian Science Press Ltd.

Hanz, U., Wienberg, C., Hebbeln, D., Duineveld, G., Lavaleye, M., Juva, K., Dullo, W.C., Freiwald, A., Tamborrino, L., Reichart, G.J., Flögel, S., Mienis, F., 2019. Environmental factors influencing cold-water coral ecosystems in the oxygen minimum zones on the Angolan and Namibian margins. *Biogeosciences*, 2019, 1-37.

Hardman-Mountford, N.J., Richardson, A.J., Agenbag, J.J., Hagen, E., Nykjaer, L., Shillington, F.A., Villacastin, C., 2003. Ocean climate of the South East Atlantic observed from satellite data and wind models. *Progress in Oceanography*, 59, 181-221.

Harris, P.T., Macmillan-Lawler, M., Rupp, J., Baker, E.K., 2014. Geomorphology of the oceans. *Marine Geology*, 352, 4-24.

Hebbeln, D., Wienberg, C., Bender, M., Bergmann, F., Dehning, K., Dullo, W.C., Eichstädter, R., Flöter, S., Freiwald, A., Gori, A., Haberkern, J., Hoffman, L., Mendes João, F., Lavaleye, M., Leymann, T., Matsuyama, K., Meyer-Schack, B., Mienis, F., Moçambique, B.I., Nowald, N., Orejas Saco del Valle, C., Cordova, C.R., Saturov, D., Seiter, C., Titschack, J., Vittori, V., Wefing, A.M., Wilsenack, M. & Wintersteller, P., 2016. ANNA - Cold-water coral ecosystems off Angola and Namibia. *Meteor Berichte*, Cruise No. M122, 1-74.

Hebbeln, D., Wienberg, C., Dullo, W.-C., Freiwald, A., Mienis, F., Orejas, C., Titschack, J., 2020. Cold-water coral reefs thriving under hypoxia. *Coral Reefs*, 39(4), 853-859.

Hecker, B., 1990. Variation in megafaunal assemblages on the continental margin south of New England. *Deep Sea Research Part A*, 37(1), 37-57.

Heezen, B.C., 1974. Atlantic-Type Continental Margins. In C.A. Burk, C.L. Drake (Eds.), *The Geology of Continental Margins* (pp. 13-24). New York: Springer-Verlag.

Heezen, B.C., Menzies, R.J., Schneider, E.D., Ewing, W.M., Granelli, N.C.L., 1964. Congo submarine canyon. *AAPG Bulletin*, 48, 1126-1149.

Helly, J.J., Levin, L.A., 2004. Global distribution of naturally occurring marine hypoxia on continental margins. *Deep Sea Research Part I*, 51, 1159-1168.

Henry, L.-A., Roberts, J.M., 2007. Biodiversity and ecological composition of macrobenthos on cold-water coral mounds and adjacent off-mound habitat in the bathyal Porcupine Seabight, NE Atlantic. *Deep Sea Research Part I*, 54(4), 654-672.

Henry, L.-A., Roberts, J.M., 2017. Global Biodiversity in Cold-Water Coral Reef Ecosystems. In S. Rossi, L. Bramanti, A. Gori, C. Orejas (Eds.), *Marine Animal Forests: The Ecology of Benthic Biodiversity Hotspots* (pp. 235-256). Cham: Springer International Publishin

Hernández-Ávila, I., Guerra-Castro, E., Bracho, C., Rada, M., Ocaña, F.A., Pech, D., 2018. Variation in species diversity of deep-water megafauna assemblages in the Caribbean across depth and ecoregions. *PLoS ONE*, 13(8), e0201269.

Heron-Allen, E., Earland, A., 1929. Some new Foraminifera from the South Atlantic. *Journal of the Royal Microscopical Society*, 49, 102-108.

Higgs, N.D., Gates, A.R., Jones, D.O.B., 2014. Fish Food in the Deep Sea: Revisiting the Role of Large Food-Falls. *PLoS ONE*, 9(5), e96016.

Hill, A.J., Southgate, J.G., Fish, P.R., Thomas, S., 2011a. Deepwater Angola part I. In S. Gourvenec, D. White (Eds.), *Frontiers in Offshore Geotechnics II* (pp. 209-214). London: CRC Press.

Hill, A.J., Evans, T.G., Mackenzie, B., Thompson, G., 2011b. Deepwater Angola part II. In S. Gourvenec, D. White (Eds.), *Frontiers in Offshore Geotechnics II* (pp. 215-220). London: CRC Press.

Hill, M.O., 1973. Diversity and evenness: A unifying notation and its consequences. *Ecology*, 54(2), 427-432.

Ho, S., Cartwright, J.A., Imbert, P., 2012. Vertical evolution of fluid venting structures in relation to gas flux, in the Neogene-Quaternary of the Lower Congo Basin, Offshore Angola. *Marine Geology*, 332-334, 40-55.

Ho, S., Imbert, P., Hovland, M., Wetzel, A., Blouet, J.-P., Carruthers, D., 2018. Downslope-shifting pockmarks: interplay between hydrocarbon leakage, sedimentations, currents and slope's topography. *International Journal of Earth Sciences*, 107(8), 2907-2929.

Holm, S., 1979. A Simple Sequentially Rejective Multiple Test Procedure. *Scandinavian Journal of Statistics*, 6(2), 65-70.

Hopkins, J., Lucas, M., Dufau, C., Sutton, M., Stum, J., Lauret, O., Channelliere, C., 2013. Detection and variability of the Congo River plume from satellite derived sea surface temperature, salinity, ocean colour and sea level. *Remote Sensing of Environment*, 139, 365-385.

Hovland, M., Gardner, J.V., Judd, A.G., 2002. The significance of pockmarks to understanding fluid flow processes and geohazards. *Geofluids*, 2(2), 127-136.

Howell, K.L., Billett, D.S.M., Tyler, P.A., 2002. Depth-related distribution and abundance of seastars (Echinodermata: Asteroidea) in the Porcupine Seabight and Porcupine Abyssal Plain, N.E. Atlantic. *Deep Sea Research Part I*, 49(10), 1901-1920.

Howell, K.L., Davies, J.S., Allcock, A.L., Braga-Henriques, A., Buhl-Mortensen, P., Carreiro-Silva, M., Dominguez-Carrió, C., Durden, J.M., Foster, N.L., Game, C.A., Hitchin, B., Horton, T., Hosking, B., Jones, D.O.B., Mah, C., Laguionie Marchais, C., Menot, L., Morato, T., Pearman, T.R.R., Piechaud, N., Ross, R.E., Ruhl, H.A., Saeedi, H., Stefanoudis, P.V., Taranto, G.H., Thompson, M.B., Taylor, J.R., Tyler, P., Vad, J., Victorero, L., Vieira, R.P., Woodall, L.C., Xavier, J.R., Wagner, D., 2019. A framework for the development of a global standardised marine taxon reference image database (SMarTaR-ID) to support image-based analyses. *PLoS ONE*, 14(12), e0218904.

Howell, K.L., Hilário, A., Allcock, A.L., Bailey, D.M., Baker, M., Clark, M.R., Colaço, A., Copley, J., Cordes, E.E., Danovaro, R., Dissanayake, A., Escobar, E., Esquete, P., Gallagher, A.J., Gates, A.R., Gaudron, S.M., German, C.R., Gjerde, K.M., Higgs, N.D., Le Bris, N., Levin, L.A., Manea, E., McClain, C., Menot, L., Mestre, N.C., Metaxas, A., Milligan, R.J., Muthumbi, A.W.N., Narayanaswamy, B.E., Ramalho, S.P., Ramirez-Llodra, E., Robson, L.M., Rogers, A.D., Sellanes, J., Sigwart, J.D., Sink, K., Snelgrove, P.V.R., Stefanoudis, P.V., Sumida, P.Y., Taylor, M.L., Thurber, A.R., Vieira, R.P., Watanabe, H.K., Woodall, L.C., Xavier, J.R., 2020. A Blueprint for an Inclusive, Global Deep-Sea Ocean Decade Field Program. *Frontiers in Marine Science*, 7(999).

Howell, K.L., Mowles, S.L., Foggo, A., 2010. Mounting evidence: near-slope seamounts are faunally indistinct from an adjacent bank. *Marine Ecology*, 31(s1), 52-62.

Hsieh, T.C., Ma, K.H., Chao, A., McInerny, G., 2016. iNEXT: an R package for rarefaction and extrapolation of species diversity (Hill numbers). *Methods in Ecology and Evolution*, 7(12), 1451-1456.

Hudec, M.R., Jackson, M.P.A., 2002. Structural segmentation, inversion, and salt tectonics on a passive margin: Evolution of the Inner Kwanza Basin, Angola. *GSA Bulletin*, 114(10), 1222-1244.

Hudec, M.R., Jackson, M.P.A., 2004. Regional restoration across the Kwanza Basin, Angola: Salt tectonics triggered by repeated uplift of a metastable passive margin. *AAPG Bulletin*, 88(7), 971-990.

Huffard, C.L., Kuhnz, L.A., Lemon, L., Sherman, A.D., Smith, K.L., 2016. Demographic indicators of change in a deposit-feeding abyssal holothurian community (Station M, 4000m). *Deep Sea Research Part I*, 109, 27-39.

Hughes, D.J., Gage, J.D., 2004. Benthic metazoan biomass, community structure and bioturbation at three contrasting deep-water sites on the northwest European continental margin. *Progress in Oceanography*, 63, 29-55.

Hughes, J.A., 2008. BP Angola Block 31 Pre-operational Environmental Survey, 2008: Integrated results and report. . *National Oceanography Centre Southampton Research and Consultancy Report, No. 56*: Southampton, UK: National Oceanography Centre, Southampton, 55pp. (Unpublished report) *Commercial in Confidence*.

Hughes, J.A., Hunt, J., 2008. MV *Sea Trident* Cruise 28 MAR - 23 APR 2008. Seabed environmental study of Angola Block 31. *National Oceanography Centre: Research & Consultancy Report No. 47*: Southampton, UK: National Oceanography Centre, Southampton, 51 pp. (Unpublished report) *Commercial in Confidence.*

Hunter, W.R., Oguri, K., Kitazato, H., Ansari, Z.A., Witte, U., 2011. Epi-benthic megafaunal zonation across an oxygen minimum zone at the Indian continental margin. *Deep Sea Research Part I*, 58(6), 699-710.

Husebø, Å., Nøttestad, L., Fosså, J.H., Furevik, D.M., Jørgensen, S.B., 2002. Distribution and abundance of fish in deep-sea coral habitats. *Hydrobiologia*, 471(1), 91-99.

Huvenne, V.A.I., Tyler, P.A., Masson, D.G., Fisher, E.H., Hauton, C., Hühnerbach, V., Le Bas, T.P., Wolff, G.A., 2011. A Picture on the Wall: Innovative Mapping Reveals Cold-Water Coral Refuge in Submarine Canyon. *PLoS ONE*, 6(12), e28755.

IMAR Survey, 2015a. BP Angola Environmental Monitoring Survey - Survey Operations Report. Survey Leg 1: 4-Jul-2014 to 12-Aug-2014, Survey Leg 2: 13-Aug-2014 to 11-Sep-2014. IMAR Report Reference 10047-10051, CON-ANG-00-5731. *Commercial in Confidence*.

IMAR Survey, 2015b. BP Angola Environmental Monitoring Survey Block 18 - Physico-Chemical Water and Sediment Results Report. IMAR Report Reference 10047.2, CON-ANG-00-5731. *Commercial in Confidence*.

IMAR Survey, 2015c. BP Angola Environmental Monitoring Survey Block 19 - Physico-Chemical Water and Sediment Results Report. IMAR Report Reference 10048.2, CON-ANG-00-5731. *Commercial in Confidence*.

IMAR Survey, 2015d. BP Angola Environmental Monitoring Survey Block 24 - Physico-Chemical Water and Sediment Results Report. IMAR Report Reference 10049.2, CON-ANG-00-5731. *Commercial in Confidence*.

IMAR Survey, 2015e. BP Angola Environmental Monitoring Survey Block 31 - Physico-Chemical Water and Sediment Results Report. IMAR Report Reference 10050-51.2, CON-ANG-00-5731. *Commercial in Confidence*.

Institute for Coastal and Marine Research, 2021. EBSA Portal, Angola. Nelson Mandela University, South Africa. https://cmr.mandela.ac.za/Research-Projects/EBSA-Portal/Angola (accessed September 2021).

Ives, A.R., Carpenter, S.R., 2007. Stability and Diversity of Ecosystems. *Science*, 317(5834), 58.

Jackson, M.P.A., Hudec, M.R., Hegarty, K.A., 2005. The great West African Tertiary coastal uplift: Fact or fiction? A perspective from the Angolan divergent margin. *Tectonics*, 24(6).

Jamieson, A.J., 2016. Landers: Baited Cameras and Traps. In M.R. Clark, M. Consalvey, A.A. Rowden (Eds.), *Biological Sampling in the Deep Sea*: Wiley Blackwell.

Jamieson, A.J., Linley, T.D., Craig, J., 2017. Baited camera survey of deep-sea demersal fishes of the West African oil provinces off Angola: 1200–2500m depth, East Atlantic Ocean. *Marine Environmental Research*, 129, 347-364.

Jansen, J.H.F., 1990. Glacial-interglacial oceanography of the southeastern atlantic Ocean and the paleoclimate of west central Africa. *Paysages quaternaires de l'Afrique centrale atlantique* (pp. 110-123). Paris: ORSTROM.

Jansen, J.H.F., Van Weering, T.C.E., Gieles, R., Van Iperen, J., 1984. Middle and late quaternary oceanography and climatology of the Zaire-Congo fan and the adjacent Eastern Angola basin. *Netherlands Journal of Sea Research*, 17(2-4), 201-249.

Jarre, A., Hutchings, L., Kirkman, S.P., Kreiner, A., Tchipalanga, P.C.M., Kainge, P., Uanivi, U., van der Plas, A.K., Blamey, L.K., Coetzee, J.C., Lamont, T., Samaai, T., Verheye, H.M., Yemane, D.G., Axelsen, B.E., Ostrowski, M., Stenevik, E.K., Loeng, H., 2015. Synthesis: climate effects on biodiversity, abundance and distribution of marine organisms in the Benguela. *Fisheries Oceanography*, 24(S1), 122-149.

Jatiault, R., Dhont, D., Loncke, L., de Madron, X.D., Dubucq, D., Channelliere, C., Bourrin, F., 2018. Deflection of natural oil droplets through the water column in deep-water environments: The case of the Lower Congo Basin. *Deep Sea Research Part I*, 136, 44-61.

Jatiault, R., Dhont, D., Loncke, L., Dubucq, D., 2017. Monitoring of natural oil seepage in the Lower Congo Basin using SAR observations. *Remote Sensing of Environment*, 191, 258-272.

Jatiault, R., Loncke, L., Dhont, D., Dubucq, D., Imbert, P., 2019b. Geophysical characterisation of active thermogenic oil seeps in the salt province of the lower Congo basin. Part II: A regional validation. *Marine and Petroleum Geology*, 103, 773-791.

Jatiault, R., Loncke, L., Dhont, D., Imbert, P., Dubucq, D., 2019a. Geophysical characterisation of active thermogenic oil seeps in the salt province of the lower Congo basin part I: Detailed study of one oil-seeping site. *Marine and Petroleum Geology*, 103, 753-772.

Jennings, S., Kaiser, M.J., 1998. The Effects of Fishing on Marine Ecosystems. In J.H.S. Blaxter, A.J. Southward, P.A. Tyler (Eds.), *Advances in Marine Biology*, Vol. 34 (pp. 201-352): Academic Press.

Jensen, A., Frederiksen, R., 1992. The fauna associated with the bank-forming deepwater coral Lophelia pertusa (Scleractinaria) on the Faroe shelf. *Sarsia*, 77(1), 53-69.

Jones, D.O.B., Bett, B.J., Tyler, P.A., 2007a. Depth-related changes in the arctic epibenthic megafaunal assemblages of Kangerdlugssuaq, East Greenland. *Marine Biology Research*, 3(5), 191-204.

Jones, D.O.B., Bett, B.J., Tyler, P.A., 2007b. Megabenthic ecology of the deep Faroe-Shetland channel: A photographic study. *Deep Sea Research Part I*, 54, 1111-1128.

Jones, D.O.B., Bett, B.J., Wynn, R.B., Masson, D.G., 2009. The use of towed camera platforms in deep-water science. *International Journal of the Society for Underwater Technology*, 28(2), 41-50.

Jones, D.O.B., Hudson, I.R., Bett, B.J., 2006. Effects of physical disturbance on the cold-water megafaunal communities of the Faroe-Shetland Channel. *Marine Ecology Progress Series*, 319, 43-54.

Jones, D.O.B., Brewer, M.E., 2012. Response of megabenthic assemblages to different scales of habitat heterogeneity on the Mauritanian slope. *Deep-Sea Research Part I*, 67, 98-110.

Jones, D.O.B., Mrabure, C.O., Gates, A.R., 2013. Changes in deep-water epibenthic megafaunal assemblages in relation to seabed slope on the Nigerian margin. *Deep Sea Research Part I*, 78, 49-57.

Jones, D.O.B., Walls, A., Clare, M., Fiske, M.S., Weiland, R.J., O'Brien, R., Touzel, D.F., 2014. Asphalt mounds and associated biota on the Angolan margin. *Deep Sea Research I*, 94, 124-136.

Jonsson, L.G., Nilsson, P.G., Floruta, F., Lund, T., 2004. Distributional patterns of macro- and megafauna associated with a reef of the cold-water coral Lophelia pertusa on the Swedish west coast. *Marine Ecology Progress Series*, 284, 163-171.

Jost, L., 2010. The relation between evenness and diversity. *Diversity*, 2(2), 207-232.

Jurasinski, G., Retzer, V., Beierkuhnlein, C., 2009. Inventory, differentiation, and proportional diversity: a consistent terminology for quantifying species diversity. *Oecologia*, 159, 15-26.

Kaiser, S., Brenke, N., 2016. Epibenthic Sledges. In M.R. Clark, M. Consalvey, A.A. Rowden (Eds.), *Biological Sampling in the Deep Sea*: Wiley Blackwell.

Karner, G.D., Driscoll, N.W., 1999. Tectonic and stratigraphic development of the West African and eastern Brazilian Margins: insights from quantitative basin modelling. In N.R. Cameron, R.H. Bate, V.S. Clure (Eds.), *The Oil and Gas Habitats of the South Atlantic*. Geological Society, London, Special Publications, 153, 11-40.

Karner, G.D., Driscoll, N.W., McGinnis, J.P., Brumbaugh, W.D., Cameron, N.R., 1997. Tectonic significance of syn-rift sediment packages across the Gabon-Cabinda continental margin. *Marine and Petroleum Geology*, 14(7), 973-1000.

Karner, G.D., Gambôa, L.A.P., 2007. Timing and origin of the South Atlantic pre-salt sag basins and their capping evaporites. *Geological Society, London, Special Publications*, 285(1), 15.

Karstensen, J., Stramma, L., Visbeck, M., 2008. Oxygen minimum zones in the eastern tropical Atlantic and Pacific oceans. *Progress in Oceanography*, 77(4), 331-350.

Kelley, C., Kerby, T., Sarradin, P.M., Sarrazin, J., Dhugal, L., 2016. Submersibles and Remotely Operated Vehicles. In M.R. Clark, M. Consalvey, A.A. Rowden (Eds.), *Biological Sampling in the Deep Sea*: Wiley Blackwell.

Kelley, D., Richards, C., 2019. oce: Analysis of Oceanographic Data. R package version 1.1-1. https://CRAN.R-project.org/package=oce.

Khripounoff, A., Vangriesheim, A., Babonneau, N., Crassous, P., Dennielou, B., Savoye, B., 2003. Direct observation of intense turbidity current activity in the Zaire submarine valley at 4000 m water depth. *Marine Geology*, 194(3-4), 151-158.

Kirkman, S.P., Blamey, L., Lamont, T., Field, J.G., Bianchi, G., Huggett, J.A., Hutchings, L., Jackson-Veitch, J., Jarre, A., Lett, C., Lipiński, M.R., Mafwila, S.W., Pfaff, M.C., Samaai, T., Shannon, L.J., Shin, Y.J., van der Lingen, C.D., Yemane, D., 2016. Spatial characterisation of the Benguela ecosystem for ecosystem-based management. *African Journal of Marine Science*, 38(1), 7-22.

Kopte, R., Brandt, P., Dengler, M., Tchipalanga, P.C.M., Macuéria, M., Ostrowski, M., 2017. The Angola Current: Flow and hydrographic characteristics as observed at 11°S. *Journal of Geophysical Research: Oceans*, 122(2), 1177-1189.

Kostianoy, A.G., Lutjeharms, J.R.E., 1999. Atmospheric effects in the Angola-Benguela frontal zone. *Journal of Geophysical Research: Oceans*, 104(C9), 20963-20970.

Kröncke, I., Reiss, H., Türkay, M., 2013. Macro- and megafauna communities in three deep basins of the South-East Atlantic. *Deep Sea Research Part I*, 81, 25-35.

Kröncke, I., Türkay, M., 2003. Structural and functional aspects of the benthic communities in the deep Angola Basin. *Marine Ecology Progress Series*, 260, 43-53.

Krylova, E.M., Cosel, R.v., 2011. A new genus of large Vesicomyidae (Mollusca, Bivalvia, Vesicomyidae, Pliocardiinae) from the Congo margin, with the first record of the subfamily Pliocardiinae in the Bay of Biscay (northeastern Atlantic). *Zoosystema*, 33(1), 83-99, 17.

Kuhnz, L.A., Ruhl, H.A., Huffard, C.L., Smith Jr, K.L., 2014. Rapid changes and long-term cycles in the benthic megafaunal community observed over 24 years in the abyssal northeast Pacific. *Progress in Oceanography*, 124, 1-11.

Kunze, E., Llewellyn-Smith, S.G., 2004. The role of small-scale topography in turbulent mixing of the global ocean. *Oceanography*, 17(1), 55-64.

Lacharité, M., Metaxas, A., 2017. Hard substrate in the deep ocean: How sediment features influence epibenthic megafauna on the eastern Canadian margin. *Deep Sea Research Part I*, 126, 50-61.

Lambshead, P.J.D., Boucher, G., 2003. Marine nematode deep-sea biodiversity – hyperdiverse or hype? *Journal of Biogeography*, 30(4), 475-485.

Lampitt, R.S., Billett, D.S.M., Martin, A.P., 2010. The sustained observatory over the Porcupine Abyssal Plain (PAP): Insights from time series observations and process studies. *Deep Sea Research Part II: Topical Studies in Oceanography*, 57(15), 1267-1271.

Lampitt, R.S., Billett, D.S.M., Rice, A.L., 1986. Biomass of the invertebrate megabenthos from 500 to 4100 m in the northeast Atlantic Ocean. *Marine Biology*, 93(1), 69-81.

Lange, G., Darr, A., Zettler, M.L., 2014. Macrozoobenthic communities in waters off Angola. *African Journal of Marine Science*, 36(3), 313-321.

Langenkämper, D., Zurowietz, M., Schoening, T., Nattkemper, T.W., 2017. BIIGLE 2.0 - Browsing and Annotating Large Marine Image Collections. *Frontiers in Marine Science*, 4(83), 10.3389/fmars.2017.00083.

Lass, H.U., Schmidt, M., Mohrholz, V., Nausch, G., 2000. Hydrographic and Current Measurements in the Area of the Angola–Benguela Front. *Journal of Physical Oceanography*, 30(10), 2589-2609.

Lavier, L.L., Steckler, M.S., Brigaud, F., 2000. An Improved Method for Reconstructing the Stratigraphy and Bathymetry of Continental Margins: Application to the Cenozoic Tectonic and Sedimentary History of the Congo Margin. *American Association of Petroleum Geologists Bulletin*, 84(7), 923-939.

Lavier, L.L., Steckler, M.S., Brigaud, F., 2001. Climatic and tectonic control on the Cenozoic evolution of the West African margin. *Marine Geology*, 178, 63-80.

Lazar, A., Polo, I., Arnault, S., and Mainsant, G., 2006. Kelvin waves activity in the eastern tropical Atlantic. Proceedings of the Symposium on 15 Years of Progress in Radar Altimetry. March 13-18, 2006. Venice, Italy.

Lebrato, M., Jones, D.O.B., 2009. Mass deposition event of *Pyrosoma atlanticum* carcasses off Ivory Coast (West Africa). *Limnology and Oceanography*, 54(4), 1197-1209.

Le Guilloux, E., Olu, K., Bourillet, J.F., Savoye, B., Iglésias, S.P., Sibuet, M., 2009. First observations of deep-sea coral reefs along the Angola margin. *Deep Sea Research Part II*, 56(23), 2394-2403.

Leturmy, P., Lucazeau, F., Brigaud, F., 2003. Dynamic interactions between the gulf of Guinea passive margin and the Congo River drainage basin: 1. Morphology and mass balance. *Journal of Geophysical Research: Solid Earth*, 108(B8).

Levin, L.A., 1991. Interactions between Metazoans and Large, Agglutinating Protozoans: Implications for the Community Structure of Deep-Sea Benthos. *American Zoologist*, 31(6), 886-900.

Levin, L.A., 2003. Oxygen Minimum Zone Benthos: Adaptation and Community Response to Hypoxia. *Oceanography and Marine Biology: an Annual Review*, 41, 1-45.

Levin, L.A., Dayton, P.K., 2009. Ecological theory and continental margins: where shallow meets deep. *Trends in Ecology & Evolution*, 24(11), 606-617.

Levin, L.A., Baco, A.R., Bowden, D.A., Colaco, A., Cordes, E.E., Cunha, M.R., Demopoulos, A.W.J., Gobin, J., Grupe, B.M., Le, J., Metaxas, A., Netburn, A.N., Rouse, G.W., Thurber, A.R., Tunnicliffe, V., Van Dover, C.L., Vanreusel, A., Watling, L., 2016. Hydrothermal Vents and Methane Seeps: Rethinking the Sphere of Influence. *Frontiers in Marine Science*, 3(72).

Levin, L.A., Bett, B.J., Gates, A.R., Heimbach, P., Howe, B.M., Janssen, F., McCurdy, A., Ruhl, H.A., Snelgrove, P., Stocks, K.I., Bailey, D., Baumann-Pickering, S., Beaverson, C., Benfield, M.C., Booth, D.J., Carreiro-Silva, M., Colaço, A., Eblé, M.C., Fowler, A.M., Gjerde, K.M., Jones, D.O.B., Katsumata, K., Kelley, D., Le Bris, N., Leonardi, A.P., Lejzerowicz, F., Macreadie, P.I., McLean, D., Meitz, F., Morato, T., Netburn, A., Pawlowski, J., Smith, C.R., Sun, S., Uchida, H., Vardaro, M.F., Venkatesan, R., Weller, R.A., 2019. Global Observing Needs in the Deep Ocean. *Frontiers in Marine Science*, 6(241).

Levin, L.A., Dayton, P.K., 2009. Ecological theory and continental margins: where shallow meets deep. *Trends in Ecology & Evolution*, 24(11), 606-617.

Levin, L.A., DeMaster, D.J., McCann, L.D., Thomas, C.L., 1986. Effects of giant protozoans (class: Xenophyophorea) on deep-seamount benthos. *Marine Ecology Progress Series*, 29(1), 99-104.

Levin, L.A., Etter, R.J., Rex, M.A., Gooday, A.J., Smith, C.R., Pineda, J., Stuart, C.T., Hessler, R.R., Pawson, D., 2001. Environmental influences on regional deep-sea species diversity. *Annual Review of Ecology and Systematics*, 32, 51-93.

Levin, L.A., Gooday, A.J., 2003. The deep Atlantic Ocean. In P.A. Tyler (Ed.), *Ecosystems of the world: Vol. 28. Ecosystems of Deep Oceans*. Amsterdam: Elsevier.

Levin, L.A., Rouse, G.W., 2020. Giant protists (xenophyophores) function as fish nurseries. *Ecology*, 101(4), e02933.

Levin, L.A., Sibuet, M., 2012. Understanding Continental Margin Biodiversity: A New Imperative *Annual Review of Marine Science*, 4, 79-112.

Levin, S.A., 1992. The Problem of Pattern and Scale in Ecology: The Robert H. MacArthur Award Lecture. *Ecology*, 73(6), 1943-1967.

Linley, T.D., Gerringer, M.E., Yancey, P.H., Drazen, J.C., Weinstock, C.L., Jamieson, A.J., 2016. Fishes of the hadal zone including new species, in situ observations and depth records of Liparidae. *Deep Sea Research Part I*, 114, 99-110.

Lopes, D.A., Hajdu, E., 2014. Carnivorous sponges from deep-sea coral mounds in the Campos Basin (SW Atlantic), with the description of six new species (Cladorhizidae, Poecilosclerida, Demospongiae). *Marine Biology Research*, 10(4), 329-356.

Lübbecke, J.F., Böning, C.W., Keenlyside, N.S., Xie, S.-P., 2010. On the connection between Benguela and equatorial Atlantic Niños and the role of the South Atlantic Anticyclone. *Journal of Geophysical Research: Oceans*, 115(C9).

Lundin, E.R., 1992. Thin-skinned extensional tectonics on a salt detachment, northern Kwanza Basin, Angola. *Marine and Petroleum Geology*, 9(4), 405-411.

Lutz, M.J., Caldeira, K., Dunbar, R.B., Behrenfeld, M.J., 2007a. Seasonal rhythms of net primary production and particulate organic carbon flux to depth describe the efficiency of biological pump in the global ocean. *Journal of Geophysical Research*, 112, C10011, doi:10.1029/2006JC003706.

Lutz, M.J., Caldeira, K., Dunbar, R.B., Behrenfield, M.J., 2007b. Seasonal rhythms of net primary production and particulate organic carbon flux to depth describe the efficiency of biological pump in the global ocean. *Journal of Geophysical Research*, 112.

Maechler, M., Rousseeuw, P., Struyf, A., Hubert, M., Hornik, K., 2019. cluster: Cluster Analysis Basics and Extensions. R package version 2.0.8.

Magurran, A.E., 2004. *Measuring Biological Diversity*. Oxford: Blackwell Publishing.

Maier, S.R., Mienis, F., de Froe, E., Soetaert, K., Lavaleye, M., Duineveld, G., Beauchard, O., van der Kaaden, A.-S., Koch, B.P., van Oevelen, D., 2021. Reef communities associated with 'dead' cold-water coral framework drive resource retention and recycling in the deep sea. *Deep Sea Research Part I*, 175, 103574.

Marcon, Y., Sahling, H., Allais, A.-G., Bohrmann, G., Olu, K., 2014. Distribution and temporal variation of mega-fauna at the Regab pockmark (Northern Congo Fan), based on a comparison of videomosaics and geographic information systems analyses. *Marine Ecology*, 35(1), 77-95.

MARISMA EBSA Workstream, 2020a. Ecologically or Biologically Significant Marine Areas in the Benguela Current Large Marine Ecosystem: Angola, Technical Report - Descriptions. MARISMA Project, Angola. Available at https://cmr.mandela.ac.za/Research-Projects/EBSA-Portal/Angola (accessed July 2021).

MARISMA EBSA Workstream, 2020b. Ecologically or Biologically Significant Marine Areas in the Benguela Current Large Marine Ecosystem: Angola, Technical Report - Descriptions, status assessment and management recommendations. MARISMA

Project, Angola. Available at https://cmr.mandela.ac.za/Research-Projects/EBSA-Portal/Angola (accessed July 2021).

Marshall, N.B., 1952. The Atlantide Expedition. *Nature*, 169(4299), 491-492.

Marsset, T., Droz, L., Dennielou, B., Pichon, E., 2009. Cycles in the architecture of the Quaternary Zaire turbidite system: a possible link with climate. In B. Kneller, O.J. Martinsen, B. McCaffrey (Eds.), *External Controls on Deep-Water Depositional Systems. SEPM Special Publication 92* (pp. 89-106). Tulsa, Oklahoma, U.S.A.: SEPM.

Martinez, M.I., Solís-Marín, F.A., Penchaszadeh, P.E., 2019. First report of Paelopatides (Synallactida, Synallactidae) for the SW Atlantic, with description of a new species from the deep-sea off Argentina. *Zoologischer Anzeiger*, 278, 21-27.

Marton, G.L., Tari, G.C., Lehmann, C.T., 2000. Evolution of the Angolan Passive Margin, West Africa, With Emphasis on Post-Salt Structural Styles. In W. Mohriak, M. Taiwani (Eds.), *Atlantic Rifts and Continental Margins Geophysical Monograph 115* (pp. 129-149). Washington, DC: American Geophysical Union.

Marzoli, A., Melluso, L., Morra, V., Renne, P.R., Sgrosso, I., D'Antonio, M., Duarte Morais, L., Morais, E.A.A., Ricci, G., 1999. Geochronology and petrology of Cretaceous basaltic magmatism in the Kwanza basin (western Angola), and relationships with the Paranà-Etendeka continental flood basalt province. *Journal of Geodynamics*, 28(4), 341-356.

Mauduit, T., Guerin, G., Brun, J.P., Lecanu, H., 1997. Raft tectonics: the effects of basal slope angle and sedimentation rate on progressive extension. *Journal of Structural Geology*, 19(9), 1219-1230.

Mayall, M., Stewart, I., 2000. The Architecture of Turbidite Slope Channels. In P. Weimar (Ed.), *GCSSEPM Foundation 20th Annual Research Conference, Deep-Water Reservoirs of the World, December 3-6, 2000*, Vol. 20 (pp. 578-586): SEPM Society for Sedimentary Geology.

Mazeika, P.A., 1967. Thermal domes in the Eastern Tropical Atlantic Ocean. *Limnology and Oceanography*, 12(3), 537-539.

McClain, C.R., Allen, A.P., Tittensor, D.P., Rex, M.A., 2012. Energetics of life on the deep seafloor. *PNAS*, 109(38), 15366-15371.

McClain, C.R., Barry, J.P., 2010. Habitat heterogeneity, disturbance, and productivity work in concert to regulate biodiversity in deep submarine canyons. *Ecology*, 91(4), 964-976.

McClain, C.R., Barry, J.P., Eernisse, D., Horton, T., Judge, J., Kakui, K., Mah, C., Warén, A., 2016. Multiple processes generate productivity–diversity relationships in experimental wood-fall communities. *Ecology*, 97(4), 885-898.

McClain, C.R., Hardy, S.M., 2010. The dynamics of biogeographic ranges in the deep sea. *Proceedings of the Royal Society of London B: Biological Sciences*, 277(1700), 3533-3546.

McClain, C.R., Rex, M.A., 2015. Toward a Conceptual Understanding of β-Diversity in the Deep-Sea Benthos. *Annual Review of Ecology, Evolution, and Systematics*, 46(1), 623-642.

McClain, C.R., Rex, M.A., Etter, R.J., 2009. Patterns in deep-sea macroecology. In J.D. Witman, K. Roy (Eds.), *Marine Macroecology*. Chicago and London: The University of Chicago Press.

McClain, C.R., Schlacher, T.A., 2015. On some hypotheses of diversity of animal life at great depths on the sea floor. *Marine Ecology*, 36(4), 849-872.

McClain, C.R., Stegen, J.C., Hurlbert, A.H., 2012. Dispersal, environmental niches and oceanic-scale turnover in deep-sea bivalves. *Proceedings of the Royal Society of London B: Biological Sciences*, 279(1735), 1993-2002.

Meeuwis, J.M., Lutjeharms, J.R.E., 1990. Surface thermal characteristics of the Angola-Benguela front. *South African Journal of Marine Science*, 9(1), 261-279.

Mengerink K., J., Van Dover Cindy, L., Ardron, J., Baker, M., Escobar-Briones, E., Gjerde, K., Koslow, J.A., Ramirez-Llodra, E., Lara-Lopez, A., Squires, D., Sutton, T., Sweetman Andrew, K., Levin Lisa, A., 2014. A Call for Deep-Ocean Stewardship. *Science*, 344(6185), 696-698.

Menot, L., Crassous, P., Desbruyères, D., Galéron, J., Khripounoff, A., Sibuet, M., 2009. Colonization patterns along the equatorial West African margin: Implications for functioning and diversity maintenance of bathyal and abyssal communities. *Deep Sea Research Part II*, 56(23), 2313-2325.

Menot, L., Galéron, J., Olu, K., Caprais, J.-C., Crassous, P., Khripounoff, A., Sibuet, M., 2010a. Spatial heterogeneity of macrofaunal communities in and near a giant pockmark area in the deep Gulf of Guinea. *Marine Ecology*, 31(1), 78-93.

Menot, L., Sibuet, M., Carney, R.S., Levin, L.A., Rowe, G.T., Billett, D.S.M., Poore, G., Kitazato, H., Vanreusel, A., Galéron, J., Lavrado, H.P., Sellanes, J., Ingole, B., Krylova, E., 2010b. New Perceptions of Continental Margin Biodiversity. In A.D. McIntyre (Ed.), *Life in the World's Oceans* (pp. 79-101).

Mercier, H., Arhan, M., Lutjeharms, J.R.E., 2003. Upper-layer circulation in the eastern Equatorial and South Atlantic Ocean in January–March 1995. *Deep Sea Research Part I*, 50(7), 863-887.

Merrett, N.R., Marshall, N.B., 1981. Observations on the ecology of deep-sea bottom-living fishes collected off northwest Africa (08-27N). *Progress in Oceanography*, 9(4), 185-244.

Meyer, K.S., Wagner, J.K.S., Ball, B., Turner, P.J., Young, C.M., Van Dover, C.L., 2016. Hyalinoecia artifex: Field notes on a charismatic and abundant epifaunal polychaete on the US Atlantic continental margin. *Invertebrate Biology*, 135(3), 211-224.

Meyers, J.B., Rosendahl, B.R., Jr, J.A.A., 1996. Deep-penetrating MCS images of the South Gabon Basin: implications for rift tectonics and post-breakup salt remobilization. *Basin Research*, 8(1), 65-84.

Miatta, M, Snelgrove, P., 2021a. Sea pen fields as biogenic habitats for macroinfaunal communities in deep-sea sediments: Evidence from the Laurentian Channel MPA. *Book of Abstracts, 16th Deep-Sea Biology Symposium*, Brest, 12-17 September 2021.

Miatta, M., Snelgrove, P.V.R., 2021b. Benthic nutrient fluxes in deep-sea sediments within the Laurentian Channel MPA (eastern Canada): The relative roles of macrofauna, environment, and sea pen octocorals. *Deep Sea Research Part I*, 178, 103655.

Miller, R.J., Smith, C.R., Demaster, D.J., Fornes, W.L., 2000. Feeding selectivity and rapid particle processing by deep-sea megafaunal deposit feeders: A 234Th tracer approach. *Journal of Marine Research*, 58(4), 653-673.

Milligan, R.J., Spence, G., Roberts, J.M., Bailey, D.M., 2016. Fish communities associated with cold-water corals vary with depth and substratum type. *Deep-Sea Research Part I*, 114, 43-54.

Milligan, R.J., Scott, E.M., Jones, D.O.B., Bett, B.J., Jamieson, A.J., O'Brien, R., Pereira Costa, S., Rowe, G.T., Ruhl, H.A., Smith Jr, K.L., de Susanne, P., Vardaro, M.F., Bailey, D.M., 2020. Evidence for seasonal cycles in deep-sea fish abundances: A great migration in the deep SE Atlantic? *Journal of Animal Ecology*, 89(7), 1593-1603.

Mohrholz, V., Bartholomae, C.H., van der Plas, A.K., Lass, H.U., 2008. The seasonal variability of the northern Benguela undercurrent and its relation to the oxygen budget on the shelf. *Continental Shelf Research*, 28(3), 424-441.

Mohriak, W.U., Macedo, J.M., Castellani, R.T., Rangel, H.D., Barros, A.Z.N., Latgé, M.A.L., Ricci, J.A., Mizusaki, A.M.P., Szatmari, P., Demercian, L.S, Rizzo, J.G., Aires, R.J., 1995. Salt tectonics and structural styles in the deep water province of the Cabo Frio region, Rio de Janeiro, Brazil, in M. P. A. Jackson, D. G. Roberts, and S. Snelson, eds., *Salt tectonics: a global perspective*: AAPG Memoir 65, p. 273–304

Mohriak, W.U., Biassusi, A.S., Fernandez, B., 2004. Salt Tectonic Domains and Structural Provinces: Analogies Between the South Atlantic and the Gulf of Mexico, in P.J. Post, D.L. Olson, K.T. Lyons, S.L. Palmes, P.F. Harrison, N.C. Rosen, eds., *Salt Sediment Interactions and Hydrocarbon Prospectivity Concepts, Applications and Case Studies for the 21st Century*, Vol. 24 (p. 0): SEPM Society for Sedimentary Geology.

Mohriak, W.U., Szatmari, P., Anjos, S., 2012. Salt: geology and tectonics of selected Brazilian basins in their global context. Geological Society, London, Special Publications, 363(1), 131.

Moore, J.A., Auster, P.J., 2009. Commensalism between Juvenile Cusk Eels and Pancake Urchins on Western North Atlantic Seamounts. *Bulletin of the Peabody Museum of Natural History*, 50, 381-386.

Morel, A., Antoine, D., Babin, M., Dandonneau, Y., 1996. Measured and modeled primary production in the northeast Atlantic (EUMELI JGOFS program): the impact of natural variations in photosynthetic parameters on model predictive skill. *Deep-Sea Research Part I*, 43(8), 1273-1304.

Morel, A., and Berthon, J.-F., 1989. Surface pigments, algal biomass profiles, and potential production of the euphotic layer: Relationships reinvestigated in view of remote-sensing applications. *Limnology and Oceanography*, 34(8), 1545-1562.

Moroshkin, K.V., Bunov, V.A., and Bulatov, R.P., 1970. Water circulation in the eastern South Atlantic Ocean. *Oceanology*, 10, 27-34.

Morris, K.J., Bett, B.J., Durden, J.M., Benoist, N.M.A., Huvenne, V.A.I., Jones, D.O.B., Robert, K., Ichino, M.C., Wolff, G.A., Ruhl, H.A., 2016. Landscape-scale spatial heterogeneity in phytodetrital cover and megafauna biomass in the abyss links to modest topographic variation. *Scientific Reports*, 6, 34080.

Morris, K.J., Bett, B.J., Durden, J.M., Huvenne, V.A.I., Milligan, R., Jones, D.O.B., McPhail, S., Robert, K., Bailey, D.M., Ruhl, H.A., 2014. A new method for ecological surveying of the abyss using autonomous underwater vehicle photography. *Limnology and Oceanography: Methods*, 12, 795-809.

Mortensen, P.B., Brattegard, T., Hovland, M., Farestveit, R., 1995. Deep water bioherms of the scleractinian coral lophelia pertusa (L.) at 64° n on the norwegian shelf: Structure and associated megafauna. *Sarsia*, 80(2), 145-158.

Mortensen, P.B., Hovland, M.T., Fossa, J.H., Furevik, D.M., 2001. Distribution, abundance and size of Lophelia pertusa coral reefs in mid-Norway in relation to seabed characteristics. *Journal of the Marine Biological Association of the United Kingdom*, 81(4), 581-597.

Mortensen, T., 1951. Report on the Echinoidea collected by the Atlantide Expedition. Atlantide Report No.2. *Scientific Results of the Danish Expedition to the Coasts of Tropical West Africa 1945-1946*, 293-303.

Mosch, T., Sommer, S., Dengler, M., Noffke, A., Bohlen, L., Pfannkuche, O., Liebetrau, V., Wallmann, K., 2012. Factors influencing the distribution of epibenthic megafauna across the Peruvian oxygen minimum zone. *Deep Sea Research Part I*, 68, 123-135.

Moulin, M., Aslanian, D., Olivet, J.L., Contrucci, I., Géli, L., Klingelhoefer, F., Nouzé, H., Matias, L., Réhault, J.P., Unternehr, P., 2005. Geological constraints on the

evolution of the Angolan margin based on reflection and refraction seismic data (ZaïAngo project). *Geophysical Journal International*, 162(3), 793-810.

Mühlenhardt-Siegel, U., 2003. A new Cumacea genus (Crustacea: Peracarida: Diastylidae) from the deep-sea expedition Diva-1 with RV'METEOR' to the Angola Basin. *Beaufortia*, 53(7), 159-165.

Mullins, H.T., Thompson, J.B., McDougall, K., Vercoutere, T.L., 1985. Oxygen-minimum zone edge effects: Evidence from the central California coastal upwelling system. *Geology*, 13(7), 491-494.

Muñoz, P.D., Patrocinio, T., Murillo, F.J., Sacau, M., Fernández, G., Gago, A., Sayago-Gil, M., González-Porto, M., González, E., 2012. Distribution patterns of deep-sea fish and benthic invertebrates from trawlable grounds of the Hatton Bank, north-east Atlantic: Effects of deep-sea bottom trawling. *Journal of the Marine Biological Association of the United Kingdom*, 92(7), 1509-1524.

Muntoni, M., Devillers, R., Koen-Alonso, M., Schindler, D.E., 2019. Science should not be left behind during the design of a marine protected area: meeting conservation priorities while integrating stakeholder interests. *FACETS*, 4(1), 472-492.

Murillo, F.J., MacDonald, B.W., Kenchington, E., Campana, S.E., Sainte-Marie, B., Sacau, M., 2018. Morphometry and growth of sea pen species from dense habitats in the Gulf of St. Lawrence, eastern Canada. *Marine Biology Research*, 14(4), 366-382.

Murray, J., Hjort, J., 1912. The Depths of the Oceans, MacMillan, London.

Mursch, A., Brenke, N., Wägele, J.W., 2008. Results of the DIVA-1 Expedition of RV "*Meteor*" (Cruise M48:1): Three new species of Munnopsidae Sars, 1864 from abyssal depths of the Angola Basin (Crustacea: Isopoda: Asellota). *Zootaxa*, 1866, 493-539.

Murty, S.J., Bett, B.J., Gooday, A.J., 2009. Megafaunal responses to strong oxygen gradients on the Pakistan margin of the Arabian Sea. *Deep Sea Research Part II*, 56(6), 472-487.

NAFO, 2021. Northwest Atlantic Fisheries Organisation: Conservation and Enforcement Measures 2021. Serial No. N7153, NAFO/COM Doc. 21-01. Available at https://www.nafo.int/Portals/0/PDFs/COM/2021/comdoc21-01.pdf (accessed October 2021).

Nørvang, A., 1961. Schizamminidae, a new family of Foraminifera. Atlantide Report No. 6. *Scientific Results of the Danish Expedition to the Coasts of Tropical West Africa 1945-1946*, 169-201.

Oksanen, J., Guillaume Blanchet, F., Friendly, M., Kindt, R., Legendre, P., McGlinn, D., Minchin, P.R., O'Hara, R.B., Simpson, G.L., Solymos, P., Stevens, M.H.H., Szoecs, E., Wagner, H., 2019. vegan: Community Ecology Package. R package version 2.5-5. https://CRAN.R-project.org/package=vegan.

Olabarria, C., 2005. Patterns of bathymetric zonation of bivalves in the Porcupine Seabight and adjacent Abyssal plain, NE Atlantic. *Deep Sea Research Part I*, 52(1), 15-31.

Olu-Le Roy, K., Caprais, J.C., Fifis, A., Fabri, M.C., Galeron, J., Budzinsky, H., Le Menach, K., Khripounoff, A., Ondreas, H., Sibuet, M., 2007. Cold-seep assemblages on a giant pockmark off West Africa: spatial patterns and environmental control. *Marine Ecology-an Evolutionary Perspective*, 28(1), 115-130.

Olu, K., 2011. WASC cruise, RV Pourquoi pas? http://dx.doi.org/10.17600/11030010.

Olu, K., Caprais, J.C., Galéron, J., Causse, R., von Cosel, R., Budzinski, H., Ménach, K.L., Roux, C.L., Levaché, D., Khripounoff, A., Sibuet, M., 2009. Influence of seep emission on the non-symbiont-bearing fauna and vagrant species at an active giant pockmark in the Gulf of Guinea (Congo–Angola margin). *Deep Sea Research Part II*, 56(23), 2380-2393.

Olu, K., Cordes, E.E., Fisher, C.R., Brooks, J.M., Sibuet, M., Desbruyères, D., 2010. Biogeography and Potential Exchanges Among the Atlantic Equatorial Belt Cold-Seep Faunas. *PLoS ONE*, 5(8), e11967.

Olu, K., Decker, C., Pastor, L., Caprais, J.C., Khripounoff, A., Morineaux, M., Ain Baziz, M., Menot, L., Rabouille, C., 2017. Cold-seep-like macrofaunal communities in organic- and sulfide-rich sediments of the Congo deep-sea fan. *Deep Sea Research Part II*, 142, 180-196.

Oluboyo, A.P., Gawthorpe, R.L., Bakke, K., Hadler-Jacobsen, F., 2014. Salt tectonic controls on deep-water turbidite depositional systems: Miocene, southwestern Lower Congo Basin, offshore Angola. *Basin Research*, 26(4), 597-620.

Ondréas, H., Olu, K., Fouquet, Y., Charlou, J.L., Gay, A., Dennielou, B., Donval, J.P., Fifis, A., Nadalig, T., Cochonat, P., Cauquil, E., Bourillet, J.F., Moigne, M.L., Sibuet, M., 2005. ROV study of a giant pockmark on the Gabon continental margin. *Geo-Marine Letters*, 25(5), 281-292.

Orejas, C., Wienberg, C., Titschack, J., Tamborrino, L., Freiwald, A., Hebbeln, D., 2021. Madrepora oculata forms large frameworks in hypoxic waters off Angola (SE Atlantic). *Scientific Reports*, 11(1), 15170.

Ostrowski, M., da Silva, J.C.B., Bazik-Sangolay, B., 2009. The response of sound scatterers to El Niño- and La Niña-like oceanographic regimes in the southeastern Atlantic. *ICES Journal of Marine Science*, 66(6), 1063-1072.

Pace, M.L., Knauer, G.A., Karl, D.M., Martin, J.H., 1987. Primary production, new production and vertical flux in the eastern Pacific Ocean. *Nature*, 325(6107), 803-804.

Palardy, J.E., Witman, J.D., 2011. Water flow drives biodiversity by mediating rarity in marine benthic communities. *Ecology Letters*, 14(1), 63-68.

Paterson, G.L.J., Lambshead, P.J.D., 1995. Bathymetric patterns of polychaete diversity in the Rockall Trough, northeast Atlantic. *Deep Sea Research Part I*, 42(7), 1199-1214.

Pautot, G., Renard, V., Daniel, J., Dupont, J., 1973. Morphology, Limits, Origin, and Age of Salt Layer along South Atlantic African Margin. *The American Association of Petroleum Geologlists Bulletin*, 57(9), 1658-1671.

Pawson, D.L., Vance, D.J., 2004. Chiridota heheva, new species, from Western Atlantic deep-sea cold seeps and anthropogenic habitats (Echinodermata : Holothuroidea : Apodida). *Zootaxa*, 534, 1-12.

Pearcy, W.G., Stein, D.L., Carney, R.S., 1982. The Deep-Sea Benthic Fish Fauna of the Northeastern Pacific Ocean on Cascadia and Tufts Abyssal Plains and Adjoining Continental Slopes. *Biological Oceanography*, 1(4), 375-428.

Pebesma, E.J., Bivand, R.S., 2005. Classes and methods for spatial data in R. https://cran.r-project.org/web/packages/sp/index.html.

Peel, F.J., Travis, C.J., Hossack, R.J., 1995, Genetic structural provinces and salt tectonics of the Cenozoic offshore U.S. Gulf of Mexico: a preliminary analysis, in M.P.A. Jackson, D.G. Roberts, and S. Snelson, eds., *Salt tectonics: a global perspective*: AAPG Memoir 65, p. 153-175.

Peterson, R.G., Stramma, L., 1991. Upper-level circulation in the South Atlantic Ocean. *Progress in Oceanography*, 26(1), 1-73.

Pfannkuche, O., Linke, P., 2003. GEOMAR Landers as long-term deep-sea observatories. *Sea Technology*, 40, 50-55.

Picaut, J., 1983. Propagation of the Seasonal Upwelling in the Eastern Equatorial Atlantic. *Journal of Physical Oceanography*, 13(1), 18-37.

Picot, M., Droz, L., Marsset, T., Dennielou, B., Bez, M., 2016. Controls on turbidite sedimentation: Insights from a quantitative approach of submarine channel and lobe architecture (Late Quaternary Congo Fan). *Marine and Petroleum Geology*, 72, 423-446.

Pierre, C., Blanc-Valleron, M.-M., Demange, J., Boudouma, O., Foucher, J.-P., Pape, T., Himmler, T., Fekete, N., Spiess, V., 2012. Authigenic carbonates from active methane seeps offshore southwest Africa. *Geo-Marine Letters*, 32(5), 501-513.

Pierre, C., Fouquet, Y., 2007. Authigenic carbonates from methane seeps of the Congo deep-sea fan. *Geo-Marine Letters*, 27, 249-257.

Poole, R., Tomczak, M., 1999. Optimum multiparameter analysis of the water mass structure in the Atlantic Ocean thermocline. *Deep Sea Research Part I*, 46(11), 1895-1921.

Pop Ristova, P., Wenzhöfer, F., Ramette, A., Zabel, M., Fischer, D., Kasten, S., Boetius, A., 2012. Bacterial diversity and biogeochemistry of different chemosynthetic habitats of the REGAB cold seep (West African margin, 3160 m water depth). *Biogeosciences*, 9(12), 5031-5048.

Priede, I.G., Godbold, J.A., King, N.J., Collins, M.A., Bailey, D.M., Gordon, J.D.M., 2010. Deep-sea demersal fish species richness in the Porcupine Seabight, NE Atlantic Ocean: global and regional patterns. *Marine Ecology*, 31(1), 247-260.

Purser, A., Thomsen, L., Barnes, C., Best, M., Chapman, R., Hofbauer, M., Menzel, M., Wagner, H., 2013. Temporal and spatial benthic data collection via an internet operated Deep Sea Crawler. *Methods in Oceanography*, 5, 1-18.

Purser, A., Orejas, C., Gori, A., Tong, R., Unnithan, V., Thomsen, L., 2013. Local variation in the distribution of benthic megafauna species associated with cold-water coral reefs on the Norwegian margin. *Continental Shelf Research*, 54, 37-51.

Puth, M.T., Neuhäuser, M., Ruxton, G.D., 2015. On the variety of methods for calculating confidence intervals by bootstrapping. *Journal of Animal Ecology*, 84(4), 892-897.

Quero, J.C., Hureau, J.C., Karrer, C., Post, A., SalDanHa, I., 1990. Check-list of the fishes of the eastern tropical Atlantic. Vol. vol. 1, 1–519, vol. 2, 520-1080, vol. 3 1081-1492. Lisbon: UNESCO.

Quirk, D.G., Schødt, N., Lassen, B., Ings, S.J., Hsu, D., Hirsch, K.K., Von Nicolai, C., 2012. Salt tectonics on passive margins: examples from Santos, Campos and Kwanza basins. *Geological Society, London, Special Publications*, 363(1), 207.

R Core Team, 2020. R: A Language and Environment for Statistical Computing. R Foundation for Statistical Computing, Vienna, Austria. URL http://www.R-project.org/.

Rabouille, C., 2011. CONGOLOBE cruise, RV Pourquoi pas? http://dx.doi.org/10.17600/11030170.

Rabouille, C., Baudin, F., Dennielou, B., Olu, K., 2017a. Organic carbon transfer and ecosystem functioning in the terminal lobes of the Congo deep-sea fan: outcomes of the Congolobe project. *Deep Sea Research Part II*, 142, 1-6.

Rabouille, C., Caprais, J.C., Lansard, B., Crassous, P., Dedieu, K., Reyss, J.L., Khripounoff, A., 2009. Organic matter budget in the Southeast Atlantic continental margin close to the Congo Canyon: In situ measurements of sediment oxygen consumption. *Deep Sea Research Part II*, 56(23), 2223-2238.

Rabouille, C., Dennielou, B., Baudin, F., Raimonet, M., Droz, L., Khripounoff, A., Martinez, P., Mejanelle, L., Michalopoulos, P., Pastor, L., Pruski, A., Ragueneau, O., Reyss, J.L., Ruffine, L., Schnyder, J., Stetten, E., Taillefert, M., Tourolle, J., Olu, K., 2019. Carbon and silica megasink in deep-sea sediments of the Congo terminal lobes. *Quaternary Science Reviews*, 222, 105854.

Rabouille, C., Olu, K., Baudin, F., Khripounoff, A., Dennielou, B., Arnaud-Haond, S., Babonneau, N., Bayle, C., Beckler, J., Bessette, S., Bombled, B., Bourgeois, S., Brandily, C., Caprais, J.C., Cathalot, C., Charlier, K., Corvaisier, R., Croguennec, C., Cruaud, P., Decker, C., Droz, L., Gayet, N., Godfroy, A., Hourdez, S., Le Bruchec, J., Saout, J., Le Saout, M., Lesongeur, F., Martinez, P., Mejanelle, L., Michalopoulos, P., Mouchel, O., Noel, P., Pastor, L., Picot, M., Pignet, P., Pozzato, L., Pruski, A.M., Rabiller, M., Raimonet, M., Ragueneau, O., Reyss, J.L., Rodier, P., Ruesch, B., Ruffine, L., Savignac, F., Senyarich, C., Schnyder, J., Sen, A., Stetten, E., Sun, M.Y., Taillefert, M., Teixeira, S., Tisnerat-Laborde, N., Toffin, L., Tourolle, J., Toussaint, F., Vétion, G., Jouanneau, J.M., Bez, M., 2017b. The Congolobe project, a multidisciplinary study of Congo deep-sea fan lobe complex: Overview of methods, strategies, observations and sampling. *Deep Sea Research Part II*, 142, 7-24.

Ramil, F., Ramos, A., 2017. An Overview on Bathyal Soft-Bottoms Megabenthos off Mauritania. In A. Ramos, F. Ramil, J. L. Sanz (eds.). *Deep-Sea Ecosystems Off Mauritania - Research of Marine Biodiversity and Habitats in the Northwest African Margin*. Springer Science and Business Media, p. 277-315.

Ramirez-Llodra, E., Brandt, A., Danovaro, R., De Mol, B., Escobar, E., German, C.R., Levin, L.A., Martinez Arbizu, P., Menot, L., Buhl-Mortensen, P., Narayanaswamy, B.E., Smith, C.R., Tittensor, D.P., Tyler, P.A., Vanreusel, A., Vecchione, M., 2010. Deep, diverse and definitely different: unique attributes of the world's largest ecosystem. *Biogeosciences*, 7(9), 2851-2899.

Ramirez-Llodra, E., Tyler, P.A., Baker, M.C., Bergstad, O.A., Clark, M.R., Escobar, E., Levin, L.A., Menot, L., Rowden, A.A., Smith, C.R., Van Dover, C.L., 2011. Man and the Last Great Wilderness: Human Impact on the Deep Sea. *PLoS ONE*, 6(8), e22588.

Rasmussen, E.S., 1996. Structural evolution and sequence formation offshore South Gabon during the Tertiary. *Tectonophysics*, 266(1), 509-523.

Reid, J.L., 1989. On the total geostrophic circulation of the South Atlantic Ocean: flow patterns, tracers, and transport. *Progress in Oceanography*, 23, 149-244.

Republic of Angola, 2010. Constitution of the Republic of Angola. National Assembly, Luanda. English version available at https://www.constituteproject.org/constitution/Angola_2010.pdf?lang=en (accessed September 2021).

Rex, M.A., 1981. Community Structure in the Deep-Sea Benthos. *Annual Review of Ecology and Systematics*, 12, 331-352.

Rex, M.A., Crame, J.A., Stuart, C.T., Clarke, A., 2005a. Large-Scale Biogeographic Patterns in Marine Mollusks: A Confluence of History and Productivity? *Ecology*, 86(9), 2288-2297.

Rex, M.A., Etter, R.J., 2010. *Deep-sea Biodiversity - Pattern and Scale*. Cambridge, Massachusetts: Harvard University Press.

Rex, M.A., Etter, R.J., Morris, J.S., Crouse, J., McClain, C.R., Johnson, N.A., Stuart, C.T., Deming, J.W., Thies, R., Avery, R., 2006. Global bathymetric patterns of standing stock and body size in the deep-sea benthos *Marine Ecology Progress Series*, 317, 1-8.

Rex, Michael A., McClain, Craig R., Johnson, Nicholas A., Etter, Ron J., Allen, John A., Bouchet, P., Warén, A., 2005b. A Source-Sink Hypothesis for Abyssal Biodiversity. *The American Naturalist*, 165(2), 163-178.

Rice, A.L., Aldred, R.G., Billett, D.S.M., Thurston, M.H., 1979. The combined use of an epibenthic sledge and a deep-sea camera to give quantitative relevance to macro-benthos samples. *Ambio*, Special Report No. 6, 59-72.

Rice, W.R., 1989. Analyzing Tables of Statistical Tests. *Evolution*, 43(1), 223-225.

Rice, A.L., Thurston, M.H., New, A.L., 1990. Dense aggregations of a hexactinellid sponge, Pheronema carpenteri, in the Porcupine Seabight (northeast Atlantic Ocean), and possible causes. *Progress in Oceanography*, 24(1), 179-196.

Ricklefs, R.E., Jenkins, D.G., 2011. Biogeography and ecology: towards the integration of two disciplines. *Philosophical Transactions: Biological Sciences*, 366(1576), 2438-2448.

Riedel, M., Scherwath, M., Römer, M., Veloso, M., Heesemann, M., Spence, G.D., 2018. Distributed natural gas venting offshore along the Cascadia margin. *Nature Communications*, 9(1), 3264.

Robert, K., Jones, D.O.B., Huvenne, V.A.I., 2014. Megafaunal distribution and biodiversity in a heterogeneous landscape: the iceberg-scoured Rockall Bank, NE Atlantic. *Marine Ecology Progress Series*, 501, 67-88.

Roberts, J.M., Brown, C.J., Long, D., Bates, C.R., 2005. Acoustic mapping using a multibeam echosounder reveals cold-water coral reefs and surrounding habitats. *Coral Reefs*, 24(4), 654-669.

Roberts, J.M., Davies, A.J., Henry, L.A., Dodds, L.A., Duineveld, G.C.A., Lavaleye, M.S.S., Maier, C., van Soest, R.W.M., Bergman, M.J.N., HühnerbachÃ‚Â , V., Huvenne, V.A.I., Sinclair, D.J., Watmough, T., Long, D., Green, S.L., van Haren, H., 2009. Mingulay reef complex: an interdisciplinary study of cold-water coral habitat, hydrography and biodiversity. *Marine Ecology Progress Series*, 397, 139-151.

Roberts, J.M., Henry, L.A., Long, D., Hartley, J.P., 2008. Cold-water coral reef frameworks, megafaunal communities and evidence for coral carbonate mounds on the Hatton Bank, north east Atlantic. *Facies*, 54(3), 297-316.

Roberts, J.M., Wheeler, A.J., Freiwald, A., 2006. Reefs of the Deep: The Biology and Geology of Cold-Water Coral Ecosystems. *Science*, 312(5773), 543.

Rodrigues, C.F., Cunha, M.R., Olu, K., Duperron, S., 2012. The smaller vesicomyid bivalves in the genus Isorropodon (Bivalvia, Vesicomyidae, Pliocardiinae) also harbour chemoautotrophic symbionts. *Symbiosis*, 56(3), 129-137.

Ross, S.W., Quattrini, A.M., 2007. The fish fauna associated with deep coral banks off the southeastern United States. *Deep Sea Research Part I*, 54(6), 975-1007.

Rouault, M., Illig, S., Bartholomae, C., Reason, C.J.C., Bentamy, A., 2007. Propagation and origin of warm anomalies in the Angola Benguela upwelling system in 2001. *Journal of Marine Systems*, 68, 473-488.

Rouby, D., Raillard, S., Guillocheau, F., Bouroullec, R., Nalpas, T., 2002. Kinematics of a growth fault/raft system on the West African margin using 3-D restoration. *Journal of Structural Geology*, 24(4), 783-796.

Rousseeuw, P.J., 1987. Silhouettes: A graphical aid to the interpretation and validation of cluster analysis. *Journal of Computational and Applied Mathematics*, 20, 53-65.

Ruhl, H.A., Smith Jr, K.L., 2004. Shifts in deep-sea community structure linked to climate and food supply. *Science*, 305(5683), 513-515.

Sabato Ceraldi, T., Hodgkinson, R.A., Backé, G., 2017. The petroleum geology of the West Africa margin: an introduction. *Geological Society, London, Special Publications*, 438(1), 1-6.

Sahling, H., Bohrmann, G., Spiess, V., Bialas, J., Breitzke, M., Ivanov, M., Kasten, S., Krastel, S., Schneider, R., 2008. Pockmarks in the Northern Congo Fan area, SW Africa: Complex seafloor features shaped by fluid flow. *Marine Geology*, 249, 206-225.

Saiz-Salinas, J.I., 2007. Sipunculans and echiurans from the deep Angola Basin. *Journal of Natural History*, 41(45-48), 2789-2800.

Saiz-Salinas, J.I., 2007. Sipunculans and echiurans from the deep Angola Basin. *Journal of Natural History*, 41(45-48), 2789-2800.

Saunders, P.M., Fofonoff, N.P., 1976. Conversion of pressure to depth in the ocean. *Deep Sea Research and Oceanographic Abstracts*, 23(1), 109-111.

Savoye, B., Babonneau, N., Dennielou, B., Bez, M., 2009. Geological overview of the Angola–Congo margin, the Congo deep-sea fan and its submarine valleys. *Deep Sea Research Part II: Topical Studies in Oceanography*, 56(23), 2169-2182.

Savoye, B., Cochonat, P., Apprioual, R., Bain, O., Baltzer, A., Bellec, V., Beuzart, P., Bourillet, J.-F., Cagna, R., Cremer, M., Crusson, A., Dennielou, B., Diebler, D., Droz, L., Ennes, J.-C., Floch, G., Guiomar, M., Harmegnies, F., Kerbrat, R., Klein, B., Kuhn, H., Landuré, J.-Y., Lasnier, C., Le Drezen, E., Le Formal, J.-P., Lopez, M., Loubrieu, B., Marsset, T., Migeon, S., Normand, A., Nouzé, H., Ondréas, H., Pelleau, P., Saget, P., Séranne, M., Sibuet, J.-C., Tofani, R., Voisset, M., 2000. Structure et évolution récente de l'éventail turbiditique du Zaïre : premiers résultats

scientifiques des missions d'exploration Zaïango1 & 2 (marge Congo–Angola). *Comptes Rendus de l'Académie des Sciences - Series IIA - Earth and Planetary Science*, 331(3), 211-220.

Schlünz, B., Schneider, R.R., 2000. Transport of terrestrial organic carbon to the oceans by rivers: re-estimating flux- and burial rates. *International Journal of Earth Sciences*, 88(4), 599-606.

Schneider, C.A., Rasband, W.S., Eliceiri, K.W., 2012. NIH Image to ImageJ: 25 years of image analysis. *Nature Methods*, 9, 671-675.

Schneider, R.R., Müller, P.J., Wefer, G., 1994. Late Quaternary paleoproductivity changes off the Congo deduced from stable carbon isotopes of planktonic foraminifera. *Palaeogeography, Palaeoclimatology, Palaeoecology*, 110(3), 255-274.

Schneider, R.R., Price, B., Mueller, P.J., Kroon, D., Alexander, I., 1997. Monsoon related variations in Zaire (Congo) sediment load and influence of fluvial silicate supply on marine productivity in the east equatorial Atlantic during the last 200,000 years. *Paleoceanography*, 12(3), 463-481.

Seifried, S., Plum, C., Schulz, M., 2007. A new species of Parabradya Lang, 1944 (Copepoda: Harpacticoida: Ectinosomatidae) from the abyssal plain of the Angola Basin. *Zootaxa*, 1432, 1-21.

Sellanes, J., Neira, C., Quiroga, E., Teixido, N., 2010. Diversity patterns along and across the Chilean margin: a continental slope encompassing oxygen gradients and methane seep benthic habitats. *Marine Ecology*, 31, 111-124.

Sen, A., Dennielou, B., Tourolle, J., Arnaubec, A., Rabouille, C., Olu, K., 2017. Fauna and habitat types driven by turbidity currents in the lobe complex of the Congo deep-sea fan. *Deep Sea Research Part II*, 142, 167-179.

Sen, A., Ondréas, H., Gaillot, A., Marcon, Y., Augustin, J.-M., Olu, K., 2016. The use of multibeam backscatter and bathymetry as a means of identifying faunal assemblages in a deep-sea cold seep. *Deep Sea Research Part I*, 110, 33-49.

Séranne, M., 1999. Early Oligocene stratigraphic turnover on the west Africa continental margin: a signature of the Tertiary greenhouse-to-icehouse transition? *Terra Nova*, 11(4), 135-140.

Seranne, M., Abeigne, C.R.N., 1999. Oligocene to Holocene sediment drifts and bottom currents on the slope of Gabon continental margin (west Africa) Consequences for sedimentation and southeast Atlantic upwelling. *Sedimentary Geology*, 128, 179-199.

Séranne, M., Anka, Z., 2005. South Atlantic continental margins of Africa: a comparison of the tectonic vs climate interplay on the evolution of equatorial west Africa and SW Africa margins. *Journal of African Earth Sciences*, 43, 283-300.

Serié, C., Huuse, M., Schødt, N.H., 2012. Gas hydrate pingoes: Deep seafloor evidence of focused fluid flow on continental margins. *Geology*, 40(3), 207-210.

Serié, C., Huuse, M., Schødt, N.H., Brooks, J.M., Williams, A., 2017. Subsurface fluid flow in the deep-water Kwanza Basin, offshore Angola. *Basin Research*, 29(2), 149-179.

Shannon, L.V., Agenbag, J.J., Buys, M.E.L., 1987. Large- and mesoscale features of the Angola-Benguela front. *South African Journal of Marine Science*, 5(1), 11-34.

Shannon, L.V., Boyd, A.J., Brundrit, G.B., Taunton-Clark, J., 1986. On the existence of an El Niño-type phenomenon in the Benguela System. *Journal of Marine Research*, 44(3), 495-520.

Shannon, L.V., Chapman, P., 1991. Evidence of Antarctic bottom water in the Angola Basin at 32°S. *Deep Sea Research Part A*, 38(10), 1299-1304.

Shepard, F.P., 1954. Nomenclature based on sand-silt-clay ratios. *Journal of Sedimentary Research*, 24(3), 151-158.

Shepard, F.P., Emery, K.O., 1973. Congo Submarine Canyon and Fan Valley. *The American Association of Petroleum Geologists Bulletin*, 57(9), 1679-1691.

Sibuet, M., 1985. Quantitative distribution of echinoderms (Holothuroidea, Asteroidea, Ophiuroidea, Echinoidea) in relation to organic matter in the sediment in deep basins of the Atlantic Ocean. In B.F. Keegan, B.D.S. O'Connor (Eds.), *Proceedings of the Fifth International Echinoderm Conference Galway, 24-29 September 1984* (pp. 99-108). Rotterdam: A.A. Balkema.

Sibuet, M., Lambert, C.E., Chesselet, R., Laubier, L., 1989. Density of the major size groups of benthic fauna and trophic input in deep basins of the Atlantic Ocean. *Journal of Marine Research*, 47(4), 851-867.

Sibuet, M., Galeron, J., Khripounoff, A., Menot, L., Olu-LeRoy, K., Durrieu, J., Mine, J., 2002. Deep Sea Ecosystems on the Equatorial African Margin : First results of a pluridisciplinary environmental programme and discovery of chemosynthetic based ecosystem. *SPE International Conference on Health, Safety and Environment in Oil and Gas Exploration and Production, 20-22 March 2002* (p. 15). Kuala Lumpur, Malaysia: Society of Petroleum Engineers.

Sibuet, M., Olu, K., 1998. Biogeography, biodiversity and fluid dependence of deep-sea cold-seep communities at active and passive margins. *Deep Sea Research Part II*, 45(1), 517-567.

Sibuet, M., Vangriesheim, A., 2009. Deep-sea environment and biodiversity of the West African Equatorial margin. *Deep Sea Research Part II*, 56(23), 2156-2168.

Simon-Lledó, E., Bett, B.J., Huvenne, V.A.I., Schoening, T., Benoist, N.M.A., Jeffreys, R.M., Durden, J.M., Jones, D.O.B., 2019a. Megafaunal variation in the abyssal

landscape of the Clarion Clipperton Zone. *Progress in Oceanography*, 170, 119-133.

Simon-Lledó, E., Bett, B.J., Huvenne, V.A.I., Schoening, T., Benoist, N.M.A., Jones, D.O.B., 2019b. Ecology of a polymetallic nodule occurrence gradient: Implications for deep-sea mining. *Limnology and Oceanography*, 64(5), 1883-1894.

Sinniger, F., Pawlowski, J., Harii, S., Gooday, A.J., Yamamoto, H., Chevaldonné, P., Cedhagen, T., Carvalho, G., Creer, S., 2016. Worldwide Analysis of Sedimentary DNA Reveals Major Gaps in Taxonomic Knowledge of Deep-Sea Benthos. *Frontiers in Marine Science*, 3(92).

Smith, C.R., Demopoulos, A.W.J., 2003. The Deep Pacific Ocean Floor. In P.A. Tyler (Ed.), *Ecosystems of the world: Vol. 28. Ecosystems of Deep Oceans*. Amsterdam: Elsevier.

Smith, C.R., Hamilton, S.C., 1983. Epibenthic megafauna of a bathyal basin off southern California: patterns of abundance, biomass, and dispersion. *Deep Sea Research Part A*, 30(9), 907-928.

Smith, K., Kaufmann, R.S., Wakefield, W.W., 1993. Mobile megafaunal activity monitored with a time-lapse camera in the abyssal North Pacific. *Deep Sea Research Part I*, 40(11-12), 2307-2324.

Smith, K.L., 1983. Metabolism of two dominant epibenthic echinoderms measured at bathyal depths in the Santa Catalina Basin. *Marine Biology*, 72(3), 249-256.

Soberón, J., 2007. Grinnellian and Eltonian niches and geographic distributions of species. *Ecology Letters*, 10(12), 1115-1123.

Sobrino, I., González, J., Hernández-González, C.L., Balguerias, E., 2012. Distribution and relative abundance of main species of grenadiers (Macrouridae, Gadiformes) from the African Atlantic Coast. *Journal of Ichthyology*, 52(10), 690-699.

Soltwedel, T., Jaeckisch, N., Ritter, N., Hasemann, C., Bergmann, M., Klages, M., 2009. Bathymetric patterns of megafaunal assemblages from the arctic deep-sea observatory HAUSGARTEN. *Deep Sea Research Part I*, 56(10), 1856-1872.

Spathopoulos, F., 1996. An insight on salt tectonics in the Angola Basin, South Atlantic. *Geological Society, London, Special Publications*, 100(1), 153-174.

Stankiewicz, J., de Wit, M.J., 2006. A proposed drainage evolution model for Central Africa - Did the Congo flow east? *Journal of African Earth Sciences*, 44(1), 75-84.

Stefanoudis, P.V., Bett, B.J., Gooday, A.J., 2016. Abyssal hills: Influence of topography on benthic foraminiferal assemblages. *Progress in Oceanography*, 148, 44-55.

Stetten, E., Baudin, F., Reyss, J.-L., Martinez, P., Charlier, K., Schnyder, J., Rabouille, C., Dennielou, B., Coston-Guarini, J., Pruski, A.M., 2015. Organic matter characterization and distribution in sediments of the terminal lobes of the Congo

deep-sea fan: Evidence for the direct influence of the Congo River. *Marine Geology*, 369, 182-195.

Stevenson, A., Rocha, C., 2013. Evidence for the bioerosion of deep-water corals by echinoids in the Northeast Atlantic. *Deep Sea Research Part I*, 71, 73-78.

Stone, R.P., 2006. Coral habitat in the Aleutian Islands of Alaska: depth distribution, fine-scale species associations, and fisheries interactions. *Coral Reefs*, 25(2), 229-238.

Storch, D., Gaston, K.J., 2004. Untangling ecological complexity on different scales of space and time. *Basic and Applied Ecology*, 5(5), 389-400.

Stramma, L., England, M., 1999. On the water masses and mean circulation of the South Atlantic Ocean. *Journal of Geophysical Research: Oceans*, 104(C9), 20863-20883.

Stramma, L., Schott, F., 1999. The mean flow field of the tropical Atlantic Ocean. *Deep Sea Research Part II*, 46(1), 279-303.

Strømme, T., Sætersdal, G., 1986. Report on the surveys of Angolas marine fish resources January 1985 - June 1986. Institute of Marine Research, Bergen.

Suess, E., 1980. Particulate organic carbon flux in the oceans - surface productivity and oxygen utilization. *Nature*, 288(5788), 260-263.

Svavarsson, J.T., 1997. Diversity of isopods (Crustacea): New data from the Arctic and Atlantic Ocean. *Biodiversity and Conservation*, 6, 1571-1579.

Swan, J.M.A., 1970. An Examination of Some Ordination Problems By Use of Simulated Vegetational Data. *Ecology*, 51(1), 89-102.

Tews, J., Brose, U., Grimm, V., Tielborger, K., Wichmann, M.C., Schwager, M., Jeltsch, F., 2004. Animal species diversity driven by habitat heterogeneity/diversity: the importance of keystone structures. *Journal of Biogeography*, 31, 79-92.

Thiem, Ø., Ravagnan, E., Fosså, J.H., Berntsen, J., 2006. Food supply mechanisms for cold-water corals along a continental shelf edge. *Journal of Marine Systems*, 60(3), 207-219.

Thomas, E.A., Liu, R., Amon, D., Copley, J.T., Glover, A.G., Helyar, S.J., Olu, K., Wiklund, H., Zhang, H., and Sigware, J., 2020. *Chiridota heheva* - the cosmopolitan holothurian. *Marine Biodiversity*, 50, 110.

Thomson, C.W., Murray, J., 1895. Report of the scientific results of the voyage of H.M.S. Challenger during the years 1873-76, London.

Thurston, M.H., Bett, B.J., Rice, A.L., Jackson, P.A.B., 1994. Variations in the invertebrate abyssal megafauna in the North Atlantic Ocean. *Deep Sea Research Part I*, 41(9), 1321-1348.

Tittensor, D.P., Rex, M.A., Stuart, C.T., McClain, C.R., Smith, C.R., 2011. Species-energy relationships in deep-sea molluscs. *Biology Letters*, 7, 718-722.

Torsvik, T.H., Rousse, S., Labails, C., Smethurst, M.A., 2009. A new scheme for the opening of the South Atlantic Ocean and the dissection of an Aptian salt basin. *Geophysical Journal International*, 177(3), 1315-1333.

Tselepides, A., 2000. Macrobenthic community structure over the continental margin of Crete (South Aegean Sea, NE Mediterranean). *Progress in Oceanography*, 46, 401-428.

Tuomisto, H., 2010a. A diversity of beta diversities: straightening up a concept gone awry. Part 1. Defining beta diversity as a function of alpha and gamma diversity. *Ecography*, 33(1), 2-22.

Tuomisto, H., 2010b. A diversity of beta diversities: straightening up a concept gone awry. Part 2. Quantifying beta diversity and related phenomena. *Ecography*, 33(1), 23-45.

Tweddle, D., Anderson, M.E., 2008. A collection of marine fishes from Angola, with notes on new distribution records. *Smithiana Bulletin*, 8, 3-24.

Tyler, P.A., 1988. Seasonality in the deep-sea. *Oceanography and Marine Biology: an Annual Review*, 26, 227-258.

Uchupi, E., 1992. Angola Basin: Geohistory and Construction of the Continental Rise. In C.W. Poag, P.C. de Graciansky (Eds.), *Geologic Evolution of Atlantic Continental Rises* (pp. 77-99). New York: Van Nostrand Reinhold.

United Nations Country Team Angola, 2019. United Nations Sustainable Development Cooperation Framework Angola 2020-2022. Available at https://angola.un.org/sites/default/files/2020-10/Doc-UNSDCF-Angola-ENG-0804.pdf (accessed September 2021).

Unterseh, S.L., 2013. Early Recognition of Seabed and Sub-Seabed Natural Hydrocarbon Seeps in Deep Offshore Angola. *Offshore Technology Conference* (p. 7). Houston, Texas, USA: Offshore Technology Conference.

Uthicke, S., Schaffelke, B., Byrne, M., 2009. A boom–bust phylum? Ecological and evolutionary consequences of density variations in echinoderms. *Ecological Monographs*, 79(1), 3-24.

Valle, P.J., Gjelberg, J.G., Helland-Hansen, W., 2001. Tectonostratigraphic development in the eastern Lower Congo Basin, offshore Angola, West Africa. *Marine and Petroleum Geology*, 18, 909-927.

Van Bennekom, A.J., Berger, G.W., 1984. Hydrography and silica budget of the Angola Basin. *Netherlands Journal of Sea Research*, 17(2-4), 149-200.

Van Bennekom, A.J., Berger, G.W., Helder, W., and De Vries, R.T.P., 1978. Nutrient distribution in the Zaire estuary and river plume. *Netherlands Journal of Sea Research*, 12(3-4), 296-323.

Van Gaever, S., Galéron, J., Sibuet, M., Vanreusel, A., 2009. Deep-sea habitat heterogeneity influence on meiofaunal communities in the Gulf of Guinea. *Deep Sea Research Part II*, 56(23), 2259-2269.

van Oevelen, D., Soetaert, K., Heip, C., 2012. Carbon flows in the benthic food web of the Porcupine Abyssal Plain: The (un)importance of labile detritus in supporting microbial and faunal carbon demands. *Limnology and Oceanography*, 57(2), 645-664.

van Soest, R.W.M., Cleary, D.F.R., de Kluijver, M.J., Lavaleye, M.S.S., Maier, C., van Duyl, F.C., 2007. Sponge diversity and community composition in Irish bathyal coral reefs. *Contributions to Zoology*, 76(2), 121-142.

van Weering, T.C.E., van Iperen, J., 1984. Fine-grained sediments of the Zaire deep-sea fan, southern Atlantic Ocean. *Geological Society, London, Special Publications*, 15(1), 95-113.

Vangriesheim, A., Khripounoff, A., Crassous, P., 2009. Turbidity events observed in situ along the Congo submarine channel. *Deep Sea Research Part I*, 56, 2208-2222.

Vangriesheim, A., Marie Treguier, A., Andre, G., 2005. Biweekly current oscillations on the continental slope of the Gulf of Guinea. *Deep Sea Research Part I*, 52(11), 2168-2183.

Vardaro, M.F., Bagley, P.M., Bailey, D.M., Bett, B.J., Jones, D.O.B., Milligan, R.J., Priede, I.G., Risien, C.M., Rowe, G.T., Ruhl, H.A., Sangolay, B.B., Smith, K.L., Walls, A., Clarke, J., 2013. A Southeast Atlantic deep-ocean observatory: first experiences and results. *Limnology and Oceanography-Methods*, 11, 304-315.

Veitch, J., 2009. Equilibrium dynamics of the Benguela system: a numerical modelling approach. PhD thesis. University of Cape Town.

von Nicolai, C., Scheck-Wenderoth, M., Warsitzka, M., Schødt, N., Andersen, J., 2013. The deep structure of the South Atlantic Kwanza Basin - Insights from 3D structural and gravimetric modelling. *Tectonophysics*, 604, 139-152.

Wacongne, S., Piton, B., 1992. The near-surface circulation in the northeastern corner of the South Atlantic ocean. *Deep Sea Research Part A*, 39(7), 1273-1298.

Wagstaff, M.C., Howell, K.L., Bett, B.J., Billett, D.S.M., Brault, S., Stuart, C.T., Rex, M.A., 2014. beta-diversity of deep-sea holothurians and asteroids along a bathymetric gradient (NE Atlantic). *Marine Ecology Progress Series*, 508, 177-185.

Wakefield, W.W., Genin, A., 1987. The use of a Canadian (perspective) grid in deep-sea photography. *Deep Sea Research Part A*, 34(3), 469-478.

Walbridge, S., Slocum, N., Pobuda, M., Wright, D.J., 2018. Unified Geomorphological Analysis Workflows with Benthic Terrain Modeler. *Geosciences*, 8(3).

Walgenwitz, F., Richert, J.P., Charpentier, P., 1992. Southwest African plate margin; thermal history and geodynamical implications. In C.W. Poag, P.C. de Graciansky (Eds.), *Geologic Evolution of Atlantic Continental Rises* (pp. 20-45). New York: Van Nostrand Reinhold.

Warén, A., Bouchet, P., 2009. New gastropods from deep-sea hydrocarbon seeps off West Africa. *Deep Sea Research Part II*, 56(23), 2326-2349.

Warwick, R.M., 1986. A new method for detecting pollution effects on marine macrobenthic communities. *Marine Biology*, 92(4), 557-562.

Wasmund, N., Lass, H.U., Nausch, G., 2005. Distribution of nutrients, chlorophyll and phytoplankton primary production in relation to hydrographic structures bordering the Benguela-Angolan frontal region. *African Journal of Marine Science*, 27(1), 177-190.

Wefing, A.-M., Arps, J., Blaser, P., Wienberg, C., Hebbeln, D., Frank, N., 2017. High precision U-series dating of scleractinian cold-water corals using an automated chromatographic U and Th extraction. *Chemical Geology*, 475, 140-148.

Wei, C.-L., Rowe, G.T., 2009. Faunal zonation of large epibenthic invertebrates off North Carolina revisited. *Deep Sea Research Part II*, 56, 1830-1833.

Wei, C.-L., Rowe, G.T., Escobar-Briones, E., Boetius, A., Soltwedel, T., Caley, M.J., Soliman, Y., Huettmann, F., Qu, F., Yu, Z., Pitcher, C.R., Haedrich, R.L., Wicksten, M.K., Rex, M.A., Baguley, J.G., Sharma, J., Danovaro, R., MacDonald, I.R., Nunnally, C.C., Deming, J.W., Montagna, P., Lévesque, M., Weslawski, J.M., Wlodarska-Kowalczuk, M., Ingole, B.S., Bett, B.J., Billett, D.S.M., Yool, A., Bluhm, B.A., Iken, K., Narayanaswamy, B.E., 2010. Global Patterns and Predictions of Seafloor Biomass Using Random Forests. *PLoS ONE*, 5(12), e15323.

Weiss, R.F., 1970. The solubility of nitrogen, oxygen and argon in water and seawater. *Deep Sea Research and Oceanographic Abstracts*, 17(4), 721-735.

Wenau, S., Spieß, V., Pape, T., Fekete, N., 2017. Controlling mechanisms of giant deep water pockmarks in the Lower Congo Basin. *Marine and Petroleum Geology*, 83, 140-157.

Wenau, S., Spiess, V., Pape, T., Fekete, N., 2015a. Cold seeps at the salt front in the Lower Congo Basin I: Current methane accumulation and active seepage. *Marine and Petroleum Geology*, 67, 894-908.

Wenau, S., Spiess, V., Pape, T., Fekete, N., 2015b. Cold seeps at the salt front in the Lower Congo Basin II: The impact of spatial and temporal evolution of salt-tectonics on hydrocarbon seepage. *Marine and Petroleum Geology*, 67, 880-893.

Wentworth, C.K., 1922. A scale of grade and class terms for clastic sediments. *Journal of Geology*, 30, 377-392.

Westphal, H., Beuck, L., Braun, S., Freiwald, A., Hanebuth, T., Hetzinger, S., Klicpera, A., Kudrass, H., Lantzsch, H., Lundälv, T., Vicens, G.M., Preto, N., Reumont, J., Schilling, S., Taviani, M., Wienberg, C., 2012. Phaeton - Paleoceanographic and paleo-climatic record on the Mauritanian Shelf. RV MariaS. Merian Cruise MSM16/3,Bremerhaven - Mindelo, 13.10. 20.11.2010., 53pp.

Wetzel, A., 1993. The Transfer of River Load to Deep-Sea Fans: A Quantitative Approach. *AAPG Bulletin*, 77(10), 1679-1692.

Whittaker, R.H., 1960. Vegetation of the Siskiyou Mountains, Oregon and California. *Ecological Monographs*, 30(3), 279-338.

Whittaker, R.H., 1967. Gradient Analysis of Vegetation. *Biological Review*, 49, 207-264.

Whittaker, R.H., 1972. Evolution and measurement of species diversity. *Taxon*, 21(2-3), 213-251.

Wienberg, C., Heidkamp, S., Hebbeln, D., Beuck, L., Freiwald, A., Pfannkuche, O., Monteys, X., 2008. Franken Mound: Facies and biocoenoses on a newly-discovered "carbonate mound" on the western Rockall Bank, NE Atlantic. *Facies*, 54(1), 1-24.

Wiens, J.J., 2011. The niche, biogeography and species interactions. *Philosophical Transactions of the Royal Society B - Biological Sciences*, 366, 2336-2350.

Williams, A., Althaus, F., Dunstan, P.K., Poore, G.C.B., Bax, N.J., Kloser, R.J., McEnnulty, F.R., 2010. Scales of habitat heterogeneity and megabenthos biodiversity on an extensive Australian continental margin (100-1100m depths). *Marine Ecology*, 31(1), 222-236.

Wishner, K., Levin, L., Gowing, M., Mullineaux, L., 1990. Involvement of the oxygen minimum in benthic zonation on a deep seamount. *Nature*, 346, 57-59.

Wittmann, K.J., 2020. Lophogastrida and Mysida (Crustacea) of the “DIVA-1” deep-sea expedition to the Angola Basin (SE-Atlantic). *European Journal of Taxonomy*, 628.

Woolley, S.N.C., Tittensor, D.P., Dunstan, P.K., Guillera-Arroita, G., Lahoz-Monfort, J.J., Wintle, B.A., Worm, B., O'Hara, T.D., 2016. Deep-sea diversity patterns are shaped by energy availability. *Nature*, doi:10.1038/nature17937.

WoRMS Editorial Board, 2020. World Register of Marine Species. Available from http://www.marinespecies.org at VLIZ. Accessed throughout 2017-2020. doi:10.14284/170.

Wright, D.H., 1983. Species-Energy Theory: An Extension of Species-Area Theory. *Oikos*, 41(3), 496-506.

Wright, J., Rothery, D.A., 2007. *The Ocean Basins: Their Structure and Evolution. 2nd Edition*: The Open University.

Yeh, J., Drazen, J.C., 2009. Depth zonation and bathymetric trends of deep-sea megafaunal scavengers of the Hawaiian Islands. *Deep Sea Research Part I*, 56(2), 251-266.

Yemane, D., Kirkman, S.P., Kathena, J., N'siangango, S.E., Axelsen, B.E., Samaai, T., 2014. Assessing changes in the distribution and range size of demersal fish populations in the Benguela Current Large Marine Ecosystem. *Reviews in Fish Biology and Fisheries*, 24(2), 463-483.

Zettler, M.L., Freiwald, A., Guerra-García, J.M., 2018. Cold-water corals off Angola as refuge for a new Aeginella species (Crustacea: Amphipoda: Caprellidae). *Zootaxa*, 4462 4, 535-546.

Zhang, G., Qu, H., Chen, G., Zhao, C., Zhang, F., Yang, H., Zhao, Z., Ma, M., 2019. Giant discoveries of oil and gas fields in global deepwaters in the past 40 years and the prospect of exploration. *Journal of Natural Gas Geoscience*, 4(1), 1-28.

Zibrowius, H., Gili, J.-M., 1990. Deep-water scleractinia (Cnidaria: Anthozoa) from Namibia, South Africa, and Walvis Ridge, southeastern Atlantic. *Scientia Marina*, 54(1), 19-46.

# Appendix A

# Photographic analysis methods

## A.1 Introduction

This appendix details the steps taken to process the seabed photographs together with the camera platforms used to acquire the imagery. Image processing steps specific to individual research questions are summarised in the respective thesis chapters.

## A.2 Camera platforms

All analysed seabed imagery was obtained with towed deep-water camera systems, which consisted of steel frames fitted with video and stills cameras, lights for illumination, flashguns, power supply, and instrumentation for vehicle navigation and tracking.

During the 2005 survey, the National Oceanography Centre's Wide-Angle Seabed Photography (WASP) camera system was employed (Figure A.1). WASP is a self-contained, off-bottom photographic platform capable of operating in water depth of up to 6000 metres (Jones et al., 2009). Seabed imagery was recorded with vertically mounted video (OceanCam6000V) and film (OSIL Mk7) cameras, both set to be automatically activated by the attached altimeter when the sensor is located less than 10 m from the seabed. The stills camera was programmed to take a photograph every 12 s (Bett, 2007), and images were printed on to 35 mm film along with frame identification number and camera altitude. Vehicle navigation was achieved using an acoustic telemetry system, which consisted of an active transmitter (10 kHz) mounted to the camera frame, a submerged downward-looking tow fish as transducer and a "Waterfall" system on the survey vessel to provide continuous monitoring of acoustic signals. Typically, the frame was towed along the seabed for 30 minutes, but failure of equipment resulted in shorter transects at several locations.

In 2008, seabed imagery was collected with a Seatronics drop frame fitted with a 5 megapixel Kongsberg OE14-208 digital stills camera, and a pair of parallel point lasers spaced 38 cm apart (Hughes and Hunt, 2008). The Seatronics DTS 6000 digital video

telemetry system provided power for cameras and lights and a real time video link to the vessel, where video was continuously recorded to VHS video and DVD. The stills camera was triggered manually to take account of varying flash recharge time and vertical movements of the camera frame caused by swell of the towing vessel. Typically, photographs were taken with a time gap of at least 10 seconds. The location of the camera frame was tracked with an ultra-short baseline (USBL) transponder beacon mounted within the vehicle and linked to the ship's geographic positioning system.

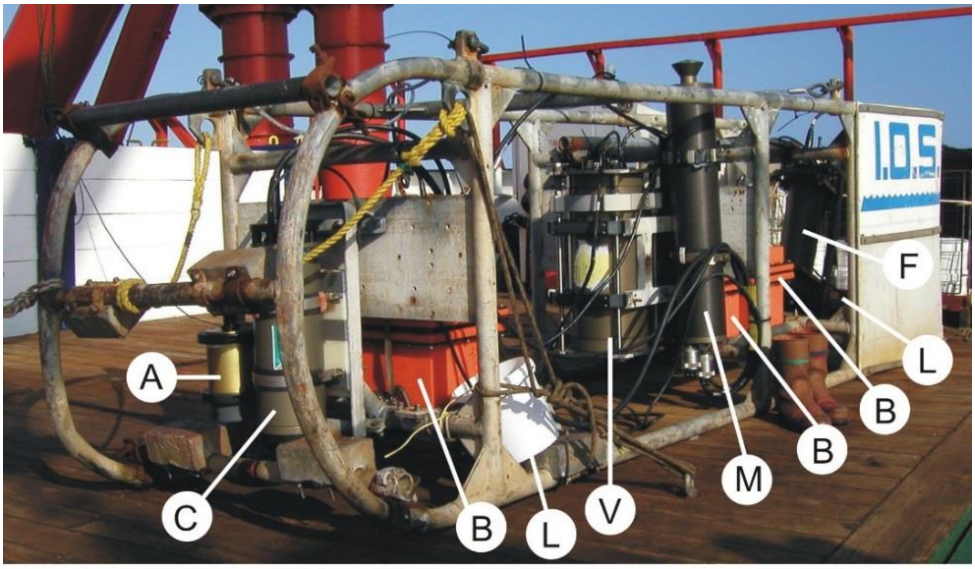


**Figure A.1** The NOC WASP camera system as an example of the towed-camera vehicles used to survey the Angolan slope, shown with the main components marked. A - altimeter, B - batteries, C - still camera, F - flashgun, L - video lamps, M - acoustic transmitter, V - video camera. Image © NOCS

During the survey conducted in 2014, the camera platform carried a wide angle high-definition video camera (SubCControl 1Cam), which was connected to the survey vessel via a coaxial cable (IMAR Survey, 2015a). Still images were initially obtained with a 14 megapixel Imenco TigerShark SDS1210 digital camera, which was later replaced by a 5 megapixel Kongsberg OE14-208 camera. Both stills cameras were programmed to take an image every 15 s. Two sets of parallel lasers spaced 7 and 10 cm apart provided capabilities for scaling. Positional information of the imaging platform was recorded at 3 second interval with an USBL beacon linked to the ship's Sonardyne USBL acoustic tracking system.

The specifications of the different camera platforms and the characteristics of the obtained photographs are summarised in Table A.1.

**Table A.1** Photographic instruments used to survey the Angolan continental slope in 2005, 2008 and 2014 with key characteristics of the obtained seabed photographs. Information was derived from the respective cruise reports (Bett, 2007; Hughes and Hunt, 2008; IMAR Survey, 2015a).

| | **2005** | **2008** | **2014** |
|---|---|---|---|
| **Vessel** | MV *Ocean Endeavour* | MV *Sea Trident* | MV *Ocean Discovery* |
| **Survey period** | 13 Oct - 6 Nov 2005 | 28 Mar - 23 April 2008 | 4 Jul - 11 Sept 2014 |
| **Camera platform** | NOC WASP system | Seatronics DTS 6000 Mini Multiplexer | Sea and Sun deep water camera system |
| **Camera orientation** | Vertical | Oblique[1] or vertical | Vertical |
| **Towing speed** | Not specified - inferred from positioning data | Not specified - inferred from positioning data | 1 to 3 knots |
| **Video camera** | OceanCam6000V loaded with a 63 minute MiniDV tape | Video recorded through stills camera because of failure of video camera focus | Wide angle SubCControl 1Cam |
| **Stills camera** | 35 mm OSIL Mk7, loaded with c. 40 m of Kodak Vision 250D, OSIL 1200J flash gun | Kongsberg/Simrad OE14-208, one strobe | Imenco TigerShark SDS1210 and Kongsberg/Simrad OE14-208, one strobe |
| **Lighting** | Two 250W DSPL video lamps | Four LED lamps | Three Bowtech LED lamps |
| **Image interval** | 12 s | > 10 s | 15 s |
| **Image trigger** | Automatic | Manual | Automatic |
| **Image scaling** | Altimeter information | Green line laser set 38 cm apart | Red point laser set 7 cm apart or green line laser set 10 cm apart |
| **Image format** | Analog, microfilm | Digital, JPEG | Digital, JPEG |
| **Pixel dimensions** | - | 2592 x 1944 pixels | 4320 x 3240[2] pixels, 2592 x 1944[3] pixels |
| **Acceptance angles[4]** | 35 x 50 | 47.8 x 36.2 | 46.7 x 36.8[2], 47.8 x 36.2[3] |
| **Altimeter** | Simrad Mesotech 200 kHz | Not used because of equipment failure | Not used because of equipment failure |
| **Positioning** | Acoustic telemetry system (10 kHz) received through tow fish and monitored with a waterfall display system | USBL transponder beacon | USBL transponder beacon |
| **Positioning accuracy** | Not specified | Not specified | ± 10 m |

[1] Images captured with oblique camera settings were not analysed as part of this study

[2] Imenco TigerShark SDS1210

[3] Kongsberg/Simrad OE14-208

[4] Field of view for stills cameras - horizontal degrees x vertical degrees

## A.3 Image selection and pre-processing

Photographs unsuitable for analysis were removed from the data sets. This included all images where suspended matter or disturbed sediments obscured view of most of the seabed, and images that were overexposed or out of focus. Photographs in which light scattering obscured view around the upper edges but which were otherwise acceptable for analysis were cropped. For the images taken in 2014, the area to be excluded was selected per image altitude bin, and subsequent cropping was carried out using the batch processing tool in Adobe Photoshop CS6. Images taken in 2008 showed a more varied distribution of areas affected by sediment clouds or backscatter compared with the photographs obtained in 2014. For these images, areas unacceptable for analysis were recorded individually for each image as part of the annotation process. Similarly, for the photographic frames collected in 2005 areas unsuitable for reliable detection and identification of megafauna were identified while annotating. Image vignetting in photographs from 2014 was further minimised by applying flatfield corrections to the intensity (V) channel of each image, implemented in MATLAB (R2015a) as described by Morris et al. (2014).

## A.4 Scaling of imagery

The seabed area covered by an image was determined either based on camera altitude or, when camera height was unknown, by using the scale provided by the parallel laser beams. Figure A.2 illustrates the geometry of a seabed image and the notations used to calculate image dimensions.

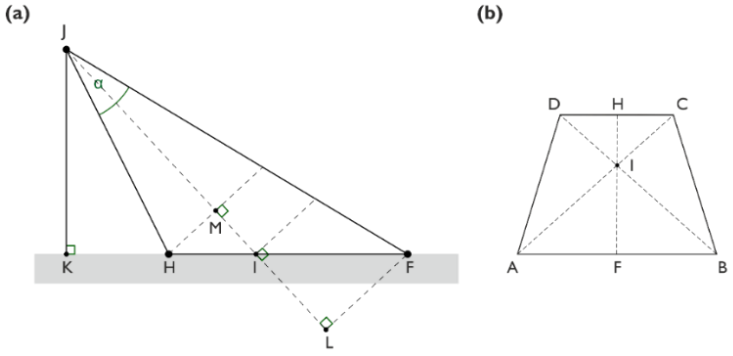


**Figure A.2** Schematic of the geometry for an image taken from an oblique angle to the seabed (redrawn from Durden et al., 2016). **(a)** Lateral view showing the camera focal point J, the camera nadir K, and the vertical acceptance angle α. The distance JK is the height of the camera above the seabed. The distance of the camera to the top and bottom edge of the image is represented by JF and JH. I denotes the principal point on the optical axis. **(b)** Top view of the area pictured on the seabed. Seafloor coverage is represented by the trapezoid ABCD with height HF. For images taken perpendicular to a flat seabed the area of view is represented by a rectangle and JK = JM = JI = JL.

### A.4.1 Scaling using altitude data

For the photographs collected with the WASP camera system, camera altitude imprinted on the photograph was used to calculate the height and width of the visible seafloor area, as:

$$AB = 2\ x\ altitude\ x \tan\left(\frac{\beta}{2}\right) \quad (1)$$

$$AD = 2\ x\ altitude\ x \tan\left(\frac{\alpha}{2}\right) \quad (2)$$

where α and β are the camera's vertical and horizontal acceptance angles, respectively. It was assumed that photographs were taken across level terrain. For the area of seafloor covered by a photograph it follows:

$$Image\ area = 4\ x\ altitude^2\ x \tan\left(\frac{\beta}{2}\right) x \tan\left(\frac{\alpha}{2}\right) \quad (3)$$

Several frames had no or incorrect altitude readings. Camera height of these frames was estimated by comparing the frame's colour and illumination patterns to those patterns in frames with known altitude. The error of approximation has been estimated as ± 0.25 m.

### A.4.2 Scaling using laser markers

For the photographic data collected in 2008 and 2014, image altitude and seafloor coverage were calculated by converting measured pixel distances between the two laser markers to seabed distances, following the trigonometric approach outlined in Wakefield and Genin (1987) and Durden et al. (2016). Whenever visible the beams of the green line laser were used for scaling to determine any deviation from a level plane caused by sloping terrain or change in inclination of the camera. Distances between the two laser lines were first measured along the upper and lower edge of the image, using the ImageJ software (Schneider et al., 2012). Seafloor coverage was then calculated as trapezoid:

$$Image\ area = \frac{1}{2} \times (AB + CD) \times HF \quad (4)$$

The bases of the trapezoid $AB$ and $CD$ were derived from converting the measured number of pixels between the two laser lines to length values, based on the known pixel dimensions of the image and the distance between the two laser markers:

$$AB = \frac{\text{Distance between laser lines [cm]} \times \text{ Horizontal number of pixels}}{\text{Number of pixels between laser lines (longer base)}} \quad (5)$$

$$CD = \frac{\text{Distance between laser lines (cm)} \times \text{ Horizontal number of pixels}}{\text{Number of pixels between laser lines (shorter base)}} \quad (6)$$

The height of the trapezoid was calculated using the law of cosines, as:

$$HF = \sqrt{JF^2 + JH^2 - (2 \times JF \times JH \times \cos(\alpha))} \quad (7)$$

The distances of the camera to the edges of the seabed area can be computed as:

$$JF = JL/\cos(\alpha/2) \quad (8)$$

$$JH = JM/\cos(\alpha/2) \quad (9)$$

with

$$JL = (AB/2)/\tan(\beta/2) \quad (10)$$

$$JM = (CD/2)/\tan(\beta/2) \quad (11)$$

The image altitude $JK$ was calculated as:

$$JK = (2 \times A)/HF \quad (12)$$

where $A$ represents the area of the triangle $JHF$. Area $A$ was derived using Heron's formulae and the semi-perimeter $s$:

$$A = \sqrt{s \times (s - JH) \times (s - JF) \times (s - HF)} \quad (13)$$

$$s = (JH + JF + HF)/2 \quad (14)$$

Images calibrated with the point lasers were assumed to be taken perpendicular to the seafloor across a flat seabed with the surface area photographed being represented by a rectangle with $AB = CD$. Image width was derived from the measured pixel distance between the two laser points using equation (5), and image area and altitude were calculated using equations (7) to (14) where $JF = JH$ and $JK = JL = JM$.

### A.4.3 Scaling using image colour components

In the case of transect 14C02 (Area C, 600-700 m) laser markers were only visible in the video footage. Seafloor coverage of images from this transect was estimated as a function of the image's red colour channel, whose suitability to predict image size was ascertained as follows:

***Scaling test images**:* First, sixty images were randomly chosen, and frame grabs from the corresponding video segments were taken. Then for each frame grab, the pixel-to-centimeter ratio for one clearly visible object (megafauna or debris) was determined from the pixel length of the object and the distance between the two laser lines. A width for each validation image was subsequently derived by first relating the pixel-to-centimeter ratio of the measured object in the video frame grab to the pixel length of the object in the corresponding still image and then converting the computed image object length to image width.

***Computing image colour components**:* Four metrics were tested for their potential to predict image size: the three colour channels of the original RGB image (red (R), green (G) and blue (B)), and the brightness/value (V) component of the image in HSV space. The metrics were chosen based on the premise that (1) the colour components of underwater images change with the distance of the camera as light is absorbed, (2) different wavelengths are attenuated differently, and (3) light intensity is expected to decrease with the distance to the light source. For each channel, a mean pixel value was computed for the 100 x 100 pixels located in the centre of the image, where light scattering and uneven illumination were assumed to be minimal. Calculation of mean pixel values and preceding image decomposition were conducted using MATLAB R2015a.

***Model fitting:*** Width of the test images plotted as a function of each colour channel suggested a negative linear relationship of width with the blue channel and negative non-linear relationships of width with the red, green and brightness channels. To test the relationships, a linear model of image width vs the blue channel and log-log and log-linear models of width vs the remaining metrics were fitted, using the base command 'lm' in R (R Core Team, 2020). Homoscedasticity, presence of influential variables, and normality assumptions of each model were verified by visual inspection of residuals, cook distance and QQ plots.

***Model results and area predictions**:* All models tested to estimate image width showed a significant fit (Table A.2). Comparison of the Akaike Information Criteria for the non-linear models indicated that power models outperformed exponential models with the red channel showing the best fit in both cases. Based on these results, the fitted power model for the red channel was chosen to predict image dimensions (Figure A.3).

**Table A.2** Regression coefficients and statistics for fitted models relating image width (W) to the mean standardised pixel value of the red (R), green (G), blue (B) and brightness (V) channels of the image. 95% CI confidence intervals for regression coefficients were calculated from the Standard Error of estimation. nc - not computed as not comparable with other models

| Model | Slope (95% CI) | Intercept (95% CI) | $F_{[1,54]}$ | $R^2$ (%) | AIC |
|---|---|---|---|---|---|
| W ~ B | -589.84 (-633.25 - -546.45) | 359.37 (344.30 -374.44) | 742.6 **** | 93.2 | nc |
| log (W) ~ log (R) | -0.78 (-0.82 - -0.74) | 4.30 (4.26 - 4.34) | 1449 **** | 96.4 | -169.3 |
| log (W) ~ log (G) | -1.05 (-1.12 - -0.99) | 4.19 (4.14 - 4.24) | 1184 **** | 95.6 | -158.5 |
| log (W) ~ log (V) | -1.05 (-1.11 - -0.99) | 4.20 (4.15 - 4.25) | 1229 **** | 95.8 | -160.5 |
| log (W) ~ R | -1.86 (-1.98 - -1.75) | 5.80 (5.75 - 5.85) | 1045 **** | 95.1 | -151.8 |
| log (W) ~ G | -2.23 (-2.37 - -2.08) | 6.07 (6.00 - 6.14) | 951.2 **** | 94.6 | -146.8 |
| log (W) ~ V | -2.19 (-2.33 - -2.04) | 6.05 (5.98 - 6.12) | 895.7 **** | 94.3 | -143.6 |

**** $p < 0.0001$

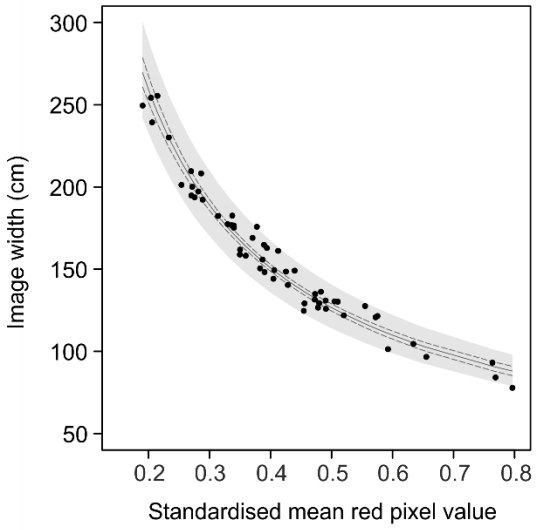


**Figure A.3** Estimated width of photographs collected at 14C02 as a function of the mean red channel pixel value across the centre of the image (100 x 100 pixels). Points represent photographs selected for prediction. The solid line represents the fitted line obtained by linear regression of the natural log-log transformed data. Dashed lines show the 95% confidence interval of the fitted values. The shaded area is the 95% prediction interval.

## A.5 Identifying overlapping images

Low tow speeds, fluctuating camera altitudes, and the occassional contact of the camera platform with the seabed resulted in some areas of the seafloor being photographed in consecutive images. To avoid double-counting of organisms and overestimating the seabed area analysed only non-overlapping images were included in quantitative analyses.

Overlaps on the digital photographs were identified by mapping each image footprint based on image position and estimated image area. For transects sampled in 2014, positioning information was extracted from the raw USBL sensor files, which contained positions of the camera frame at 3 second intervals. Following the removal of erronous records, the positions were smoothened using either a 9-point, 13-point or 21-point centred weighted moving average to correct recording errors, which may have been caused by abrupt movements of the camera frame or high suspended sediment loads. Smoothing bins were chosen based on the degree of scatter of image positions around the transect line. To map image footprints, coordinates were assigned to the centre of each image using the USBL position recorded at the time that most closely matched the image's EXIF timestamp. Then, the xy positions for each image corner were calculated from the image dimension that were obtained during scaling. To account for camera rotation, corner positions were adjusted for camera heading. For transects with no heading information, camera orientation was estimated from the direction of camera movement observed in the corresponding video footage. Final image positions were mapped as spatial polygons in R (R Core Team, 2020) using various functions from the 'sp' (Pebesma and Bivand, 2005) and 'rgdal' (Bivand et al., 2019) packages. Sets of overlapping images were listed using the 'over' command from the 'stringi' package (Gagolewski, 2019) and reduced to a single image, with a preference to retain images taken between 0.5 and 4 m above the seabed.

Overlaps between photographs taken during the 2008 survey were mapped using uncorrected image coordinates because plotted image positions showed only small deviations from the expected transect lines. For the film material collected in 2005 positioning information could not reliably be matched to individual frames. In this case, potential overlaps were first estimated from calculated vessel speeds, and then verified during the annotation process.

## A.6 Camera altitude

The ability to detect and identify specimens in underwater photographs depends inherently on the image's properties, which vary substantially as a function of camera altitude. For instance, as the distance between the seabed and the camera increases light intensity decreases, which can lead to a decrease in brightness around an image's edges (vignetting). Additionally, haze due to the scattering of light by suspended particles increases with distance, as does the dominance of blue tones since the different wavelengths of light are subjected to different rates of attenuation (Chiang and Chen, 2012). Corrections for one or several image properties may be applied during image processing to improve overall image quality or to optimise the visibility of particular features (Durden et al., 2016). In addition, analysis may be restricted to photographs that were taken within a specified distance from the seabed. The optimal altitude range is dependent on the questions to be investigated and the number of captured images (Jones et al., 2009). For example, if the aim is to study the distribution of habitat features, lower resolution photographs covering a larger area may be sufficient. If, however, species diversity and community structure are to be investigated, then image resolution becomes more critical. In this case, altitude range should be large enough to capture a reasonable number of individuals for quantitative analysis, but small enough so that specimens can be consistently detected and identified to a common level of taxonomic resolution (Jones et al., 2009).

In the present study, photographic material was collected with different camera platforms over a large depth gradient under different environmental conditions, yielding images of varying quality and altitudes (Figure A.4). For analysis of morphospecies diversity, standing stocks and assemblage structure (as applied in Chapters 3 to 5), all images above 4 m were excluded prior to annotating owing to a combination of strong blue hue, low illumination, and high backscatter, which affected large parts of these images. For the remaining photographs, segments suffering from non-uniform illumination or low contrast were either corrected or excluded from analysis, as described in Section A.3.

A comparison of the size of metazoan megafauna among images from different altitude ranges indicated a decrease in the detectability of specimens < 1 cm in digital images taken above 2-2.5 m from the seabed (Figure A.5c-g). For specimens > 1 cm, a reduction in detectability is suggested for image altitudes of > 3-3.5m, although the number of images

taken at these higher altitudes is comparatively low. For subsequent analyses of faunal patterns, specimens < 1 cm in maximal dimensions were omitted. Furthermore, for analysis conducted in Chapters 3 and 5, only images taken between 0.8 to 3.5 m from the seabed were retained to strike a balance between sampling a representative proportion of the smallest specimens and providing sufficiently large numbers of images to allow quantification of ecological parameters that are more sensitive to sampling effort (e.g. morphospecies richness). To assess the structure of megafaunal communities associated with cold-water coral reef habitats (Chapter 4), all images below 4 m were retained to ensure that for each photographic site an adequate number of images was available to compare ecological parameters among defined substratum classes.

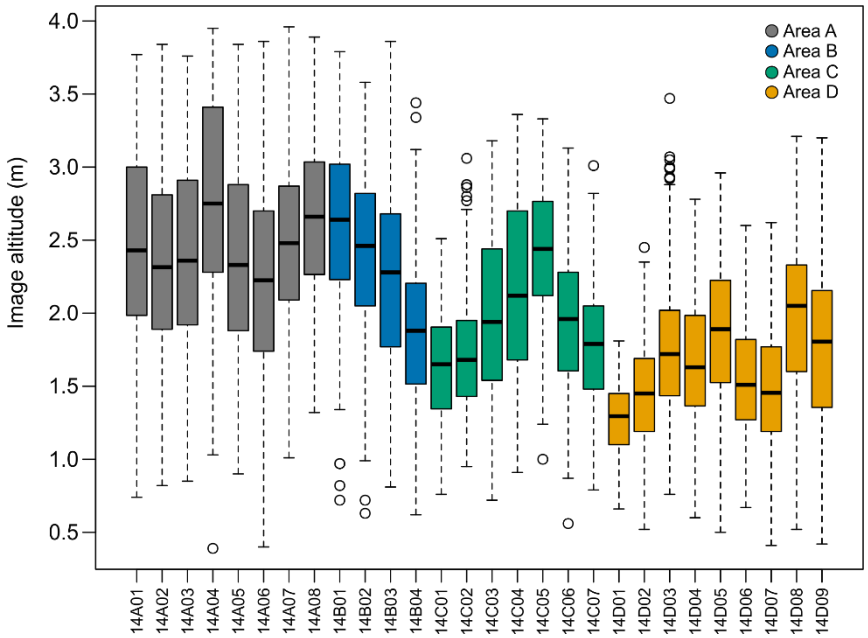


**Figure A.4** Boxplot showing the variation in image altitude for each photographic transect sampled across soft substratum in 2014, including all non-overlapping, annotated photographs. For transect codes see Table S3.1.

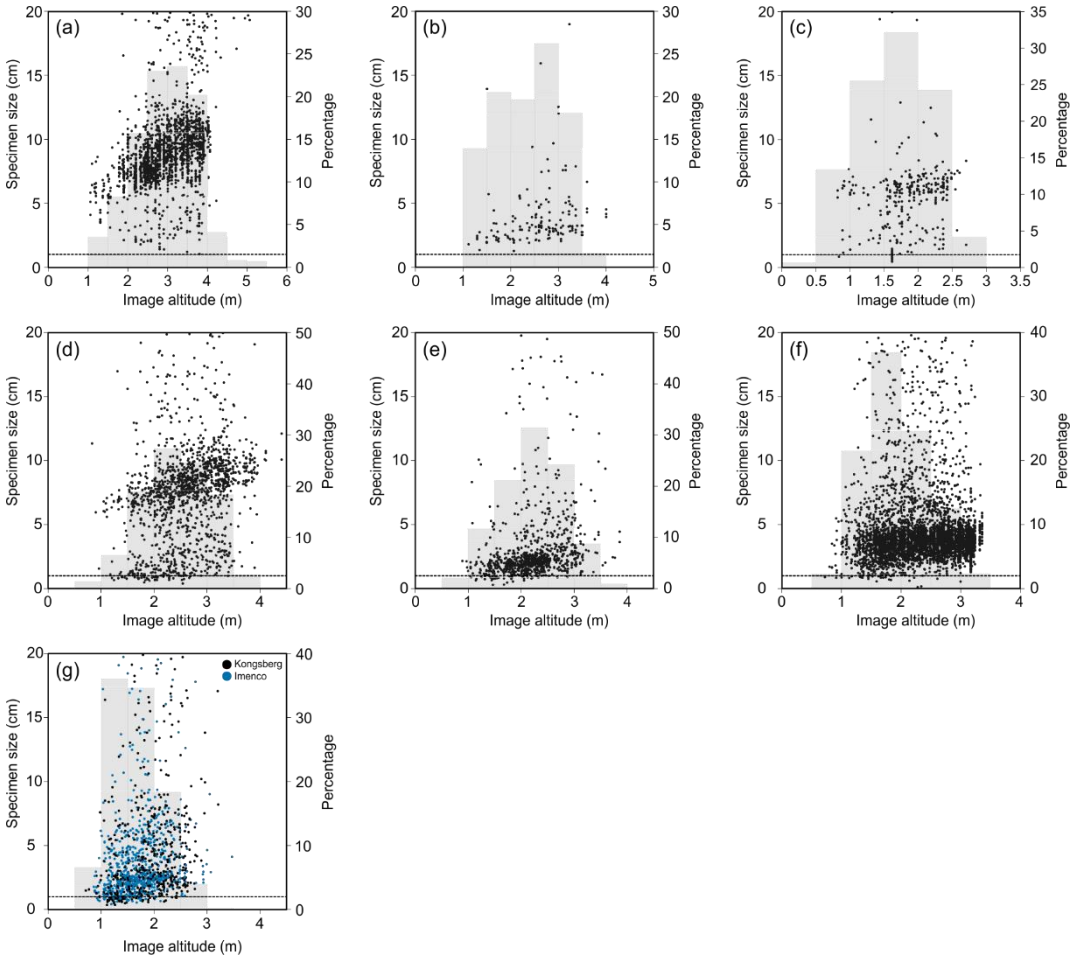


**Figure A.5** Variation in the recorded size of metazoan megafauna with image altitude for photographs taken across sedimentary habitats along the Angolan continental slope in 2005, 2008 and 2014 (as analysed in Chapter 3). 2005: Area A **(a)** and Area B **(b)**; 2008: Area A **(c)**; 2014: Area A **(d)**, Area B **(e)**, Area C **(f)**, and Area D **(g)**. Histograms show the proportion of annotated photographs at different image altitude ranges. Specimen sizes represent maximum visible dimensions, which were obtained by multiplying the standard length measured during annotation with a taxa-specific factor that takes account of tentacles, appendages, legs etc. Dashed line shows 1 cm specimen size. For better readability only specimens with a maximum dimension of < 20 cm are shown. Specimens recorded at transects 14C01, 14C02, 14D01 and 14D02 were excluded because images from these transects were collected at lower altitudes (Figure A.4).

# Appendix B

# Epibenthic and benthopelagic megafauna photographed along the Angolan Continental

This Appendix includes representative images of the megabenthic and benthopelagic morphospecies that were included in the faunal analyses conducted as part of this study. The methods and criteria by which morphospecies were classified are given in the respective thesis chapters. For each morphotype, at least one image is provided. For morphotypes that are likely to include several species multiple images are included to illustrate morphological differences.

The following experts were consulted for advice on the classification of the morphospecies: A. Goineau and A. Gooday (Foraminifera); S. De Grave, T. Horton and M. Thurston (Crustacea); D. Billett (Echinodermata); E. Anderson, A. Jamieson and K. Sulak (Chordata); B. Bett, J. Durden, A. Gates and D. Jones (various faunal groups). Visual identification material and peer-reviewed literature consulted to facilitate taxa identification and classification are listed at the end of the appendix.

Work on the image catalogue is ongoing with the aim of providing a comprehensive publicly available reference image guide for benthic and benthopelagic megafauna observed in seabed images and video collected from the Angolan deep continental margin. Besides the morphospecies shown here, the catalogue is intended to include (1) morphospecies classified as part of this study but excluded from analyses (e.g. morphotypes recorded exclusively off-bottom or smaller than 1 cm), and (2) morphospecies identified during previous image-based studies in the region (e.g. Jones et al., 2014). The final publication format of the image catalogue has yet to be decided.

# Porifera


Porifera msp-1


Porifera msp-2


Porifera msp-3


Porifera msp-4, cf. *Cladorhiza*


Porifera msp-5


Porifera msp-6, cf. Latruncullidae

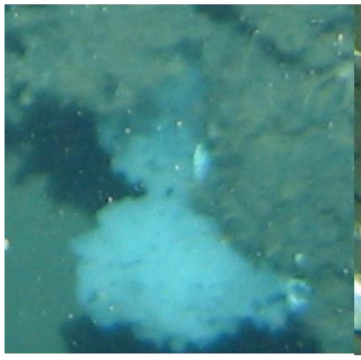
Porifera msp-7


Porifera msp-8


Porifera msp-9


Porifera msp-10


Porifera msp-10


Porifera msp-12

Porifera msp-13 Porifera msp-13 Porifera msp-13

Porifera msp-14 Porifera msp-14 Porifera msp-15

Porifera msp-16 Porifera msp-16 Porifera msp-17

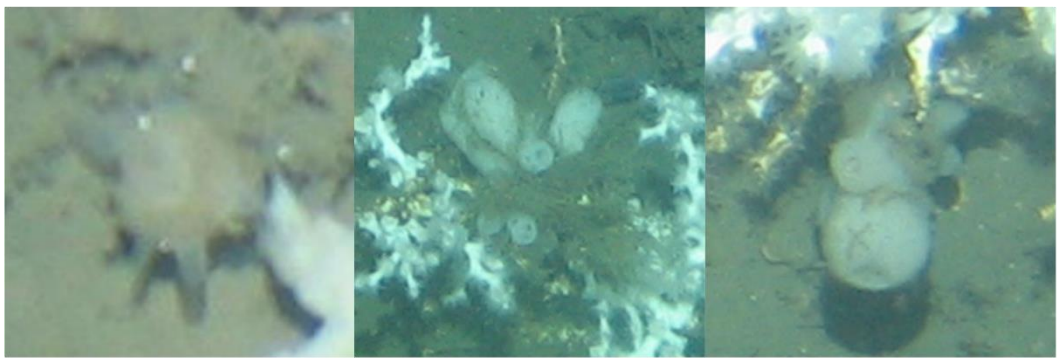

Porifera msp-18 Porifera msp-20 Porifera msp-20


Porifera msp-21


Porifera msp-22

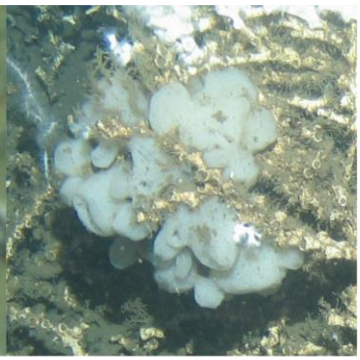
Porifera msp-23


Porifera msp-24


Porifera msp-24


Porifera msp-25


Porifera msp-25


Porifera msp-26


Porifera msp-27


Porifera msp-27


Porifera msp-27


Porifera msp-27

Porifera msp-27

Porifera msp-27

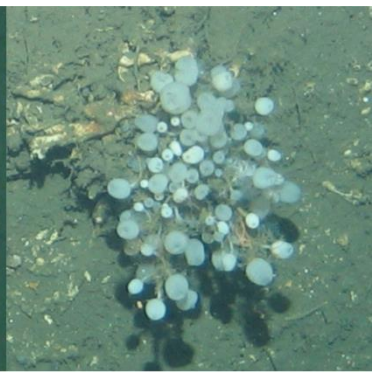

*Sympagella* msp-1

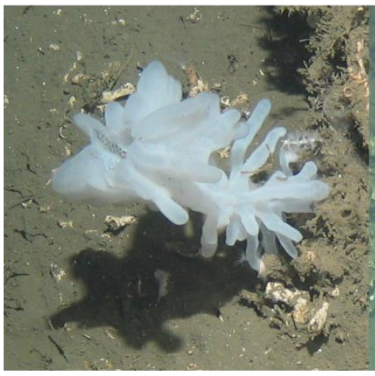

*Aphrocallistes* msp-1

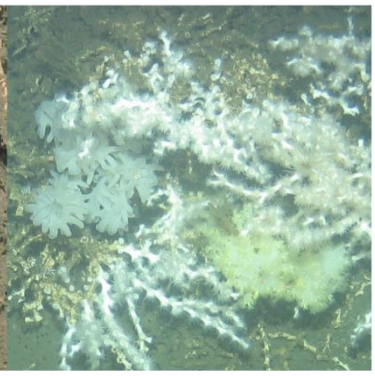

*Aphrocallistes* msp-1

# Cnidaria

Actiniaria msp-1 | Actiniaria msp-2 | Actiniaria msp-3

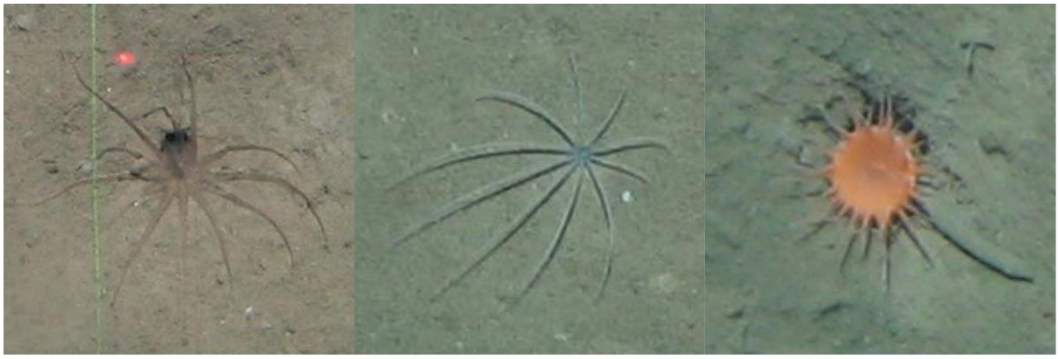

Actiniaria msp-4 | Actiniaria msp-5 | Actiniaria msp-6

Actiniaria msp-7 | Actiniaria msp-8 | Actiniaria msp-9

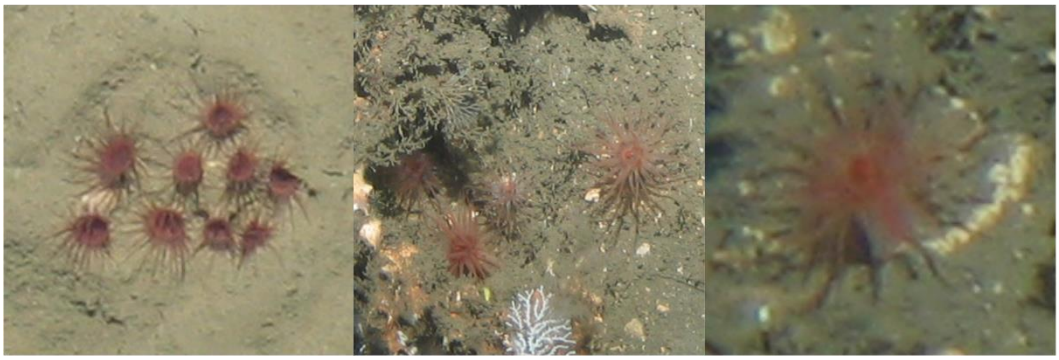

Actiniaria msp-10 | Actiniaria msp-11, cf. *Halcurias* | Actiniaria msp-11, cf. *Halcurias*


Actiniaria msp-12

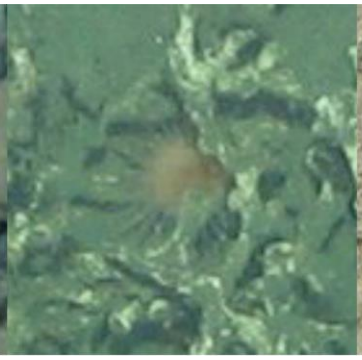
Actiniaria msp-13


Actiniaria msp-14


Actiniaria msp-15


Actiniaria msp-16


Actiniaria msp-18


Actiniaria msp-18


Actiniaria msp-19, cf. *Clavularia*


Actiniaria msp-20


Actiniaria msp-20


Actiniaria msp-21


Actiniaria msp-25


Actiniaria msp-26


Actiniaria msp-27

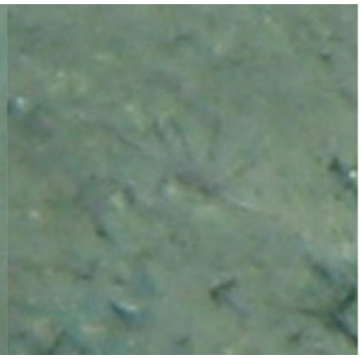
Actiniaria msp-28


Actiniaria msp-30, on asphalt mounds


Actiniaria msp-31

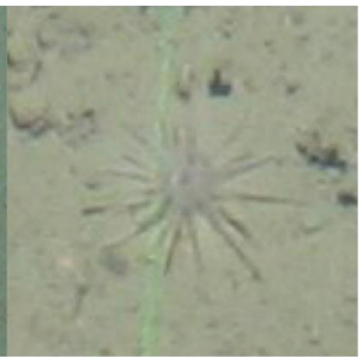
Actiniaria msp-32


Actiniaria msp-33


Actiniaria msp-34


Actinoscyphiidae msp-1


Actinoscyphiidae msp-2

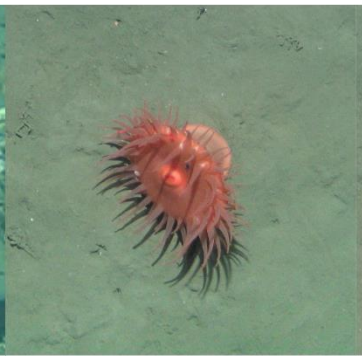
Actinostolidae msp-1


Metridioidea msp-1

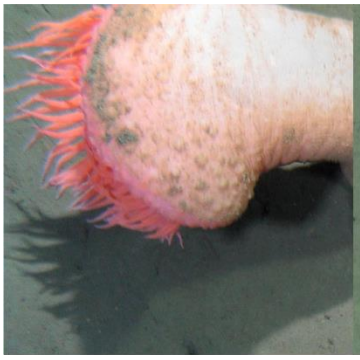
Metridioidea msp-2


Metridioidea msp-3


Metridioidea msp-5


Antipatharia msp-1

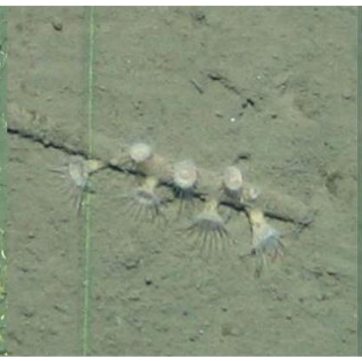
Zoantharia msp-1


Zoantharia msp-2

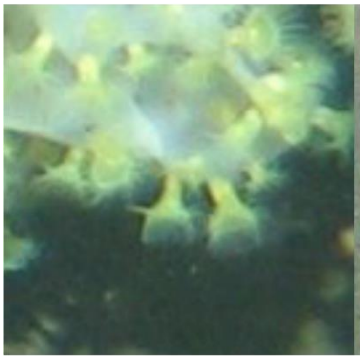
Zoantharia msp-3


Epizoanthidae

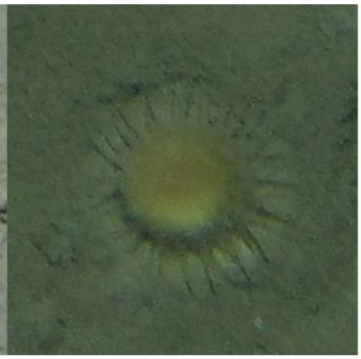
Scleractinia msp-1

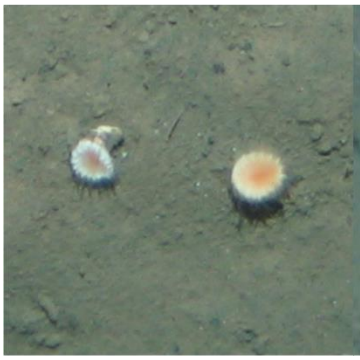
Scleractinia msp-2


Scleractinia msp-3, *Caryophyllia* sp.


Scleractinia msp-3, *Caryophyllia* sp.

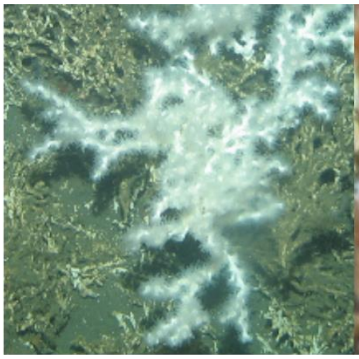
*Desmophyllum pertusum*

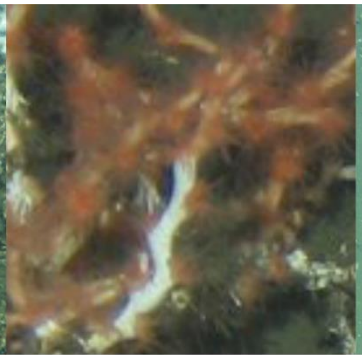
*Desmophyllum pertusum*

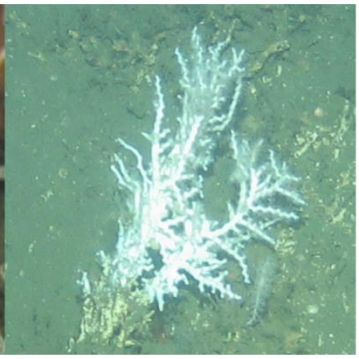
*Madrepora oculata*


Hexacorallia msp-1


Hexacorallia msp-2


Hexacorallia msp-4

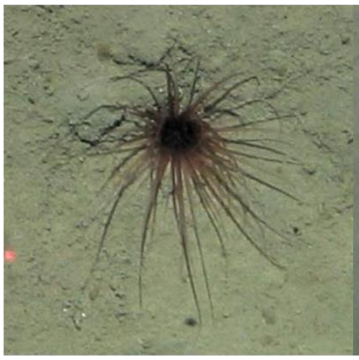
Ceriantharia msp-1


Ceriantharia msp-1


Ceriantharia msp-2


Ceriantharia msp-3


Ceriantharia msp-4


Ceriantharia msp-5


Ceriantharia msp-6


Ceriantharia msp-7


Pennatulacea msp-1, cf. Virgularidae


Pennatulacea msp-2


Pennatulacea msp-3


Pennatulacea msp-5


Pennatulacea msp-6


Pennatulacea msp-6


Pennatulacea msp-7


Pennatulacea msp-8


Pennatulacea msp-10


Pennatulacea msp-11


*Umbellula* msp-1


Alcyoniidae msp-1

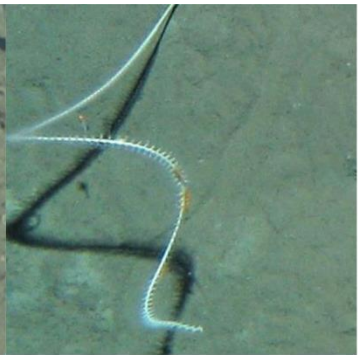
Alcyonacea msp-1


Alcyonacea msp-2

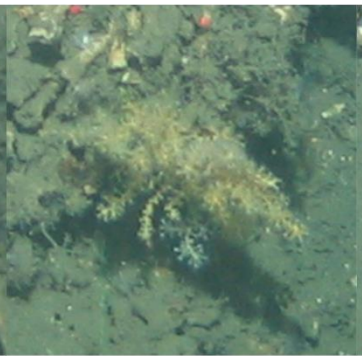
Alcyonacea msp-2

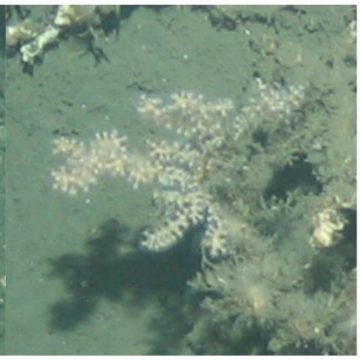
Alcyonacea msp-2


Alcyonacea msp-3


Octocorallia msp-1


Octocorallia msp-3


Octocorallia msp-4


Octocorallia msp-5


Actiniaria msp-36

Anthozoa msp-1 | Anthozoa msp-2 | Anthozoa msp-3

Anthozoa msp-4, cf. Ceriantharia | Anthozoa msp-5, cf. Ceriantharia | Anthozoa msp-6

Anthozoa msp-7 | Anthozoa msp-8 | Anthozoa msp-9

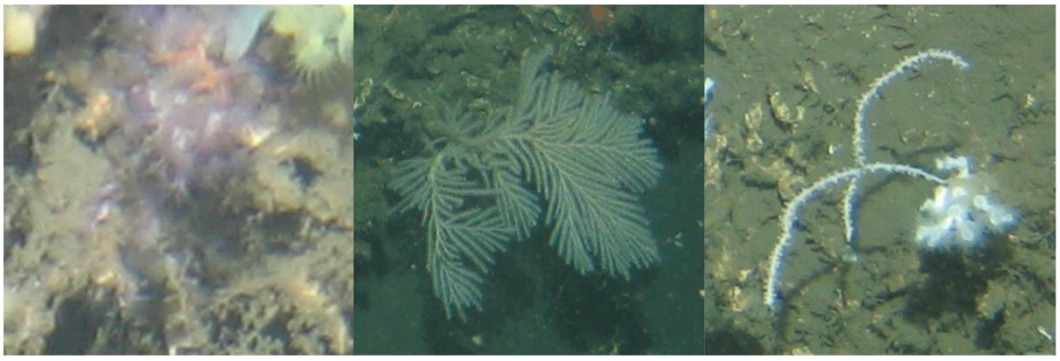

Anthozoa msp-10 | Anthozoa msp-11 | Anthozoa msp-12

Anthozoa msp-13 Anthozoa msp-14 Anthozoa msp-15

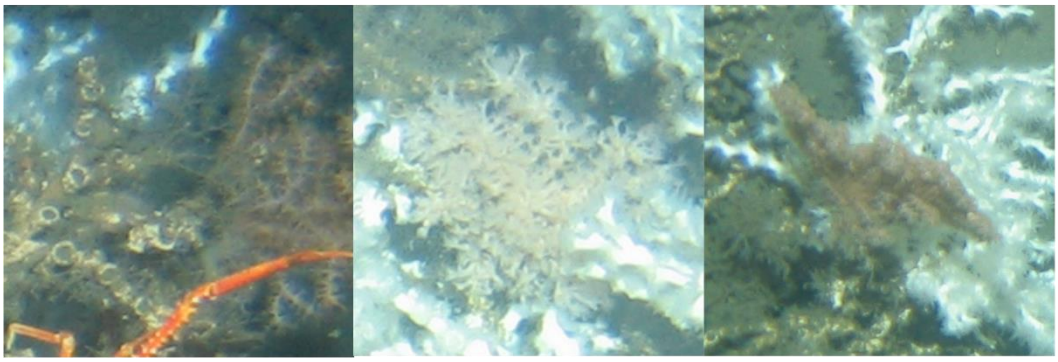

Anthozoa msp-16 Anthozoa msp-17 Anthozoa msp-18

Anthozoa msp-19 Anthozoa msp-20 Anthozoa msp-21

Anthozoa msp-22 Anthozoa msp-23 Anthozoa msp-24


Cnidaria msp-1


Cnidaria msp-2


Cnidaria msp-2


Cnidaria msp-3


Cnidaria msp-4

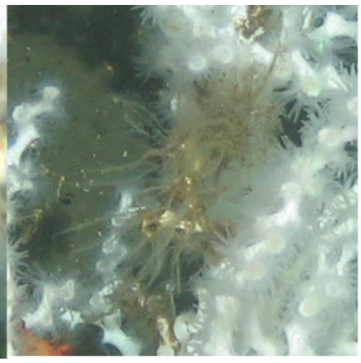
Cnidaria msp-4


Cnidaria msp-5

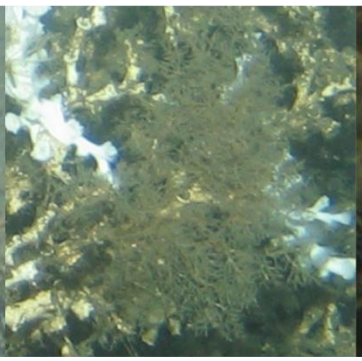
Cnidaria msp-6


Cnidaria msp-7


Cnidaria msp-8

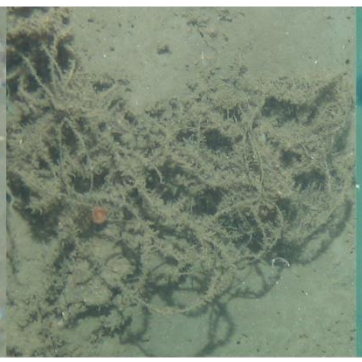
Cnidaria msp-9


Corymorphidae

# Arthropoda


Anomura msp-1, cf. Galatheoidea


Anomura msp-2, cf. Galatheoidea


Anomura msp-3


Anomura msp-4


Anomura msp-4


Anomura msp-5


Anomura msp-6, cf. Munidopsidae


Anomura msp-7


Anomura msp-8, cf. Munidopsidae


Anomura msp-9


Anomura msp-10


*Eumunida* msp-1


Paguroidea


Paguroidea


*Polycheles* msp-1


*Bathynectes* msp-1


Geryonidae


Geryonidae


Brachyura msp-4


Brachyura msp-5


Brachyura msp-6, cf. Homolidae


Brachyura msp-8


Brachyura msp-9, cf. Dormiidae


Cirrepedia

Isopoda msp-1, cf. Janiroidea | Isopoda msp-2, cf. Janiroidea | Isopoda msp-3, cf. Janiroidea

Isopoda msp-1, Aegidae | Isopoda msp-5 | Isopoda msp-6, cf. Janiroidea

*Bythocaris* msp-1 | Caridea msp-1 | Caridea msp-2

Caridea msp-3 | Caridea msp-3 | Caridea msp-4

Caridea msp-5 | *Nematocarcinus* msp-1 | *Nematocarcinus* msp-1

Caridoid msp-1 | Caridoid msp-3 | Caridoid msp-3

Caridoid msp-5 | Caridoid msp-7 | Caridoid msp-7

Caridoid msp-9 | Caridea msp-11 | Caridea indet.

Aristeidae msp-1

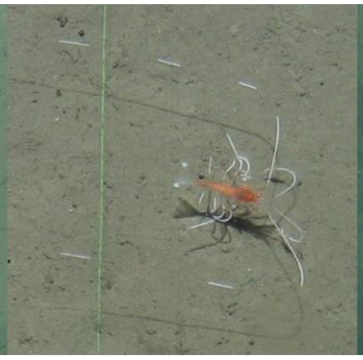

Aristeidae msp-2

Aristeidae msp-5

Aristeidae msp-3

Malacostraca msp-1

Malacostraca msp-2

Decapoda msp-1

Decapoda msp-2

Decapoda msp-3

# Gastropoda


Gastropoda msp-1


Gastropoda msp-2


Gastropoda msp-7


Gastropoda msp-8


Gastropoda msp-8


Gastropoda msp-9


Gastropoda msp-13


Gastropoda msp-15


Gastropoda msp-16


Gastropoda msp-19


Gastropoda msp-21


Gastropoda msp-22


Gastropoda msp-24


Gastropoda msp-25


*Acesta* msp-1


Bivalvia msp-1


Bivalvia msp-2


*Bathymodiolus* msp-1

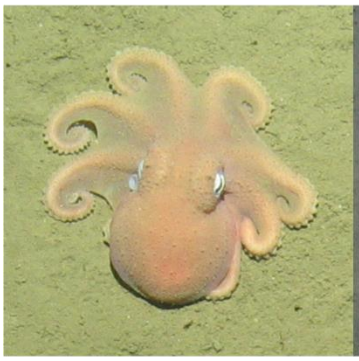
Cephalopoda msp-1


Cephalopoda msp-2


Cephalopoda msp-4


Cephalopoda msp-5

# Echinodermata: Asteroidea


Asteroidea msp-01


Asteroidea msp-02


Asteroidea msp-02

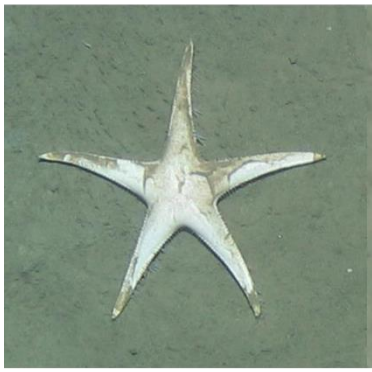
Asteroidea msp-03

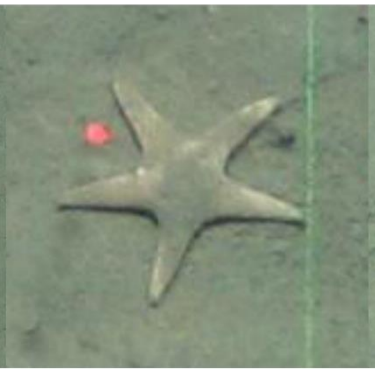
Asteroidea msp-04


Asteroidea msp-05


Asteroidea msp-05


Asteroidea msp-05


Asteroidea msp-06


Asteroidea msp-07


Asteroidea msp-07


Asteroidea msp-07

Asteroidea msp-9

Asteroidea msp-11

Asteroidea msp-14

Asteroidea msp-15, cf. *Coronaster*

Asteroidea msp-16, cf. *Asterias*

Goniasteridae msp-1

Goniasteridae msp-2

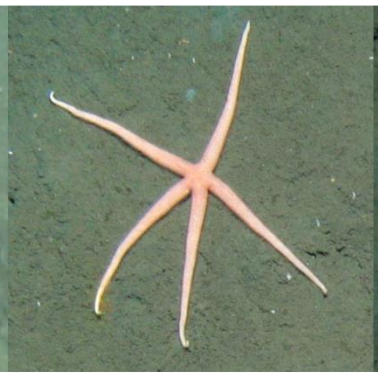

Zoroasteridae

Zoroasteridae

Comatulida msp-1

Comatulida msp-2

# Echinodermata: Holothuroidea

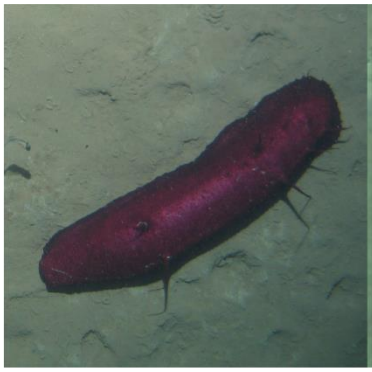

*Benthodytes* msp-01

*Benthodytes* msp-02

Holothuroidea msp-01

*Benthothuria* msp-01

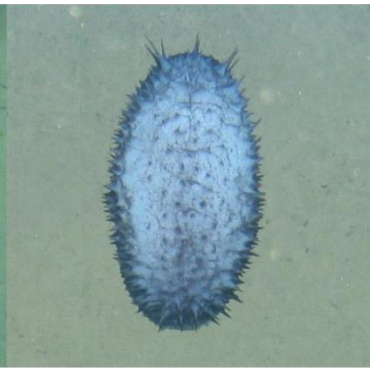

Holothuroidea msp-02

*Elpidia* msp-01

*Elpidia* msp-01

Elpidiidae msp-02

*Paelopatides* msp-01

*Paelopatides* msp-01

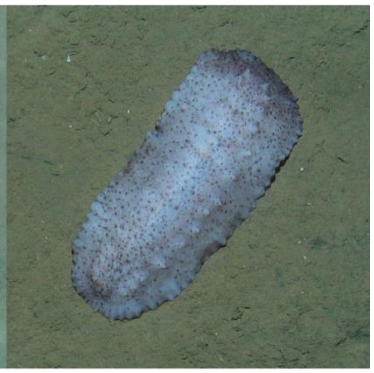

*Paelopatides* msp-01

# Echinodermata: Holothuroidea


*Psychropotes* msp-01


*Psychropotes* msp-01


Holothuroidea msp-07


*Peniagone* msp-01


*Peniagone* msp-01


*Peniagone* msp-02

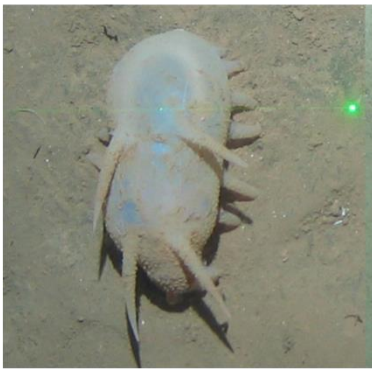
*Scotoplanes* msp-01


*Scotoplanes* msp-01


*Mesothuria* msp-01


Holothuroidea msp-04


Holothuroidea msp-04


Holothuroidea msp-04


Holothuroidea msp-6


Holothuroidea msp-7


Holothuroidea msp-7


*Chiridota* msp-1


*Chiridota* msp-1

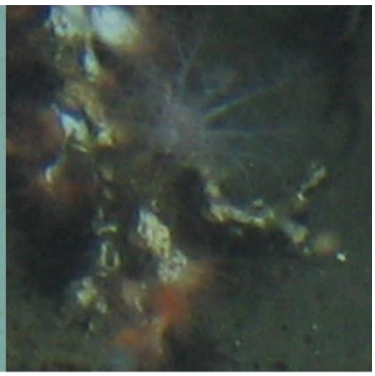
Psolidae

# Echinodermata: Echinoidea

Echinidae msp-1, cf. *Echinus*

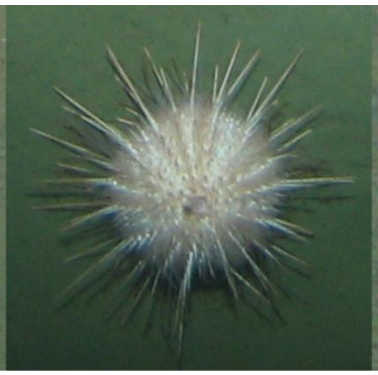

Echinidae msp-1, cf. *Echinus*

Echinidae msp-2

Echinidae msp-2

Echinidae msp-3, cf. *Gracilechinus*

Echinidae msp-4

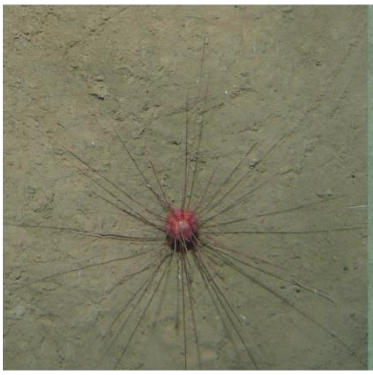

Aspidodiadematidae

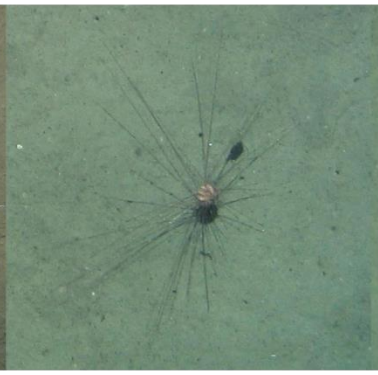

Aspidodiadematidae

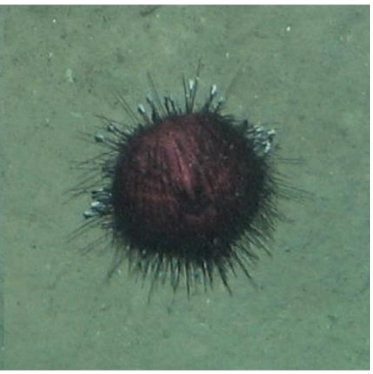

*Hygrosoma* msp-1

*Phormosoma* msp-1

*Phormosoma* msp-1

*Pourtalesia* msp-1

Echinoidea msp-3

Echinoidea msp-4

Echinoidea msp-4

Echinoidea msp-5

Echinoidea msp-6

Echinoidea msp-7

Echinoidea msp-8

# Holothuroidea: Ophiuroidea

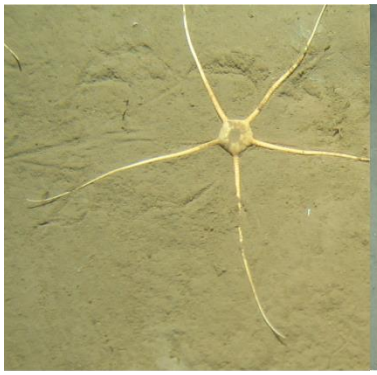
Ophiuroidea msp-1, cf. Ophiomusaidae

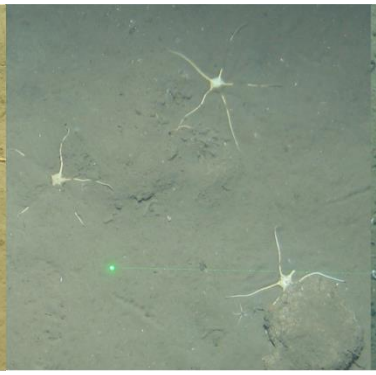
Ophiuroidea msp-1, cf. Ophiomusaidae

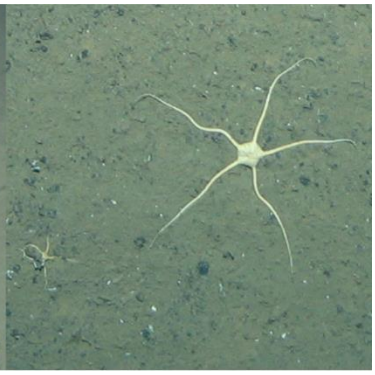
Ophiuroidea msp-1, cf. Ophiomusaidae

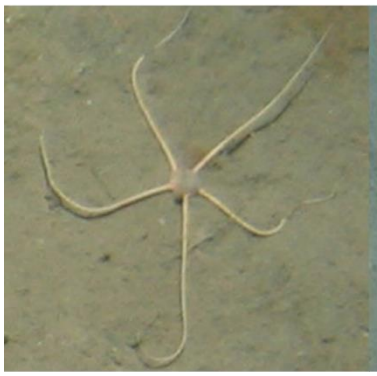
Ophiuroidea msp-2


Ophiuroidea msp-2


Ophiuroidea msp-2

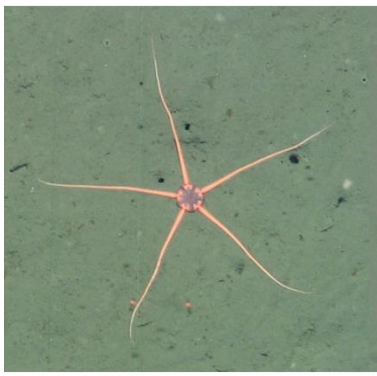
Ophiuroidea msp-3

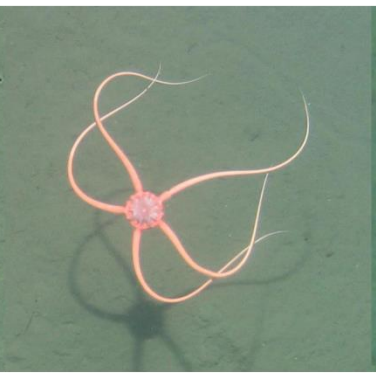
Ophiuroidea msp-3


Ophiuroidea msp-4


Ophiuroidea msp-4

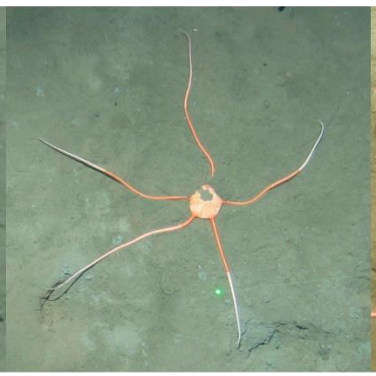
Ophiuroidea msp-5

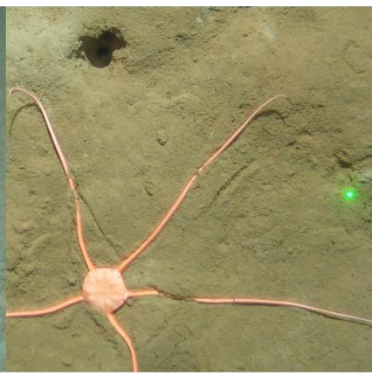
Ophiuroidea msp-5

Ophiuroidea msp-6

Ophiuroidea msp-7

Ophiuroidea msp-7

Ophiuroidea msp-8

Ophiuroidea msp-8

Ophiuroidea msp-9

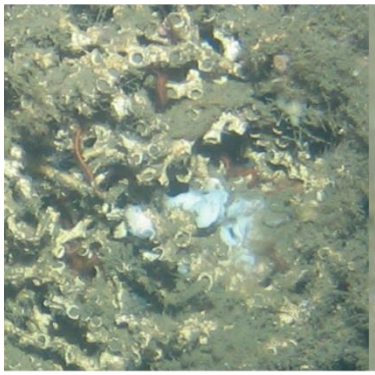

Ophiuroidea msp-10

Ophiuroidea msp-11

# Invertebrates: Miscellaneous


Tunicata msp-1


Tunicata msp-2


Tunicata msp-3


Brachiopoda msp-1


Sabellidae msp-1


Sabellidae msp-2


Serpulidae


Serpulidae

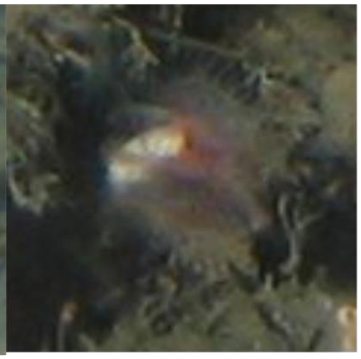
Serpulidae


Bryozoa msp-1


Bryozoa msp-1


Bryozoa msp-1


Bryozoa msp-2

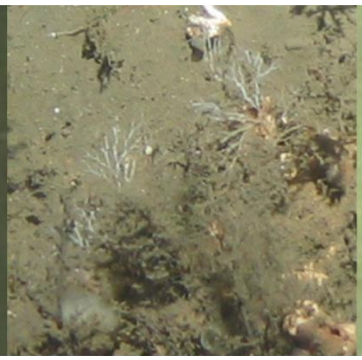
Bryozoa msp-2


Polychaeta msp-1


Polychaeta msp-2


Polychaeta msp-3


Polychaeta msp-5


Polychaeta msp-5


Polychaeta msp-6


Polychaeta msp-9, cf. Terebellidae


Onuphidae


Onuphidae


Vermiform msp-1


Vermiform msp-6


Vermiform msp-7


Vermiform msp-8


Annelida msp-1


Animalia indet. msp-2


Animalia indet. msp-


Animalia indet. msp-4


Animalia indet. msp-4


Animalia indet. msp-4


Animalia indet. msp-5


Animalia indet. msp-13


Animalia indet. msp-17


Animalia indet. msp-19


Animalia indet. msp-33


Animalia indet. msp-34


Animalia indet. msp-35


Animalia indet. msp-39


Animalia indet. msp-42


Animalia indet. msp-45


Animalia indet. msp-46


Animalia indet. msp-47


Animalia indet. msp-48

Animalia indet. msp-50 Animalia indet. msp-53 Animalia indet. msp-56

Animalia indet. msp-57 Animalia indet. msp-58 Animalia indet. msp-59

Animalia indet. msp-60 Animalia indet. msp-61 Animalia indet. msp-62

Animalia indet. msp-63 Animalia indet. msp-64 Animalia indet. msp-65

# Foraminifera

Foraminifera msp-1, *Schizammina*

Foraminifera msp-2, cf. *Bathysiphon*

? Foraminifera msp-3, cf. *Bathysiphon*

? Foraminifera msp-3, cf. *Bathysiphon*

Foraminifera msp-4

Foraminifera msp-6

Foraminifera msp-6

? Foraminifera msp-7

Xenophyophoroidea msp-1

Xenophyophoroidea msp-1

Xenophyophoroidea msp-2

Xenophyophoroidea msp-2


Xenophyophoroidea msp-4


Xenophyophoroidea msp-5


Xenophyophoroidea msp-5

# Chordata

*Simenchelys* msp-01

*Ilyophis* msp-01

*Synaphobranchus* msp-01

Synaphobranchidae msp-04, cf. *Ilyophis* sp.

*Nettastomatidae* msp-01

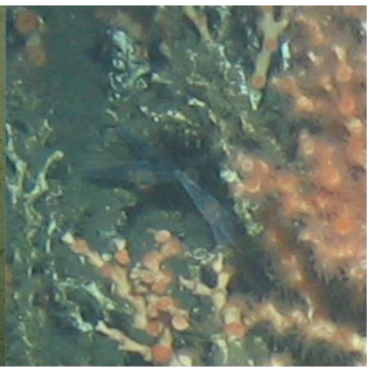

*Nettastomatidae* msp-01

Anguilliformes msp-01

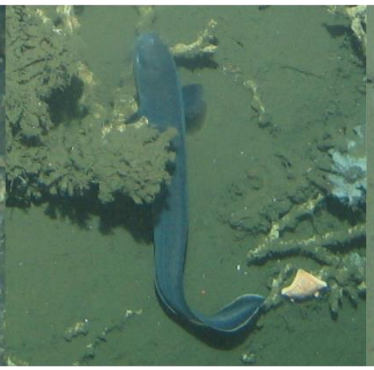

*Coloconger* msp-01

Ophichthidae msp-01

Chaunacidae msp-01, cf. *Chaunax* sp.

Chaunacidae msp-02, potential colour morph of msp-01

Lophiidae msp-01

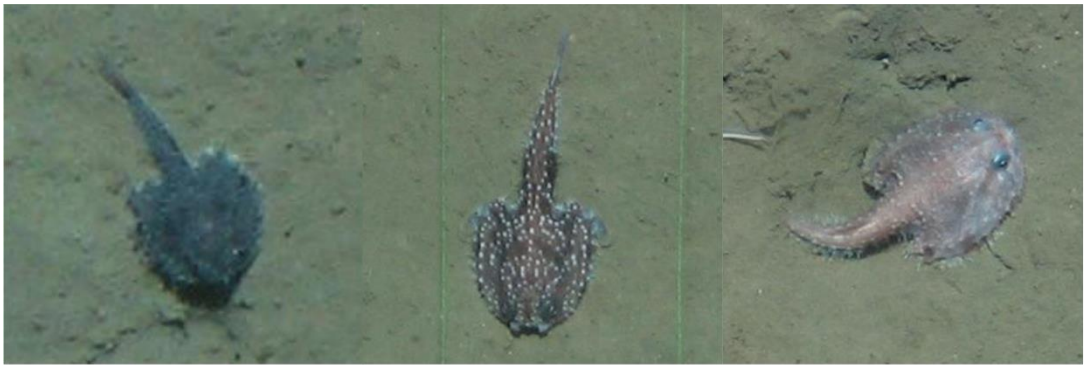

Ogcocephalidae msp-01 | Ogcocephalidae msp-02 | Ogcocephalidae msp-02

Lophiidae msp-02, cf. *Lophiodes* sp. | *Antimora* msp-01 | *Laemonema* msp-01, cf. Guinea codling *L. laureysi*

*Trachyrincus* msp-01 | *Coelorinchus* msp-01 | *Coelorinchus* msp-01

Macrouridae msp-01 | Macrouridae msp-02 | Macrouridae msp-04


Macrouridae msp-03


Macrouridae msp-03

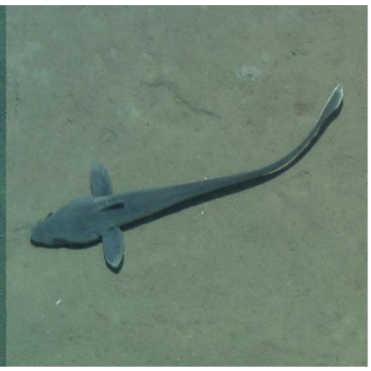
Macrouridae msp-04


Macrouridae msp-05


Macrouridae msp-06, cf. *Hymenocephalus* sp.

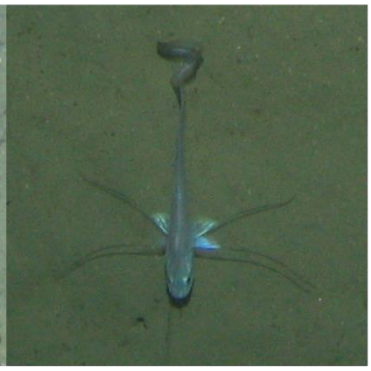
Macrouridae msp-07, cf. *Gadomus* sp.

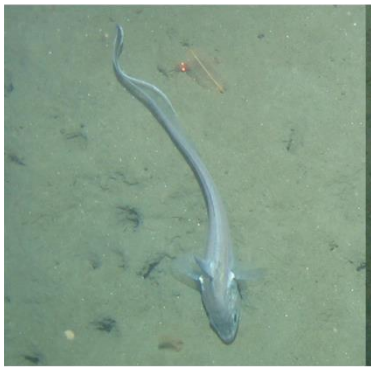
Macrouridae msp-08


Macrouridae spp.


Macrouridae spp.


Macrouridae spp.

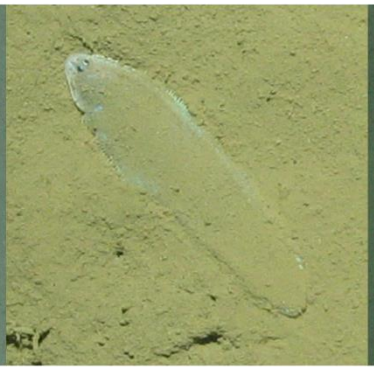
Cynoglossidae, cf. *Cynoglossus* sp.


Soleidae

Halosauridae, cf. *Halosaurus* sp.

Halosauridae

Halosauridae

Alepocephalidae

Alepocephalidae

Alepocephalidae

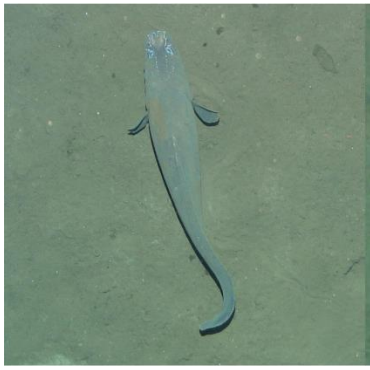

*Cataetyx* msp-01

*Dicrolene* spp.

*Dicrolene* spp.

Ophidiiformes msp-01

Ophidiiformes msp-02

Ophidiiformes msp-03, cf. pearlfish

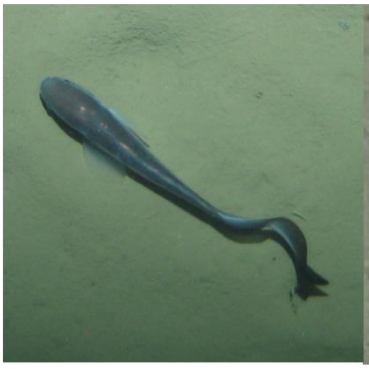

Ophidiiformes msp-04

Ophidiiformes msp-05

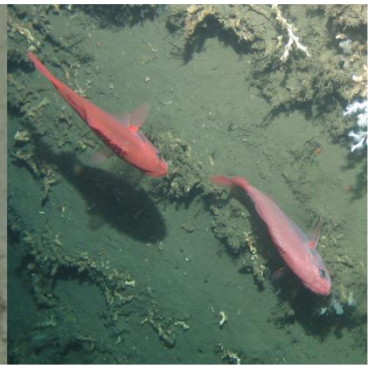

Beryciformes msp-01, cf. *Gephyroberyx*

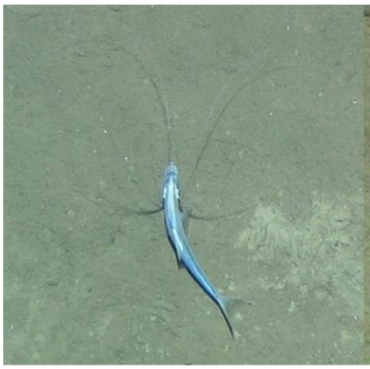

*Bathypterois* spp.

*Bathypterois* spp.

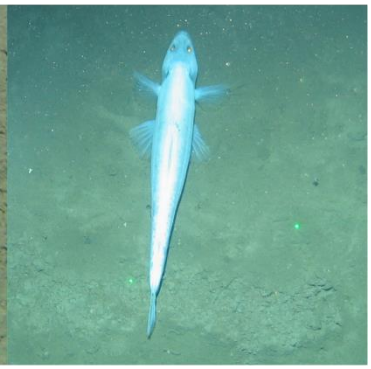

*Bathysaurus* msp-01

Chlorophthalmidae, cf. greeneyes
*Chlorophthalmus* sp.

Scorpaeniformes msp-01,
cf. *Trachyscorpia* or *Setarches*

Scorpaeniformes msp-02,
cf. *Helicolenus* sp.

Scorpaeniformes msp-02,
cf. *Helicolenus* sp.

Scorpaeniformes msp-03

*Psychrolutes* msp-01


Actinopterygii msp-09


Actinopterygii msp-10


Actinopterygii msp-12


Actinopterygii msp-13


Actinopterygii msp-14


Actinopterygii msp-15


Actinopterygii msp-16


Actinopterygii msp-19


Actinopterygii msp-20


Actinopterygii msp-21


Actinopterygii msp-22


Actinopterygii msp-23

Actinopterygii msp-24

Actinopterygii msp-25

Squaliformes, cf. *Centroscymnus* sp.

Rajiformes spp.

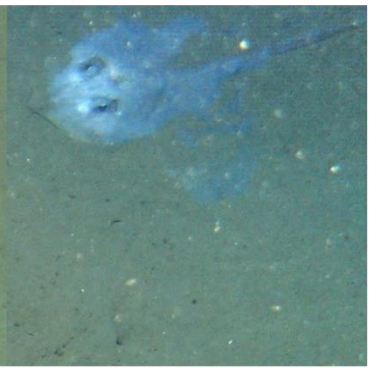

Rajiformes spp.

## Consulted visual identification material

Alt, C. H. (2012). On the Benthic Invertebrate Megafauna at the Mid-Atlantic Ridge, in the Vicinity of the Charlie-Gibbs Fracture Zone (Appendix E). University of Southampton, School of Ocean and Earth Science, Doctoral Thesis, 279pp. https://eprints.soton.ac.uk/351272/

Durden, J. M. (2016). Spatial and temporal variation in abyssal megabenthic communities, as assessed with seabed photography (Appendix A). University of Southampton, School of Ocean and Earth Science, Doctoral Thesis, 203pp. https://eprints.soton.ac.uk/396583/

Gates, A.R. (2016). Deep-sea Life of Tanzania. UK: National Oceanography Centre, Southampton, 87pp. ISBN: 0-904175-61-8. http://nora.nerc.ac.uk/id/eprint/513680/

Glover A.G., Higgs N.D., Horton T., Porrer, A. (2015). Deep Sea ID v.1.2 A Field Guide to the Marine Life of the Deep Sea 2015. http://www.marinespecies.org/deepsea/app.php

Howell, K.L., Davies, J.S., van den Beld I. (2017). Deep-sea species image catalogue. University of Plymouth, Ifremer, NOAA. http://www.deepseacatalogue.fr/ On-line version 3, 2017.

Jones D.O.B., Gates A.R., Curry R.A., Thomson M., Pile A., Benfield M. (Eds) (2009). SERPENT project. Media database archive. http://archive.serpentproject.com/

Jones D.O.B., Gates A.R. (2010). Deep-sea life of Scotland and Norway. UK: Ophiura, 77pp. ISBN: 978-0-9565832-0-8. https://eprints.soton.ac.uk/175317/

MBARI Deep-Sea Guide (2015). http://dsg.mbari.org/dsg/home

NEPTUNE Canada Marine Life Field Guide, First Edition 2012. https://www.oceannetworks.ca/now-available-marine-life-field-guide

NOAA Office of Ocean Exploration and Research Benthic Deepwater Animal Identification Guide. https://oceanexplorer.noaa.gov/okeanos/animal_guide/animal_guide.html

Stone, R.P., Lehnert, H., Reiswig, H. (2011). A guide to the deep-water sponges of the Aleutian Island Archipelago. NOAA Professional Paper NMFS 12. https://spo.nmfs.noaa.gov/content/guide-deepwater-sponges-aleutian-island-archipelago

Tyler, P., Hauton, C., Pattenden, A., Masson, D., Huvenne, V. Megafauna of canyons of the NE Atlantic and Portuguese Margin. Unpublished.

University of Hawai‘i Undersea Research Laboratory (HURL) Deep-sea Animal Identification Guide. http://www.soest.hawaii.edu/

## Consulted peer-reviewed literature

Alt, C.H.S., Kremenetskaia, A., Gebruk, A.V., Gooday, A.J., Jones, D.O.B., 2019. Bathyal benthic megafauna from the Mid-Atlantic Ridge in the region of the Charlie-Gibbs fracture zone based on remotely operated vehicle observations. *Deep Sea Research Part I: Oceanographic Research Papers*, 145, 1-12.

Amon, D.J., Ziegler, A.F., Drazen, J.C., Grischenko, A.V., Leitner, A.B., Lindsay, D.J., Voight, J.R., Wicksten, M.K., Young, C.M., Smith, C.R., 2017. Megafauna of the UKSRL exploration contract area and eastern Clarion-Clipperton Zone in the Pacific Ocean: Annelida, Arthropoda, Bryozoa, Chordata, Ctenophora, Mollusca. *Biodiversity Data Journal*, 5, e14598.

Amon, D.J., Ziegler, A.F., Kremenetskaia, A., Mah, C.L., Mooi, R., O'Hara, T., Pawson, D.L., Roux, M., Smith, C.R., 2017. Megafauna of the UKSRL exploration contract area and eastern Clarion-Clipperton Zone in the Pacific Ocean: Echinodermata. *Biodiversity Data Journal*, 5, e11794.

Bianchi, G., 1992. Demersal assemblages of the continental-shelf and upper slope of Angola. *Marine Ecology-Progress Series*, 81(2), 101-120.

Bianchi, G., Carpenter, K.E., Roux, J.-P., Molloy, F.J., Boyer, D., Boyer, H.J., 1999. FAO species identification field guide for fishery purposes. The living marine resources of Namibia. Rome, FAO. 265 p., 11 colour plates.

Bluhm, H., Gebruk, A., 1999. Holothuroidea (Echinodermata) of the Peru basin - Ecological and taxonomic remarks based on underwater images. *MARINE ECOLOGY-PUBBLICAZIONI DELLA STAZIONE ZOOLOGICA DI NAPOLI I*, 20(2), 167-195.

Boury-Esnault, N., Vacelet, J., Reiswig, H.M., Fourt, M., Aguilar, R., Chevaldonné, P., 2014. Mediterranean hexactinellid sponges, with the description of a new Sympagella species (Porifera, Hexactinellida). *Journal of the Marine Biological Association of the United Kingdom*, 95(7), 1353-1364.

Buhl-Mortensen, L., Serigstad, B., Buhl-Mortensen, P., Olsen, M.N., Ostrowski, M., Błażewicz-Paszkowycz, M., Appoh, E., 2017. First observations of the structure and megafaunal community of a large Lophelia reef on the Ghanaian shelf (the Gulf of Guinea). *Deep-Sea Research Part II: Topical Studies in Oceanography*, 137, 148-156.

Jamieson, A.J., Linley, T.D., Craig, J., 2017. Baited camera survey of deep-sea demersal fishes of the West African oil provinces off Angola: 1200–2500m depth, East Atlantic Ocean. *Marine Environmental Research*, 129, 347-364.

Jones, D.O.B., Brewer, M.E., 2012. Response of megabenthic assemblages to different scales of habitat heterogeneity on the Mauritanian slope. *Deep-Sea Research Part I*, 67, 98-110.

Jones, D.O.B., Mrabure, C.O., Gates, A.R., 2013. Changes in deep-water epibenthic megafaunal assemblages in relation to seabed slope on the Nigerian margin. *Deep-Sea Research Part I*, 78, 49-57.

Jones, D.O.B., Walls, A., Clare, M., Fiske, M.S., Weiland, R.J., O'Brien, R., Touzel, D.F., 2014. Asphalt mounds and associated biota on the Angolan margin. *Deep-Sea Research I*, 94, 124-136.

Le Guilloux, E., Olu, K., Bourillet, J.F., Savoye, B., Iglésias, S.P., Sibuet, M., 2009. First observations of deep-sea coral reefs along the Angola margin. *Deep Sea Research Part II: Topical Studies in Oceanography*, 56(23), 2394-2403.

Levin, L.A., Childers, S.E., Smith, C.R., 1991. Epibenthic, agglutinating foraminiferans in the Santa Catalina Basin and their response to disturbance. *Deep Sea Research Part A. Oceanographic Research Papers*, 38(4), 465-483.

Merrett, N.R., Marshall, N.B., 1981. Observations on the ecology of deep-sea bottom-living fishes collected off northwest Africa (08-27N). *Progress in Oceanography*, 9(4), 185-244.

Nørvang, A., 1961. Schizamminidae, a new family of Foraminifera. Atlantide Report No. 6. *Scientific Results of the Danish Expedition to the Coasts of Tropical West Africa 1945-1946*, 169-201.

O'Hara T.D., Stöhr S., Hugall A.F., Thuy B., Martynov A., 2018. Morphological diagnoses of higher taxa in Ophiuroidea (Echinodermata) in support of a new classification. *European Journal of Taxonomy* 416: 1–35.

Pajuelo, J.G., Seoane, J., Biscoito, M., Freitas, M., González, J.A., 2016. Assemblages of deep-sea fishes on the middle slope off Northwest Africa (26°–33° N, eastern Atlantic). *Deep Sea Research Part I: Oceanographic Research Papers*, 118, 66-83.

Pawson, D.L., Ames, C.L., Pawson, D.J., Nizinski, M.S., 2015. Deep-sea echinoids and holothurians (Echinodermata) near cold seeps and coral communities in the northern Gulf of Mexico. *Bulletin of Marine Science*, 91(2), 167-204.

Pawson, D.L., Vance, D.J., 2004. Chiridota heheva, new species, from Western Atlantic deep-sea cold seeps and anthropogenic habitats (Echinodermata : Holothuroidea : Apodida). *Zootaxa*, 534, 1-12.

Rogacheva, A., Gebruk, A., Alt, C.H.S., 2013. Holothuroidea of the Charlie Gibbs Fracture Zone area, northern Mid-Atlantic Ridge. *Marine Biology Research*, 9(5-6), 587-623.

Tendal, O.S.C., T., 2007. *Schizammina andamana* N. sp., a large foraminiferan (protozoa, granuloreticulosa) from the shelf West of Thailand. *Phuket mar. biol. Cent. Res. Bull.*, 68, 11-19.

Vardaro, M.F., Bagley, P.M., Bailey, D.M., Bett, B.J., Jones, D.O.B., Milligan, R.J., Priede, I.G., Risien, C.M., Rowe, G.T., Ruhl, H.A., Sangolay, B.B., Smith, K.L., Walls, A., Clarke, J., 2013. A Southeast Atlantic deep-ocean observatory: first experiences and results. *Limnology and Oceanography-Methods*, 11, 304-315.

# Appendix C
# Environmental data

This Appendix contains information about environmental data provided by BP, which have been used throughout Chapters 3 to 5.

## C.1 Hydrographic data

Oceanographic properties were assessed using CTD data collected during the 2014 survey. CTD casts were obtained from 20 stations across all four study areas (Table C.1) with a Valeport 606+ multiparameter instrument mounted on a 24-Niskin rosette sampler and fitted with sensors to record temperature (ºC), conductivity (mS $cm^{-1}$), pressure (dbar), dissolved oxygen (% saturation) and turbidity (FTU) (IMAR Survey, 2015a). For analysis of hydrographic profiles, downcast data were retrieved and water depths computed from pressure and latitude based on the method of Saunders and Fofonoff (1976) with the formula modified to fit the UNESCO equation of state (Fofonoff and Millard, 1983). Oxygen saturation levels were converted to dissolved oxygen concentrations (ml $l^{-1}$) as per Weiss (1970), and salinity (PSU) and potential temperature ($\theta$) were computed as per Fofonoff and Millard (1983). Calculations were carried out in R using the 'oce' package (Kelley and Richards, 2019).

**Table C.1** Location, date and depth for CTD deployments across the Angolan continental slope in 2014 (IMAR Survey, 2015a). Depth represents the deployment depth of each CTD cast.

| Area | Station | Date | Latitude (º) | Longitude (º) | Depth (m) |
|---|---|---|---|---|---|
| A | CTD ER | 22/08/2014 | -6.26945 | 10.77694 | 1877.74 |
| A | CTD WR | 20/08/2014 | -6.34663 | 10.67154 | 1925.34 |
| A | 3000m NE | 22/08/2014 | -6.22830 | 10.75827 | 1945.32 |
| A | 3000m SW | 21/08/2014 | -6.25434 | 10.71065 | 1988.19 |
| A | MICROR | 21/08/2014 | -6.34800 | 10.72988 | 1998.99 |
| A | N4 | 15/08/2014 | -6.20575 | 10.51950 | 2227.21 |
| B | rnd4C | 26/08/2014 | -7.83557 | 12.16352 | 1256.81 |
| B | 3000W | 28/08/2014 | -7.84706 | 12.08783 | 1313.19 |
| B | 3000S | 28/08/2014 | -7.87411 | 12.11341 | 1350.41 |
| B | B18CTDWR | 28/08/2014 | -7.88236 | 12.07779 | 1368.36 |
| B | B18CTDER | 31/08/2014 | -7.91700 | 12.18533 | 1389.09 |
| C | CTD SE | 05/08/2014 | -9.12983 | 12.58889 | 684.51 |
| C | CTD SW | 08/08/2014 | -9.12825 | 12.36158 | 1240.05 |
| C | CTD ME | 10/08/2014 | -8.81353 | 12.59099 | 1279.20 |
| C | CTD MW | 11/08/2014 | -8.81192 | 12.36384 | 1492.13 |
| D | CTD ME | 27/07/2014 | -11.91369 | 13.23711 | 894.19 |
| D | CTD SE | 20/07/2014 | -12.16225 | 13.23552 | 945.58 |
| D | CTD SW | 31/07/2014 | -12.15951 | 12.84050 | 1461.01 |
| D | CTD SW | 31/07/2014 | -12.15951 | 12.84050 | 1462.30 |
| D | CTD MW | 28/07/2014 | -11.91096 | 12.84247 | 1547.66 |

# C.2 Analytical methods - Sediment core analysis

**Table C.2** Summary of analytical methods employed by BP to measure grain size distributions and concentrations of hydrocarbons, nitrogen, and inorganic and organic material in surficial sediment samples obtained across the Angolan continental slope in 2005, 2008 and 2014. Sediment samples were collected with a hydraulically damped megacorer. A minimum of two samples were retained at each coring site for the analysis of sediment properties. Analysis of hydrocarbon concentrations included total hydrocarbon, individual n-alkanes, the isoprenoids Pristane and Phytane, and polynuclear aromatic hydrocarbons (PAHs). Information about analytical procedures was extracted from unpublished survey and data reports: ERT (2006), Bett (2007), ERT (2008), Hughes (2008), and IMAR Survey (2015a-e).

| Parameter | 2005 | 2008 | 2014 |
|---|---|---|---|
| **Sample horizon** | Hydrocarbon sample from the top 3 cm, stored in a pre-cleaned glass jar and frozen at -20°C. Sample for the remaining parameters from the top 4 cm, stored in a plastic bag and frozen at -20°C. | Hydrocarbon sample from the top 2 cm, stored in a pre-cleaned metal tin and frozen at -20°C. Sample for the remaining parameters from the top 5 cm, stored in a plastic bag and frozen at -20°C. | Two samples retained for physiochemical analyses, both from the top 3 cm of the respective cores. One hydrocarbon sample, stored in a metal tin and frozen at -20°C. One sample for the remaining parameters with residual top water retained, stored in a plastic bag and frozen onboard at -20°C. |
| **Grain size distribution** | Sediment samples for grain size distributions were pre-treated with 30% hydrogen peroxide to remove organic material. The samples were then filtered and washed with distilled water to remove any remaining salts and dried in an oven at approximately 60 °C. The treated material larger than 500 µm was dry sieved using nested sieves with mesh apertures between 4,000 and 500 µm (0.5 phi interval). A small subsample (1 to 2 g) of the material < 500 µm was analysed by laser diffraction at 0.5 phi interval between 500 µm to 63 µm, and at 1 phi interval for material < 63 µm, using a Malvern Mastersizer S (active beam length 2.4 mm, range 300RF with 0.05 to 900 µm). | | Sediment samples were separated into particles > 2 mm and < 2 mm by wet sieving. The dry weights of both fractions were recorded separately and the sum of these was calculated as the total dry weight of the untreated sample. Material > 2 mm was then dry sieved using nested sieves at 0.5 phi interval mesh sizes. Material < 2 mm was pre-treated with 30% hydrogen peroxide to remove organic material. The organic-free material > 1 mm was dry sieved using nested sieves at 0.5 phi interval mesh sizes. The sediment particle size distributions below 1 mm were determined by laser diffraction using a Malvern Mastersizer particle sizer at 0.5 phi interval. |
| **Total organic matter (TOM)** | By loss-on-ignition, after removal of carbonate; expressed as % w/w (dry sediment): Samples for TOM analysis were dried, weighed and then treated with hydrochloric acid to remove inorganic carbon in the form of carbonate. Fresh acid was added until all effervescence ceased; the sediment was then washed over a glass-fibre filter and the residue dried to a constant weight before being ignited in a muffle furnace at 600 °C for two hours. The organic content of the sample was then calculated using the weight difference from the original dry weight to the ignited residue, taking into account the loss of carbonate. | | By loss-on-ignition, expressed as % w/w (dry sediment): Samples for TOM analysis were air-dried, ground (particle size < 118 µm), dried at 50 ± 2.5°C and weighed, before being ignited at 450 ± 25°C for four and a half hours. The organic content of the sediment was then calculated using the weight difference from the original dry weight to the ignited residue, accounting for the amount of carbonate in the sample, which was determined separately by titration (see method below). |
| **Sediment carbonates** | Weight loss after acidification with hydrochloric acid (see TOM) | | Back titration method: An aliquot of the air-dried and ground sample was shaken with 100 ml of hydrochloric acid (HCl) until it ceased to effervesce. The clear supernatant liquid from this mixture was then titrated against sodium hydroxide (NaOH) to pH 7.0. A reference sample, comprising 25 ml of the HCl solution, was analysed with each sample batch. The mass of hydrochloric acid neutralised by the carbonate in the sample was calculated from the difference in the titre added to the reference solution and the sample. This was converted into the equivalent mass of carbonate present in the sample, and expressed as percent carbonate. |

**Table C.2** continued

| Parameter | 2005 | 2008 | 2014 |
|---|---|---|---|
| **Total organic carbon (TOC)** | Removal of inorganic carbon using acidification by dilute mineral acid (type not specified), followed by measurement of TOC using combustion analysis with an automatic Dumas elemental analyser. | | Dry combustion after removal of inorganic carbon using acidification by sulphurous acid: A 0.25 g aliquot of the air dried and ground (particle size < 118 μm) sample was mixed with 10 ml of sulphurous acid and allowed to effervesce at 40°C for fourteen hours in order to remove any inorganic carbon. The digested sample was then heated to 105°C until any remaining acid had evaporated and the sample had dried. The dried residue was then combusted at 1600 °C in an Eltra induction furnace fitted with a non-dispersive infrared (NDIR) cell, which measures the organic carbon content of the sample as liberated $CO_2$ concentration. |
| **Total organic nitrogen (TN)** | Removal of inorganic carbon using acidification by dilute mineral acid (type not specified), followed by measurement of TN using combustion analysis with an automatic Dumas elemental analyser. | | Combustion analysis using an automatic elemental analyser (type not specified). A known mass of sample was combusted in oxygen. The concentration of nitrogen gas were then measured by thermal conductivity cells. |
| **Hydrocarbon concentrations** | Ultrasonic extraction followed by clean-up and gas chromatography analysis for total hydrocarbons and individual n-alkanes $nC_{12}$-$nC_{36}$, and gas chromatography-mass spectrometry analysis for PAHs. | | Wet vortex extraction followed by clean-up and gas chromatography analysis with flame ionisation detection for total hydrocarbons and individual n-alkanes $nC_{10}$-$nC_{37}$, and gas chromatography-mass spectrometry analysis for PAHs. |